Regulation of endothelial calcium-dependent phenomena by calcium-regulated proteins

Lesley Anne Wilson

Submitted in accordance with the requirements for the degree of Doctor of Philosophy

The University of Leeds

School of Biomedical Sciences

September, 2013

The candidate confirms that the work submitted is her own and that appropriate credit has been given where reference has been made to the work of others.

Acknowledgements

Abstract

The inner lining of the vasculature is a monolayer of endothelial cells that performs a multitude of functions with importance for cardiovascular health. Many of the functions are regulated by or are dependent on the calcium ion (Ca^{2+}), a major intracellular signalling factor.

The overall aim of this thesis was to investigate molecular mechanisms and pharmacology of Ca^{2+} entry mechanisms and their downstream signalling in endothelial cells. Molecular, biochemical and electrophysiology techniques and cell functional assays were used to address two main objectives. The first objective was to investigate putative Ca^{2+} channel regulator proteins, CRACR2A and golli-MBP. Based on previous reported studies, it was hypothesised that both of these proteins would have a role in regulating endothelial cell store-operated Ca^{2+} entry. However, unexpectedly these proteins had Ca^{2+} channel-independent functions, leading to alternative hypotheses about their roles in endothelial cells. The second objective was to generate new information about pharmacology targeted to a Ca^{2+} channel subunit, TRPC6, which has been suggested to be important in endothelial cell biology. Specifically, it was hypothesised that the anti-cancer agent carboxyamidotriazole (CAI) and the flavanol galangin and its derivatives, which have previously been shown to inhibit intracellular Ca^{2+}, were TRPC6 channel inhibitors.

Endothelial cells did not express CRACR2A as reported for T cells (Srikanth et al., 2010) but did express a longer splice variant arising from the same gene, EFCAB4B isoform *a* (EFCAB4B-a). CRACR2A and EFCAB4B-a have the same putative Ca^{2+} binding domains at their N termini but EFCAB4B-a, unlike CRACR2A, had no role in the regulation of Ca^{2+} release-activated Ca^{2+} (CRAC) channels. Instead, EFCAB4B-a contained a predicted Rab domain in its C terminus and was therefore a putative monomeric G protein. It localised to endothelial cell specific Weibel-Palade bodies and influenced the abundance of the pro-thrombotic agent von Willebrand factor. Golli-MBP was found expressed

in endothelial cells but again there was little effect on CRAC channel activity. Instead golli-MBP was identified as a positive regulator of the important endothelial growth factor receptor, VEGFR2.

The small-molecule CAI, was identified as an inhibitor of TRPC6 channels without effect on TRPC5 or TRPV4 channels. A range of flavonol compounds was also identified as TRPC6 inhibitors.

In summary, this research has generated new information and hypotheses about a putative Ca^{2+}-regulated Rab protein of Weibel-Palade bodies, a novel regulator of a key endothelial growth factor receptor, and a molecular target for CAI. It has, therefore, led to understanding of molecular mechanisms and pharmacology in endothelial cells which may be useful for devising strategies to treat life-threatening conditions such as cardiovascular disease and cancer.

Table of Contents

List of Figures

Chapter 4

Chapter 5

Chapter 6

List of Tables

List of Abbreviations

2-APB	2-aminoethoxydiphenyl borate
AA	Arachidonic acid
ATP	Adenosine triphosphate
bp	Base pair
BSA	Bovine serum albumin
Ca^{2+}	Calcium ion
CAI	Carboxyamidotriazole
CHO	Chinese hamster ovary
CRAC	Calcium-release activated calcium
DAG	Diacylglycerol
DAPI	4',6-diamidino-2-phenylindole
DMSO	Dimethylsulphoxide
DN	Dominant negative
dNTP	Deoxyribonucleotide triphosphate
DTT	1,4-Dithiothreitol
EC	Endothelial cell
EGM	Endothelial growth medium
ELISA	Enzyme linked immunosorbent assay
ER	Endoplasmic reticulum
Fura-2 AM	Fura-2-acetoxymethyl ester
GAP	GTPase activating protein
Gd^{3+}	Gadolinium
GEF	Guanine exchange factor
GFP	Green fluorescent protein
Golli-MBP	Gene of oligodendrocyte lineage-myelin basic protein
GPCR	G-protein coupled receptor
GSP	Gene specific primer
GTP	Guanosine triphosphate
HBdMEC	Human bladder microvascular endothelial cell
HCMEC	Human cardiac microvascular endothelial cell
HCoMEC	Human colonic microvascular endothelial cell
HDMEC	Human dermal microvascular endothelial cell
HEK	Human embryonic kidney
HPAEC	Human pulmonary artery endothelial cell
HPMEC	Human pulmonary microvascular endothelial cell
HUAEC	Human umbilical artery endothelial cell
HUVEC	Human umbilical vein endothelial cell
ICC	Immunocytochemisty
IL	Interleukin

IP$_3$	Inositol trisphosphate
KDR	Kinase insert domain receptor, also known as vascular endothelial growth factor receptor 2
MAP kinase	Mitogen-activated protein kinase
Mg^{2+}	Magnesium ion
NCX	Sodium calcium exchanger
NFAT	Nuclear factor of activated T cells
OAG	1-Oleoyl-2-acetyl-sn-glycerol
PCR	Polymerase chain reaction
PKC	Protein kinase C
PLC	Phospholipase C
PMCA	Plasma membrane calcium ATPase
ROC	Receptor-operated channel
RT (+/-)	With (+) or without (-) reverse transcriptase
RT-PCR	Reverse transcriptase PCR
RTK	Receptor tyrosine kinase
SBS	Standard bath solution
SCID	Severe combined immune deficiency
SDS	Sodium dodecyl sulfate
SERCA	Sarco-endoplasmic reticulum calcium ATPase
siRNA	Short interfering RNA
SOCE	Store-operated calcium entry
STIM	Stromal interacting molecule
TG	Thapsigargin
TRP	Transient receptor potential
TRPC	Classical transient receptor potential
TRPV	Vanilloid transient receptor potential
VEGF	Vascular endothelial growth factor
VGCC	Voltage-gated calcium channel
VPF	Vascular permeability factor
vWF	Von Willebrand Factor
WB	Western blot
WPB	Weibel-Palade body

Publications

Amer MS, McKeown L, Tumova S, Liu R, Seymour VA, **Wilson LA**, Naylor J, Reenhalgh K, Hou B, Majeed Y, Turner P, Sedo A, O'Regan DJ, Li J, Bon RS, Porter KE, Beech DJ. **Inhibition of endothelial cell Ca(2+) entry and Transient Receptor Potential channels by Sigma-1 receptor ligands**. Br J Pharmacol. 2013 Mar; 168(6):1445-55.

Sukumar P, Sedo A, Li J, **Wilson LA**, O'Regan D, Lippiat JD, Porter KE, Kearney MT, Ainscough JF, Beech DJ. **Constitutively active TRPC channels of adipocytes confer a mechanism for sensing dietary fatty acids and regulating adiponectin**. Circ Res. 2012 Jul 6;111(2):191-200.

Li J, Cubbon RM, **Wilson LA**, Amer MS, McKeown L, Hou B, Majeed Y, Tumova S, Seymour VA, Taylor H, Stacey M, O'Regan D, Foster R, Porter KE, Kearney MT, Beech DJ. **Orai1 and CRAC channel dependence of VEGF-activated Ca^{2+} entry and endothelial tube formation.** Circ Res. 2011 May 13;108(10):1190-8.

Majeed Y, Bahnasi Y, Seymour VA, **Wilson LA**, Milligan CJ, Agarwal AK, Sukumar P, Naylor J, Beech DJ. **Rapid and contrasting effects of rosiglitazone on transient receptor potential TRPM3 and TRPC5 channels.** Mol Pharmacol. 2011 Jun;79(6):1023-30.

Manuscripts submitted or in preparation

Wilson LA, McKeown L, Tumova S, Li J, Main M, Barry S, Beech DJ. **Identification of a novel Ca^{2+}-regulated Rab protein in endothelial cells.**

Wilson LA, Li J, Main M, Barry S, Beech DJ. **Carboxyamidotriazole inhibits TRPC6 channels.**

Communications

Identification of a novel EF-hand Rab-like protein that regulates VEGF receptor expression (presentation). Yorkshire Cancer Research U.K. Symposium, Leeds 2012.

Novel Ca^{2+} channels: targets for colorectal and liver cancers? (presentation). The Management of Liver Disease, Radisson Blu Hotel Leeds. 2012.

Identification of a novel putative Rab protein in endothelial cells (presentation). Postgraduate Symposium. University of Leeds. 2013 and Endothelial Retreat, Lake District, 2013.

Transient Receptor Potential Ion Channels in Tumour Angiogenesis. (poster presentation). Postgraduate Symposium. University of Leeds. 2010.

Inhibition of TRPC6 Channels by Carboxyamidotriazole. (poster presentation). Postgraduate Symposium. University of Leeds. 2011.

The putative anti-cancer drug carboxyamidotriazole inhibits TRPC6 but not TRPC5 or TRPV4 channels. (poster presentation). International Meeting on Ion Transport and Cancer. Wurzburg, Germany. 2012.

CHAPTER 1. INTRODUCTION

Lining the inner surface of the entire vasculature is a monolayer of endothelial cells which together make up the endothelium. The endothelium forms a semi-permeable barrier between the blood and tissues and performs vital physiological functions such as regulation of blood flow and blood pressure, haemostasis, inflammatory responses and angiogenesis (Khazaei et al., 2008). Endothelial cells also play a key role in pathophysiological processes such as tumour angiogenesis (Hoeben et al., 2004) and endothelial dysfunction is a hallmark of many cardiovascular diseases such as atherosclerosis and hypertension (Khazaei et al., 2008). Endothelial cells have therefore become an attractive therapeutic target. Many endothelial cell processes depend on calcium, an important signalling factor in endothelial cells. Research in our laboratory is focused on calcium entry mechanisms and the downstream effects of calcium on endothelial cell processes in the context of cardiovascular disease and cancer. This introductory chapter will provide a short background on endothelial cell anatomy and physiology; endothelial cell dysfunction and cardiovascular disease; calcium regulation in endothelial cells with a particular focus on store-operated calcium entry (SOCE) channels, and therapeutic targeting of endothelial cell calcium.

1.1. The vascular endothelium: physiology and function

The human endothelium is a dynamic, multifunctional 'organ' composed of approximately 1×10^{13} endothelial cells (ECs) with a combined mass of around 1 kg, which is approximately 1% of body mass (Galley and Webster, 2004, Khazaei et al., 2008). Lining the inner surface of the vasculature, ECs have an important role in regulating the transfer of molecules between the circulating blood and tissues. In this regard the endothelium is often referred to as the 'blood-tissue barrier'. Being in direct contact with the circulating blood, ECs are

responsible for detecting and responding to changes in hemodynamic forces via membrane receptor mechanisms and the synthesis and release of vasoactive substances (Khazaei et al., 2008). In the same way, ECs contribute to the regulation of blood flow and blood pressure through the release of vasodilator and vasoconstrictor substances, which are important for controlling vascular tone (Khazaei et al., 2008). A major vasodilator synthesised and released by ECs is nitric oxide (NO). NO has several beneficial effects on the cardiovascular system including inhibition of platelet aggregation, smooth muscle cell proliferation and anti-atherosclerotic effects (Khazaei et al., 2008). ECs release vasoconstrictors and these include endothelin (ET)-1 and prostaglandin H2. Other important vasomotor factors are shown in Figure 1-1. In addition to hemodynamic functions, ECs also regulate thrombosis and thrombolysis. An important substance involved in thrombosis and coagulation is von Willebrand factor (vWF), which is synthesised by ECs and stored in organelles, unique to ECs called Weibel-Palade bodies (Valentijn et al., 2011). These are rod-shaped secretory-like granules that release large multimers of vWF during inflammatory processes or infection (Sumpio et al., 2002). ECs are involved in a number of other key processes, including platelet activation and aggregation, inflammation and immune modulation, vascular smooth muscle cell proliferation, vascular permeability, vasculogenesis and angiogenesis, some of which will be discussed in more detail below. Figure 1-2 shows schematically the general organisation of the endothelial cell.

1.1.1. *Angiogenesis*

One of the most important EC functions is angiogenesis. Angiogenesis is defined as the growth of new blood vessels from pre-existing ones and is vital for physiological processes such as wound healing, growth and reproduction (Hoeben et al., 2004, Khazaei et al., 2008). Pathologically, angiogenesis is important for tumour growth, psoriasis, diabetic retinopathy and rheumatoid arthritis (Hoeben et al., 2004). Angiogenesis involves endothelial cell migration and proliferation, the selective breakdown of the extracellular matrix by proteases such as collagenase, further migration and sprout formation (Khazaei

et al., 2008). During normal physiological conditions a delicate balance of pro (stimulatory) and anti (inhibitory) angiogenic factors circulate in the blood (Hoeben et al., 2004). A change in the balance of these circulating factors can result in a switch to a pro-angiogenic phenotype. The most potent stimulators of angiogenesis are growth factors, of which one of the most important is vascular endothelial growth factor (VEGF).

VEGF

VEGF was first discovered in the late 1970s as a tumour-secreted protein which was found to greatly increase microvascular permeability to circulating macromolecules and hence was given the name vascular permeability factor (VPF) (Dvorak et al., 1979). VPF was shown to increase permeability at concentrations as low as 1 nmol/L, 50,000 times more potently than histamine (Dvorak et al., 1999, Dvorak, 2002).

VEGF family

VPF (also known as VEGF-A) is member of the platelet-derived growth factor (PDGF) superfamily of growth factors (Dvorak, 2002). Other members of this family include VEGF-B, VEGF-C, VEGF-D and placenta-derived growth factor, PIGF (Hoeben et al., 2004). All of these growth factors are dimeric glycoproteins and all contain a conserved VEGF homology domain (Hoeben et al., 2004). VEGF-A is the most well characterised of the VEGF proteins. VEGF-A is a 34 - 45 kDa protein with highest mRNA levels found in the adult lung, heart, kidney and adrenal gland and lower levels in the gastric mucosa, spleen and liver (Hoeben et al., 2004). There are different isoforms of VEGF-A but VEGF-A$_{165}$ is often the predominant form (Hoeben et al., 2004). VEGF-A has several unique properties: it is essential for the development of a vascular system as evidenced by both the null (VEGF-A$^{-/-}$) and heterozygote (VEGF-A$^{+/-}$) animals that are embryonic lethal (Carmeliet et al., 1996, Ferrara et al., 1996); it is selective for ECs since its major receptor, VEGFR2, is selectively expressed on vascular endothelium, compared to other growth factors that are comparatively less selective for ECs (Dvorak, 2002), it can increase vascular permeability (Dvorak et al., 1979) and it is up-regulated in many human cancers (Duncan et al., 2008).

VEGF receptors

In the early 1990s the VEGF receptors were characterised (reviewed by (Shibuya and Claesson-Welsh, 2006). The 3 tyrosine kinase receptors identified are structurally highly related; they are: VEGFR1, VEGFR2 (also known as KDR in humans) and VEGFR3 (Hoeben et al., 2004). VEGFR2 and VEGFR3 are more active kinases than VEGFR1, which has 10 times lower kinase activity than VEGFR2 (Shibuya and Claesson-Welsh, 2006). VEGFR2 binds VEGF-C and VEGF-D but is most important for its role in VEGF-A-induced vascular permeability and angiogenesis (Hoeben et al., 2004). VEGF-A binding to VEGFR2 results in the autophosphorylation of various tyrosine residues on VEGFR2 (Hoeben et al., 2004). Autophosphorylation of Tyr1175 results in the binding of phospholipase C (PLCγ1) which generates an increase in inositol 1,4,5-triphosphate (IP_3) and diacylglycerol (DAG) leading to a rise in intracellular Ca^{2+} but also activating protein kinase C (PKC), which subsequently activates Ras, which is involved in downstream gene transcription events (Hoeben et al., 2004).

Tumour angiogenesis

For a tumour to grow beyond 1-2 mm^3 it must develop its own blood supply – a process which is termed tumour angiogenesis (Hanahan and Weinberg, 2000). When a tumour reaches 1-2 mm^3 the balance of pro- and anti-angiogenic factors is shifted in favour of angiogenesis. ECs isolated from tumour blood vessels are phenotypically and genetically different from 'normal' endothelial cells and are often described as dysfunctional (Dudley, 2012). Tumour blood vessels are often chaotic and leaky and no longer form a single layer of regular shaped cells, but instead take on an irregular shape and size with cytoplasmic protrusions stretching across the lumen of the vessel (Dudley, 2012). There still remains some debate as to the origin of tumour blood vessels - whether they have developed from pre-existing 'normal' vessels or whether stem-like tumour cells have trans-differentiated to form an endothelium (Hendrix et al., 2003).

However, regardless of origin, the endothelial lining of these vessels is morphologically and genetically distinct from 'normal' vessels.

1.1.2. Endothelial permeability

ECs form a barrier between the circulating blood and tissues (Goddard and Iruela-Arispe, 2013) The integrity of this barrier is regulated in various ways including intercellular junctions such as tight junctions and adherence junctions (Goddard and Iruela-Arispe, 2013). Tight junction proteins include claudin-5, occludin and junctional adhesion molecules and vascular permeability is increased when these proteins become phosphorylated (Goddard and Iruela-Arispe, 2013). Adherence junctions are mainly composed of the calcium-dependent VE-cadherin proteins (Goddard and Iruela-Arispe, 2013). When ECs become exposed to permeability factors such as thrombin, VEGF and histamine, VE-cadherins become phosphorylated and internalise, which disrupts the integrity of the barrier (Goddard and Iruela-Arispe, 2013). Different adherent proteins exist in different vascular beds. In particular, in tumour blood vessels, junctions are very weak and hence vessels are very leaky (Dudley, 2012). VEGF is the most potent permeability factor and the mechanisms involved in VEGF-induced increases in permeability include junctional remodelling, induction of fenestrae and other downstream signalling events such as PLC-dependent increase in intracellular Ca^{2+}, phosphorylation and internalisation of junctional proteins, eNOS signalling and dissociation of VE-cadherin complexes (Goddard and Iruela-Arispe, 2013). Other permeability factors include the inflammatory mediators histamine, thrombin and bradykinin, all of which evoke a transient increase in vascular permeability followed by barrier stabilisation (Goddard and Iruela-Arispe, 2013).

1.1.3. Haemostasis

Another important role of ECs is in haemostasis, a physiological process that allows bleeding to stop. Circulating in the blood is a balance of prothrombotic and antithrombotic factors (Figure 1-1), which maintain haemostasis. During

normal physiological conditions, ECs produce prostacylin and NO, which work to prevent the adhesion of platelets and subsequent aggregation (Khazaei et al., 2008). However, during vessel damage and wound healing ECs increase their release of pro-thrombotic factors such as von Willebrand factor (vWF) through Ca^{2+}-dependent exocytosis, which interacts with the platelet glycoprotein complex allowing platelet adhesion and aggregation resulting in clot formation (Khazaei et al., 2008).

1.2. Endothelial dysfunction

Endothelial dysfunction occurs as a result of phenotypic changes to healthy ECs and is characterised by an increase in contracting factors combined with an overall shift towards a proinflammatory, procoagulatory and proliferative environment along with an increase in vascular permeability (Bonetti et al., 2003, Widlansky et al., 2003). These phenotypic alterations mark an early step in the development of atherosclerosis, a major precursor of cardiovascular disease, which is the main cause of death in Europe responsible for over 4 million deaths each year (European Cardiovascular Disease Statistics 2012 edition) (Widlansky et al., 2003).

Atherosclerosis is a disease of the arterial vessels, which involves the thickening of the vessel wall through accumulation of fatty material and importantly low density lipoprotein (LDL) (Singh et al., 2002). Lipoproteins, monocytes and macrophages are able to accumulate in the vessel due to an increase in vessel permeability, a key characteristic of endothelial dysfunction (Khazaei et al., 2008). The build-up of fatty material or 'streaks' in the vessel wall is a trigger for an inflammatory response (Weber and Noels, 2011, Esper et al., 2006). When the LDL becomes oxidised within the vessel wall by reactive oxygen species or enzymes, this triggers further immune response including expression of adhesion molecules and secretion of chemokines by the ECs, which results in T cells and macrophages travelling to the damaged site and absorbing the oxidised LDL (Weber and Noels, 2011, Esper et al., 2006). Since the oxidised LDL cannot be effectively broken down, it builds-up and can rupture releasing cholesterol into the circulation, triggering further immune

responses, amplifying the problem. If the process continues then eventually a cholesterol plaque is formed as a result of the inflammation and vascular smooth muscle cells form a hard cover over the affected area, which ultimately narrows the vessel, decreases blood flow and increases blood pressure. During this inflammatory cascade, the normal antithrombotic milieu is disrupted, decreasing the anticoagulatory potential of the endothelium and increasing procoagulatory mediators resulting in a thrombotic vascular environment (Esper et al., 2006).

Hypertension represents another risk factor for cardiovascular disease, however there remains some debate as to whether hypertension is the cause or result of endothelial dysfunction (Dharmashankar and Widlansky, 2010, Panza et al., 1993).
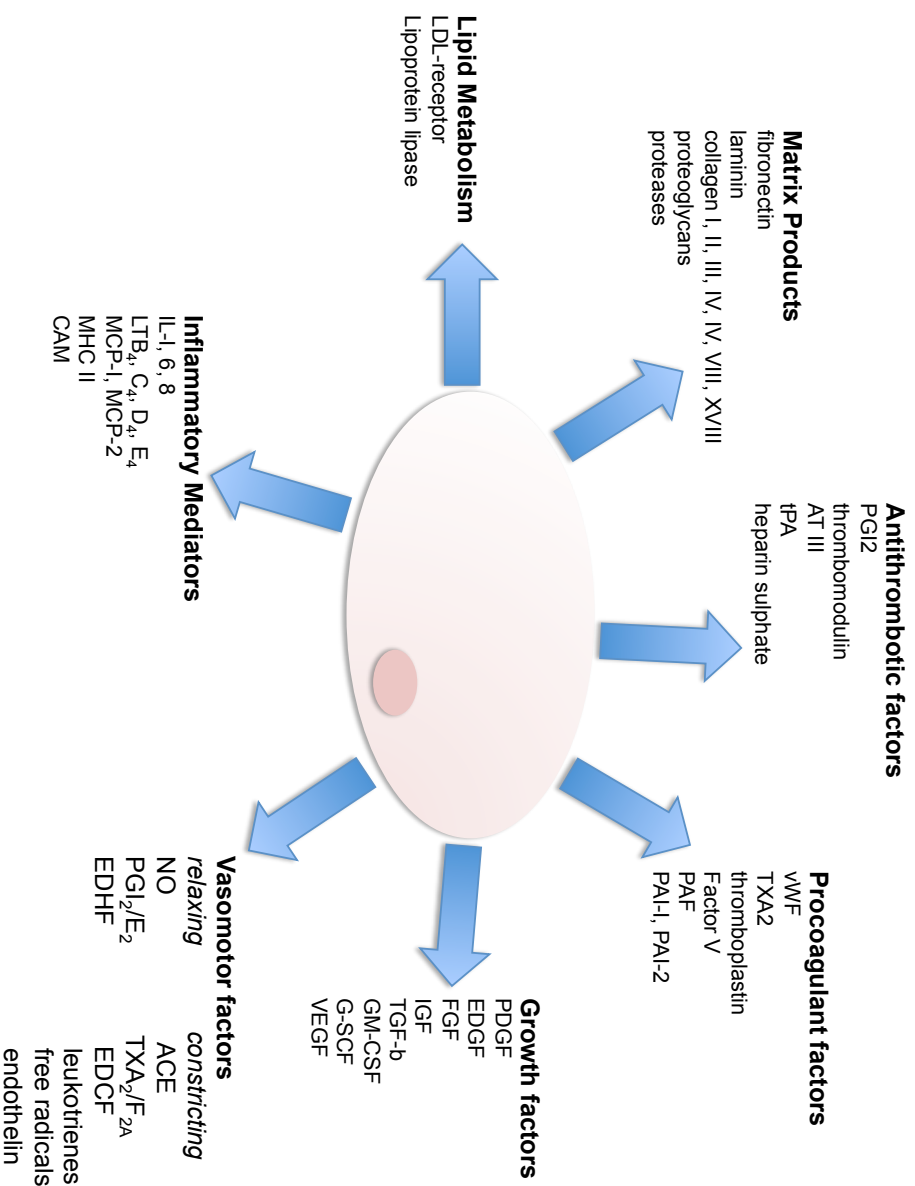
Figure 1-1 Secretory and expression products of vascular ECs.

Antithrombotic factors
PGI2
thrombomodulin
AT III
tPA
heparin sulphate

Procoagulant factors
vWF
TXA2
thromboplastin
Factor V
PAF
PAI-I, PAI-2

Growth factors
PDGF
EDGF
FGF
IGF
TGF-b
GM-CSF
G-SCF
VEGF

Vasomotor factors
relaxing
NO
PGI$_2$/E$_2$
EDHF
constricting
ACE
TXA$_2$/F$_{2A}$
EDCF
leukotrienes
free radicals
endothelin

Inflammatory Mediators
IL-I, 6, 8
LTB$_4$, C$_4$, D$_4$, E$_4$
MCP-I, MCP-2
MHC II
CAM

Lipid Metabolism
LDL-receptor
Lipoprotein lipase

Matrix Products
fibronectin
laminin
collagen I, II, III, IV, IV, VIII, XVIII
proteoglycans
proteases

8

PGI$_2$ prostacyclin; AT III antithrombin; tPA tissue plasminogen activator; TXA$_2$ thromboxane A2; PAF platelet activating factor; PAI plasminogen activator inhibitor; PDGF platelet derived growth factor; EDGF epidermal growth factor; FGF fibroblast growth factor; IGF insulin growth factor; TGF transforming growth factor; GM-CSF Granulocyte macrophage-colony stimulating factor; G-SCF granulocyte-colony stimulating factor; NO nitric oxide; EDCF endothelium-dependent contracting factor; EDHF Endothelium-Derived Hyperpolarizing Factor; IL interleukin; LTB$_4$ leukotriene B4; MCP Monocyte chemoattractant protein; MHC major histocompatibility complex; CAM cell adhesion molecules; LDL low density lipoprotein. Adapted from *Sumpio et al* (2002).
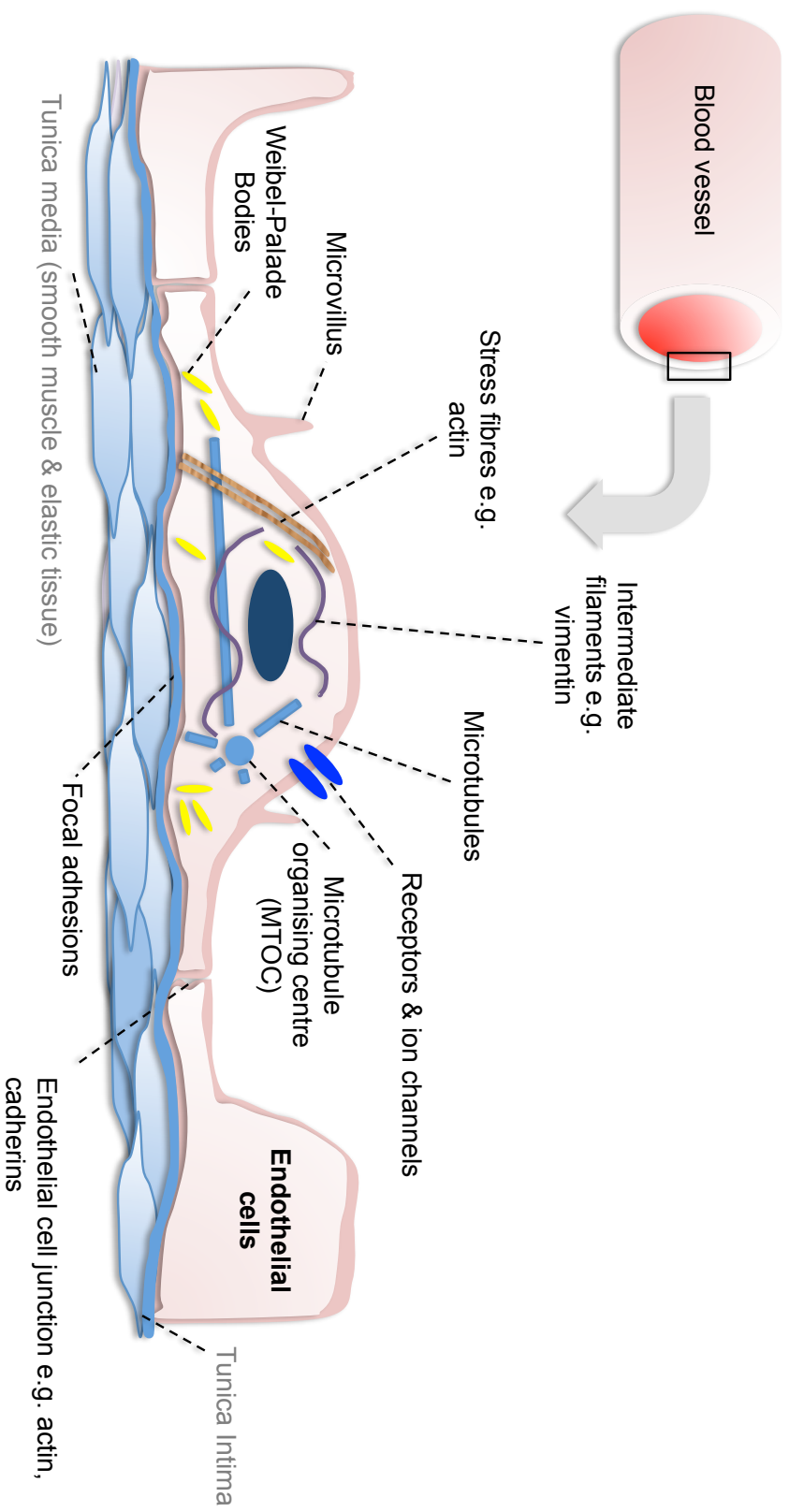
Figure 1-2 Diagram illustrating endothelial cell anatomy.

Adapted from Drenckham and Ness 1997 (Esper et al., 2006).

Blood vessel

Intermediate filaments e.g. vimentin

Stress fibres e.g. actin

Microvillus

Weibel-Palade Bodies

Tunica media (smooth muscle & elastic tissue)

Focal adhesions

Microtubules

Receptors & ion channels

Microtubule organising centre (MTOC)

Endothelial cells

Endothelial cell junction e.g. actin, cadherins

Tunica Intima

1.3. Endothelial cell signalling pathways

For endothelial cells to effectively communicate and perform the range of functions that they do, many different signalling mechanisms exist. Signalling cascades are often initiated by extracellular signalling molecules that bind and activate cell surface receptors. The signalling of one molecule often signals to another and then to another and so on, amplifying the signal as it goes and finally distributing the signal to the appropriate effector molecule for example gene regulatory proteins or ion channels (Alberts et al., 2008). There are two key families of cell-surface receptors that are important in endothelial cells - G-protein-coupled receptors and enzyme-coupled receptors. In addition, there are several principal intracellular signalling pathways activated by these receptors that are important for endothelial cell function including the RAS/Raf/MEK/ERK, PI3K/AKT, and IP_3/DAG pathways (Figure 1-3). The first two of these pathways will be discussed below and the third will be discussed in greater detail in section 1.4.

1.3.1. RAS/Raf/MEK/ERK pathway

The RAS/Raf/MEK/ERK pathway is a conserved signal transduction pathway involved primarily in cell growth and proliferation. This pathway is stimulated by growth factors acting on their target receptor tyrosine kinase (RTK) at the plasma membrane (Alberts et al., 2008). RAS is part of a superfamily of monomeric GTPases and is involved in relaying signals from the cell surface through to effector molecules such as transcription factors and thereby affecting gene expression (Alberts et al., 2008). As with all small GTPases, RAS switches between an active GTP-bound state and an inactive GDP-bound state. Regulating this switch are numerous effector and adaptor molecules called guanine-nucleotide exchange factors (GEFs) that speed up the activation of RAS and GTPase activating proteins (GAPs) that increase the rate of hydrolysis and inactivate RAS (Colicelli, 2004) (Figure 1-4). RTKs couple to RAS via adaptor molecules called Grb2 and Shc and a GEF called "son of sevenless"

SOs (Alberts et al., 2008). Activation of RAS then phosphorylates the effector molecule Raf, which subsequently phosphorylates MEK and ERK. The ERK kinase then enters the nucleus and is involved in gene transcription. RAF, MEK and ERK are all mitogen-activated protein (MAP) kinases and therefore this signalling pathway is often referred to as the MAP kinase signalling pathway. Mutations in RAS are common in cancer and around 15% of human cancers have activating RAS mutations, which lead to aberrant cell growth (Malumbres and Barbacid, 2003). Evidence for the importance of this signalling pathway in endothelial cells is clear; MEK1 knockout mice show defective angiogenesis in the placenta and are embryonic lethal (Giroux et al., 1999). Two studies use a dominant negative (DN) approach and show that DN Raf results in endothelial cell apoptosis and inhibits tumour growth (Hood and Cheresh, 2002), and that DN MEK1 results in a decrease in the vascularisation of a tumour (Mavria et al., 2006). In addition the ERK-MAPK pathway is essential for proliferation (Meadows et al., 2001).

1.3.2. PI3K/Akt pathway

Akt is a serine/threonine protein kinase, activated by a range of different growth factors including angiogenic growth factors such as VEGF, in a PI3 kinase (PI3K)-dependent manner (Shiojima and Walsh, 2002). Upon growth factor stimulation, the pleckstrin homology (PH) domain of Akt binds to the lipid products of PI3K, resulting in recruitment of Akt to the plasma membrane. Akt then becomes phosphorylated, yielding a fully activated kinase. The Akt/PI3K pathway is most widely known for its role as a cell-survival pathway since studies have shown that constitutive activation of this pathway is able to block cell death induced by a range of apoptotic stimuli, and that mutation of Akt in Drosophila results in embryonic lethality. However, this signalling pathway is also important for angiogenesis, since activating mutations in the PI3K pathway can suppress tumour vascularisation (Yuan and Cantley, 2008, Graupera and Potente, 2013).
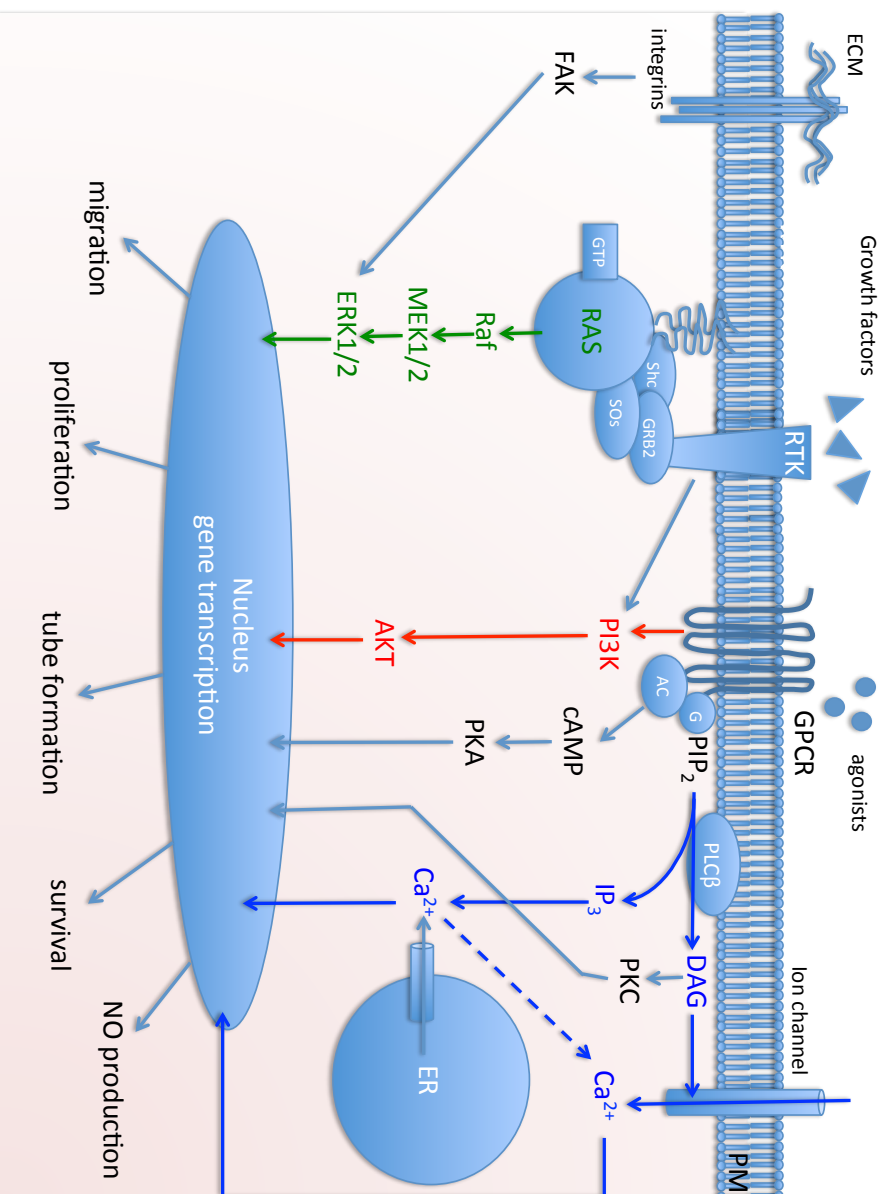
Figure 1-3 Important signalling cascades in endothelial cells.

The figure schematically shows the RAS/Raf/MEK/ERK, PI3K and IP$_3$/DAG signalling mechanisms in endothelial cells. ECM, extracellular matrix; RTK, receptor tyrosine kinase; GPCR, G-protein coupled receptor; PM, plasma membrane; PLC, phospholipase C; FAK, focal adhesion kinase; PI3K, phosphatidylinositol-3 kinase; Shc, src homologous and collagen; GRB2, growth factor receptor-bound protein 2; SOs, son of seveless; ER, endoplasmic reticulum; DAG, diacylglycerol.
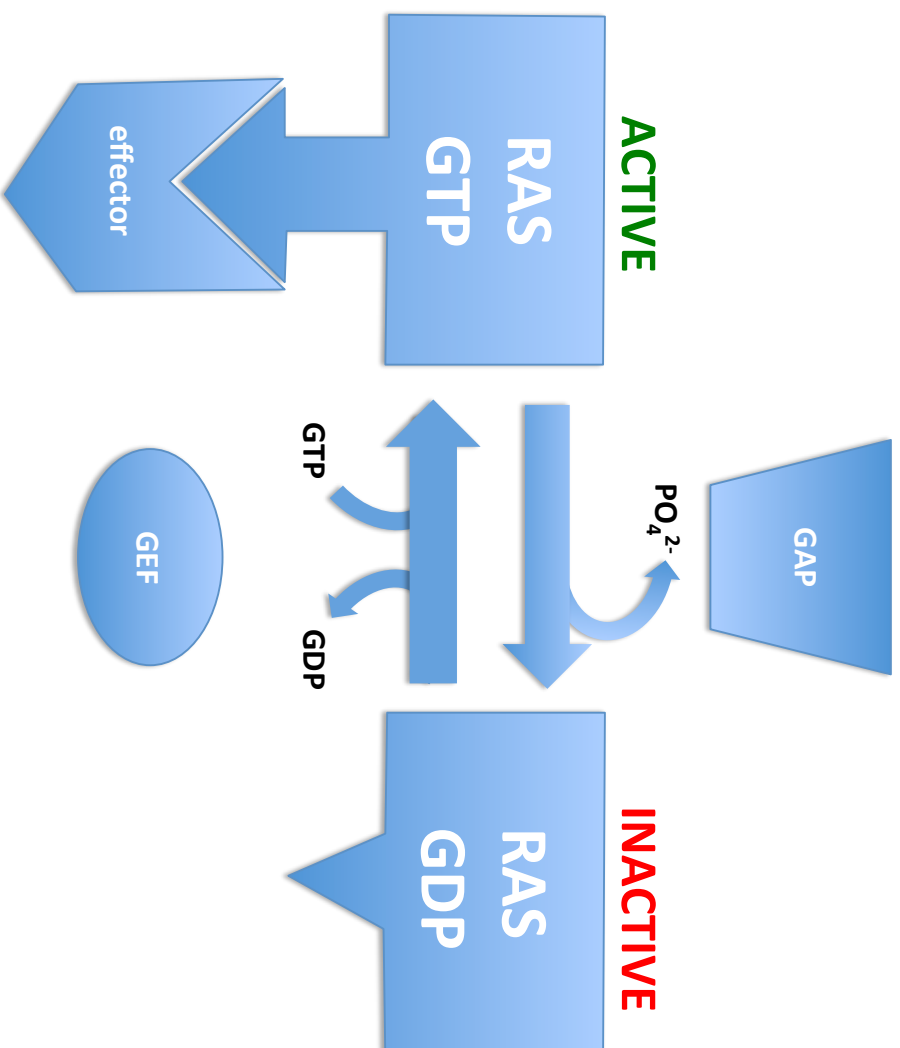
Figure 1-4 Regulation of small GTPases of the RAS superfamily.

The figure schematically shows how RAS GTPases are regulated, switching between active GTP-bound states to inactive GDP-bound states. GTPase activating proteins (GAPs) increase the rate of hydrolysis and inactivate RAS while guanine-nucleotide exchange factors (GEFs) speed up the activation of RAS. Adapted from Colicelli (2004).

1.4. The calcium ion – a major signalling ion in ECs

Calcium (Ca^{2+}) can be described as the chief intracellular signal, as it regulates a diverse range of cellular processes from rapid processes such as exocytosis (within microseconds), to longer-acting processes such as transcription (over several hours) (Berridge et al., 2003). In ECs, Ca^{2+} is required for many vital functions such as vasodilation and constriction, angiogenesis, vessel permeability and haemostasis (Khazaei et al., 2008, Tran et al., 2000). Control of cellular Ca^{2+} is carefully regulated so that the intracellular Ca^{2+} concentration is maintained at ~100 nM, whereas extracellular Ca^{2+} concentration is in the mM range creating a concentration gradient of around 20,000-fold (Clapham, 2007a). With Ca^{2+} being so avidly extruded from the cytosol, the cell has evolved ways to exert control over Ca^{2+} levels, such as chelation, compartmentalisation and extrusion (Clapham, 2007a). This requires a balance of 'on' reactions that allow Ca^{2+} into the cytoplasm and 'off' reactions that remove Ca^{2+} (Berridge et al., 2003). Figure 1-5 schematically shows the mechanisms that a cell uses to control Ca^{2+} homeostasis. The details in this diagram such as major storage sites for intracellular Ca^{2+} and the various mechanisms that endothelial cells use to carefully control the balance of Ca^{2+} in the cell will be discussed in the next sections.
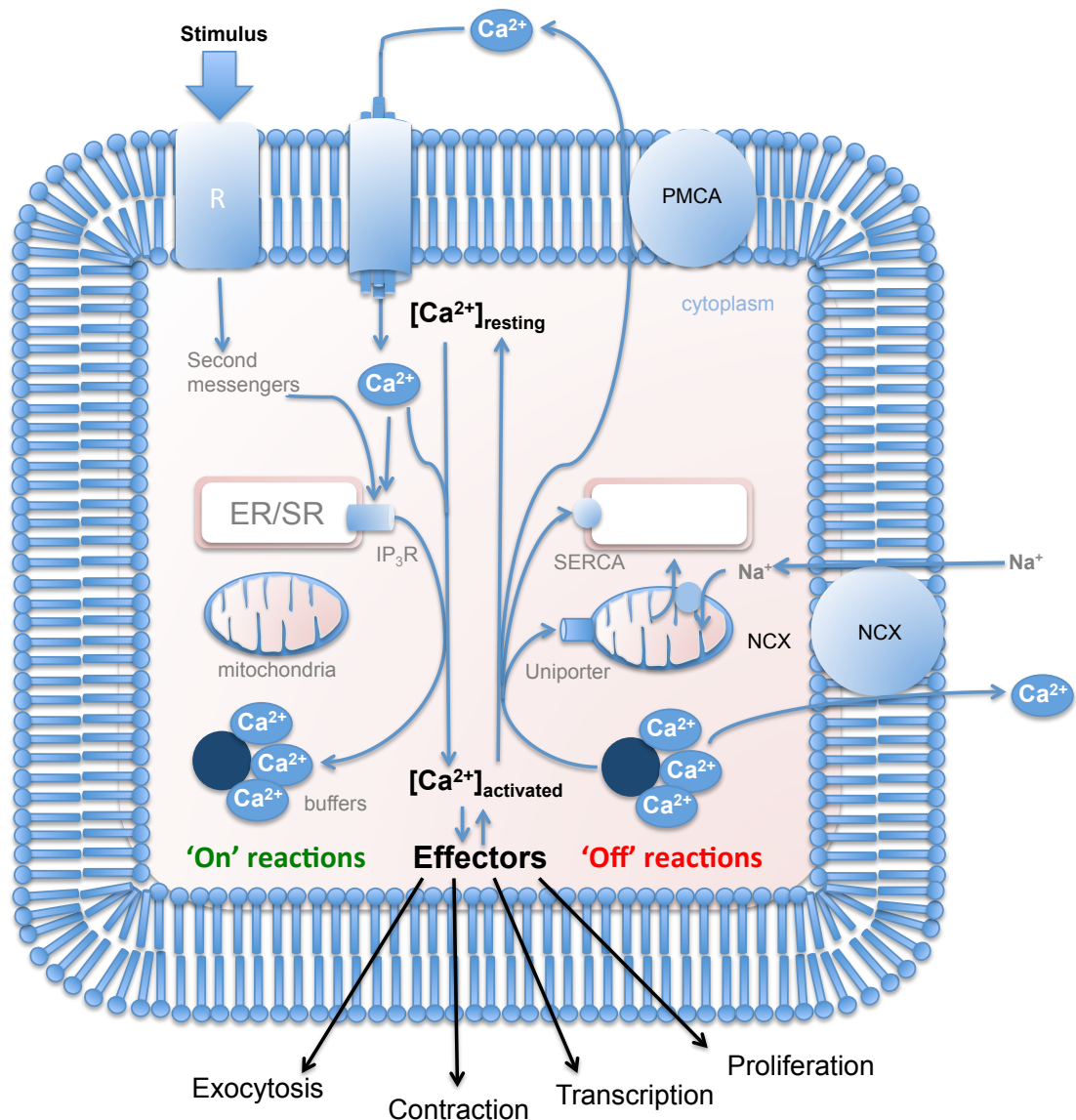
Figure 1-5 Intracellular Ca^{2+} handling.

The diagram illustrates Ca^{2+} handling in the cell. The Ca^{2+} concentration in the cell must be carefully controlled. Increases in cellular Ca^{2+} arise through various 'on' reactions such as Ca^{2+} entry through membrane ion channels or the release of Ca^{2+} from the endoplasmic reticulum (ER). Decreases in cellular Ca^{2+} occur through various 'off' reactions, such as uptake into the ER or mitochondria or extrusion through the NCX or PMCA in the plasma membrane. Ca^{2+} buffers in the cell also contribute to regulating the amount of Ca^{2+} in the cell. Ca^{2+} is a critical second messenger for many cell reactions such as exocytosis, contraction, transcription and proliferation. PMCA: plasma membrane Ca^{2+} ATPase; R: receptor; ER/SR: endoplasmic reticulum/sarcoplasmic reticulum; NCX: Na^{2+}/Ca^{2+} exchanger; SERCA: sarcoendoplasmic reticulum ATPase. Adapted from Berridge *et al* (2003).

1.4.1. Storage sites of Ca^{2+}

Endoplasmic reticulum

The endoplasmic reticulum (ER) is a multifunctional signalling organelle involved in the synthesis and packaging of proteins, but is also essential for many signalling processes (Berridge, 2002). With regard to the latter, the ER is the major intracellular store of Ca^{2+}, where the Ca^{2+} concentration is maintained at 100-500 μM but can reach as high as 3 mM (Berridge, 2002, Tran et al., 2000). In endothelial cells, 75% of the total intracellular Ca^{2+} is stored in the ER (Tran et al., 2000). It is vital that the ER maintains a constant luminal level of Ca^{2+} for the post-translational processing, folding and export of proteins (Berridge, 2002). In order to maintain a constant Ca^{2+} concentration, the ER contains buffers such as calreticulin that have a large capacity for Ca^{2+}. In addition the ER contains Ca^{2+}-sensitive chaperones such as GRP94 and calnexin which act in concert with the buffers to maintain a constant level of Ca^{2+} (Berridge, 2002). Should the ER Ca^{2+} level decline, this can have catastrophic effects due to activation of ER stress signalling pathways (Berridge, 2002).

Mitochondria

The remaining 25% of intracellular Ca^{2+} in ECs is contained in the mitochondria (Tran et al., 2000). The ER and the mitochondria are intimately connected and the two organelles cooperate to generate Ca^{2+} signals (Berridge, 2002). The mitochondria are important in sequestering Ca^{2+} that has been released from the ER but if large amounts of Ca^{2+} move from the ER to the mitochondria, a number of stress signals are induced (Berridge, 2002).

Other intracellular Ca^{2+} stores

Whilst the ER and mitochondria are the best-characterised cellular compartments for storing and releasing Ca^{2+}, other vesicular compartments have been shown to accumulate Ca^{2+} including the Golgi, secretory vesicles and lysosomes (Dickson et al., 2012). Since these organelles are highly

localised within the cell, they have the capacity to take up or release Ca^{2+} in select 'microdomains', the importance of which is still under investigation.

1.4.2. Regulation of Ca^{2+}

Pumps and exchangers

A number of Ca^{2+} pumps and exchangers are important for maintaining the resting level of Ca^{2+} in the cell at ~100 nM and ensuring that internal stores are kept loaded (Berridge et al., 2003). In order to perform these functions, the pumps are located on the plasma and ER membranes. For example, the plasma membrane Ca^{2+}-ATPase (PMCA) removes Ca^{2+} from the cell to the extracellular environment (Holton et al., 2010). The PMCA operates with high Ca^{2+} affinity and low transport capacity such that one Ca^{2+} is removed for each ATP hydrolysed (Moccia et al., 2012) which means the PMCA is efficient at maintaining low levels of intracellular Ca^{2+} over long durations (Clapham, 2007a). PMCA1, 2 and 4 are expressed on the vascular endothelium but PMCA1 appears to be the predominant isoform (Szewczyk et al., 2007).

Also localised on the plasma membrane, and responsible for extruding Ca^{2+} from the cell are members of the sodium/calcium exchanger family, NCX. (Berridge et al., 2003). This family comprises NCX1-3 and functions by extruding one Ca^{2+} ion for the uptake of 3 Na^+ ions. The NCX therefore operates with low Ca^{2+} affinity and high transport capacity, which makes it suitable for making rapid adjustments in Ca^{2+} concentration (Clapham, 2007a).

Unlike the PMCA and NCX, which extrude Ca^{2+} from the cell, the sarco(endo)plasmic reticulum ATPase (SERCA) located on the ER membrane functions to pump Ca^{2+} against a concentration gradient into the ER at the expense of ATP (Berridge et al., 2003). Uniporters on mitochondria also serve to rapidly sequester Ca^{2+} that is then released more slowly back into the cytosol where it is sequestered by the SERCA and PMCA (Berridge et al., 2003).

1.4.3. Intracellular Ca^{2+} permeable ion channels

Ca^{2+} release and uptake channels on the ER

In ECs, the predominant Ca^{2+} release channels on the ER are the IP$_3$Rs (Berridge, 2002), of which there are 3 forms (Moccia et al., 2012, Tran et al., 2000). The second messenger IP$_3$ activates these channels and this allows Ca^{2+} to be released from the intracellular store into the cytoplasm (Tran et al., 2000). In addition to Ca^{2+} release from the ER through IP$_3$Rs, Ca^{2+} can also leak out of the ER down its concentration gradient into the cytosol (Tran et al., 2000). This Ca^{2+} leak is often compensated for by uptake of Ca^{2+} by ER Ca^{2+} ATPases such as SERCA which is faster at taking up Ca^{2+} than the leak channels are at releasing it, thereby maintaining Ca^{2+} homeostasis (Tran et al., 2000).

1.4.4. Plasma membrane Ca^{2+} permeable ion channels

ECs express a multitude of Ca^{2+} permeable ion channels on their cell surface, all of which open and close in response to various stimuli. The next section will discuss voltage-operated Ca^{2+} channels and the Transient Receptor Potential (TRP) family of ion channels that act as cellular sensors for various stimuli.

Voltage-gated Ca^{2+} channels

Voltage-gated Ca^{2+} channels (VGCCs) have a high selectivity for Ca^{2+} and open in response to cell membrane depolarisation. VGCCs are predominantly found in neurons and muscle, where they are involved in excitation and contraction (Vinet and Vargas, 1999). ECs are generally considered 'electrically non-excitable' and to not express VGCCs, however a number of reports have shown expression and function of these channels in ECs (Bossu et al., 1992a, Bossu et al., 1992b, Bossu et al., 1989, Zhou and Wu, 2006). Interestingly, all of these publications report expression in microvascular ECs and the publication by Zhou *et al* shows almost no expression in macrovascular ECs, suggesting a possible specific role of VGCCs in small diameter blood vessel ECs (Zhou and

Wu, 2006). Further studies are needed in this area to determine the significance of this finding.

Endothelial Ca^{2+}-permeable TRP channels

The TRP family of ion channels were discovered in the *Drosophila melanogaster* visual system in 1989 (Montell and Rubin, 1989) and many are expressed in mammalian ECs. These include all known members of the canonical (TRPC) family, 3 members of the vanilloid (TRPV) family including TRPV1, TRPV2 and TRPV4, all of the melastatin (TRPM) family except TRPM5, and 2 members of the polycystin (TRPP) family, TRPP1 and TRPP2. All of these channels except TRPM4 are Ca^{2+} permeable ion channels (Kwan et al., 2007) that act as cellular sensors for a variety of different internal and external stimuli. The literature around endothelial TRP channels is vast, and so the next sections will focus on three important endothelial Ca^{2+}-permeable TRP channels that have distinct mechanisms of activation: TRPC6, TRPV4 and TRPM2.

TRPC6: a receptor-operated Ca^{2+} channel

Activation of receptor-operated channels occurs as a result of plasma membrane G-protein coupled receptor (GPCR) stimulation, leading to activation of phospholipase C (PLC) and the hydrolysis of PIP_2 into IP_3 and diacylglycerol (DAG). Generation of IP_3 activates IP_3 receptors on the ER that results in Ca^{2+} release from the ER and this triggers Ca^{2+} entry through receptor-operated channels (Janssen and Kwan, 2007). Alternatively, DAG can directly activate receptor-operated channels in the plasma membrane for example TRPC6 (Estacion et al., 2004). The muscarinic family of GPCRs are an example of GPCR that couple to ROCs (Shapiro et al., 2001).

TRPV4: an arachidonic acid-sensitive Ca^{2+} channel

TRPV4 is activated endogenously by arachidonic acid (Nilius et al., 2004). Stimulation with arachidonic acid causes a robust Ca^{2+} influx which has been found important in migration and angiogenesis of tumour-derived endothelial cells (Fiorio Pla et al., 2010).

TRPM2: a cellular redox sensing Ca^{2+} channel

TRPM2 is expressed on endothelial cells and has been shown to contribute to endothelial cell permeability through its sensing and responding to oxidative stress for example through the generation of reactive oxygen species such as hydrogen peroxide (Hecquet et al., 2008). However, TRPM2 not only acts as a cellular redox sensor but also uniquely behaves as an enzyme, via a region with homology with the ADP-ribose pyrophosphatase NUDT9 at its C terminus (Perraud et al., 2001). When ADP-ribose binds to this region, TRPM2 becomes activated, but the enzymatic function of TRPM2 remains to be determined. For this reason, TRPM2 is sometimes referred to as a 'chanzyme' due to its potential dual roles as an ion channel and an enzyme.

Store-operated Ca^{2+} entry (SOCE) channels

The first evidence for SOCE came from Casteels and Droogmans in 1981 (Casteels and Droogmans, 1981), but it was Jim Putney in 1986 who coined the term 'capacitiative calcium entry'. This was following experiments which showed that Ca^{2+} entry triggered by muscarinic receptor agonists was more closely linked to the emptiness of the ER Ca^{2+} store than to increases in IP$_3$ or occupation of the muscarinic receptor (Putney, 1986). Today, SOCE is recognised as a major pathway in nearly all animal cells, both excitable and non-excitable, and the defining feature of SOCE channels is their activation by the reduction of Ca^{2+} concentration in the lumen of the ER rather than by receptor-associated signalling molecules such as G-proteins, PLC or IP$_3$ (Lewis, 2011, Park et al., 2009). Physiologically, this often occurs when phospholipase-C (PLC) coupled receptors in the plasma membrane become activated which leads to the production of inositol 1,4,5-triphosphate (IP$_3$), and the activation of IP$_3$ receptors on the ER membrane, causing release of Ca^{2+} from stores (Lewis, 2011).

Identifying the molecular nature of SOCE channels has been the subject of much research over the last 25 years. The development of fluorescent Ca^{2+} indicator dyes such as Fura-2 (Grynkiewicz et al., 1985) and the identification of sarcoendoplasmic reticulum Ca^{2+}-ATPase (SERCA) inhibitors (that have the

ability to deplete ER Ca^{2+} stores independently of receptors and IP_3) such as thapsigargin (Thastrup et al., 1989) have had a significant positive impact on determining the molecular make-up of these channels. TRPC channels have long been associated with SOCE, however whether they are truly store-dependent is still under debate (Lewis, 2011).

In 1992 a major breakthrough was made in the search for the channel underlying SOCE. Hoth and Penner identified an inwardly-rectifying ion channel current in mast cells, activated during whole-cell patch recordings either spontaneously (by Ca^{2+} chelators) or by IP_3 or ionomycin, that was highly Ca^{2+}-selective. They called this current the 'Ca^{2+} release-activated Ca^{2+} (CRAC) current (I_{CRAC}) (Hoth and Penner, 1992). Research efforts over the subsequent 13 years led to the identification of the genes underlying I_{CRAC} and in 2005 and 2006, STIM1, the ER Ca^{2+}-sensor and Orai1, the CRAC channel protein were discovered (Zhang et al., 2005, Roos et al., 2005, Vig et al., 2006a, Vig et al., 2006b). These important discoveries have greatly advanced our understanding of the role of these channels in physiology and disease, and have created new directions for research (Lewis, 2011). In addition to Orai1, two other Orai homologues exist, Orai2 and 3, both of which also form SOCE channels (Lis et al., 2007). However the role of Orai2 and 3 in physiology and pathophysiology remains to be determined. The functions of STIM1 and Orai1 and their relevance to health and disease will be discussed in the next section.

1.5. CRAC channel composition and function

1.5.1. ER Ca^{2+} sensors: STIM1 and STIM2

Mammalian cells ubiquitously express the Ca^{2+} binding proteins STIM1 and STIM2 (Williams et al., 2001). STIM1 was originally identified as a tumour suppressor gene called GOK (Sabbioni et al., 1999) but was later identified as a molecular component of store-operated Ca^{2+} signalling through RNAi screening by two independent research groups, and is now recognised as the primary ER Ca^{2+} sensor (Liou et al., 2005, Roos et al., 2005). In addition, a close family member (STIM2, which shares 61% sequence similarity with STIM1) is also an ER Ca^{2+} sensor but has lower Ca^{2+} binding affinity compared to STIM1 and has been suggested to activate CRAC channels following mild store depletion (Thiel et al., 2013, Soboloff et al., 2012). Studies revealed that whilst STIM1 could trigger SOCE, it did not form the CRAC channel itself. It was only in the next year through genetic and RNAi studies, that Orai1 was identified as the pore forming protein of the CRAC channel. Orai1 and CRAC channel function will be discussed below. STIM1 is predominantly localised in the ER, but 20-30% is detected at the plasma membrane (Manji et al., 2000). STIM1 is an ER membrane protein with one transmembrane region (Cahalan, 2009). The amino terminal of STIM1 resides in the lumen of the ER and has a pair of low affinity EF-hands that sense ER Ca^{2+} levels (Zhang et al., 2005). This Ca^{2+} binding domain has since proven critical for STIM1 function as an ER Ca^{2+} sensor. In addition, STIM1 also contains a sterile alpha motif or SAM domain located on the ER luminal side of the protein that is important for its function, since SAM-deletion mutants are unable to form ER-PM punctae required for SOCE (Cahalan, 2009, Stathopulos et al., 2008). In the resting cell when ER Ca^{2+} stores are filled, STIM1 exists as a dimer, stabilised by C-terminal coiled-coil interactions (Penna et al., 2008).

STIM1 mRNA is widely expressed and can be found in the heart, central nervous system, skeletal muscle and platelets (Feske, 2010). Genetic ablation of the STIM1 gene is lethal and mice die perinatally due to skeletal muscle myopathy (Oh-Hora et al., 2008). In comparison, STIM2 knockout mice survive to 4-5 weeks after birth (Oh-hora et al 2008). T cells derived from STIM1 knockout mice have smaller and shorter Ca^{2+} influx responses and impaired interleukin-2 production compared to cells derived from wild-type mice (Oh-Hora et al., 2008). This is in contrast to T cells derived from STIM2 knockout mice that have relatively normal Ca^{2+} influx responses and interleukin-2 production. Despite this however, overexpression of STIM2 is unable to fully compensate for the loss of STIM1 in T cells derived from STIM1 knockout mice compared to overexpression of STIM1 (Oh-Hora et al., 2008). Ablating both STIM1 and STIM2 in mice leads to a lymphoproliferative phenotype characterised by signs of autoimmunity (Oh-Hora et al., 2008).

Studies in endothelial cells have shown that knockdown of STIM1 using short interfering RNA (siRNA) results in a smaller CRAC channel response compared to controls (Abdullaev et al., 2008).

1.5.2. CRAC channels and the Orai family of ion channels

The Orai family of ion channels comprises 3 homologues: Orai1, 2 and 3 (Feske et al., 2006). Like STIM1, the Orai family (named after the Greek keepers of Heaven's gate and also known as CRACM channels), was discovered in RNAi based screens, and was found to include the molecular components that form the CRAC channel. At the same time a linkage analysis study in patients with severe combined immune deficiency (SCID, which is caused by a defect in Ca^{2+} entry of T cells), identified Orai1 (also called CRACM1 or TMEM142a), suggesting a role for the Orai1 gene product in SOCE (Feske et al., 2006). Importantly, in T cells obtained from SCID patients, a SOCE response could be restored by overexpression of Orai1. The SOCE defect in SCID patients was subsequently found to be due to a mutation (encoding the amino acid change

R91W) in the Orai1 gene on chromosome 12, highlighting the importance of this gene in the immune system. Further studies clarified Orai1 was an ion channel by demonstrating that the R91W mutation could significantly affect ion selectivity (Feske et al., 2006, Prakriya et al., 2006, Vig et al., 2006b, Yeromin et al., 2006). Orai proteins have no sequence homology with other Ca^{2+} permeable ion channels, and therefore represent a structurally unique family of ion channels (Rothberg et al., 2013).

A key characteristic of CRAC channels is their high selectivity for Ca^{2+} over monovalent ions (PCa/PNa > 1000) (Yamashita et al., 2007), which renders them functionally unique (Rothberg et al., 2013). Biophysically, CRAC channels are highly Ca^{2+} selective ion channels producing inwardly-rectifying currents with a calculated single channel conductance of <1 pS (Parekh and Putney, 2005). The CRAC channel current can be blocked by micromolar La^{3+} and 2-aminoethoxydiphenyl borate (2-APB) (Parekh and Putney, 2005). Other blockers of the current include the non-selective Ca^{2+} channel blocker SKF96365, a 3,5-trifluoromethyl pyrazole derivative BTP2 (YM-58483) and a structurally similar compound Synta 66 (3-fluoropyridine-4-carboxylic acid (2′,5′-dimethoxybiphenyl-4-yl)amide) which blocks I_{CRAC} with an IC_{50} of approximately 3 μM in immune cells, and with 100-fold greater potentcy in ECs with an IC_{50} of approximately 25 nM (Li et al., 2011, Parekh, 2010).

Sequence analysis predicts that Orai1 has four transmembrane helices (M1 to M4; Figure 1-6) and multiple studies have indicated that Orai1 channels are multimers, with most studies predicting a tetrameric configuration (Ji et al., 2008, Penna et al., 2008, Zhou et al., 2010). However the crystal structure of a large component of the *Drosophila melanogaster* Orai channel has been solved (Hou et al., 2012), revealing an unexpected hexameric assembly of Orai proteins (Hou et al., 2012). This structure shares 73% sequence similarity with the human version within its transmembrane region (Hou et al., 2012). Figure 1-7 shows the newly solved crystal structure of *d*Orai.

Orai1 knockout mice are smaller than their wild-type litter-mates and have eyelid irritation and sporadic hair loss (Gwack et al., 2008). Despite T cells

developing normally in the Orai1 knockout mouse, their function is impaired (Gwack et al., 2008).

In endothelial cells, knockdown of Orai1 using siRNA resulted in smaller store-operated Ca^{2+} responses and an inhibition of VEGF-mediated Ca^{2+} signalling and endothelial cell tube formation (Abdullaev et al., 2008, Li et al., 2011).

Both Orai2 and Orai3 are also able to complex with STIM1 and form Ca^{2+} channels (DeHaven et al., 2007, Lis et al., 2007). The Ca^{2+} channels involving Orai2 and Orai3 have similar biophysical properties to those involving Orai1, but differ in their activation and inactivation kinetics. For example, Ca^{2+} entry via Orai3 channels is potentiated by 2-APB, which is the opposite of the effect seen on Orai1 channels (Lis et al., 2007). Despite these similarities, it has been shown that Orai2 is unable to compensate for the loss of Orai1 in T cells derived from SCID patients, and overexpression of Orai3 is only able to partially compensate (Gwack et al 2007).

There is little information regarding the physiological role of Orai2 or Orai3 channels in endothelial cells however in smooth muscle cells Orai3 knockdown *in vivo* inhibited neointimal formation (Gonzalez-Cobos et al., 2013). Orai3 also underlies SOCE in estrogen receptor positive breast cancer cells compated to estrogen receptor negative cells where Orai1 underlies the SOCE response (Motiani et al., 2013).

Orai3 is also suggested to complex with Orai1 to form arachidonic-acid activated channels, and these channels have been shown to function in a store-independent manner (Mignen and Shuttleworth, 2000, Mignen et al., 2008). Both Orai1 and Orai3 are expressed on ECs but the existence or physiological relevance of the Arc channel remains to be determined.
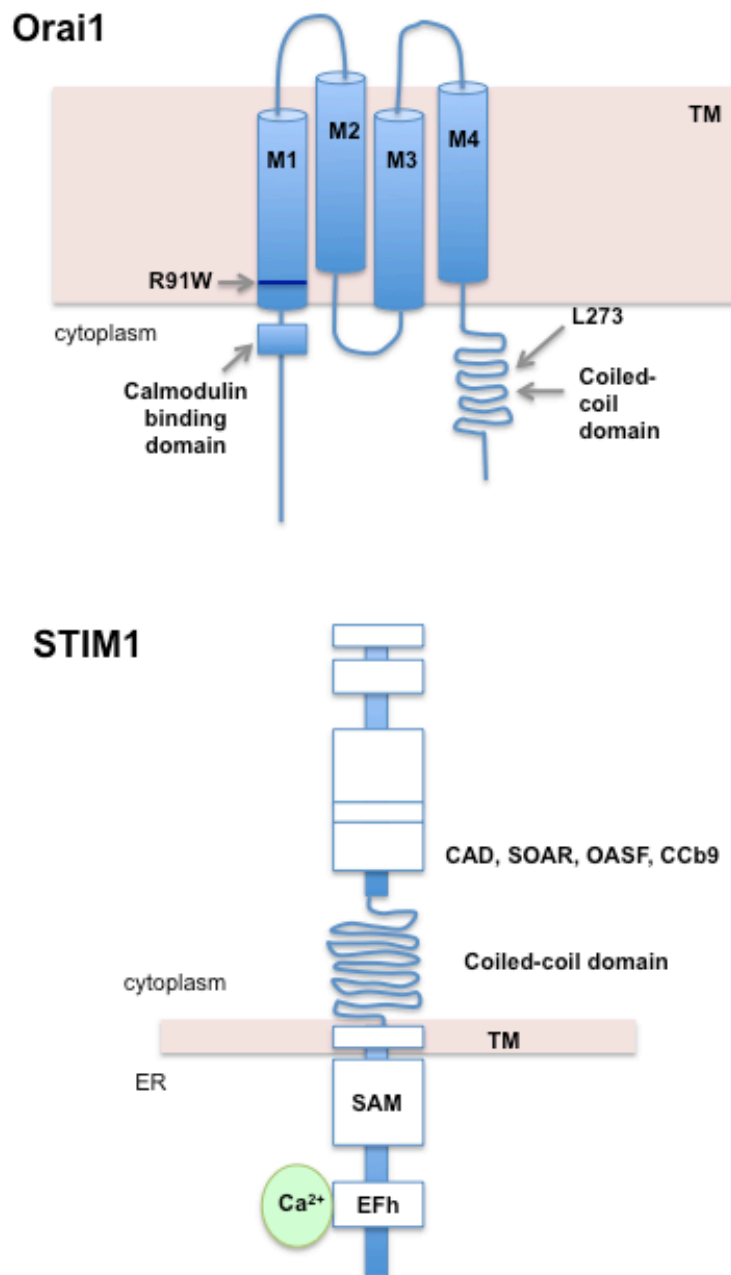
Figure 1-6 Functional domains in Orai1 and STIM1.

Orai1 comprises 4 transmembrane domains M1-M4. The M1 transmembrane helix lines the channel pore. Orai1 has a calmodulin binding site on the cytoplasmic side. L273 is a region important for STIM1 binding. The R91W mutation is shown and is important for Orai1 function. STIM1 has an N-terminus that resides in the ER and contains 2 EF-hand domains responsible for Ca^{2+} binding. STIM1 also contains a sterile alpha motif (SAM) located in the ER. The CAD/SOAR/OASF/CCb9 region, which is important for Orai1 binding is located in the cytoplasm. Adapted from Feske (2010).
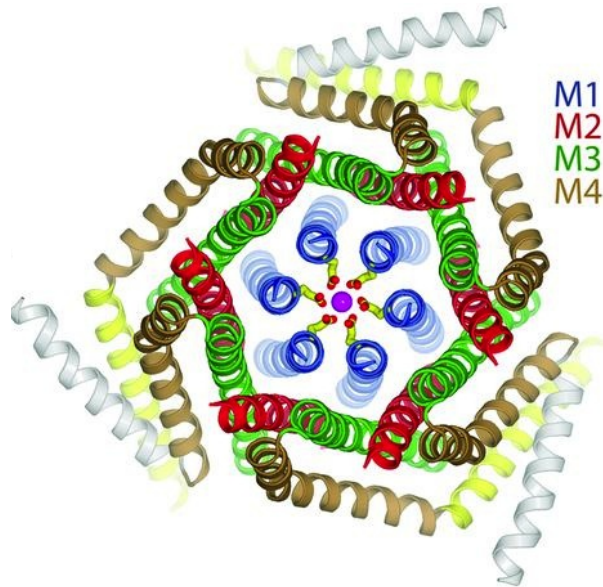
Figure 1-7 The structure of the Orai1 channel hexamer.

View from the extracellular side showing the four transmembrane helices of each of the Orai1 subunits (M1-M4) with the M1 helices lining the channel pore (Hou et al., 2012). Reprinted with permission from AAAS.

1.5.3. Orai1, STIM1 and CRAC channel function

During resting conditions STIM1 binds to Ca^{2+} via its EF-hands that lie in the ER lumen, and Orai1 resides in the plasma membrane (Hogan et al., 2010). When cells become stimulated in such a way that IP_3 is increased, IP_3 interacts with IP_3 receptors on the ER membrane allowing Ca^{2+} release. This Ca^{2+} release is detected by STIM1 through its EF hands. Depletion of Ca^{2+} from the ER causes Ca^{2+} to dissociate from the EF hands (Hogan et al., 2010). It is the dissociation of Ca^{2+} that causes a conformational change in STIM1 by unfolding the adjacent EF-SAM domains, allowing it to oligomerise (Liou et al., 2005, Muik et al., 2008, Stathopulos et al., 2006). STIM1 dimers translocate to regions of the ER membrane that are in close association with the plasma membrane (10-25 nm) forming large aggregates or 'puncta' (Wu et al., 2006). In response to this movement, Orai1 accumulates in these ER-PM junctions where it can interact with STIM1 (Luik et al., 2006, Muik et al., 2008, Park et al., 2009, Xu et al., 2006, Yuan et al., 2009, Kawasaki et al., 2009) The recent breakthrough with the crystal structure of *Drosophila* Orai suggests that Orai1 subunits form a hexameric assembly around a central pore lined by the M1 transmembrane helices (Hou et al., 2012, Rothberg et al., 2013). It is the clustering of Orai1 and STIM1 that allows the entry of Ca^{2+} into the cell in a process termed SOCE. Ca^{2+} that enters the cell is then used to replenish Ca^{2+} ER stores and for downstream signalling pathways. The mechanism of STIM1/Orai1 CRAC channel activation is shown schematically in Figure 1-8.

1.5.4. Regulation of CRAC channel activity

In immune T cells, 2 novel regulatory proteins of CRAC channels, called CRACR2A and junctate have been identified by protein affinity purification (Srikanth et al., 2012, Srikanth et al., 2010). CRACR2A is a cytosolic protein that has been shown to interact with both Orai1 and STIM1 to regulate Ca^{2+} entry through Orai1 channels. The role of these proteins in non-immune cells remains to be determined. Junctate is an ER-Ca^{2+}-sensing protein that has

been found to be part of the ER-PM complex made up of Orai1 and STIM1 during CRAC channel activation in immune T cells (Srikanth et al., 2012).

Also described in immune T cells is a negative regulator of CRAC channels, a protein called Golli (gene of oligodendrocyte lineage), which is an isoform of myelin basic protein (Walsh et al., 2010). Overexpression of Golli in immune cells inhibits Ca^{2+} entry through CRAC channels. Further studies are required to understand the physiological relevance of this protein.

1.5.5. Ca^{2+} channels in EC physiology and pathophysiology

The function of Orai1 and STIM1 in SOCE in ECs was first described in 2008 (Abdullaev et al., 2008). Knockdown of Orai1 and STIM1 in human umbilical vein endothelial cells (HUVECs) and in human pulmonary artery endothelial cells (HPAECs) resulted in an inhibition of EC proliferation (Abdullaev et al., 2008). Subsequent studies have identified CRAC channels as a major Ca^{2+} entry route in ECs: knockdown of Orai1 using siRNA significantly inhibited the Ca^{2+} entry and inhibited angiogenesis both *in vitro* (in the co-culture tube formation assay) and *in vivo* (in the chick chorioallantoic membrane) (Li et al., 2011). A CRAC channel blocker called Synta66 was found to also inhibit VEGF-stimulated angiogenesis, further supporting a role of CRAC channels in angiogenesis. A study by Antigny *et al* found no effect of Orai1 in *in vitro* tube formation, but found that TRPC1 and TRPC4 were important (Antigny et al., 2013).

Hamdollah Zadeh *et al* (2008) were the first to report TRPC channel involvement in the VEGF induced microvascular endothelial cell proliferation and tube formation (Hamdollah Zadeh et al., 2008). Using a dominant negative TRPC6 (DNTRPC6) lentivirus, they showed a significant inhibition of VEGF-induced human microvascular endothelial cell tube formation *in vitro*. These results were later confirmed by Ge *et al*, who demonstrated that DNTRPC6 could inhibit VEGF-induced tube formation in human umbilical vein endothelial cells (HUVECs; (Ge et al., 2009). To date there are no *in vivo* data which

support this role of TRPC6 in tumour angiogenesis, although this may be partly due to a lack of selective tools to study TRPC channels. Ge *et al* (2009), however, did demonstrate an inhibition of blood vessel growth in *in vivo* chorioallantoic membrane (CAM) using the non-selective blocker SKF 96365 that has previously been shown to block TRPC6 (Inoue et al., 2001, Ge et al., 2009).

A recent report has shown for the first time an important role for TRPC1 in angiogenesis (Yu et al., 2010). The authors showed that knockdown of TRPC1 by antisense morpholino oligonucleotides severely disrupted angiogenic sprouting of intersegmental vessels in zebrafish larvae. In addition they showed that TRPC1 acted synergistically with VEGF in controlling vessel growth, and that TRPC1 appeared to be downstream of VEGF in controlling angiogenesis. This study supports an earlier study by Jho *et al* (2005), who showed that blocking TRPC1 inhibits VEGF-induced permeability in endothelial cells (Jho et al., 2005).
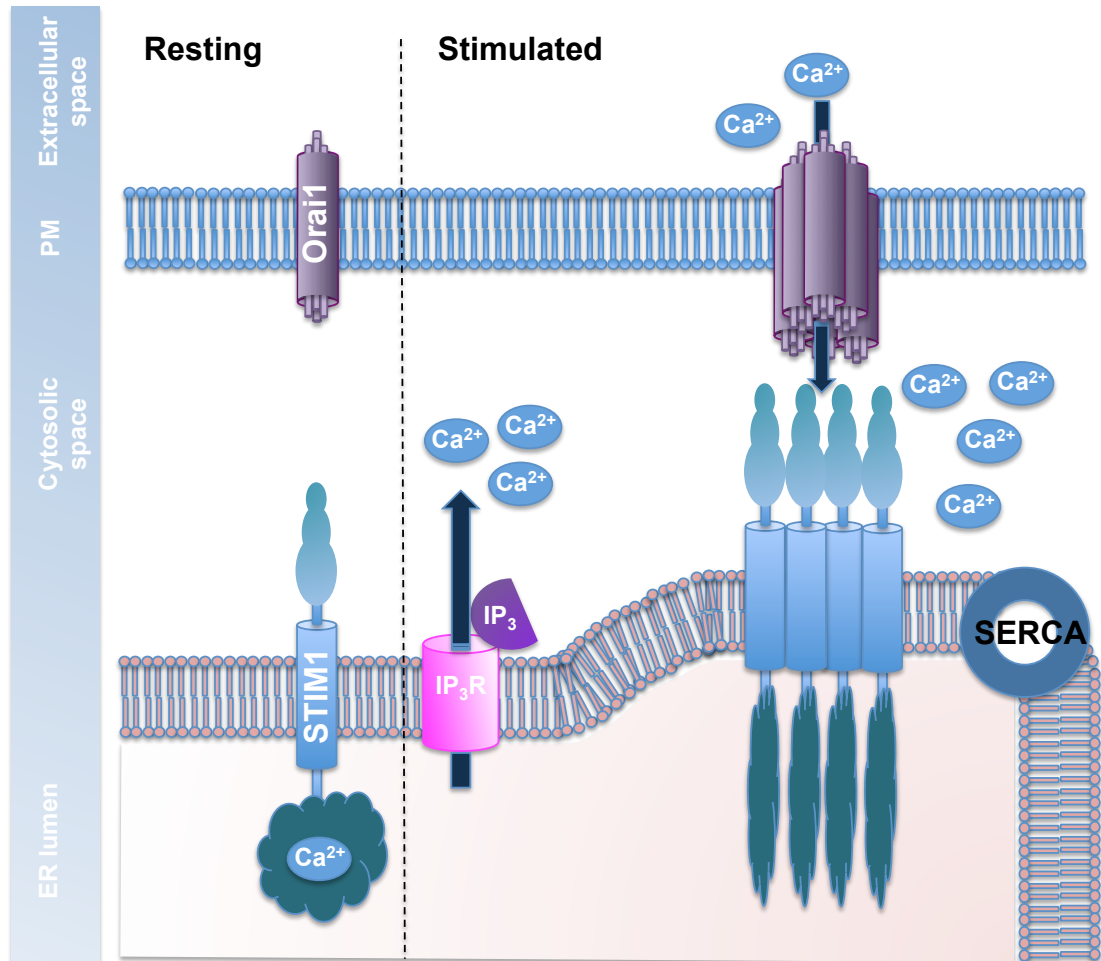
Figure 1-8 CRAC channel function.

In the resting state, STIM1 resides in the ER membrane and Orai1 subunits in the plasma membrane. When cells are stimulated, IP_3 activates IP_3Rs on the ER membrane releasing Ca^{2+}, which depletes the ER of Ca^{2+} and causes a conformational change in the STIM1 protein. STIM1 clusters at ER-PM junctions where it interacts with hexameric assemblies of Orai1 channels leading to CRAC channel activation and Ca^{2+} entry into the cell.

1.6. Downstream signalling as a result of Ca^{2+} entry

Ca^{2+} is important for both short- and long-term cellular responses. The next section will discuss recent studies linking Ca^{2+} entry through Ca^{2+} permeable ion channels with downstream signalling events: gene transcription and small GTPase activity.

1.6.1. Ca^{2+}-regulated gene transcription

Accumulating evidence suggests that Ca^{2+} entry through CRAC channels is not only important for short-term cellular responses such as exocytosis and muscle contraction but also for long-term responses such as gene transcription (Kar et al., 2012). A common mechanism for the activation of gene transcription in non-excitable cells involves Ca^{2+} entry followed by stimulation of the Ca^{2+}-calmodulin-dependent protein phosphatase calcineurin (Macian, 2005). Calcineurin dephosphorylates the highly phosphorylated nuclear factor of activated T cells (NFAT) that resides in the cytosol (Macian, 2005). This dephosphorylation exposes a nuclear localisation motif in NFAT, which causes it to be imported into the nucleus where it interacts with other transcription factors to initiate the transcription of genes such as interleukin 2 and 4 (Hogan et al., 2003, Kar et al., 2011, Parekh and Putney, 2005). It has been shown that in immune cells, CRAC channels are responsible for this Ca^{2+} entry required for NFAT activation (Parekh and Putney, 2005). Further evidence for an important role of Ca^{2+} entry through CRAC channels in NFAT translocation and transcription comes from SCID patients who carry a mutation in their *Orai1* gene; these patients fail to activate the IL-2 and and IL-4 genes (Feske et al., 2000).

NFAT activation in endothelial cells is critical for vascular development and function (Hernandez et al., 2001). VEGF activates NFATc translocation and transcription, which is important for endothelial cell migration and angiogenesis since the NFAT inhibitor cyclosporin-A inhibits these processes (Hernandez et

al., 2001). There is evidence linking Ca^{2+} entry through CRAC channels to NFAT translocation and transcription in HEK293 cells (Kar et al., 2011) which suggests this might also be true in other cell types, however there is currently no definitive study investigating this in endothelial cells. Despite this, three lines of evidence support a role for CRAC channels and NFAT activation in endothelial cells: firstly, NFAT activation is not evoked by Ca^{2+} release from the ER but involves Ca^{2+} entry via a SOCE channel (Rinne et al., 2009); secondly, Ca^{2+} entry into endothelial cells occurs via CRAC channels (Li et al., 2011); and finally VEGF, through activation of VEGFR2, causes Ca^{2+} entry through CRAC channels, which is important for cell migration and angiogenesis. An independent study shows that VEGF can activate NFATc translocation and transcription in ECs (Hernandez et al., 2001).

1.6.2. Ca^{2+} entry channels and small GTPases

The Rho family of small GTPases are important regulators of cytoskeletal dynamics in events such as cell migration, vesicle trafficking and endocytosis (Etienne-Manneville and Hall, 2002, Pertz, 2010). Members of the Rho family include cdc42 and Rac1, which have been found at the leading edge of migrating cells and are important in the formation of filopodia and lamellipodia respectively (Lamalice et al., 2007, Pertz, 2010) and RhoA, which regulates cell motility through activation of kinases such as phosphatidyinositol 3-kinase (PI3K) (Lamalice et al., 2007). Ca^{2+} is important for cell migration and it has been shown that Ca^{2+} flickers appeared at the leading edge of migrating cells, and that the stretch-activated ion channel TRPM7 was responsible for these flickers (Wei et al., 2009). A more recent study showed a direct link between Ca^{2+} influx and small GTPase activity in cell motility (Tian et al., 2010). The authors showed that TRPC5 exists in a molecular complex with Rac1, and that Ca^{2+} entry through TRPC5 channels promotes cell migration (Tian et al., 2010). Conversely, it was found that TRPC6 worked in an antagonistic manner in a complex with RhoA to inhibit cell migration.

1.7. Therapeutic targeting of Ca^{2+}

1.7.1. Ca^{2+} channel blockers

With cardiovascular disease and cancer being two of the biggest causes of death worldwide, there is a growing need to develop new drugs to treat these life-threatening conditions. Targeting intracellular Ca^{2+} is a promising therapeutic avenue to explore since Ca^{2+} channel blocking drugs have already proven successful in treating hypertension. Drugs such as verapamil and nifedipine inhibit voltage-gated Ca^{2+} channels in the heart and increase vasodilation (McDonagh et al., 2005). These drugs indicate that calcium channels represent druggable targets, and set a precedent for the development of other Ca^{2+} channel blocking drugs for other therapeutic uses.

1.7.2. Rationale for targeting Ca^{2+} permeable ion channels in cancer

It is widely accepted that Ca^{2+} is an important signalling factor in tumour progression, as it is needed for cell migration, proliferation and angiogenesis (Monteith et al., 2012). Increasing numbers of studies are showing altered expression levels of Ca^{2+} channels or pumps in cancer. A recent review provided a table of examples of ion channels and pumps that are differentially regulated in cancer (Monteith et al., 2012). In the TRPC family of non-selective Ca^{2+} channels, TRPC3 is up-regulated in breast cancer and ovarian cancer compared to healthy controls (Aydar et al., 2009, Yang et al., 2009); TRPC4 is down-regulated in renal cell carcinoma cells (Veliceasa et al., 2007) and TRPC6 was found to be the predominant Ca^{2+} channel expressed in breast cancer but was absent in normal breast tissue (Aydar et al., 2009). TRPC6 was also found elevated in specimens from oesophageal squamous cell carcinoma patients compared to normal oesophageal tissue (Shi et al., 2009). In the TRPM family, TRPM8 is up-regulated in prostate, pancreatic, breast, colorectal and lung cancers (Dhennin-Duthille et al., 2011, Schmidt et al., 2006, Tsavaler et al.,

2001, Yee et al., 2010) whilst TRPM7 is involved in pancreatic and breast cancer (Dhennin-Duthille et al., 2011, Rybarczyk et al., 2012). TRPV1 is down-regulated in bladder and up-regulated in prostate (Czifra et al., 2009, Kalogris et al., 2010) and TRPV6 in breast, prostate, thyroid, colon and ovarian cancers (Bolanz et al., 2008, Dhennin-Duthille et al., 2011, Fixemer et al., 2003). In addition both Orai1 and Orai3 are over-expressed in breast cancer (McAndrew et al., 2011, Motiani et al., 2010).

1.7.3. Targeting downstream Ca^{2+} pathways

One example of a pathway downstream of Ca^{2+} signalling that was discussed earlier was NFAT activation. In cancer, NFAT isoforms have been found to be upregulated (Jauliac et al., 2002, Mancini and Toker, 2009, Medyouf et al., 2007, Ryeom et al., 2008). It is predicted that inhibiting NFAT activation using small molecule inhibitors could suppress tumorigenesis (Mancini and Toker, 2009).

In summary, targeting Ca^{2+}, either by inhibiting Ca^{2+} entry pathways or by targeting its downstream effectors, is a potential route to develop novel therapeutics to inhibit tumour progression.

1.8. Aims and objectives

The aim of this research was to develop a better understanding of the molecular mechanisms and pharmacology of Ca^{2+} entry and its downstream signalling in endothelial cells, with the overall purpose of devising new strategies to treat major health problems such as cardiovascular disease and cancer.

Specifically, this project addressed 3 main objectives. The first objective was to investigate the novel EF-hand protein, CRACR2A. CRACR2A was identified as a binding partner for Orai1 and STIM1, and is involved in CRAC channel activity in immune T cells. Emerging evidence suggests that Orai1 and STIM1 are important in endothelial cell function, and it was therefore hypothesised that CRACR2A may also be important. RT-PCR and Western blotting will be used to investigate the expression of CRACR2A in endothelial cells and where CRACR2A is expressed, Ca^{2+} measurement and functional cell assays will be used to characterise its function.

The second objective was to investigate the expression and function of golli-MBP in endothelial cells. Golli-MBP has been identified as a novel binding partner for STIM1. It was therefore hypothesised that Golli-MBP may interact with STIM1 in endothelial cells and be an important regulator of store-operated Ca^{2+} entry. RT-PCR and Western blotting will be used to investigate the expression of golli-MBP in endothelial cells and should golli-MBP be expressed, Ca^{2+} measurement and functional cell assays will be used to characterise its function.

The final objective was to investigate the anti-cancer agent carboxyamidotriazole (CAI) as a potential TRPC6 channel inhibitor. CAI is a small molecule, Ca^{2+} influx inhibitor with anti-cancer properties. CAI has been tested in numerous clinical trials as an anti-cancer drug, but the mechanism of action remains to be determined. Several lines of evidence suggest that TRPC6 is an important Ca^{2+} channel involved in angiogenesis and cancer progression.

In this section, the hypothesis that CAI is a TRPC6 channel inhibitor is proposed. Using a recombinant mouse TRPC6 cell line, pharmacological experiments involving Ca^{2+} measurements and whole-cell voltage patch clamp will be used to determine whether CAI is a TRPC6 channel inhibitor.

CHAPTER 2. MATERIALS AND METHODS

2.1. Ionic solutions

2.1.1. Standard Bath Solution (SBS) for Ca^{2+} imaging experiments

SBS contained (mM): NaCl 130, KCl 5, $MgCl_2$ 1.2, $CaCl_2$ 1.5, D-Glucose 8, HEPES 10; Osmolarity adjusted to 290 mOsm with NaCl; pH was titrated to 7.4 with 4 M NaOH.

Ca^{2+}-free SBS was prepared by omitting $CaCl_2$.

For TRPV4 FlexStation experiments, 0.1% BSA was added to the SBS during washing and recording stages.

2.1.2. Solutions for Whole Cell Patch Clamp

For TRPC5 whole cell recordings the bath solution contained (mM): NaCl 130, KCl 5, $MgCl_2$ 1.2, $CaCl_2$ 1.5, D-Glucose 8, HEPES 10; Osmolarity was adjusted to 290 mOsm with NaCl; pH was titrated to 7.4 with 4M NaOH.

TRPC5 patch pipette solution contained (mM): EGTA 1, CsCl 135, $MgCl_2$ 2, HEPES 10, Na_2ATP 5, Na_2GTP 0.1; Osmolarity adjusted to 290 mOsm with CsCl; pH was titrated to 7.2 with 4M CsOH.

For TRPC6 whole cell recordings the bath solution contained (mM): NaCl 140, KCl 5, $MgCl_2$ 1.2, $BaCl_2$ 1, HEPES 10, D-Glucose 10; Osmolarity was adjusted to 290 mOsm with 4M NaOH; pH titrated to 7.2 with Tris Base.

TRPC6 patch pipette solution contained (mM): CsOH (monohydrate) 48, L-Glutamic acid 48, Hepes 10, Na_2ATP 1, NaCl 8, $MgCl_2$ 2, $CaCl_2$ 17, EGTA 40; Osmolarity adjusted to 300 mOsm. pH 7.2.

2.1.3. Chemicals and reagents

All general salts and solutions were purchased from Sigma along with the following chemicals: N-Methyl-D-glucamine (NMDG), gadolinium chloride, carbachol, vascular endothelial growth factor A (VEGF-A_{165}), thapsigargin, histamine, 2-aminoethoxydiphenyl borate (2-APB) and 4α-phorbol 12,13-didecanoate (4αPDD). Carboxyamidotriazole (L,651,582) was purchased from Tocris. 1-Oleoyl-2-acetyl-sn-glycerol (OAG) was purchased from Cayman Chemical.

OAG was supplied as a solution in acetonitrile. To change solvent to DMSO, the OAG was evaporated under a gentle stream of nitrogen and DMSO immediately added to make a final concentration of 50 mM. OAG aliquots were stored at -80°C.

2.2. Cell culture

2.2.1. Stably-expressing TRPC6 Human Embryonic Kidney (HEK) Cells

Stably expressing mouse TRPC6 HEK293 cells (Boulay, 2002) were maintained in Dulbecco's Modified Eagle's Medium (DMEM; Gibco) supplemented with 10% Fetal Bovine Serum (FBS) and 100 unit ml penicillin-streptomycin. The selection antibiotic G418 (0.4 mg/ml; Sigma) was used to maintain TRPC6 channel expression.

2.2.2. TRPC5-Inducible HEK Cells

A stable cell line for the tetracycline-regulated expression of full length human TRPC5 (accession number AF054568), previously developed within this laboratory (Zeng et al., 2004), was used to investigate TRPC5 function.

This cell line includes a TRPC5 expression vector that has been modified to include two tetracycline operator sequences (TetO$_2$) between the CMV promoter site and the transcription start site, and a regulator vector that constitutively expresses the tetracycline repressor protein (TR). In the absence of tetracycline, the TR protein binds to the TetO$_2$ sequence and inhibits the initiation of transcription of the TRPC5 gene.

24 hours prior to experiments TRPC5 expression was switched on by adding tetracycline (1 μg/ml) to the culture medium. TRPC5 cells were maintained in DMEM-F12 + Glutamax (GIBCO) supplemented with 10% FBS, 100 U/ml penicillin and 100 µg/ml streptomycin (Gibco) and the selection antibiotics (10 µg/ml blasticidin and 400 µg/ml zeocin).

2.2.3. Stably-expressing TRPV4 chinese hamster ovary (CHO) cells

Wild-type CHO cells or stably expressing human TRPV4 CHO K1 cells were maintained in Hams F12 glutamax medium (Gibco) supplemented with 10% FBS and 100 unit ml^{-1} penicillin-streptomycin. The selection antibiotic geneticin (G418; Sigma; 1 mg/ml) was used to maintain TRPV4 channel expression.

2.2.4. HEK-Macrophage-scavenging receptor (MSR) cells

HEK-MSR cells are a genetically engineered cell line derived from the HEK293 parent line that are more adherent than their parent HEK293 cells making them more suitable for transfection. The macrophage scavenging receptor is expressed on a pCMV.SPORT6MSR.neomycin plasmid, whose expression is controlled by the SV40 promoter. Geneticin (G418) is used routinely in the culture of HEK-MSR cells to maintain selection. Cells were maintained in

DMEM-F12 + Glutamax (GIBCO) supplemented with 10% FBS, 100 U/ml penicillin, 100 μg/ml streptomycin (Gibco) and the selection antibiotic G418 (50 μg/ml).

2.2.5. Human Umbilical Vein Endothelial Cells (HUVECs)

Pooled HUVECs were purchased from Lonza. Cells were maintained in Endothelial Growth Medium (EGM-2) supplemented with 2% Fetal Calf Serum (FCS) and growth factors (supplied as a bullet kit; Lonza). Experiments were performed on passage 2-10 cells.

2.2.6. Normal Human Dermal Fibroblasts (NHDFs)

NHDFs were purchased from Promocell and maintained in Fibroblast Growth Medium (Promocell). Experiments were performed on passage 1-12 cells.

2.2.7. Human Colonic Microvascular Endothelial Cells (HCoMECs)

HCoMECs were purchased from Sciencell and maintained in endothelial cell medium (Sciencell).

All cells were maintained in a humidified incubator gassed with 95% air and 5% CO_2.

2.3. Transfections

2.3.1. cDNA Transfection

HUVECs and MSR-HEK cells were transfected using Lipofectamine™ 2000 (Invitrogen) or FuGene HD transfection reagent (Roche) according to the manufacturer protocols.

Fugene

Briefly, 3 µl of FuGene and 1 µg of cDNA were added to 150 µl Opti-MEM medium (Gibco) and this was incubated at room temperature for 20 minutes before adding it onto 90-95% confluent cells in one well of a six well plate containing 2 ml of cell culture medium. Alternatively cells plated onto glass cover slips in a 24 well plate were transfected with 200 ng cDNA/well of a 24 well plate. Experiments were performed 24-48 hrs post-transfection.

Lipofectamine™2000

Briefly, 2 µl Lipofectamine™2000 was added to 150 µl Opti-MEM medium (Gibco) in tube 1 and 0.5 – 1 µg of cDNA was added to 150 µl Opti-MEM medium in tube 2. Tubes were incubated at room temperature for 5 minutes then tubes 1 and 2 were combined and left to incubate at room temperature for 20 minutes. The transfection mixture was added to 90-95% confluent cells in 1 well of a six well plate containing 2 ml of cell culture medium. 4-6 hours after transfection the medium was removed and fresh cell culture medium added. Alternatively, cells plated onto glass coverslips in a 24 well plate were transfected with 200 ng cDNA/well of a 24 well plate. Experiments were performed 24-48 hours post-transfection.

2.3.2. Short-interfering RNA (siRNA) transfection

HUVECs were transfected with 20 nmol/L of siRNA (Ambion) using Lipofectamine™2000. Briefly, for 1 well of a 6 well plate: 0.42 µl siRNA (stock concentration 50 µM in water) was added to 210 µl Opti-MEM in tube 1 and 4.2 µl Lipofectamine^{TM}2000 was added to 210 µl Opti-MEM in tube 2. The tubes were incubated at room temperature for 5 minutes. After this time, 200 µl of tube 1 was added to 200 µl of tube 2 and the mixture was incubated at room temperature for 20 minutes. The 400 µl transfection mixture was added to 90-95% confluent HUVECs in 1 well of a 6 well plate containing 600 µl of cell culture medium. After 4-6 hours the medium was removed and replaced with fresh cell culture medium. Experiments were performed 48-72 hours post-transfection. siRNA sequences are shown in Table 2-1. The scrambled control siRNA (sc.si) was a 19 bp scrambled sequence Lipofectamine™2000 with no

significant homology to human gene sequences (Silencer Negative Control number 1, Ambion). Knockdown efficiency was quantified by qPCR as described in section 2.9 or Western blotting as described in section 2.7.

Gene	siRNA Sequence 5' – 3'
hCRACR2A.si.1	CAACAAAUCAAAAGUGAGAtt
hCRACR2A.si.2	GGAGUUCACUACUGGAUUUtt
hGolli.si.1	GUUUCUUUAUUCAAAAGCAtt
hGolli.si.2	GAAUAGUGAAACUAACAGAtt
hOrai1.si.	GGGAAGAGGAUUUUUAUAAtt
hSTIM1.si.	CAAUUCGGCAAAACUCUGCtg

Table 2-1 List of siRNA target sequences.

Table showing siRNA target sequences used to knockdown CRACR2A, Golli, Orai1 and STIM1.

2.4. Intracellular Ca^{2+} measurement

2.4.1. Fluo-4 acetoxymethyl ester (Fluo-4 AM)

Fluo-4 is a Ca^{2+} indicator dye (Gee et al., 2000) with an acetoxymethyl moiety that confers membrane-solubility. Once inside the cell, nonspecific esterases de-esterify the compound, generating a charged and active form of fluo-4 that exhibits increased fluorescence when bound to Ca^{2+}. Fluo-4 AM is excited at 485 nm and emits at 525 nm. Fluo-4 AM was purchased from Invitrogen and made up to 1 mM in DMSO. Cells were loaded with 2 µM Fluo-4 AM in the presence of 0.01% pluronic acid (Biotium) and 2.5 mM probenecid (Sigma) in SBS for 1 hour at 37°C. Cells were washed for 30 minutes in SBS prior to FlexStation recordings.

Pluronic is a non-ionic surfactant that is used with Fluo-4 AM and Fura-2 AM to increase their aqueous solubility. Pluronic was made up as a 10% solution in water. Probenecid inhibits organic anion transporters located in the cell membrane. These transporters can prevent dyes and indicators getting across the membrane and into the cell, which contributes to poor dye loading or high background signal in FlexStation II[384] assays. Probenecid was made up fresh each day in 1M NaOH to a stock concentration of 0.5 M. The final concentration in SBS was 2.5 mM. This was titrated with concentrated HCl to pH 7.4.

2.4.2. Fura-2 acetoxymethyl ester (Fura-2 AM)

Fura-2 AM is often the preferred choice when choosing a Ca^{2+} indicator dye since it is ratiometric and has high Ca^{2+} binding affinity. Fura-2 AM is excited at 340 and 380 nm wavelengths and emits at 510 nm. Use of a ratiometric dye minimises experimental error due to uneven loading of dye, dye leakage from the cell and photobleaching (Grynkiewicz et al., 1985). Fura-2 AM (Invitrogen) was made up to 1 mM in DMSO. Cells were loaded with 2 µM Fura-2 AM in the

presence of 0.01 % pluronic acid for 1 hour at 37°C. Cells were washed for 30 minutes in SBS prior to FlexStation recordings.

2.4.3. Ca^{2+} measurements using the FlexStation II^{384}

Intracellular Ca^{2+} measurements were made using the Flexstation II^{384} (Molecular Devices). The FlexStation II^{384} is a bench-top high throughput fluorescence plate reader that has the ability to read 96 and 384 well plates. The Flexstation II^{384} has 3 drawers for tips, a cell plate and compound plate and has a built in 8-head dispenser that can be programmed to deliver compounds to the cell plate at designated time points. The Flexstation II^{384} is programmed to read across the plate, column by column. Cells were grown to 90-100% confluence in 96 well plates (for HUVECs, non-coated plates (NUNC) were used and for HEK and CHO cell experiments poly-D-lysine coated plates (Corning) were used). Cells were loaded with a Ca^{2+} indicator dye for 1 hour at 37°C, washed and placed in the lower drawer of the FlexStation II^{384}. The compounds were prepared at 5x final concentration and placed in the middle drawer. The tip box was placed in the upper drawer. Experimental setup and data collection was performed using the software program Softmax® Pro 4.7.1. All experiments were performed at room temperature.

2.5. Whole cell patch clamp electrophysiology

2.5.1. Patch pipettes

Borosilicate glass capillaries with an outside diameter of 1 mm and an inside diameter of 0.58 mm (Harvard Apparatus) were pulled into patch pipettes using a PP830 vertical 2-stage pipette puller (Narishige, Tokyo, Japan). Pipette resistances were between 2 and 6 MΩ. Immediately before patching, pipettes were fire-polished. In all experiments series resistance was 5-15 MΩ. All recordings were made at room temperature, which was 21 ± 2 °C.

2.5.2. Whole cell voltage patch clamp

A silver wire electrode was coated with chloride using a battery and concentrated NaCl solution. Cells were seeded onto glass coverslips 24 hours before recording. For TRPC5, cells were induced with 1 μg/ml tetracycline. Whole cell configuration was achieved by gentle suction on the cell to obtain a gigaseal followed by a small increase in pressure to result in breakthrough. Resulting series resistances were around 5-15 MΩ. Voltage ramps of 200 ms duration spanning the voltage range of -100 to +100 mV were delivered continuously every 10s. pClamp software was used to capture data which was analysed using Clampfit and Origin 7 software (OriginLab corporation). Currents at -80 mV and +80 mV were measured before and after drug application.

Compounds were administered to the bath using a 'push-pull' syringe mechanism to ensure rapid bath exchange. To calculate the time to 90% bath exchange, recordings were made using tetracycline-induced TRPC5 cells. TRPC5 currents were activated with gadolinium and whilst keeping gadolinium constant, Na^+ in the extracellular solution was exchanged for $NMDG^+$ (Figure 2-1). $NMDG^+$ is larger than Na^+ and so does not pass through the channel resulting in a rapid inhibition of gadolinium-induced current. Figure 2-1 shows a recording where Na^+ was replaced with $NMDG^+$ 5 times repeatedly. The time to 90% bath exchange was calculated for each of the 5 repeats as shown in Fig 2-1. The mean time to 90% bath exchange for the on rate was calculated as 56 ± 7.6 s and for the off rate calculated as 31 ± 4 s.
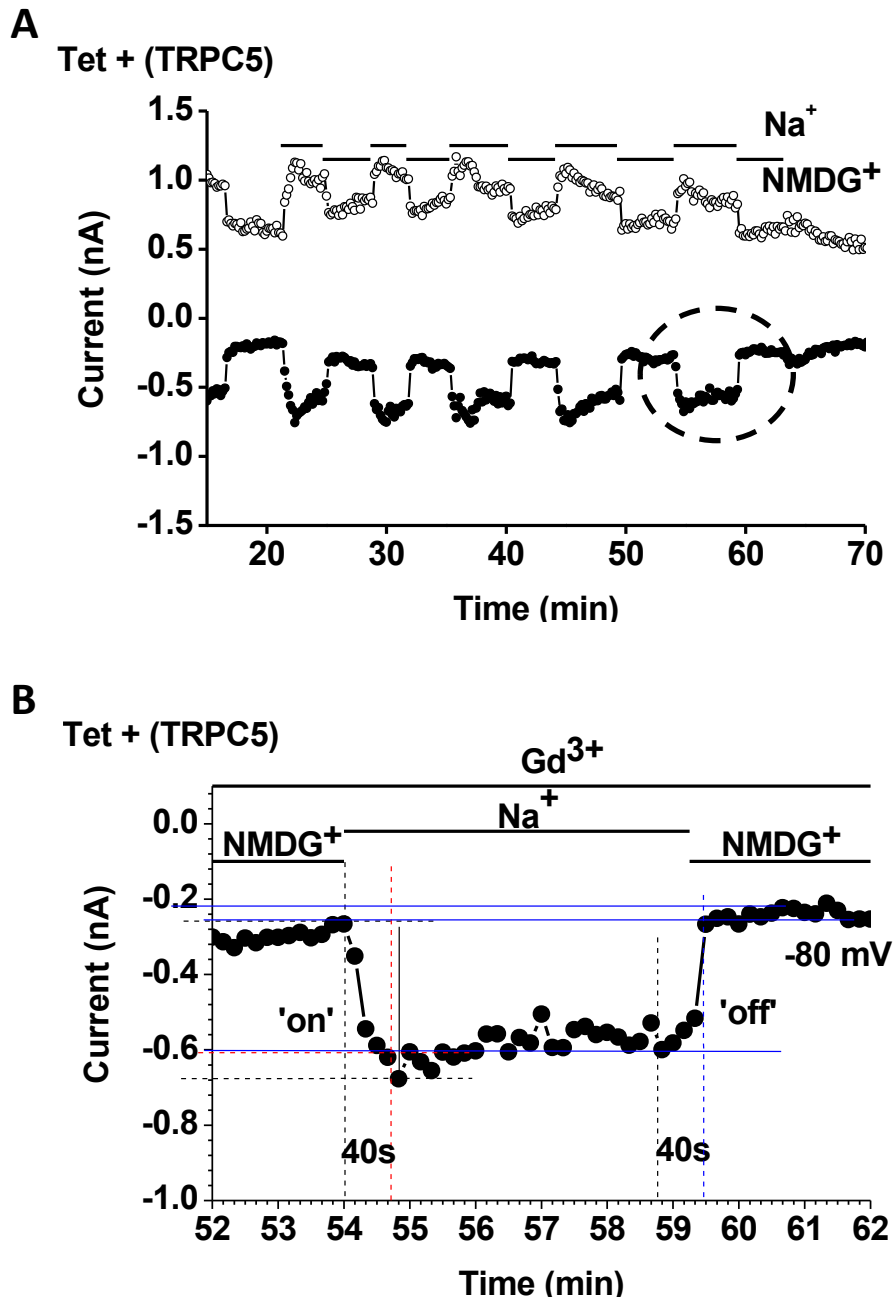
Figure 2-1 Time taken for bath exchange to occur during whole-cell voltage-clamp patch experiments.

A. Example patch clamp trace showing Gd^{3+} activated TRPC5 currents in tet + TRPC5 cells in Na^+ containing SBS followed by a switch to NMDG containing SBS. **B**. Enlargement of the highlighted region in A. Time to 90% change for 'on rate' = 56 ± 7.6 s and for 'off rate' = 31 ± 4 s (n=5 repeats).

2.6. Co-culture tube formation assay

Normal Human Dermal Fibroblasts were seeded into a 96 well plate (Greiner) at a density of 2×10^3 cells/well and incubated at 37℃ in a 5% CO_2 incubator for 72 hours. The cell culture medium was removed and HUVECs at a density of 5.4×10^4 cells/well were seeded on top of the fibroblasts in endothelial cell growth medium containing 3 ng/ml VEGF-A_{165} and 2% FBS. Co-cultures were incubated for 7 days then fixed with ice-cold methanol for 10 minutes. Non-specific binding sites were blocked with 5% donkey serum (in PBS) for 30 minutes at 37ºC. HUVEC tubes were visualised by staining with a primary monoclonal mouse anti-human CD31 antibody (1:500 in 1% donkey serum for 1 hour at room temperature). After 3 washes in PBS a secondary Alexa Fluor 488 antibody was added for 1 hour at room temperature. Plates were imaged using an IncuCyte (Essen Bioscience) and tube formation was quantified using the IncuCyte angiogenesis v2.0 software. Parameters measured included tube length, tube area and number of branching points.

2.7. Western blotting

2.7.1. Sample preparation

Cells were washed in PBS and harvested in lysis buffer containing: 0.5% NP40, 10 mM Tris (pH 7.5), 150 mM NaCl, 0.5 mM EDTA and a 1:100 protease inhibitor cocktail (Fermentas). Lysates were centrifuged at 16,000g at 4℃ for 5 minutes. The supernatant containing the soluble fraction was retained while the in-soluble fraction was discarded. For quantitative experiments, the protein concentration in each sample was measured using a detergent compatible Bio-Rad Assay (Bio-Rad Laboratories) as per the manufacturer's protocol. Protein concentrations in each sample were estimated by comparison against serial dilutions of BSA protein.

2.7.2. Sodium dodecyl sulfate polyacrylamide gel electrophoresis (SDS-PAGE)

Western blotting is a biochemical method used to detect specific protein expression in cells. SDS-PAGE separates denatured proteins by their electrophoretic mobility. SDS linearises proteins and coats them with an overall negative charge, which means that the proteins are then separated by approximate size. Reducing conditions were used to break disulphide bonds.

Equal amounts (10-20 µg) of samples were mixed with a 4x SDS running buffer (containing: 200 mM Tris-HCl pH 6.8, 8% SDS, 40% glycerol, 400 mM DTT, traces of bromophenol blue) and boiled for 5 minutes at 95°C to fully denature the proteins. Samples were loaded onto a 10% acrylamide gel alongside a protein marker (ThermoScientific) and run for 50 minutes at 170 V in running buffer, which allowed full separation of proteins in the sample. The composition of the SDS gels were as follows:

Resolving gel (10%): 4050 µl water, 3300 µl 30% acrylamide/bis-acrylamide (Sigma), 2500 µl 1.5M Tris pH 8.8, 50 µl 20% SDS, 100 µl 10% ammonium persulphate (APS), 8 µl TEMED.

Stacking gel: 4120 µl water, 1000 µl 30% acrylamide/bis-acrylamide, 750 µl 0.5M Tris pH 6.8, 60 µl 10% SDS, 100 µl 10% ammonium persulphate, 8 µl TEMED.

The separated proteins in the gel were then transferred onto PVDF membranes (Millipore) for 80 minutes at 50 mA, using a semi-dry transfer unit (BioRad). The transfer buffer contained: Tris Base 48 mM, glycine 39 mM, SDS 20%, methanol 20%.

2.7.3. Western blotting

The transferred membrane was incubated in 5% non-fat milk (in 0.1% Tween, 150 mM NaCl, 10 mM Tris, pH 7.4) for 1 hour at room temperature to block non-

specific binding sites. The membrane was then incubated either overnight at 4°C or for 1 hour at room temperature, in primary antibody diluted in 2.5% milk (For antibodies and dilutions see Table 2-2). Membranes were washed three times at room temperature in TBS-Tween, and then incubated for one hour at room temperature with secondary antibody, which was conjugated with horseradish peroxidase. Membranes were washed again in TBS-Tween (as above) and treated with Supersignal West Femto (Thermoscientific) for 5 minutes. This chemiluminescent substrate is made up of an enhancer solution and a stable peroxide solution and serves for detection of horseradish peroxidase activity. The blots were exposed to photographic paper (Kodak), developed and fixed (Photosol) to detect chemiluminescence.

2.8. Immunocytochemistry

Cells seeded onto glass coverslips were fixed with 2% paraformaldehyde (in PBS) for 10 minutes at room temperature, then permeabilised with 10% Triton-X solution for 10 minutes at room temperature. Non-specific binding sites were blocked with 5% donkey serum (in PBS) for 1 hour at room temperature. All antibodies were made up in 2.5% donkey serum and incubated at room temperature (For antibodies and dilutions see Table 2-3). Donkey serum was used since all secondary conjugated antibodies were raised in donkey. Cells were incubated in primary antibody for 1 hour followed by three washes in PBS and secondary antibodies for 1 hour. Cells were washed three times in PBS and briefly incubated in DAPI (nuclear stain) before being mounted onto imaging slides using Prolong Gold Anti-fade reagent (Invitrogen). Cells were imaged on either the Delta Vision microscope (Applied Precision) or confocal microscope (Zeiss). Images were prepared using Biophotonics ImageJ software (Opensource).

2.8.1. Delta Vision wide-field deconvolution microscopy

Delta vision (Applied Precision) microscopy uses white light from a mercury lamp, which is passed through an optical filter to give the correct excitation wavelength to illuminate the sample. To take an image, the sample is focused

by looking down the microscope then the upper and lower limits of the focus are set on the DV (Z-series) along with the number of images to take and how far apart the images should be (lowest is 1 µm). The DV then takes a series of images. Many of the images will be blurred. Once the images have been acquired the Delta Vision performs a restorative deconvolution or 'nearest neighbour' algorithm, which means it extracts information out of the blurred regions of an image in order to clean it up. The filter sets used were DAPI (excitation 360/40 and emission 457/50); FITC/GFP/Cy2 (excitation 490/20 and emission 528/38) and TRITC/Rhodamine/Cy3/DsRed (excitation 555/28 and emission 617/73). The objectives used were 40x/1.35 Oil Iris and 60x/1.4 Oil. Image acquisition and analysis was performed using SoftWoRx software.

2.8.2. Confocal laser scanning microscopy

Images were taken on a Zeiss laser scanning (LSM510) META Inverted confocal microscope, which was controlled using Zen 2009 imaging software. Confocal laser scanning microscopy uses point illumination and a spatial pinhole to get rid of out-of-focus light in a sample this in contrast to conventional wide-field microscopy that uses either a mercury or xenon lamp to flood the entire sample with light resulting in background blur. Since only a single point in the sample is illuminated during confocal microscopy, scanning over a regular raster is required. Confocal microscopy takes thin optical sections between 0.5-1.5 µm thick. The objectives used were the 40x/1.3 Oil Plan-Neofluar and the 63x/1.4 Oil Plan-Apochromat. The lasers used were the 405 nm Diode lase; Argon/2 (458, 477, 488, 514 nm); HeNe 543 nm and HeNe 633 nm. Figure 2-2 is a schematic illustrating the principle of confocal laser scanning microscopy.
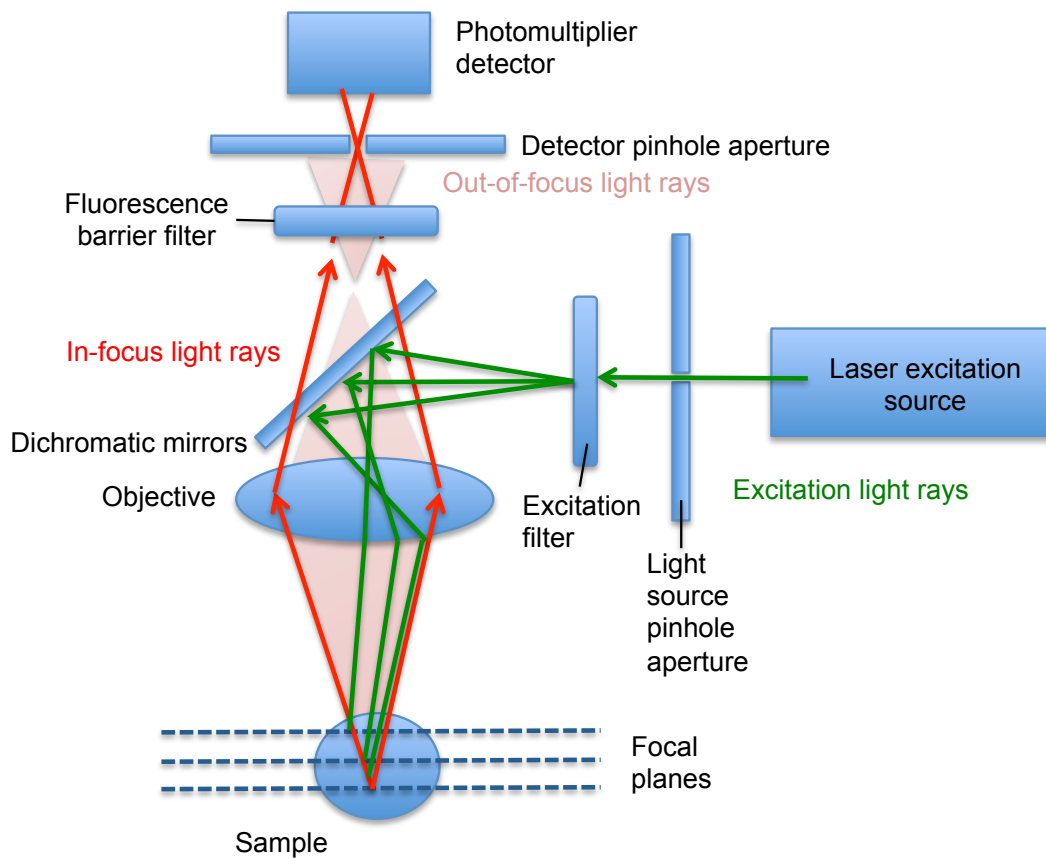
Figure 2-2 Laser scanning confocal microscopy.

The diagram shows the set-up of a confocal microscope. Adapted from http://www.olympusmicro.com.

54

Table 2-2 List of antibodies used for Western blotting.

Primary Antibody	Host species	Working dilution	Supplier	Order code	Secondary Antibody	Working dilution	Supplier	Order Code
Anti-human KDR	goat	1:1000	R&D systems	AF357	Peroxidase-conjugated AffiniPure Donkey Anti-Goat IgG (H+L)	1:20000	Jackson Immuno Research Labs	705-035-003
Anti-human EFCAB4B (polyclonal)	rabbit	1:800	Source Bioscience Lifesciences	15206-1-AP	Peroxidase-conjugated AffiniPure Donkey Anti-Rabbit IgG (H+L)	1:10000	Jackson Immuno Research Labs	711-035-152
Anti-human β actin (C4)	mouse	1:2000	Santa Cruz Biotechnology	Sc-47778	Peroxidase-conjugated AffiniPure goat Anti-mouse IgG (H+L)	1:20000	Jackson Immuno Research Labs	115-035-003
Anti-human vWF	mouse	1:800	DAKO	MO616				

Table showing the primary and secondary antibodies used for Western blotting, working dilutions and supplier details. The antigen used to raise the anti-EFCAB4B antibody was the full length (395 amino acid) CRACR2A protein.

Table 2-3 List of antibodies used for ICC and for staining co-culture assays.

	Primary Antibody	Host species	Working dilution	Supplier	Order code	Secondary Antibody	Working dilution	Supplier	Order Code
ICC	Anti-human EFCAB4B (polyclonal)	rabbit	1:50-1:200	Source Bioscience Lifesciences	15206-1-AP	Alexa Fluor® 488-AffiniPure Donkey Anti-Rabbit IgG (H+L)	1:300	Jackson Immuno Research Labs	711-545-152
	Anti-human GM130	mouse	1:50	BD Transduction Laboratories	610822	DyLight™594-conjugated AffiniPure donkey anti-mouse IgG (H+L)	1:300	Jackson Immuno Research Labs	715-515-150
	Anti-human vWF	mouse	1:100	DAKO	MO616				
Co-culture	Anti-human CD31	mouse	1:500	DAKO	MO823	Alexa Fluor® 488-AffiniPure Donkey Anti-Rabbit IgG (H+L)	1:300	Jackson Immuno Research Labs	711-545-152

Table showing the primary and secondary antibodies used for ICC (immunocytochemistry) and for staining co-culture assays.

2.9. RNA isolation, cDNA preparation and real-time polymerase chain reaction (PCR)

2.9.1. RNA isolation

HUVECs were grown to confluence in six well tissue culture plates and total RNA was extracted from HUVECs using a standard TRI-reagent protocol: briefly, medium was removed and the cells were washed twice with phosphate buffered saline (PBS). 1 ml TRI reagent (Sigma) was added to each well for 1 minute, and the cell suspension was carefully transferred to a 1.5 ml eppendorf tube then placed immediately on ice. Phenol and guanidine thiocyanate in Tri-reagent quickly lyse the cells and inactivate endogenous RNases. 12.5 μl Glycogen (Roche) was added to bind the RNA, and the mixture was vortexed thoroughly. 100 μl 1-bromo-3-chloro-propane (BCP) was then added, and the mixture vortexed once more before being left at room temperature for 15 minutes. Tubes were centrifuged at 13, 000 rpm at 4°C for 15 minutes, which separated the RNA (found in the top aqueous layer) from the DNA (in the middle layer) and the protein (bottom layer). The RNA was carefully separated from the DNA and protein and an equal volume of ice-chilled isopropanol was added in order to precipitate the RNA. This was vortexed again and left on ice for 15 minutes. Meanwhile, fresh 75% ethanol was made up in RNase free water. Following the 15 minute incubation, tubes were centrifuged at 13,000 rpm at 4°C for 20 minutes. The isoproponol was decanted and all residual isoproponol was removed from the pellet using a pipette. Each pellet was washed in 750 μl of 75% ethanol and centrifuged at 13,000 rpm at 4°C for 5 minutes. Supernatants were removed and the pellets were left to air dry for 5 minutes. Each pellet was resuspended in 10 μl of RNase free water and left on ice ready for DNase I digestion.

2.9.2. DNase I Digestion

To 10 µl of RNA solution, 1.3 µl of 10x DNase buffer (Ambion) and 3 µl of DNase I enzyme (Ambion) were added. This was incubated for 1 hour at 37°C. This was spun down using a bench-top centrifuge and 3 µl of Inactivation Reagent (Ambion) was added to pellet the DNA. This was gently mixed and left on ice for 2 minutes then bench-centrifuged again for 1 minute and supernatants containing the RNA were removed to fresh tubes.

2.9.3. Ribogreen Assay

The RNA concentration in each sample was measured using Ribogreen assay. Ribogreen is a dye that fluoresces upon nucleic acid binding. It is excited at 470 nm of light and emits light at 530 nm when it is nucleic acid bound. The Ribogreen assay gives an absorbance reading that can be converted into a concentration of RNA in a sample. A 1:200 dilution of Ribogreen solution and a 1:100 dilution of RNA solution were prepared in a 1x Tris-EDTA buffer. 10 µl of the diluted Ribogreen solution was added to 10 µl of the diluted RNA solution and loaded into glass capillaries (Roche). As a control 10 µl of Tris-EDTA buffer and 10 µl of the diluted Ribogreen solution were loaded into capillaries. Samples were mixed by centrifugation and left at room temperature for 5 minutes before fluorescence emission was measured in a real-time fluorimeter (Roche). In order to determine RNA concentrations in the samples, slope equation values from a standard curve were used. The following straight-line equation was used to determine the concentration of RNA:

Straight-line equation: $y = mx+c$, where m is the slope, c is the Y intercept, x is RNA concentration in µg/µl.

This equation rearranged to determine the RNA concentration is:

$$x = (y-c)/m$$

The m value obtained for the Ribogreen solution used in this study was 15.96. Therefore to convert the readings into RNA concentrations in μg/μl, the following equation was used:

$$x \text{ (μg/μl)} = (y - (-0.2607))/15.96 * 0.2$$

where,

y = emission of the test sample at 530 nm (background subtracted)

x = RNA concentration (μg/μl)

(multiplied by 0.2 because of the Ribogreen and RNA dilutions)

2.9.4. Reverse Transcription

To generate cDNA from the RNA samples, a high capacity RNA-to-cDNA master-mix was used (Applied Biosystems). 600 ng of RNA was reverse transcribed using 4 μl of a reverse transcription master-mix (Applied Biosystems) and a calculated volume of water to bring the total volume to 20 μl. A separate control with no reverse transcriptase ('no RT') was carried out for each reaction. The mix was incubated at 42°C for 30 minutes followed by a heat-inactivating step at 85°C for 5 minutes.

2.9.5. Real-time polymerase chain reaction (PCR)

Real-time PCR was used to quantify messenger RNA (mRNA) using the Roche Light Cycler II system and SYBR Green I (Roche). cDNA template (0.5 μl) was added to the reactions in glass capillaries containing 0.5 μM of each primer (forward and reverse; Table 2-4), 4 mM $MgCl_2$ and 1x SYBR Green I master mix (Roche, UK) to make up a final volume of 5 μl. DNA was amplified using the following protocol: 10 minute hot start at 95°C; 40 cycles of 10 seconds at 95°C, 6 seconds at 55°C, and 16 seconds at 72°C.

2.9.6. Agarose gel electrophoresis

Real time PCR products were analysed by 2% agarose gel electrophoresis. Briefly, 5 μl of PCR product was mixed with 1 μl loading buffer (Promega) and

resolved against a 100 bp DNA ladder on a 2% agarose gel containing 0.5 mg/ml ethidium bromide. Ethidium bromide intercalates between DNA base-pairs and allows DNA bands to be visualised under UV light. Electrophoresis was performed at 70 V for 70 minutes in a 1x TAE buffer.

2.9.7. Quantification of siRNA knockdown

Real time PCR crossing point (CP) values were used to determine the % gene knockdown achieved following siRNA transfection. The fold difference in gene expression in siRNA (target gene) treated versus scrambled siRNA treated cells, was determined using the following formula:

$$\text{Fold Difference} = 2^{-\Delta CP}$$

Where ΔCP is the difference in the crossing point values between test and control samples (i.e. CP in test sample - CP in control sample).

Target gene expression was normalised to actin.

2.9.8. Primer design

Real-time PCR primers were designed using Lightcycler Probe Design Software (Roche). Primers used in this study are shown in Table 2-4.

Gene (accession no.)	Primer 5' – 3'	Predicted amplicon (bp)
CRACR2A & EFCAB4B-a	**F** GAGATGGAACAACAAATCAAAAG **R** CGCTGTAGACTCTCCGT	365
EFCAB4B-a (NM_001144958.1)	**F** CGTCATGTACGATCTCAC **R** GTGACCAGAGTAGGCG	214
CRACR2A (NM_032680.3)	**F** GGTCATCCTTGCCTACG **R** GCTCGCATGAGATCAAGT	222
Orai1 (NM_032790.3)	**F** GCACAATCTCAACTCGG **R** GCGAAGACGATAAAGATCAG	300
βactin (NM_001101.3)	**F** TCGAGCAAGAGATGGC **R** TGAAGGTAGTTTCGTTGGATG	194
STIM1 (NM_001277961.1)	**F** CTCTCTTGACTCGCCA **R** GCTTAGCAAGGTTGATCT	276

Table 2-4 List of RT-PCR primers used in this study.

Table showing primers for CRACR2A and EFCAB4B-a (detects both isoforms), EFCAB4B-a, CRACR2A, Orai1, β actin, and STIM1 along with their predicted amplicon size (bp). F, forward; R, reverse.

2.10. Cloning EFCAB4B-a

2.10.1. Generation of EFCAB4B-a-enriched cDNA using an EFCAB4B-a-specific primer

Reverse transcription of HUVEC total RNA (isolated as per above protocol) was performed using Superscript II Reverse Transcriptase (Invitrogen) and an EFCAB4B-a gene specific primer (GSP; Crac2rainsertR; Table 2-5) following the manufacturers guidelines. Briefly, 2 pmoles EFCAB4B-a GSP was added to 600 ng HUVEC RNA, 2 µl dNTP mix (Promega) in a final volume of 50 µl. The mixture was heated to 65°C for 5 minutes and quickly chilled on ice. Reaction buffer was added to the mixture, which was then heated to 42°C for 2 minutes. 200 units of Superscript II enzyme was then added followed by incubation at 42°C for 50 minutes. The reaction was inactivated at 70°C for 15 minutes. DNA concentration was measured at 260 nm wavelength on a spectrophotometer.

2.10.2. Amplification of EFCAB4B-a

EFCAB4B-a was amplified from the enriched cDNA (described above) using GoTaq Green (Promega) and cloning primers (Crac2rainsertF and Crac2rainsertR; Table 2-5) designed to be compatible with the Infusion-HD vector (Clontech). PCR reaction conditions were as follows: 95ºC for 2 minutes (initial denaturation stage) followed by 40 cycles of: 95ºC for 30 seconds, 53ºC for 30 seconds, 73ºC for 2.5 minutes followed by a final extension at 73ºC for 5 minutes.

The resulting PCR product was resolved on a 1% agarose gel (at 80 V for 1 hour; Figure 2-3) then excised and the DNA was extracted using a Zymoclean™Gel DNA Recovery Kit (Zymo Research). The extracted DNA was sequenced and confirmed to be EFCAB4B-a (NM_001144958.1) before being further amplified by a second round of PCR using the high fidelity DNA polymerase Phusion (Thermoscientific).

2.10.3. Linearising the eGFP-C1 plasmid by inverse PCR

The aim was to make constructs expressing either untagged EFCAB4B-a or GFP-EFCAB4B-a fusion. To generate these constructs the eGFP-C1 plasmid (kanamycin resistant; Clontech; 4731 bp) was used, with inverse PCR to delete the GFP portion of the plasmid as needed.

2.10.4. Linearisation of plasmid with deletion of eGFP:

To make the plasmid expressing EFCAB4B-a alone, the 798 bp eGFP sequence was removed from the eGFP-C1 plasmid by inverse PCR using the DNA polymerase Phusion and inverse PCR using primers designed so that the forward primer (eGFP2Inverse-F) started at the 3' end of the GFP sequence and the reverse primer (eGFP2-Inverse-R) at the 5' end of the GFP sequence, meaning that only the vector backbone (minus eGFP) was amplified. The reaction contained: 0.5 µl eGFP-C1 cDNA, 1 µl dNTPs, 3 µl DMSO, 1 µl forward primer, 1 µl reverse primer, 0.5 µl Phusion, 10 µl Phusion reaction buffer and 34 µl water. The PCR reaction conditions were: initial denaturation at 98°C for 1 minute followed by 25 cycles of: 98°C for 30 seconds, 59°C for 30 seconds and 72°C for 2.5 minutes followed by a 5 minute extension step at 72°C. The PCR product was resolved on a 1% agarose gel, the band was excised and the DNA extracted using the Zymoclean™Gel DNA Recovery Kit.

2.10.5. Linearisation of plasmid without deletion of eGFP

To make the plasmid expressing N-terminal eGFP-tagged EFCAB4B-a, primers eGFP2Inverse-R and GFPinverse-R were designed to linearise the eGFP-C1 plasmid whilst retaining the eGFP gene. The EFCAB4B-a primers were CRACR2AsGFPF and CRAC2rainsertR (Table 2-5).

2.10.6. Infusion reaction to generate eGFP- EFCAB4B-a plasmids

The small overhangs on the EFCAB4B-a primers were used to combine the EFCAB4B-a PCR product with the eGFP-C1 vector backbone using an In-Fusion HD (Clontech) reaction. The Infusion reaction is a ligation independent cloning method. The Infusion enzyme has 3'-5' exonuclease activity and attacks exposed ends of broken double stranded DNA resulting in single stranded stretches of the vector and EFCAB4B-a insert allowing complementary pairing during the Infusion reaction. For this reaction 4 µl 5x Infusion HD enzyme premix (Clontech), 8 µl linearised eGFP-C1 vector, 4 µl EFCAB4B-a product and 4 µl water were mixed and incubated at 50°C for 15 minutes.

2.10.7. Transformation

XL10 Gold ultracompetent cells (Agilent Technologies) were used for transforming the EFCAB4B-a plasmids. Briefly, 2 µl of β-mercaptoethanol was incubated with 45 µl of cells for 10 minutes on ice 2.5 µl of the Infusion reaction mixture was added and incubated on ice for 30 minutes. The cells were then heat-shocked for 45 seconds at 42°C and put back on ice. 400 µl of LB broth was added and incubated in a 37°C shaker oven for 1 hour. 200 µl of the cell mixture was spread onto kanamycin agar plates and incubated overnight at 37°C.

2.10.8. Colony PCR

The following day, colony PCR was performed to identify clones containing the correct insert. For this, 10 colonies were selected from each plate and mixed with 5 µl water in PCR tubes. The residual left on the tip was used to streak onto labelled kanamycin plates for subsequent culture as needed. Tubes were boiled for 5 minutes at 95°C and small volume PCR was performed using the following: 12.5 µl GoTaqGreen, 5 µl of water/colony mix, 0.5 µl of primers and 6.5 µl water; 95°C for 2 minutes followed by 40 cycles of: 95°C for 30 seconds, 53°C for 30 seconds, 73°C for 30 seconds, followed by an extension at 73°C for 5 minutes. The primers used for the colony PCR were the eGFP2 reverse primer and EFCAB4B-a forward primer. PCR products were run on a 2% agarose gel at 100

V for 30 minutes. Colonies that contained the desired insert were identified by a correct band size. The correct colonies were selected from the streaked kanamycin plate the following day and grown up using a mini-prep kit (Qiagen). The clones were then sequenced (Beckman Coulter) to verify the presence and orientation of the correct insert, and plasmid Maxi-preps (Qiagen) were prepared from verified clones. Maxi-prep DNA was fully sequenced.

2.10.9. Generation of C-terminal tagged EFCAB4B-a -GFP construct

To make the EFCAB4B-a-GFP (C-terminal tagged) construct, the EFCAB4B-a plasmid was linearised using the following primers: CRACR2ALinverseR and CRACR2ALinverseF (Table 2-5). eGFP was cloned from the eGFP-C1 vector using the following primers: GFP forward primer and GFP reverse primer (Table 2-5). eGFP was then inserted into the linearised plasmid by an Infusion reaction (as described above).

2.10.10. Cloning CRACR2A

CRACR2A (NM_032680.3) clone (clone ID 3531511) was purchased from Thermo Fisher. Inverse PCR was performed to linearise the eGFP-C1 vector. Insertion of CRACR2A into the eGFP-C1 vector was performed as above for CRACR2A- but using CRACR2A primers as shown in Table 2-5.

2.11. EFCAB4B-a mutagenesis

Site-directed mutations encoding single amino acid changes (Q604L and N658I) were introduced into the EFCAB4B-a gene using a Quikchange Lightning site-directed mutagenesis kit (Agilent technologies) according to the manufacturer's protocol. Mutagenic primers are shown in Table 2-6. Phusion DNA polymerase was used for the reaction. PCR products were treated with the enzyme Dpn1 to digest any (non-mutated) methylated DNA strands. The mutated plasmid was transformed as per the protocol above and grown up using the mini-prep kit

(Qiagen). The presence of each desired mutation was confirmed by sequencing (Beckman-Coulter).

2.12. von Willebrand factor (vWF) Enzyme-linked immunosorbent assay (ELISA)

The concentration of secreted vWF was measured using an IMUBIND ELISA kit (American Diagnostica) according to the manufacturer's protocol. This ELISA is a 'sandwich' ELISA and uses a goat polyclonal vWF antibody as the capture antibody. When samples are incubated with pre-coated test plates pre-coated with this antibody, the vWF in the sample binds to the antibody, and is subsequently detected using a second, horse-radish peroxidase (HRP)-conjugated antibody. In brief, HUVECs were seeded into 6 well plates. The following day, cells were transfected with siRNA using the protocol described above. 72 hours later, the medium was removed and cells were washed once with pre-warmed, serum- and growth factor-free endothelial medium (EGM-2, Lonza) and then incubated in 1 ml of the same pre-warmed medium for 30 minutes at 37°C and 4% CO_2. VEGF-A$_{165}$ made up in the same medium was then added to the wells and incubated for 30 minutes at 37°C and 4% CO_2. A 100 µl sample was removed for each well and diluted in the same volume of medium. Two 100 µl samples were then added to the ELISA plate and the assay was performed as per the manufacturer's protocol. The concentration of vWF in each sample was determined by comparison with a standard curve. Values obtained from wells that had no VEGF-A$_{165}$ treatment were used as controls and subtracted from the sample values so that only VEGF-stimulated release was measured.
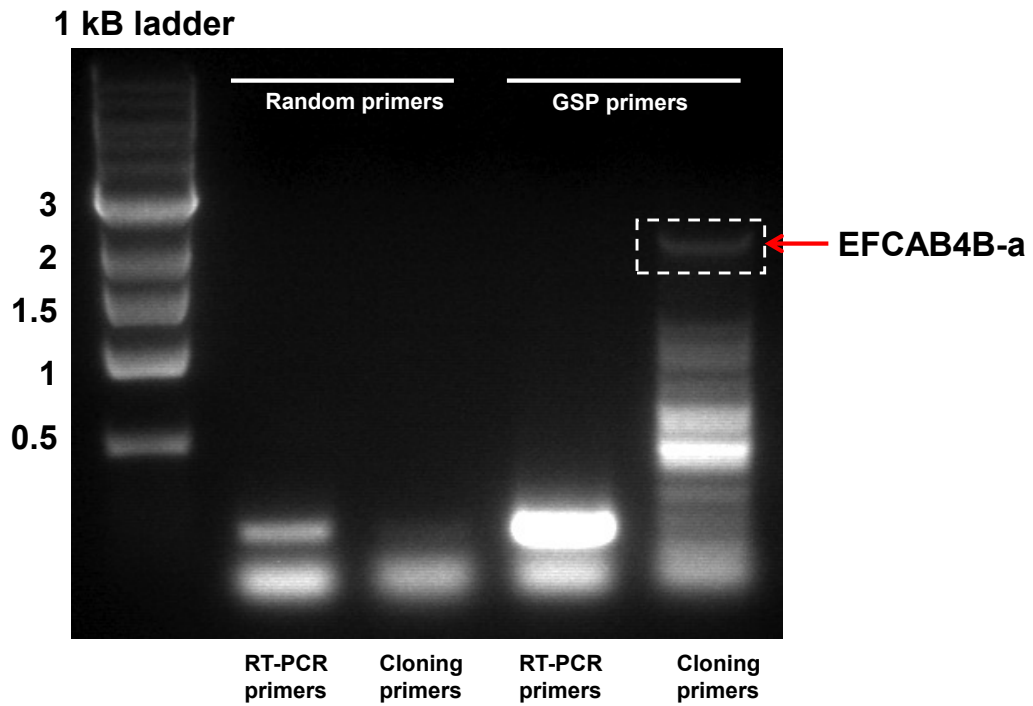
Figure 2-3 EFCAB4B-a amplified from HUVEC cDNA.

The figure shows an electrophoresis gel of EFCAB4B-a product that was amplified from EFCAB4B-a enriched HUVEC cDNA. Amplification of EFCAB4B-a was not successful from random-primed cDNA (first 2 columns). The band was excised sequenced to confirm it was EFCAB4B-a. Expected size of product: 2,795 bp.

Primer	5' – 3' sequence
EFCAB4B-a	
Crac2rainsertF	GATCCGCTAGCGCTACACCATGGCTGCCCCTGACGGG
Crac2rainsertR	GGTATGGCTGACCTTGTAGGACCCTATCA
eGFP2Inverse-F	TCAGCCATACCACATTTGTAGAGG
eGFP2Inverse-R	GTAGCGCTAGCGGATCTG
GFP- EFCAB4B-a	
eGFP2Inverse-F	TCAGCCATACCACATTTGTAGAGG
GFP Inverse-R	CGAAGCTTGAGCTCGAGAT
CRACR2AsGFP-F	GAGCTCAAGCTTCGGGTGGTATGGCTGCCCCTGAC
Crac2rainsertR	GGTATGGCTGACCTTGTAGGACCCTATCA
EFCAB4B-a-GFP	
CRACR2ALinverseR	GCCACAGCAGGATTTCTTCT
CRACR2ALinverseF	TGATAGGGTCCTACAAGGTCAG
GFP forward primer	TCCTGCTGTGGCGGTGGTGTGAGCAAGGGCGA
GFP reverse primer	TAGGACCCTATCACGAAGCTTGAGCTCG
CRACR2A	
eGFP2Inverse-F	TCAGCCATACCACATTTGTAGAGG
eGFP2Inverse-R	GTAGCGCTAGCGGATCTG
Crac2rainsertF	GATCCGCTAGCGCTACACCATGGCTGCCCCTGACGGG
CRACR2As Insert-R	GGTATGGCTGATTAGACTGGTCCTTCCGAC
GFP-CRACR2A	
eGFP2Inverse-F	TCAGCCATACCACATTTGTAGAGG
GFP Inverse-R	CGAAGCTTGAGCTCGAGAT
CRACR2AsGFP-F	GAGCTCAAGCTTCGGGTGGTATGGCTGCCCCTGAC

Table 2-5 Cloning primers.

Table showing cloning primers used in this study

Mutation	Primers (5'-3')
Q604L	**F**: TGGGACACGGCTGGGCTGGAGAGGTACCGGTGC
	R: GCACCGGTACCTCTCCAGCCCAGCCGTGTCCCA
N658I	**F**: TGTTCTTCTGCTGGGTATTAAGCTTGACAACGAG
	R: CTCGTTGTCAAGCTTAATACCCAGCAGAAGAACA

Table 2-6 List of primers for EFCAB4B-a mutagenesis.

Table showing primer sequences used to generate Q604L and N658I mutations in EFCAB4B-a. F, forward primer; R, reverse primer.

2.13. Wound assay

HUVECs were transfected with siRNA as per above protocol. Transfected cells were seeded into a 96 well Essen ImageLock plate and incubated at 37ºC/4% CO_2 overnight. A 96-pin Woundmaker (Essen) was then used as per the manufacturer's protocol to create a wound in a confluent monolayer of cells. The plate was then placed into the IncuCyte and wound images were taken every hour for up to 48 hours. The integrated IncuCyte technology calculated the Relative Wound Density, which was then used for data analysis.

2.14. Data analysis

Data were analysed and figures prepared using Origin 7.5 software (OriginLab Corporation). For FlexStation and cell migration experiments data are presented as 'n/N', which represents the 'number of independent experiments/number of individual wells used in 96-well plates across all experiments'. For patch-clamp data 'n' represents the total number of individual cells from which recordings were made. For Western blot and ELISA data 'n' represents the number of independent experiments.

Data sets were compared using two- tailed Student's *t*-tests and expressed as ± standard error of the mean (SEM). For tube formation assays the mean ± standard error of the mean (SEM) was generated for each individual experiment due to variation in tube growth between assays. A difference where $P<0.05$ was judged to be significant (*). Any difference where the P-value was greater than 0.05 was deemed not significant (n.s).

CHAPTER 3. EFCAB4B-A: A NOVEL PUTATIVE CALCIUM-REGULATED RAB PROTEIN IN ENDOTHELIAL CELLS

3.1. Introduction

Store-operated Ca^{2+} entry involving Orai1 and STIM1 is an important signalling mechanism in many cell types including immune and endothelial cells (Feske et al., 2006, Li et al., 2011). In 2010, a novel Ca^{2+} binding protein called CRACR2A (also called EFCAB4B) was identified as a binding partner for Orai1 (Srikanth et al., 2010). This came about through a study looking for novel regulators of the CRAC channel. In this study, HeLa cells stably expressing Orai1 and STIM1 were stimulated with the SERCA inhibitor thapsigargin (TG) to trigger store-depletion, and a macromolecular complex that contained putative interactors (one of which was CRACR2A) was identified through immunoaffinity purification (Srikanth et al., 2010).

CRACR2A is a cytosolic EF-hand protein (Srikanth et al., 2010). The EF-hand is one of the most common structural motifs in the human genome and constitutes a helix-loop-helix domain. EF-hand proteins bind Ca^{2+} and are important regulators of Ca^{2+} signalling events, having diverse roles ranging from the opening and closing of Ca^{2+} channels to the transduction of biochemical responses (Chazin, 2011). CRACR2A has 2 EF-hands at its N terminus and Srikanth *et al* showed that mutating the second EF-hand abolished Ca^{2+} binding. In addition, results from this study showed that the binding of Ca^{2+} to CRACR2A was important for its interaction with Orai1 in Jurkat T cells (Srikanth et al., 2010). It was found that in the absence of extracellular Ca^{2+}, CRACR2A had a strong association with Orai1 and that this was reduced in the presence of 2 mM extracellular Ca^{2+}. Figure 3-1 illustrates the role of CRACR2A in SOCE, as evidenced in Jurkat T cells and HEK293 cells. In addition, it was shown that knocking down CRACR2A with siRNA reduced Orai1 clustering - an

important mechanism involved in CRAC channel activation. Interestingly, CRACR2A could also bind to Orai2, Orai3 and STIM1. A second EF-hand protein named CRACR2B (also called EFCAB4A) that shares 36% sequence similarity with CRACR2A was also found to be an effective modulator of SOCE (Srikanth et al 2010).

Orai1 has been identified as the main ion channel underlying SOCE in endothelial cells (Li et al., 2011). The aim of this chapter was to investigate whether CRACR2A was expressed and functional in endothelial cells. RT-PCR and Western blotting was used to investigate expression of CRACR2A. Ca^{2+} imaging on HUVECs transfected with either scrambled or CRACR2A siRNA was used to address whether CRACR2A had any effect on SOCE in endothelial cells. Results from this chapter showed no expression of the CRACR2A protein in endothelial cells. However, a novel long isoform of CRACR2A that contains a putative Rab domain was discovered. This chapter reveals for the first time the expression and function of this novel putative Ca^{2+}-regulated Rab protein in endothelial cells.
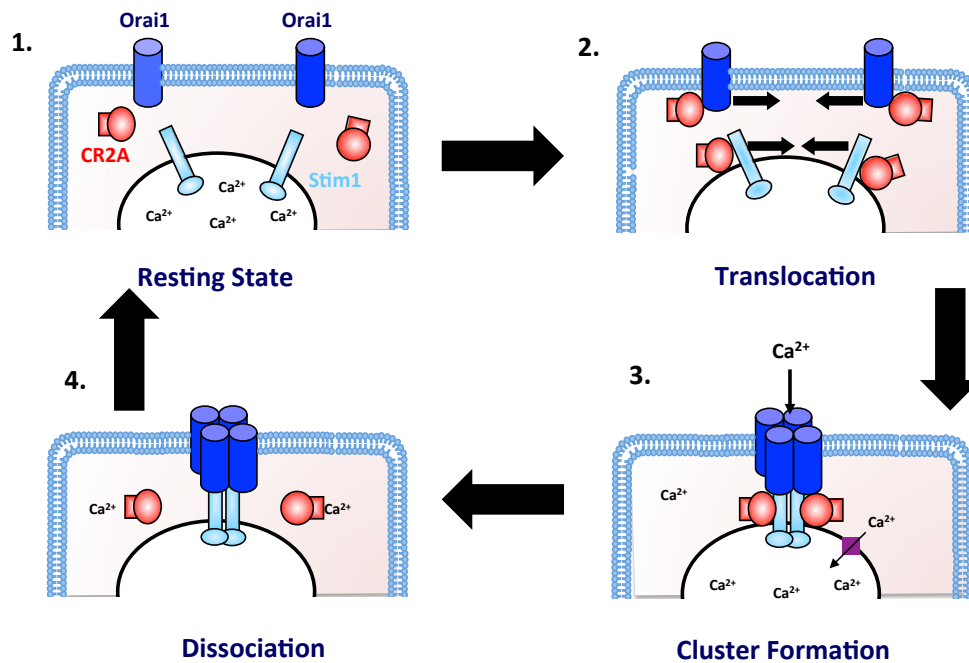
Figure 3-1 CRACR2A (CR2A) interacts with Orai1 and STIM1 and regulates Ca^{2+} entry through Orai1 channels in Jurkat T cells.

1. At rest, CR2A resides in the cytoplasm; 2. Upon release of Ca^{2+} from the endoplasmic reticulum, CR2A binds to Orai1 and STIM1; 3. Orai1 and STIM1 cluster together in a complex with CR2A and Ca^{2+} enters the cell via Orai1 channels; 4. CR2A dissociates from Orai1 and STIM1 at elevated Ca^{2+} levels returning to resting state. Adapted from Srikanth *et al* (2010).

3.2. Endothelial cells express a longer isoform of CRACR2A

First, to determine if endothelial cells expressed CRACR2A, total RNA was isolated from human umbilical vein endothelial cells (HUVECs) and reverse transcribed to generate cDNA. Real-time PCR (RT-PCR) was performed using CRACR2A primers that were designed using the LightCycler software (Roche) and products were resolved on a 2% agarose gel by electrophoresis. Since CRACR2A interacts with Orai1 and STIM1, RT-PCR was performed to confirm their expression. The gel image shows the mRNA expression of CRACR2A, Orai1 and STIM1 in HUVECs (Figure 3-2).

To determine whether CRACR2A was expressed at the protein level, Western blotting was performed using HUVEC lysate. The lysate was probed with a commercially available polyclonal anti-CRACR2A antibody (antibody details in Table 2-2). The antigen peptide used to generate the anti-CRACR2A antibody was the full length CRACR2A protein (395 amino acids). Since CRACR2A has already been detected in Jurket T cells, a Jurkat T cell lysate was used as a positive control. Surprisingly, the blots showed no expression of the 46 kDa CRACR2A protein in HUVECs compared to Jurkat T cells using a 1:400 antibody dilution and a 10 second exposure (Figure 3-3). However in both lysates the antibody detected a further 3 protein bands, one with a significantly greater abundance with an approximate molecular weight of 100 kDa (Figure 3-3). The same band could be detected using four times less lysate and a 1:800 antibody dilution, demonstrating its relatively higher abundance (Figure 3-5).

Because of this unexpected result, sequence analysis and BLAST searches were performed on the CRACR2A gene sequence. These searches revealed that the CRACR2A gene (Ensembl number: ENSG00000130038, located on humans chromosome 12p.13.32) is alternatively spliced giving rise to a possible seven predicted variants. Four of the variants are predicted to be protein coding but only two are verified and recorded in the consensus coding DNA sequence (CDS) database. These are CRACR2A, and a putative longer isoform (isoform

A; accession number NP_001138430.1) that has a predicted mass of 83 kDa. This longer isoform shares 52% sequence similarity with CRACR2A (Figure 3-4), but its expression has not been confirmed experimentally.

Therefore to determine if the larger protein detected by Western blot was the longer isoform of CRACR2A, short interfering RNA (siRNA) that targets both long and short isoforms was used to knock down gene expression. Two different siRNAs (CR2A.si.1 and CR2A.si.2) were individually transfected into HUVECs using Lipofectamine 2000™ and 72 hours post-transfection the cells were lysed and Western blotting was performed. Figure 3-5a shows that there was no expression of the 46 kDa-CRACR2A protein and that both CR2A.si.1 and CR2A.si.2 significantly reduced the amount of protein in this larger band by 80% and 95% respectively (Figure 3-5). Actin was used as a loading control to demonstrate equal protein amounts in scrambled and siRNA samples (Figure 3-5b). These data confirm that a longer isoform of CRACR2A is present in HUVECs, and from this point on the longer isoform will be referred to as EFCAB4B-a.

To further confirm that EFCAB4B-a was expressed, RT-PCR primers were designed in the C-terminal region of the EFCAB4B-a nucleotide sequence so that they were specific for EFCAB4B-a over CRACR2A. RT-PCR was performed using these primers on HUVEC cDNA. Electrophoresis gel images show that EFCAB4B-a was expressed at the mRNA level (Figure 3-6). In addition, these primers were tested on cDNA from a range of other micro- and macro-vascular endothelial cells, and the mRNA gel confirmed that EFCAB4B-a was widely expressed across a large range of endothelial cell types (Figure 3-6).
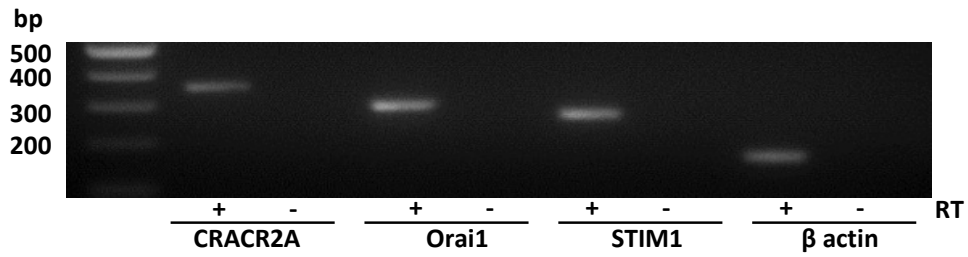
Figure 3-2 Expression of CRACR2A, Orai1 and STIM1 in HUVECs.

Gel electrophoresis showing products from RT-PCR analysis of RNA isolated from HUVECs. Reactions were performed with (+) or without (-) reverse transcriptase (RT). Expected sizes of the products were 365 bp (CRACR2A), 300 bp (Orai1) and 276 bp (STIM1), 194 bp (β actin).
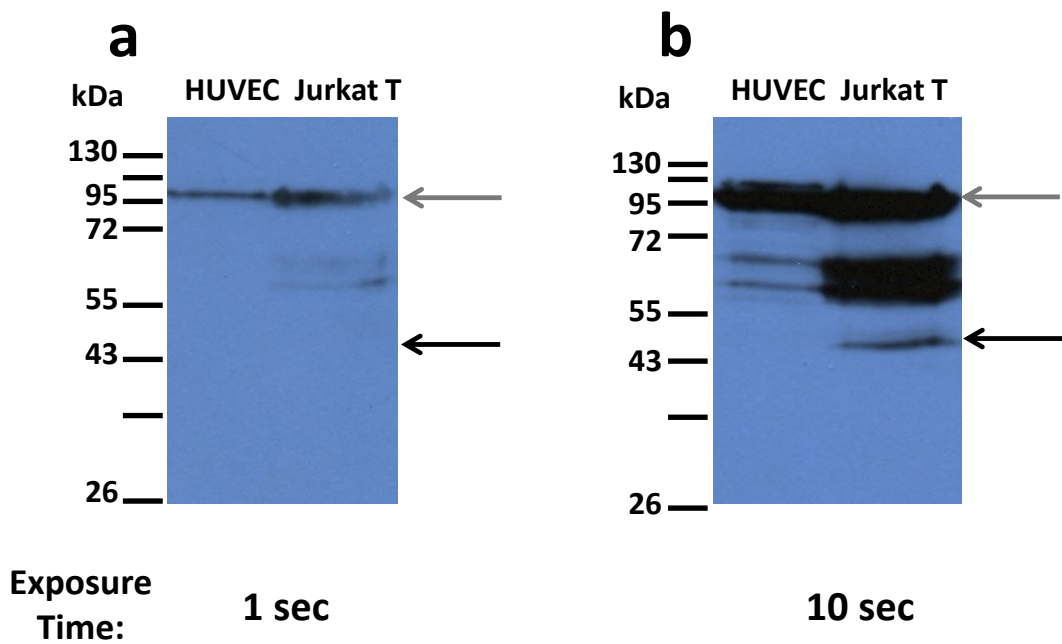
Figure 3-3 46 kDa CRACR2A is not detected in HUVECs.

Representative Western blots of whole-cell lysate from HUVECs and Jurkat T cells using an anti-CRACR2A antibody (1:400) and a 1 (**a**) and 10 (**b**) exposure times (sec) showing a band at 46 kDa corresponding to CRACR2A in Jurkat T cells but not in HUVECs (black arrows). A larger band at around 100 kDa was detected in both HUVEC and Jurkat T cell lysates (grey arrows).

```
EFCAB4Biso.c    MAAPDGRVVSRPQRLGQGSGQGPKGSGACLHPLDSLEQKETQEQTSGQLVMLRKAQEFFQ 60
EFCAB4Biso.a    MAAPDGRVVSRPQRLGQGSGQGPKGSGACLHPLDSLEQKETQEQTSGQLVMLRKAQEFFQ 60
                ************************************************************

EFCAB4Biso.c    TCDAEGKGFIARKDMQRLHKELPLSLEELEDVFDALDADGNGYLTPQEFTTGFSHFFFSQ 120
EFCAB4Biso.a    TCDAEGKGFIARKDMQRLHKELPLSLEELEDVFDALDADGNGYLTPQEFTTGFSHFFFSQ 120
                ************************************************************

EFCAB4Biso.c    NNPSQEDAGEQVAQRHEEKVYLSRGDEDLGDMGEDEEAQFRMLMDRLGAQKVLEDESDVK 180
EFCAB4Biso.a    NNPSQEDAGEQVAQRHEEKVYLSRGDEDLGDMGEDEEAQFRMLMDRLGAQKVLEDESDVK 180
                ************************************************************

EFCAB4Biso.c    QLWLQLKKEEPHLLSNFEDFLTRIISQLQEAHEEKNELECALKRKIAAYDEEIQHLYEEM 240
EFCAB4Biso.a    QLWLQLKKEEPHLLSNFEDFLTRIISQLQEAHEEKNELECALKRKIAAYDEEIQHLYEEM 240
                ************************************************************

EFCAB4Biso.c    EQQIKSEKEQFLLKDTERFQARSQELEQKLLCKEQELEQLTQKQKRLEGQCTALHHDKHE 300
EFCAB4Biso.a    EQQIKSEKEQFLLKDTERFQARSQELEQKLLCKEQELEQLTQKQKRLEGQCTALHHDKHE 300
                ************************************************************

EFCAB4Biso.c    TKAENTKLKLTNQELARELERTSWELQDAQQQLESLQQEACKLHQEKEMEVYRVTESLQR 360
EFCAB4Biso.a    TKAENTKLKLTNQELARELERTSWELQDAQQQLESLQQEACKLHQEKEMEVYRVTESLQR 360
                ************************************************************

EFCAB4Biso.c    EKAGLLKQLDFLR----------------------------------------------- 373
EFCAB4Biso.a    EKAGLLKQLDFLRERNKHLRDERDICFQKNKAAKANTAASRASWKKRSGSVIGKYVDSRG 420
                *************

EFCAB4Biso.c    ------------------------------------CVGGHWP--------------- 380
EFCAB4Biso.a    ILRSQSEEEEEVFGIPRRSSLGLSGYPLTEEEPGTGEPGPGGPYPRPLRRIISVEEDPLP 480
                                                    ** :*

EFCAB4Biso.c    ---------------------------VLRAPPRSLGSEGPV----------------- 395
EFCAB4Biso.a    QLLDGGFEQPLSKCSEEEEVSDQGVQGQIPEAPPLKLTPTSPRGQPVGKEALCKEESSPS 540
                                           : .*** .* . .*

EFCAB4Biso.c    ------------------------------------------------------------
EFCAB4Biso.a    APDRLFKIVFVGNSAVGKTSFLRRFCEDRFSPGMAATVGIDYRVKTLNVDNSQVALQLWD 600


EFCAB4Biso.c    ------------------------------------------------------------
EFCAB4Biso.a    TAGQERYRCITQQFFRKADGVIVMYDLTDKQSFLSVRRWLSSVEEAVGDRVPVLLLGNKL 660


EFCAB4Biso.c    ------------------------------------------------------------
EFCAB4Biso.a    DNEKEREVPRGLGEQLATENNLIFYECSAYSGHNTKESLLHLARFLKEQEDTVREDTIQV 720


EFCAB4Biso.c    -----------
EFCAB4Biso.a    GHPAKKKSCCG 731
```

Figure 3-4 CRACR2A has a longer isoform.

Protein sequence alignment of CRACR2A isoform c (EFCAB4Biso.c) and the predicted longer isoform a (EFCAB4Biso.a.), which has yet to be confirmed experimentally. The 2 isoforms share 52% sequence similarity (highlighted). EFCAB4biso.a. has a predicted mass of 83 kDa.
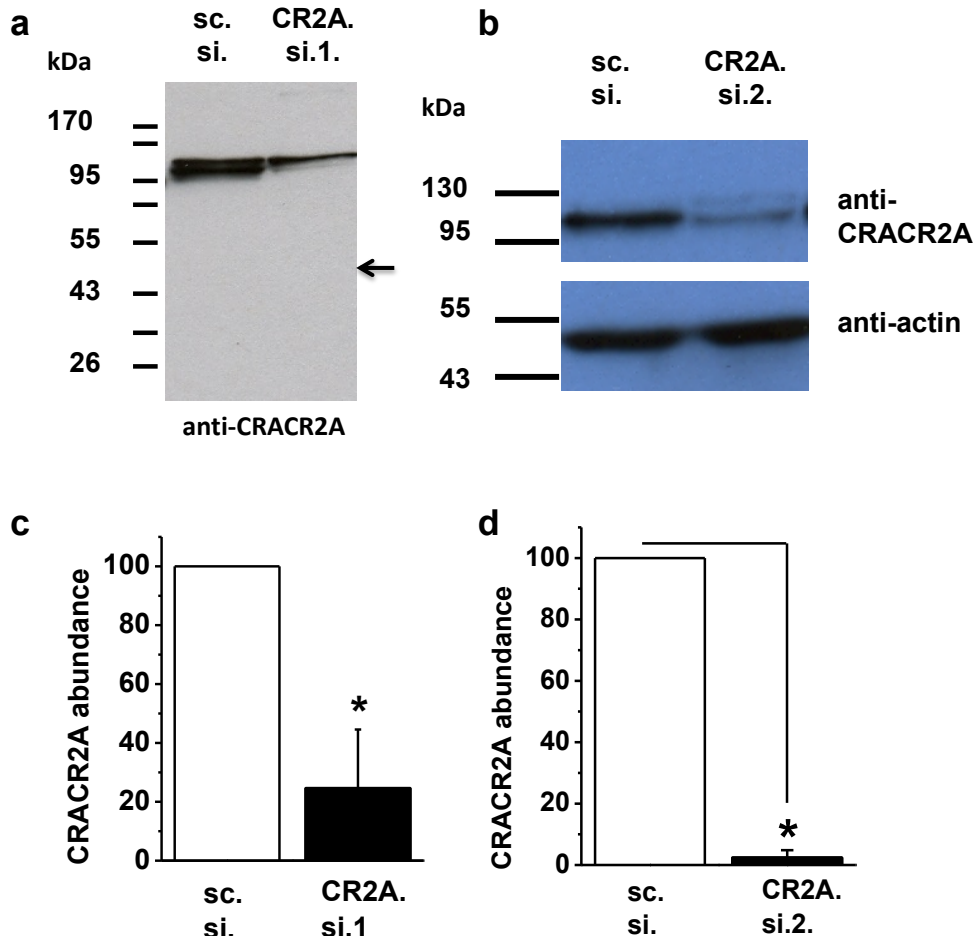
Figure 3-5 HUVECs express CRACR2A isoform a.

HUVECs were transfected with 2 different CRACR2A siRNAs and lysed after 72 hours. Western blots using an anti-CRACR2A antibody did not detect the 46 kDa CRACR2A protein (arrow; **a**) but did detect a larger protein that was down-regulated following siRNA knockdown with CRACR2A siRNA 1 (CR2A.si.1; a; n=3) and CRACR2A siRNA 2 (CR2A.si.2; b; n=3). Protein levels were quantified by densitometry and the mean levels of CRACR2A (large isoform) are shown in **c** (CR2A.si.1; *$P<0.05$) and **d** (CR2A.si.2; *$P<0.05$).
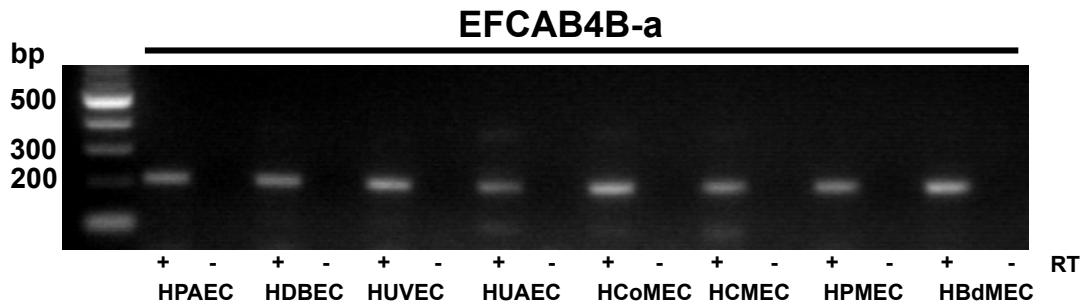
Figure 3-6 EFCAB4B-a mRNA is expressed in a range of macro- and micro-vascular endothelial cells.

The image shows an electrophoresis gel of PCR products showing expression of EFCAB4B-a in: HPAEC (pulmonary artery); HDBEC (dermal blood); HUVEC (umbilical vein); HUAEC (umbilical artery); HCoMEC (colonic microvascular); HCMEC (cardiac microvascular); HPMEC (pulmonary microvascular; HDMEC (dermal microvascular) and HBdMEC (bladder microvascular). Reactions were performed with (+) or without (-) reverse transcriptase (RT). Expected size of the EFCAB4B-a product was 214 bp.

3.3. EFCAB4B-a has no effect on store-operated Ca^{2+} entry in endothelial cells

CRACR2A was found to interact with Orai1 and STIM1 to regulate Ca^{2+} entry into cells via the Orai1 ion channel (Srikanth et al., 2010). To determine whether EFCAB4B-a shared a similar function with CRACR2A, the effect of EFCAB4B-a knockdown on store-operated Ca^{2+} entry (SOCE) was investigated. Since HUVECs showed no expression of CRACR2A at the protein level, it was assumed that any effect observed with the CRACR2A siRNA (which target the identical N-terminus of both isoforms) was an effect mediated by EFCAB4B-a. Two different siRNAs and a scrambled control siRNA were individually transfected into HUVECs. Seventy-two hours post-transfection, cells were loaded with the Ca^{2+} indicator dye Fura-2 AM and SOCE was measured in multi-well intracellular Ca^{2+} ($[Ca^{2+}]_i$) measurement experiments using the FlexStation. To measure SOCE, cells were treated with the SERCA inhibitor thapsigargin (TG), in the absence of extracellular Ca^{2+} in order to evoke a release of Ca^{2+} from intracellular stores. Extracellular Ca^{2+} was then added back and the Ca^{2+} entry response measured. Interestingly, siRNA mediated knockdown of EFCAB4B-a had no effect on SOCE in HUVECs. As a control, Orai1 and STIM1 siRNA-transfected cells showed a significant inhibition of the SOCE response (Figure 3-7).
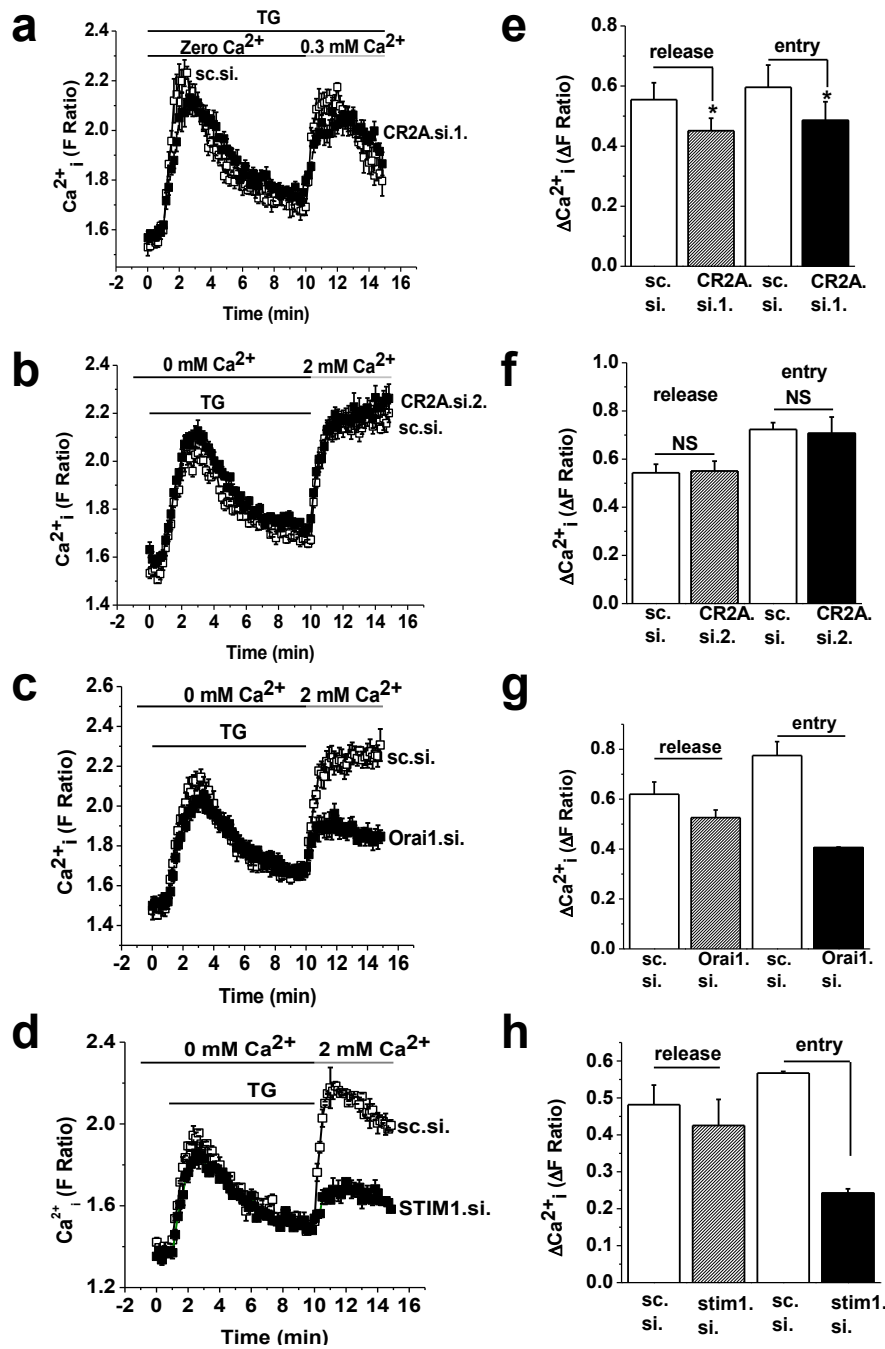
Figure 3-7 EFCAB4B-a has no effect on SOCE.

siRNA transfected HUVECs loaded with Fura-2 AM were treated with TG (1 μM) in the absence of extracellular Ca^{2+} before Ca^{2+} add-back. Example traces for **a.** CRACR2A siRNA 1 (CR2A.si.1; N=4), **b.** CRACR2A siRNA 2 (CR2A.si.2.; N=4), **c.** Orai 1 siRNA (Orai1.si.; N=7) and **d.** STIM1 siRNA (STIM1.si.; N=2). **e-h**. Summary data (Mean ± SEM) for the experiments of the type illustrated in a-d showing measurements for the Ca^{2+} release and Ca^{2+} entry effects with: **e**. CR2A.si.1 (n/N=6/28; *P<0.05), f. CR2A.si.2 (n/N=5/23; NS, non-significant), g. Orai1.si. (n/N=2/9) and h. STIM1.si. (n/N=2/8).

3.4. EFCAB4B-a contains a putative Rab domain

CRACR2A and EFCAB4B-a have identical N-termini, encoding 2 EF-hand domains and a coiled-coil region. However EFCAB4B-a also contains a putative Rab domain located at its C-terminus at 542-731 residues (Figure 3-8). Since knocking-down EFCAB4B-a using siRNA had no effect on SOCE, the C-terminus of EFCAB4B-a must influence its function. Sequence analysis showed that the putative Rab domain encoded by EFCAB4B-a contains all of the conserved Rab motifs (Figure 3-8) (Colicelli, 2004). EFCAB4B-a is therefore a putative Rab protein expressed in endothelial cells. The aims of the project from this point were to investigate whether it is a novel Rab protein, and to investigate its role in endothelial cells.

In order to obtain unbiased insight into the significance of EFCAB4B-a in endothelial cells, the subcellular localisation of EFCAB4B-a was investigated. To examine the endogenous localisation of EFCAB4B-a, HUVECs were seeded onto glass coverslips, fixed and labelled with the commercially available anti-CRACR2A antibody (1:50) and visualised using a fluorescent anti-rabbit secondary antibody. Immunofluorescence was visualised using the Delta Vision microscope. The images showed staining in the cell cytoplasm and nuclei (Figure 3-9). Since this antibody did detect other protein bands by Western blot (Figure 3-3), the staining observed could not be attributed purely to EFCAB4B-a. Since no EFCAB4B-a-specific antibodies were available it was decided to clone EFCAB4B-a from HUVECs and to generate an overexpression construct in order to further investigate its localisation.

a

N   84   119 181   213   542   731   C

EF-hands   coiled-coil
domain

CRACR2A

putative Rab
domain

EFCAB4B-a

b

MAAPDGRVVSRPQRLGQGSGQGPKGSGACLHPLDSLEQKFTQEQTSGQLVMLRKAQEFFQTCDAEGKGFIARKDMQRLHKELPLSLEELEDVFDALD 97

ADGNGYLTPQEFTTGFSHFFSQNNPSQEDAGEQVAQRHEEKVYLSRGDEDLGDMGEDEEAQFRMLMDRLGAQKVLEDESDVKQLWLQLKKEEPH 192

LSNFEDFLTRIISQLQEAHEEKNELECALKRKIAAYDEEIQHLYEEMEQQIKSEKEQFLKDTERFQARSQELEQKILLCKEQELEQLTQKQKRLEGQCTALH 295

HDKHETKAENTLKLTNQELARELERTSWELQDAQOQLESLQQEACKLHQEKEMEVYRVTESLQREKAGLLKQLDFLRERNKHLRDERDICFQKNKAA 393

KANTAASRASWKKRSGSVIGKYVDSRGILRSQSEEEEVFGIPRRSSLGLSGYPLTEEEPGTGEPGPGGPYPRPLRRIISVEEDPLPQLLDGGFEQPLSKCSE 496

EEEVSDQGVQGQIPEAPPLKLTPTSPRGQPVGKEALCKEESSPSAPDRLF KIVFVGNSAVGKT SFLRRFCEDRRFSPGMAATVGIDYRVKTLNVDNSQVAL 596
                                                    G1   G2

QLWDTAGQE RYRCITQQFFRKADGVIVMYDLTDKQSFLSVRRWLSSVEEAAVGDRVPVLLLGNKLDNEKEREVPRGLGEQLATENNLIFYECSAYSGHHNT 695
G3   G4   G5

KESLLHLARFLKEQEDTIVREDTIQVGHPAKKKSCCG 731

Figure 3-8 Sequence and putative domains of EFCAB4B-a.

Schematic comparing the basic structures of CRACR2A with EFCAB4B-a. **b.** Protein sequence for EFCAB4B-a highlighting the G box consensus residues in blue. Residues that are highly conserved in 90% of Rab family members are highlighted in red. C-terminal cysteines, which may be important for prenylation are highlighted in green. C-terminal basic residues are highlighted in orange. Information regarding conserved motifs has come from Colicelli (2004).
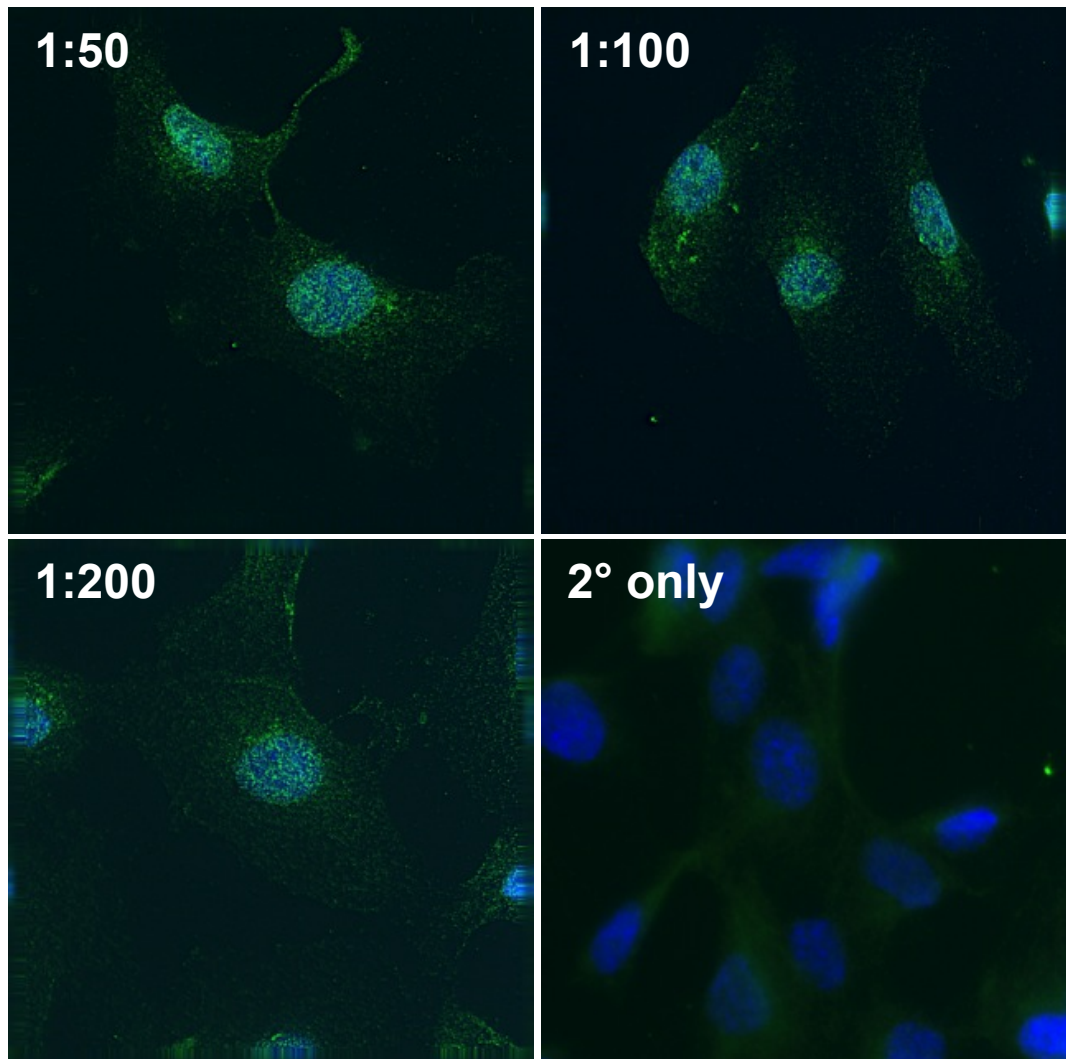
Figure 3-9 Staining observed with the anti-CRACR2A antibody.

 HUVECs were fixed and permeabilised then incubated with the anti-CRACR2A antibody at 1:50, 1:100 and 1:200 dilutions. Secondary antibody (2º) was Alexa Fluor 488 donkey anti-rabbit. Nuclei are stained with DAPI. Cells were imaged by Bing Hou on the Delta Vision microscope.

3.5. Cloning EFCAB4B-a from HUVECs confirms its expression

EFCAB4B-a was cloned from HUVEC cDNA that had been enriched using a EFCAB4B-a gene specific primer (Crac2rainsertR; Table 2-5) for reverse transcription. Nucleotide sequencing confirmed its identity as the predicted long isoform of EFCAB4B, although the sequencing results indicated that EFCAB4B-a cloned from HUVECs had 3 extra nucleotides in its sequence (encoding an additional amino acid between serine424 and glutamamine425) compared to the published sequence (NM_001144958.1). This most likely represents a genuine variation from the sequence published, since the same insertion was detected in human pulmonary artery, human dermal microvascular and human colonic microvascular endothelial cells, by RT-PCR. EFCAB4B-a was then cloned into an eGFP-C1 expression vector by Infusion reaction. Two different constructs were generated, one that expressed GFP tagged to the N-terminus of EFCAB4B-a (GFP-EFCAB4B-a), and one that expressed untagged EFCAB4B-a.

In order to compare the intracellular localisation of EFCAB4B-a with CRACR2A, a CRACR2A construct (clone ID 3531511) was purchased. Using the same cloning methods as described for EFCAB4B-a, CRACR2A was inserted into the same eGFP-C1 vector, plus and minus expression of GFP at the N-terminus and constructs were verified by sequencing.

In order to confirm the expression and detection of each gene product by the anti-CRACR2A antibody, the constructs were transfected into HUVECs, and lysates from transfected cells were probed by Western blotting. The results are shown in Figure 3-10 – in untransfected cells (lane 1), only endogenous EFCAB4B-a is detected; in transfected cells, both the endogenous protein and the overexpressed recombinant proteins (CRACR2A, lane 2; EFCAB4B-a, lane 3; GFP-EFCAB4B-a, lane 4) are detected. These data confirm that the high molecular weight band detected by this antibody is the predicted long isoform EFCAB4B-a.
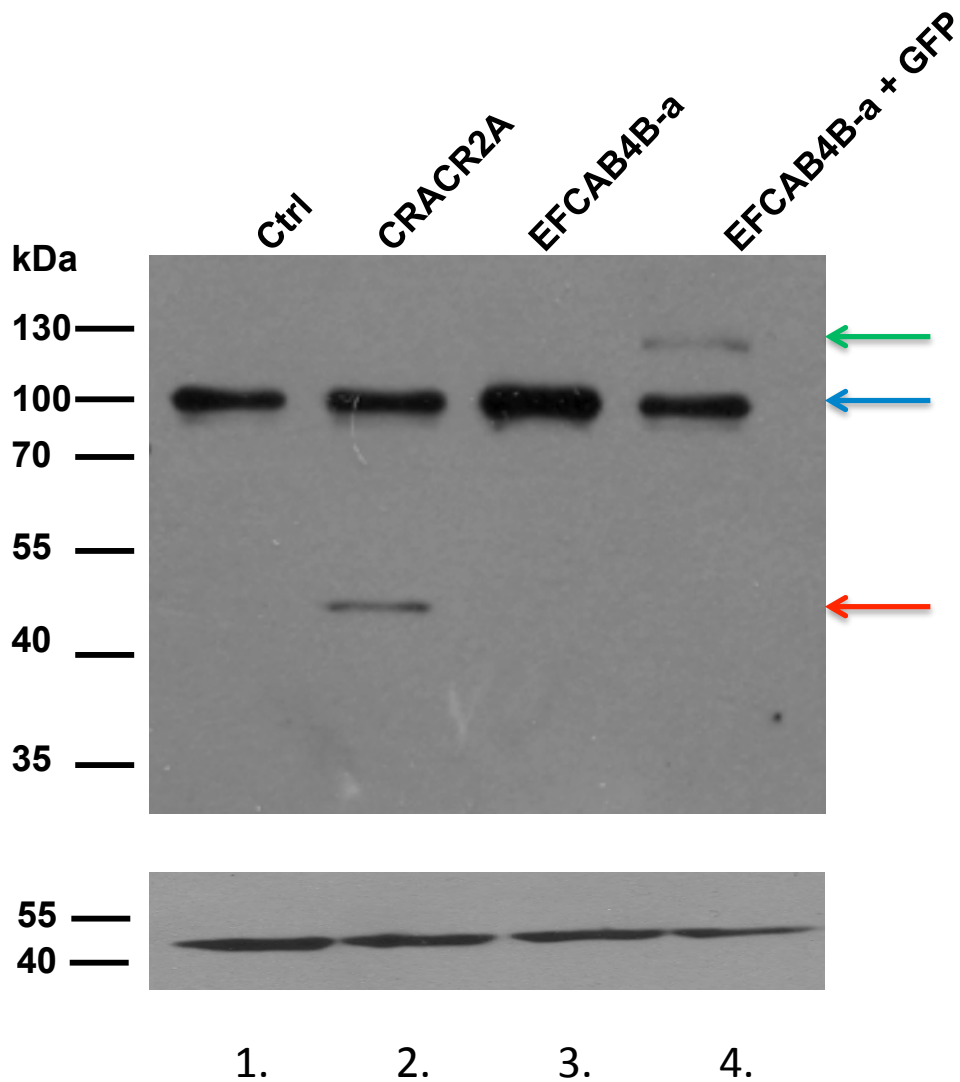
Figure 3-10 The anti-CRACR2A antibody cross reacts with EFCAB4B-a protein.

Constructs expressing either CRACR2A (lane 2), EFCAB4B-a (lane 3) or GFP-EFCAB4B-a (lane 4) were transiently transfected into HUVECs, and Western blotting was performed on cell lysates. The anti-CRACR2A antibody (1:800) detected both endogenous and overexpressed CRACR2A and EFCAB4B-a proteins. Lane 1: control transfected cells with pcDNA3.1. Lane 2: red arrow shows overexpressed 46 kDa CRACR2A. Lane 3: shows overexpressed EFCAB4B-a (blue arrow). Lane 4: Green arrow shows overexpressed GFP-EFCAB4B-a. Bottom blot shows actin loading controls.

3.6. EFCAB4B-a localises to endothelial cell-specific Weibel-Palade Bodies

To determine the localisation of EFCAB4B-a, EFCAB4B-a constructs were transiently transfected into HUVECs using Lipofectamine 2000™ in a 6-well dish. After 24 hours, cells were transferred onto glass coverslips and immunostaining was performed at 48 hours post-transfection. Constructs expressing CRACR2A were also transfected into separate cells to compare its localisation with that of EFCAB4B-a. Overexpressed proteins were visualised either by the GFP-tag or by staining with the anti-CRACR2A antibody and fluorescently labelled secondary antibodies.

CRACR2A, as expected, showed a cytosolic localisation with some plasma membrane expression (Figure 3-11). EFCAB4B-a showed a very different localisation to CRACR2A. Immediately obvious was a strong expression in the peri-nuclear region. A similar localisation had previously been observed for Rab45 (also known as RASEF), a Rab protein with a very similar structure to EFCAB4B-a with 2 EF-hands, a coiled-coil region and a Rab domain (Shintani et al., 2007). Since the Golgi has a peri-nuclear localisation, transfected cells were immunostained with the *cis*-Golgi marker GM130, in order to determine whether EFCAB4B-a was present in the Golgi. No co-localisation occurred between the Golgi marker and EFCAB4B-a (Figure 3-12). No co-localisation occurred with the *trans*-golgi marker, anti-TGN-46 either. Instead, EFCAB4B-a appeared to disrupt the Golgi (Figure 3-12).

Although the majority of cells displayed this peri-nuclear localisation, in some cells, EFCAB4B-a was found in small rod-shaped vesicles clustered around the peri-nuclear region. These rod-shaped vesicles resembled endothelial-cell specific Weibel-Palade bodies (WPBs) (Weibel and Palade, 1964). WPBs are secretory-like vesicles involved in exocytosis (Valentijn et al., 2011). WPBs can be 0.1-0.3 µm in diameter and 1-5 µm in length and the main constituent of these vesicles is the prothrombotic agent, von Willebrand Factor (vWF) (Valentijn et al., 2011). To investigate whether these rod-shaped vesicles

containing EFCAB4B-a were WPBs, HUVECs overexpressing EFCAB4B-a were fixed and immunostained with a primary anti-vWF antibody. vWF staining was visualised using a fluorescently tagged anti-mouse secondary antibody. The cells were then imaged on the DeltaVision microscope.

vWF staining, as expected, appeared in rod-shaped structures resembling WPBs. The dimensions of these structures were measured using Image J software (http://uhnresearch.ca/wcif/imagej). A total of 150 structures in cells from 6 images were measured and the results were plotted in a frequency histogram (Figure 3-13). The dimensions of the structures were consistent with those previously described for WPBs (Valentijn et al., 2011).

To investigate any potential colocalisation between EFCAB4B-a and vWF, HUVECs were transfected with non-tagged EFCAB4B-a, fixed and stained with the anti-CRACR2A and anti-vWF antibodies. Across four independent experiments, a total of eighteen images of cells expressing EFCAB4B-a in the field of view were analysed. Of those 18 images, eleven (65%) included cells showing evidence of colocalisation between vWF (red stain) and EFCAB4B-a (green stain). The degree of this colocalisation was quantified using Image J software and the Colocalisation Threshold PlugIn (http://uhnresearch.ca/wcif/imagej). This software generates an Rcolocalisation (Rcoloc) value, which is a measure of the linear correlation between the red (vWF) and green (EFCAB4B-a) channels. A value of 1 represents a complete positive correlation and zero indicates no correlation. The mean Rcoloc value across the images analysed was 0.8, indicating a strong correlation between EFCAB4B-a and vWF localisation. Seven of eighteen images analysed (41%) showed co-localisation of EFCAB4B-a and vWF in structures that resembled WPBs (Figures 3-14 and 3-15). In addition to these structures, the colocalisation was frequently observed in the peri-nuclear region. The significance of this peri-nuclear staining remains to be determined.

Although up to 97% of EFCAB4B-a was found to colocalise with vWF (Rcoloc=0.88), the extent of colocalisation varied widely between cells (5-97%).

Similar results were also obtained when cells transfected with GFP-tagged EFCAB4B-a were costained with anti-vWF (Figure 3-16).

Whilst 65% of cells showed colocalisation of EFCAB4B-a with vWF, the remaining 35% of EFCAB4B-a-expressing cells showed no detectable vWF staining (Figure 3-17) suggesting that overexpression of EFCAB4B-a reduces the total amount of cellular vWF.
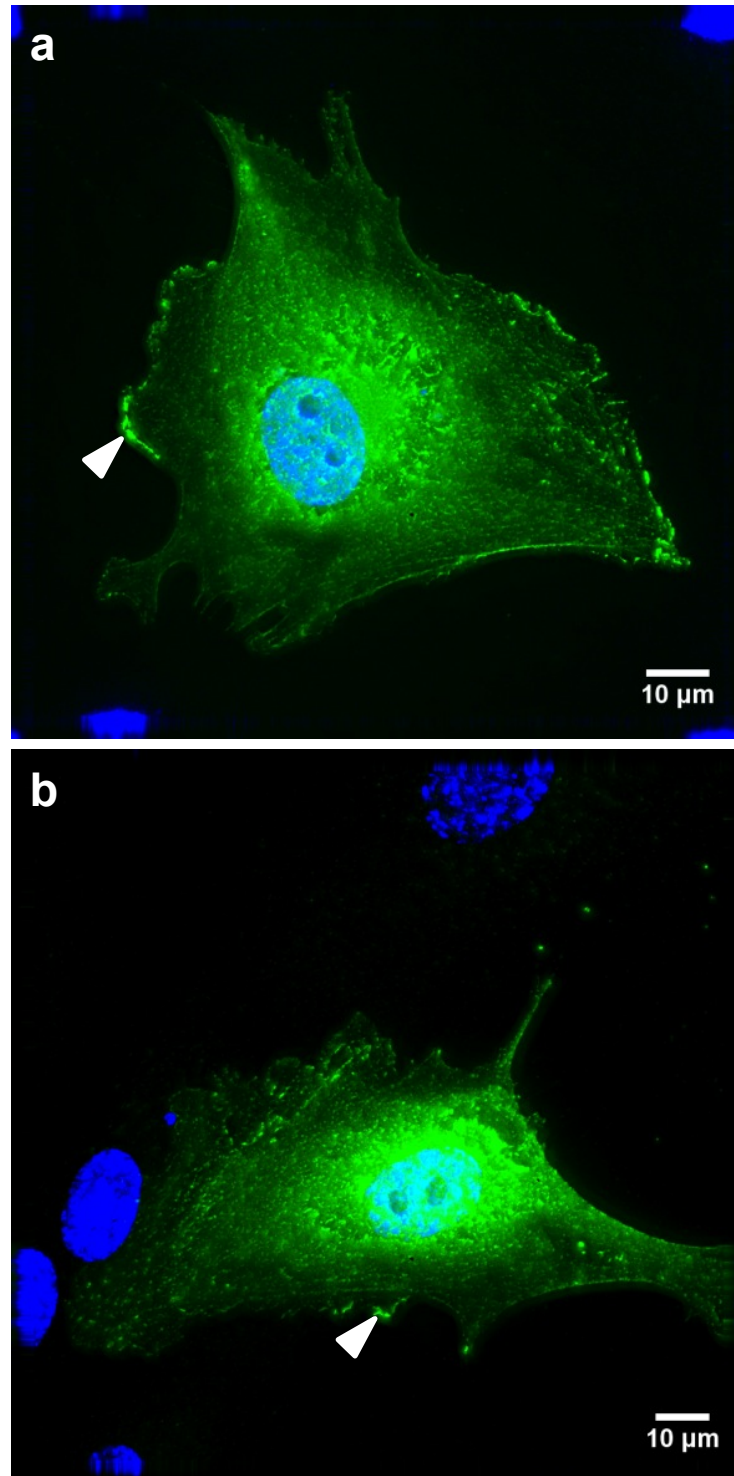
Figure 3-11 CRACR2A has a cytoplasmic and plasma membrane localisation in HUVECs.

HUVECs were transfected with a CRACR2A expressing plasmid. 48 hours later cells were fixed, stained with the anti-CRAC2A antibody and analysed by Delta Vision microscopy. The nuclei were stained with DAPI. The figures are representative images from 2 experiments showing CRACR2A expression in the cytoplasm and at the plasma membrane (arrow heads).

Figure 3-12 EFCAB4B-a does not localise to the Golgi.

HUVECs were transfected with a GFP-EFCAB4B-a expressing plasmid. 48 hours later cells were fixed, stained with a primary cis-Golgi marker, anti-GM130 antibody (1:50) and analysed by Delta Vision microscopy. DyLight594-conjugated anti-mouse IgG was used for visualisation of the Golgi (red). The nuclei were stained with DAPI (blue). The figures are representative images showing GFP-EFCAB4B-a (green) and cis-Golgi (red).
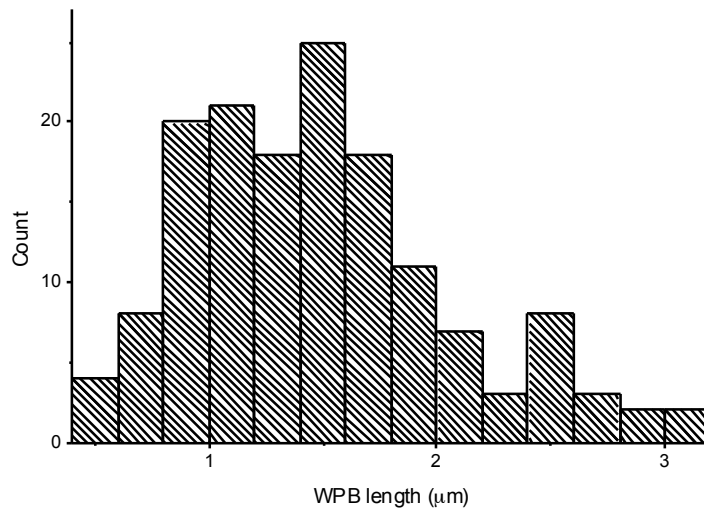
Figure 3-13 Frequency distribution of WPBs in HUVECs.

150 WPBs were counted from a total of 6 images. The length of each WPB was measured using Image J software. Data were plotted in a statistical histogram.
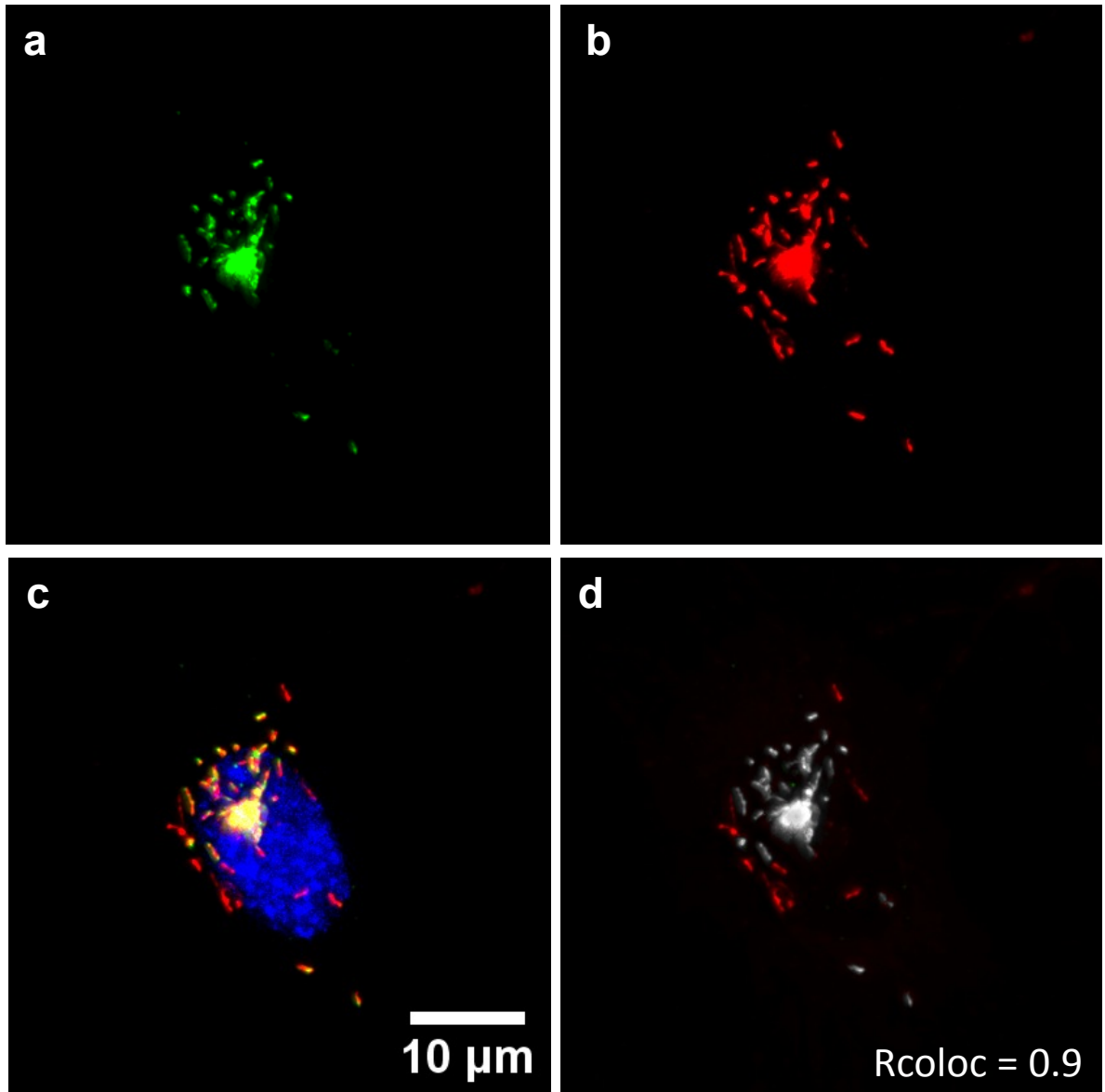
Figure 3-14 EFCAB4B-a localises to WPBs.

HUVECs were transfected with the EFCAB4B-a construct. Two days later cells were fixed, immunostained with primary monoclonal anti-vWF (shown in red) and primary polyclonal anti-CRACR2A (shown in green) antibodies and analysed by Delta Vision microscopy. DyLight594-conjugated anti-mouse IgG was used for visualisation of vWF (red). Nuclei were stained with DAPI (blue). The figure is a representative image from 4 independent experiments showing **a**. EFCAB4B-a expression (green) **b**. anti-vWF expression (red) and **c**. merged image, showing co-localisation (yellow) of EFCAB4B-a with vWF. Colocalisation was measured using Image J software and the 'Colocalisation Threshold' Plugin. The grey colour shown in **d** highlights the mask applied to generate the Rcoloc. Rcoloc=0.9.

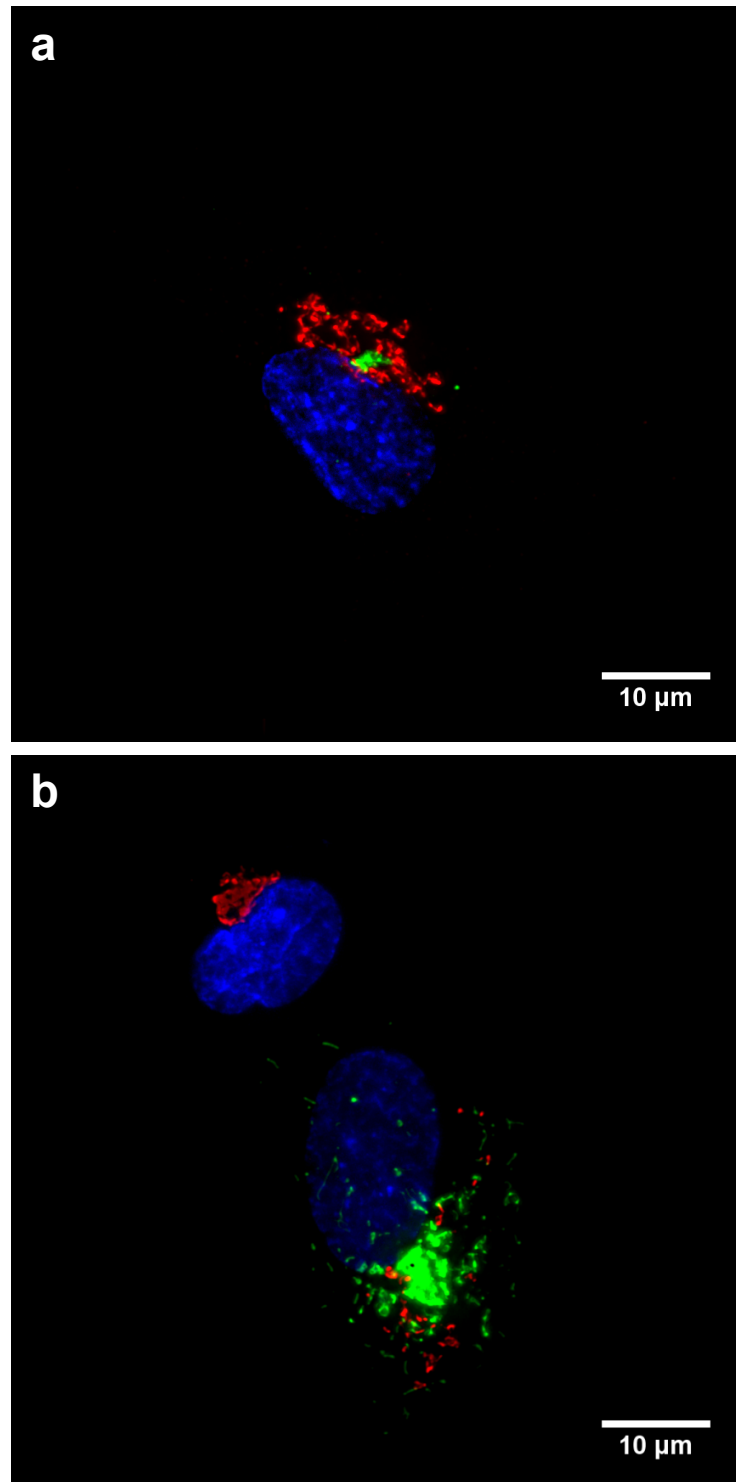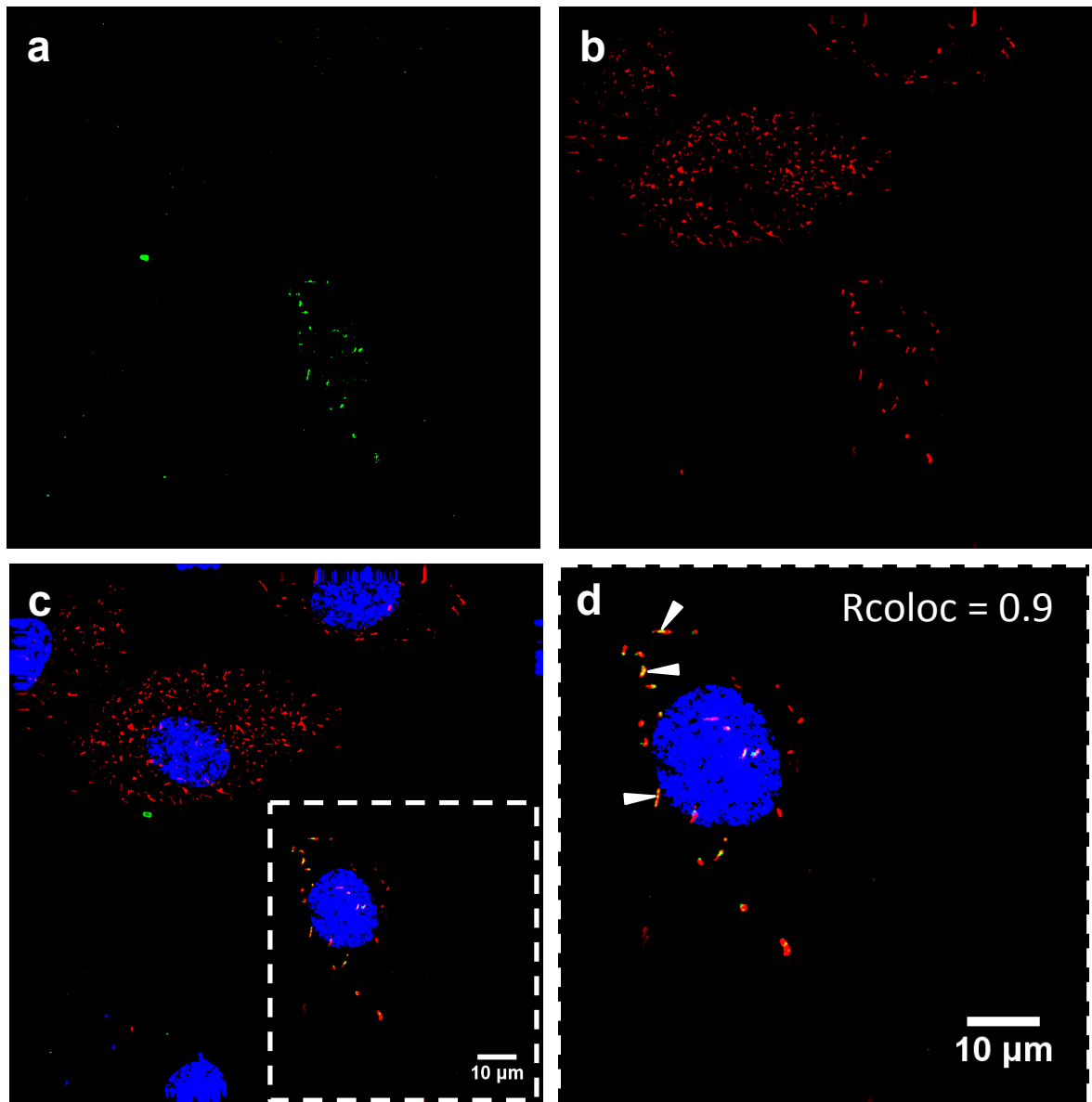**Figure 3-15 EFCAB4B-a localises to WPBs.**

HUVECs were transfected with a EFCAB4B-a expressing plasmid. 48 hours later cells were fixed, stained with a primary anti-vWF antibody (1:200) and primary anti-CRACR2A antibody and analysed by Delta Vision microscopy. DyLight594-conjugated anti-mouse IgG (red) was used for visualisation of vWF. The nucleus was stained with DAPI (blue). The figure shows representative images from 3 experiments showing **a**. EFCAB4B-a expression (green) **b**. anti-vWF expression (red) and **c**. merged image, showing co-localisation (yellow) of EFCAB4B-a with vWF. The image in panel d shows an enalarged image of the highlighted section in panel c. arrows indicate colocalisation. Rcoloc=0.9.
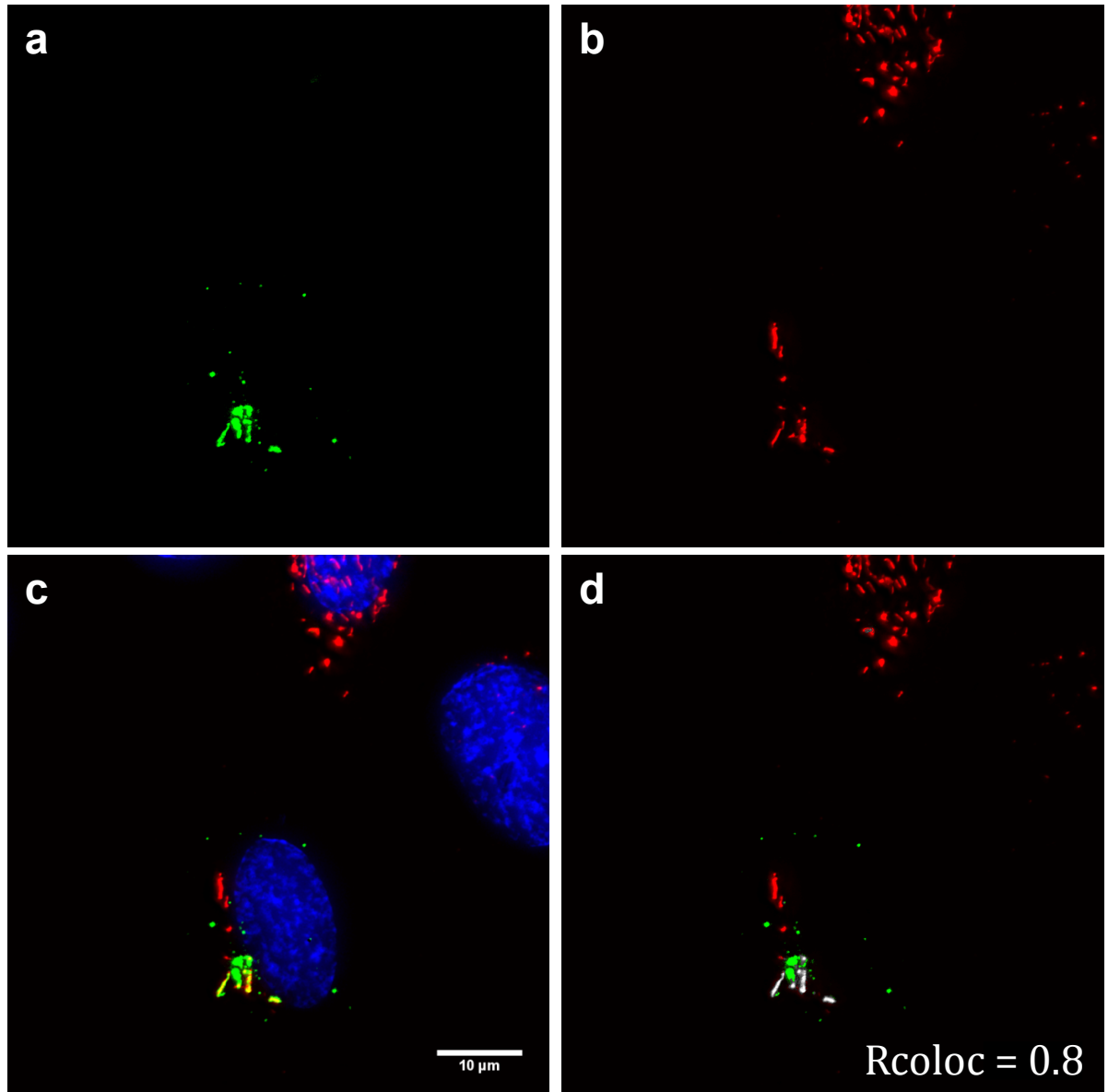
Figure 3-16 GFP-EFCAB4B localises to WPBs.

HUVECs were transfected with the GFP-EFCAB4B-a construct and immunostained with anti-vWF. Cells were imaged on the Delta Vision microscope. Nuclei are stained with DAPI (blue). **a**. expression of GFP-EFCAB4B-a (green). **b**. anti-vWF staining (red). **c.** colocalisation of GFP-EFCAB4B-a and vWF (yellow). **d**. colocalisation analysis was performed using ImageJ PlugIn : Correlation Threshold. Rcoloc = 0.8.
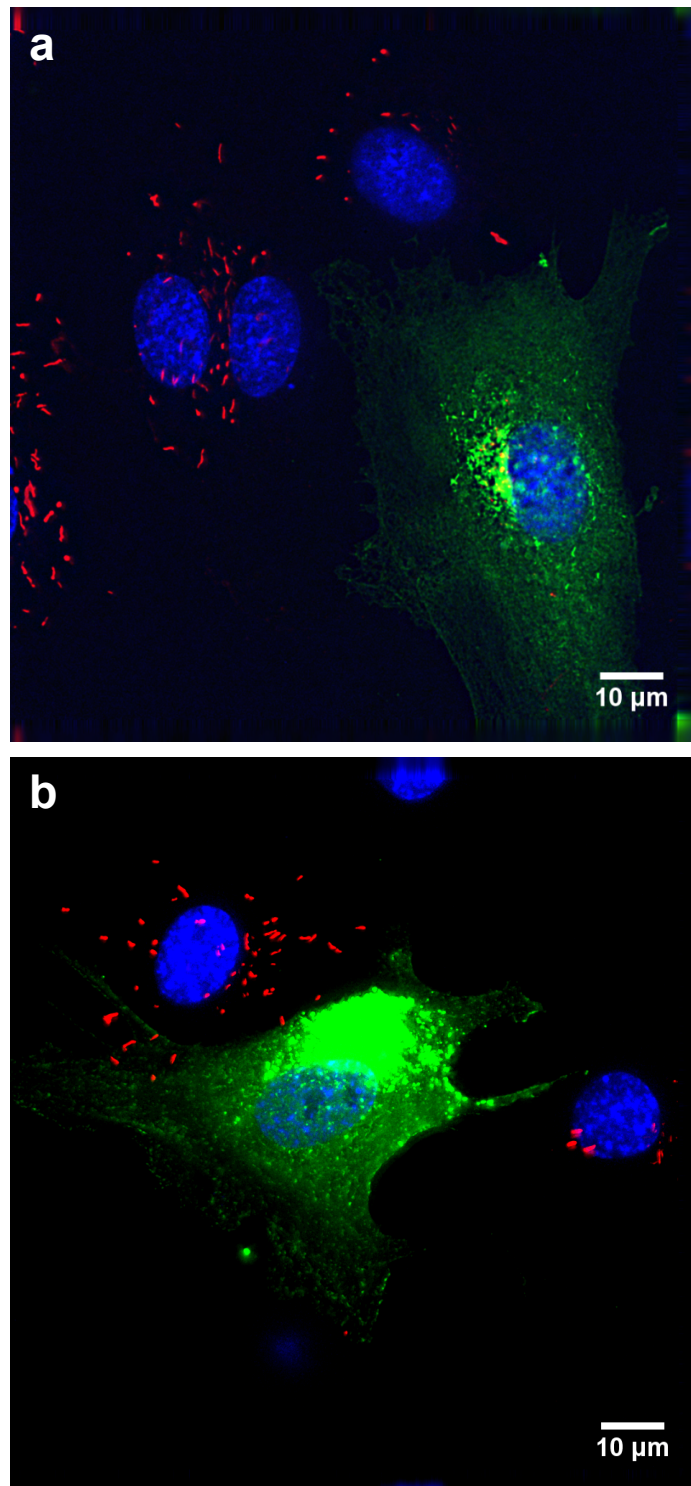
Figure 3-17 Over-expression of EFCAB4B-a reduces vWF expression.

HUVECs were transfected with a EFCAB4B-a expressing plasmid. 48 hours later cells were fixed, stained with a primary anti-vWF antibody and primary anti-CRACR2A antibody and analysed by Delta Vision microscopy. DyLight594-conjugated anti-mouse IgG was used for visualisation of vWF (red). The nuclei were stained with DAPI (blue). The figures are 2 representative images from 3 experiments showing strong EFCAB4B-a over-expression reduced vWF expression.

3.7. A conserved GTP-binding motif is important for the localisation of EFCAB4B-a.

Rab proteins function by cycling between an active GTP-bound state and an inactive GDP-bound state (Colicelli, 2004). When Rab proteins are in their GTP-bound conformation they are often membrane bound, whilst when they are in their GDP-bound confirmation they often reside in the cytoplasm (Colicelli, 2004). Conserved motifs in Rab GTPase sequences are responsible for GTP binding and hydrolysis. Rab proteins have 5 conserved "G box" motifs (Figure 3-8) (Colicelli, 2004). The G1 box is important for purine nucleotide binding; the G2 box is important for downstream effector binding; the G3 box is important in binding nucleotide-associated Mg^{2+} ions; the G4 box is important for direct interaction with the nucleotide and the residues in the G5 box are less well conserved but are primarily important for indirect associations with the guanine nucleotide (Colicelli, 2004). One of the most widely-used Rab mutations involves mutating the conserved catalytic glutamine in the G3 box residue to leucine, which prevents GTP hydrolysis and locks the protein in a permanently active state (Lee et al., 2009). On the other hand, mutations in the G4 box lead to a constitutively inactive protein that has reduced affinity for guanine nucleotides (Knop et al., 2004). In light of this information, two GFP-EFCAB4B-a mutant constructs were generated to determine whether GTP binding was important for the localisation of EFCAB4B-a. The first mutation in the G3 box was GFP-EFCAB4B-a[Q604L] and the second mutation in the G4 box was GFP-EFCAB4B-a[N658I]. The mutations were made by site-directed mutagenesis on the GFP-EFCAB4B-a construct using the primers shown in Table 2-8. Both constructs were sequenced to confirm the successful mutagenesis.

Mutated constructs were transiently transfected into HUVECs and 24 hours later, the cells were fixed and immunostained with the anti-vWF antibody to label the WPBs and then analysed on the confocal microscope. Results from five images across three independent experiments suggested that the GTP-

locked GFP-EFCAB4B-a^{Q604L} mutant had a peri-nuclear localisation, but no co-localisation with vWF was observed. In contrast, the GTP-deficient mutant (GFP-EFCAB4B-a^{N658I}) showed a more diffuse, cytosolic distribution (n=9 images from 3 independent experiments) (Figure 3-18). These findings suggest that the conserved GTP-binding motif is important for EFCAB4B-a function.

At the C-termini of Rab proteins is a prenylation motif, which acts as a localisation signal and is important for the insertion of the protein into the membrane (Gomes et al., 2003). The putative prenylation motif in EFCAB4B-a consists of two cysteine residues (–SCCG; Figure 3-8). It has been shown for other Rab proteins that disrupting this prenylation motif prevents membrane insertion and function (Gomes et al., 2003). In line with this, it has been shown that tagging fusion proteins, such as GFP, to the C-termini of Rab proteins can mask their localisation signal and result in mislocalisation (Wink, 2006). In this study, another EFCAB4B-a construct was made but this time GFP was tagged to the C-terminus of EFCAB4B-a. When this construct was transfected into HUVECs, it had a general cytosolic distribution (Figure 3-19), similar to that observed with the GFP-EFCAB4B-a^{N658I} mutation construct (Figure 3-18a). This may have occurred because the C-terminal disrupted a prenylation event that is important for WPB association.

Together these data suggest that the Rab domain and prenylation motif are important for the localisation of EFCAB4B-a to WPBs.

At a late stage in this thesis work it was appreciated that the sequence of EFCAB4B-a, cloned from HUVEC cells contained a nucleotide resulting in a single amino acid substitution (L532P). This substitution was outside the EF-hand and Rab domains but could have had an effect on function. Therefore, in order to determine whether the substitution had an effect, a construct expressing GFP-tagged gene containing the EFCAB4B-a sequence as deposited in the gene database (L532) was generated by site-directed mutagenesis, overexpressed in HUVECs and visualised using the DeltaVision microscope.

The overexpression pattern observed for the L532 construct was consistent with that observed for the constructs containing P532. A total of 19 images were taken of HUVECs expressing EFCAB4B-a^{L532}. Of those images, eight (42%) showed colocalisation with vWF and four (21%) showed co-localisation with vWF in structures that resembled WPBs (R=0.6; Figure 3-20). These experiments suggest that this amino acid (L532) is not important for the localisation of EFCAB4B-a.
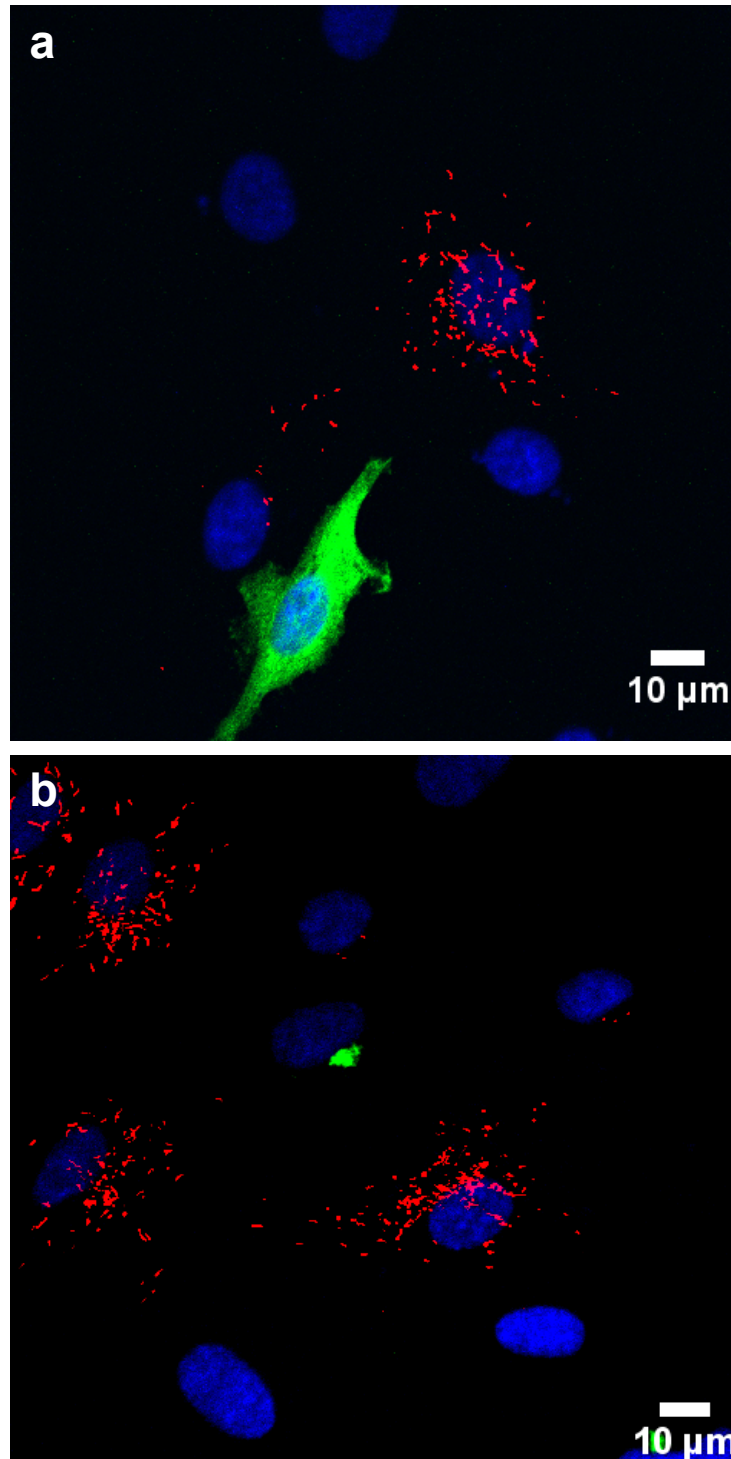
Figure 3-18 Mutating a conserved GTP-binding region in EFCAB4B-a results in a cytoplasmic localisation.

HUVECs were transfected with plasmids encoding GFP-EFCAB4B-a mutants. 24 hours later cells were stained with a primary anti-vWF antibody and visualised using the confocal microscope. Nuclei were stained with DAPI (blue). HUVECs expressing the GTP-deficient mutant GFP-EFCAB4B-a^{N658I} showed a cytoplasmic distribution (**a**) whereas the constitutively active mutant GFP-EFCAB4B-a ^{Q604L} showed a peri-nuclear and localisation (**b**). Images are representative images from 3 experiments.
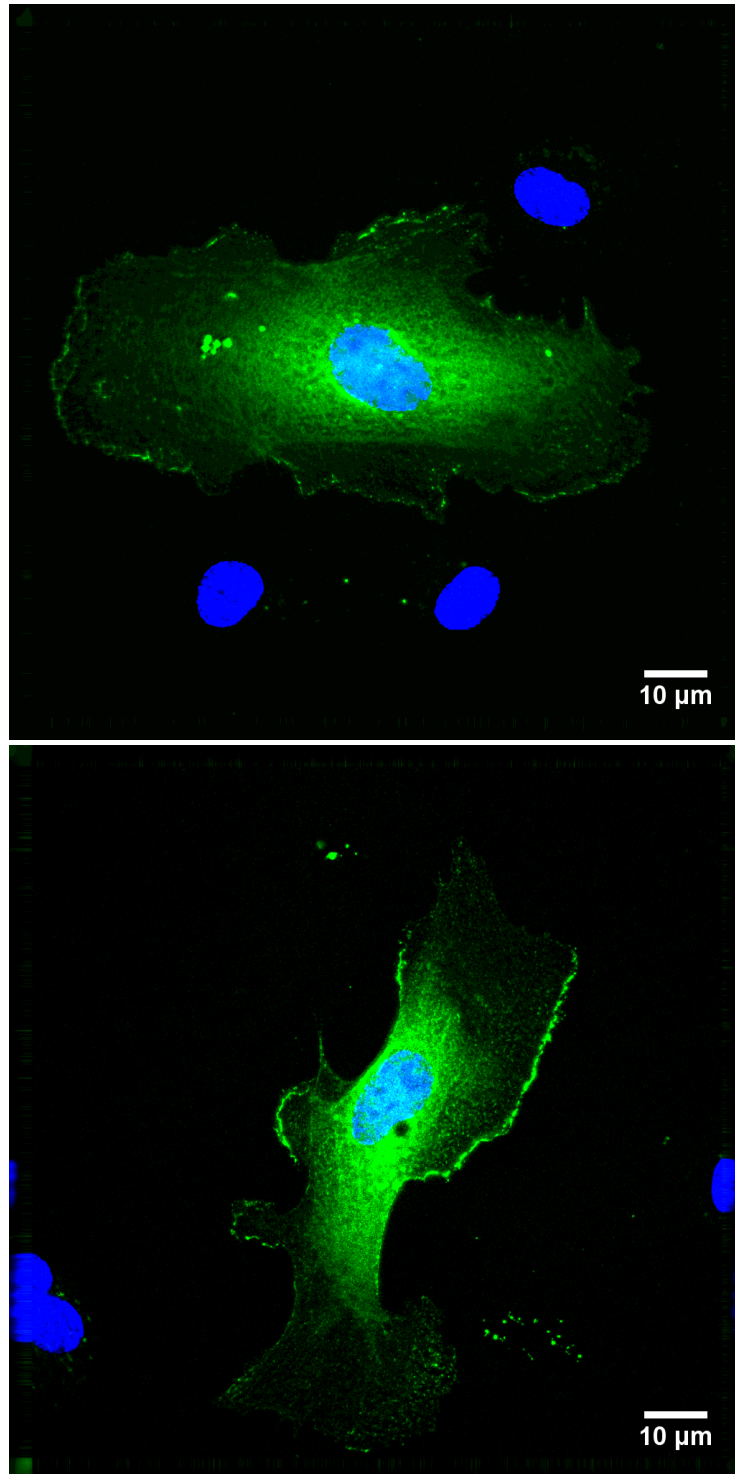
Figure 3-19 EFCAB4B-a-GFP has a cytosolic localisation.

HUVECs were transfected with EFCAB4B-a-GFP. 48 hours later cells were fixed then analysed by Delta Vision microscopy. The nuclei were stained with DAPI (blue). The figures are 2 representative images from 1 experiment showing EFCAB4B-a -GFP has a cytoplasmic localisation in HUVECs (green).
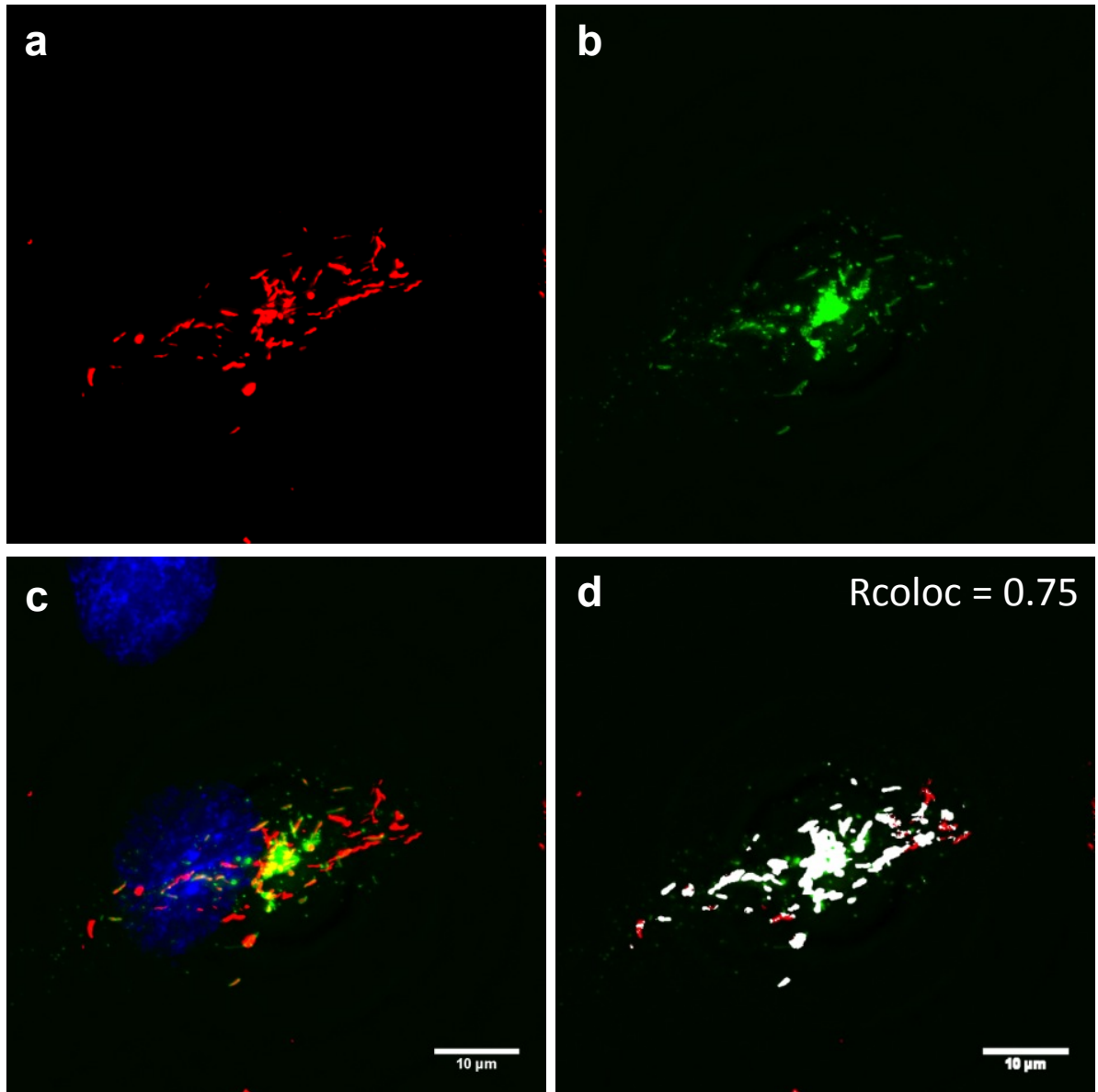
Figure 3-20 Amino acid substitution at position 532 does not affect the sub-cellular localisation of EFCAB4B-a.

HUVECs were transfected with GFP-EFCAB4B-a expressing Lysine at position 532. 48 hours post-transfection, cells were fixed and stained with the anti-vWF antibody (red) and colocalisation with GFP-EFCAB4B-a (green) was visualised using the Delta Vision microscope. The nuclei were stained with DAPI (blue). Rcoloc=0.75.

3.8. Knockdown of EFCAB4B-a has no effect on VEGF-A$_{165}$-stimulated vWF secretion

A major role of Rab proteins is in vesicle trafficking (Diekmann et al., 2011). Several other Rab proteins including Rab3, Rab33, Rab37, Rab27 and Rab15 have been found expressed in WPBs (Zografou et al., 2012) and 3 of these Rabs (Rab3d, Rab27a and Rab15) have reported roles in the trafficking and secretion of vWF (Bierings et al., 2012, Knop et al., 2004, Nightingale et al., 2009, Zografou et al., 2012). To determine if EFCAB4B-a was involved in the secretion of vWF, vWF ELISA assays were performed.

The secretion of vWF occurs mostly in a Ca^{2+}-regulated manner by exocytosis. Many different factors have been shown to activate WPB exocytosis including endogenous chemicals such as ATP and histamine; polypeptides such as thrombin and VEGF, and lipids such as ceramide and sphingosine-1-phosphate (Lowenstein et al., 2005). In this study, VEGF-A$_{165}$ was used to stimulate secretion of vWF since it is a major signalling cytokine involved in driving endothelial cell migration, proliferation and tube formation, although it also promotes vascular inflammation (Matsushita et al., 2005).

A concentration response curve to VEGF-A$_{165}$ was performed to determine a sub-maximal concentration to stimulate vWF secretion (Figure 3-21). HUVECs treated with either scrambled or EFCAB4B-a siRNA were incubated in growth factor- and serum- free media for 30 minutes at 37°C 4% CO_2. Thirty minutes later the cell medium was exchanged for medium containing 30 ng/ml VEGF-A$_{165}$. A previous study showed that 30 minutes treatment evoked a significant increase in secreted vWF (Matsushita et al., 2005). After this time two 100 µl supernatant samples were removed, and vWF levels were measured using a vWF ELISA assay. To determine the constitutive secretion of vWF, control experiments were performed where water was substituted for VEGF-A$_{165}$.

As confirmation that EFCAB4B-a had been knocked down in these experiments, the cells used in these experiments were lysed and Western

blotting was performed using the anti-CRACR2A antibody. The results showed that siRNA treatment had no significant effect on basal (constitutive) or regulated (VEGF-stimulated) vWF secretion (Figure 3-21), despite a significant reduction in EFCAB4B-a protein levels (Figure 3-22 a and b). However, the basal levels of intracellular vWF were significantly increased (Figure 3-22).
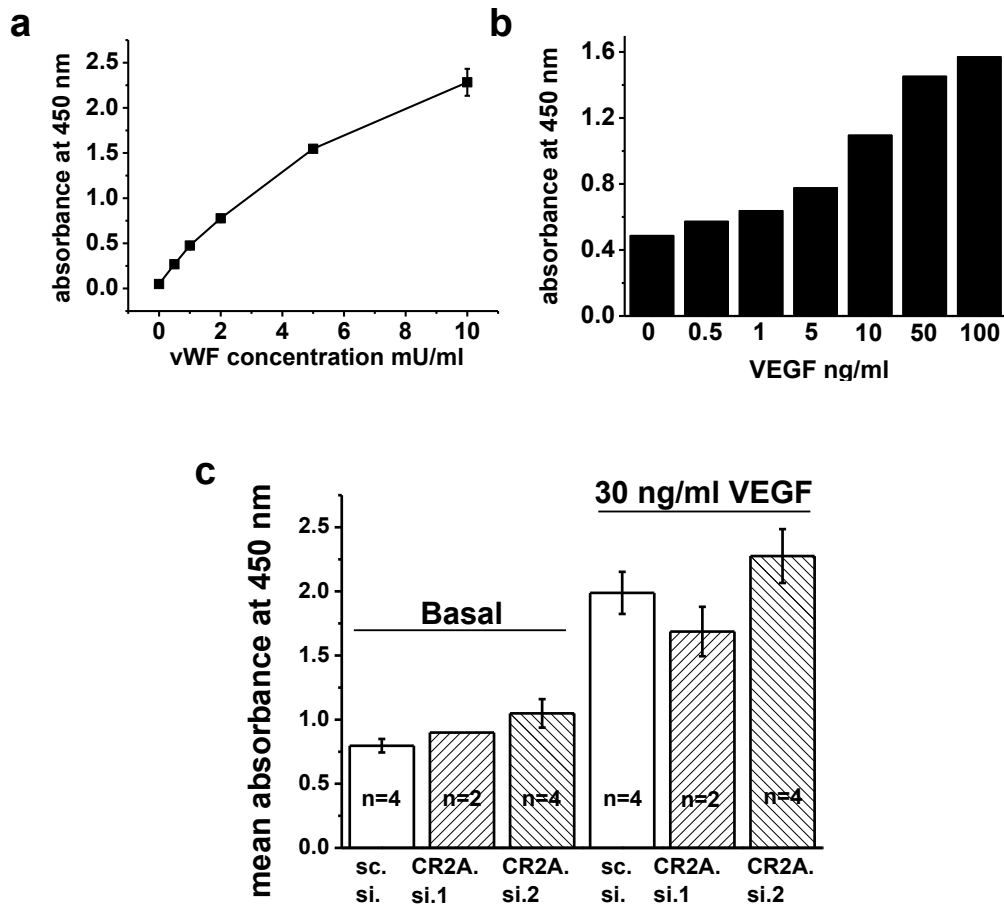
Figure 3-21 siRNA-mediated knockdown of EFCAB4B-a has no significant effect on constitutive or VEGF-stimulated vWF secretion.

a. Standard curve showing absorbance at 450 nm increases with increasing vWF concentrations. **b**. HUVECs were stimulated with a range of concentrations of VEGF-A_{165} for 30 minutes. Samples of cell media were removed and the amount of vWF was measured by ELISA assay. **c**. HUVECs treated with scrambled or EFCAB4B-a siRNA for 72 hours were treated with 30 ng/ml VEGF-A_{165} or water control (basal). The amount of vWF released was quantified by ELISA. The histogram shows the mean absorbance at 450 nm for control and knockdown cells. n numbers are shown in the histogram bars. No significant difference was observed between scrambled and knockdown treated cells.
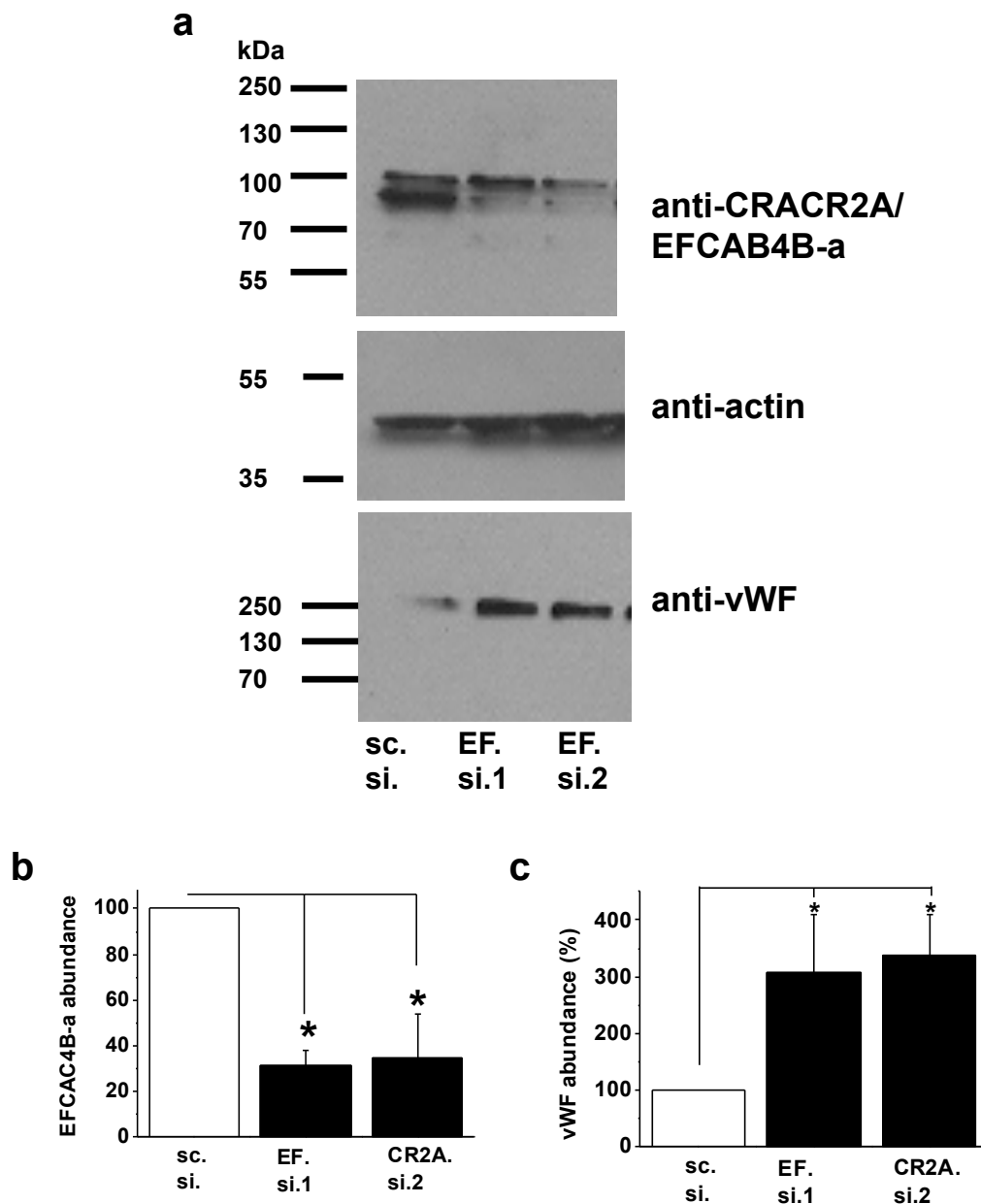
Figure 3-22 Knockdown of EFCAB4B-a increases the amount of cellular vWF.

HUVECs were transfected with scrambled or 2 different EFCAB4B-a siRNA (EF.si.1 and EF.si.2). 72 hours post-transfection, cells were lysed and Western blotting performed using an anti-CRACR2A/EFCAB4B-a antibody to confirm knockdown, anti-actin to confirm equal protein loading and anti-vWF to determine if knock-down of EFCAB4B-a had any effect on cellular vWF levels. **a**. Representative Westen blot showing successful knockdown of EFCAB4B-a and increased amount of vWF in EFCAB4B-a siRNA-treated cells. **b**. Quantification of knockdown results, showing EFCAB4B-a abundance is significantly reduced following siRNA treatment (n=3; $P<0.05$). **c**. Quantification of Western blot results showing increased expression of vWF when EFCAB4B-a is knocked down with two different siRNAs (n=3; $*P<0.05$).

3.9. Knockdown of EFCAB4B-a suppresses VEGFR2 receptor expression and function

As a separate investigation to explore other roles of EFCAB4B-a in endothelial cells, the effect of EFCAB4B-a knockdown on the VEGF-A$_{165}$-induced Ca^{2+} response was investigated. HUVECs transfected with either scrambled or CRACR2A siRNA were loaded with the Ca^{2+} indicator dye Fura-2 AM and Ca^{2+} responses were measured on the FlexStation. In the presence of extracellular Ca^{2+}, VEGF-A$_{165}$ evoked a transient Ca^{2+} elevation followed by a sustained Ca^{2+} response (Figure 3-23). siRNA mediated knockdown of EFCAB4B-a significantly reduced the transient and sustained VEGF-A$_{165}$-induced Ca^{2+} responses (Figure 3-23 a-c). The effect of EFCAB4B-a on VEGF-A$_{165}$-induced Ca^{2+} release in the absence of extracellular Ca^{2+} was also tested. The data showed that knockdown of EFCAB4B-a also inhibited the Ca^{2+} release response (Figure 3-23d). The data suggest that EFCAB4B-a has a positive impact on VEGF responsiveness without effect on the CRAC channel, which is in line with the studies discussed above with thapsigargin (Figure 3-7).

Because EFCAB4B-a knockdown inhibited the Ca^{2+} release response, it was hypothesised that this could be due to the EFCAB4B-a knockdown suppressing VEGF receptor 2 (VEGFR2; also known as KDR/Flk-1) expression, which could be responsible for the reduced Ca^{2+} signal observed in the EFCAB4B-a siRNA transfected cells. In endothelial cells VEGFR2 can be detected as an immature form with a molecular mass of around 200 kDa and a mature fully glycosylated 230 kDa form which is expressed on the cell surface (Takahashi and Shibuya, 1997). Western blot experiments using an anti-VEGFR2 antibody on HUVEC lysates were performed to confirm VEGFR2 expression. The Western blots consistently showed expression of the mature form, with less reliable detection of the immature form, possibly due to a difference in antibody recognition between the two forms. To investigate if EFCAB4B-a affected VEGFR2 expression, HUVECs were treated with two different EFCAB4B-a siRNAs (CR2A.si.1 or CR2A.si.2) and 72 hours post-transfection the cells were lysed

and Western blotting was performed with the anti-VEGFR2 antibody. The blots showed that the 2 different siRNAs reduced VEGFR2 protein abundance by 48 and 55% respectively (Figure 3-24). The data suggest that EFCAB4B-a positively affects VEGFR2 expression and function.
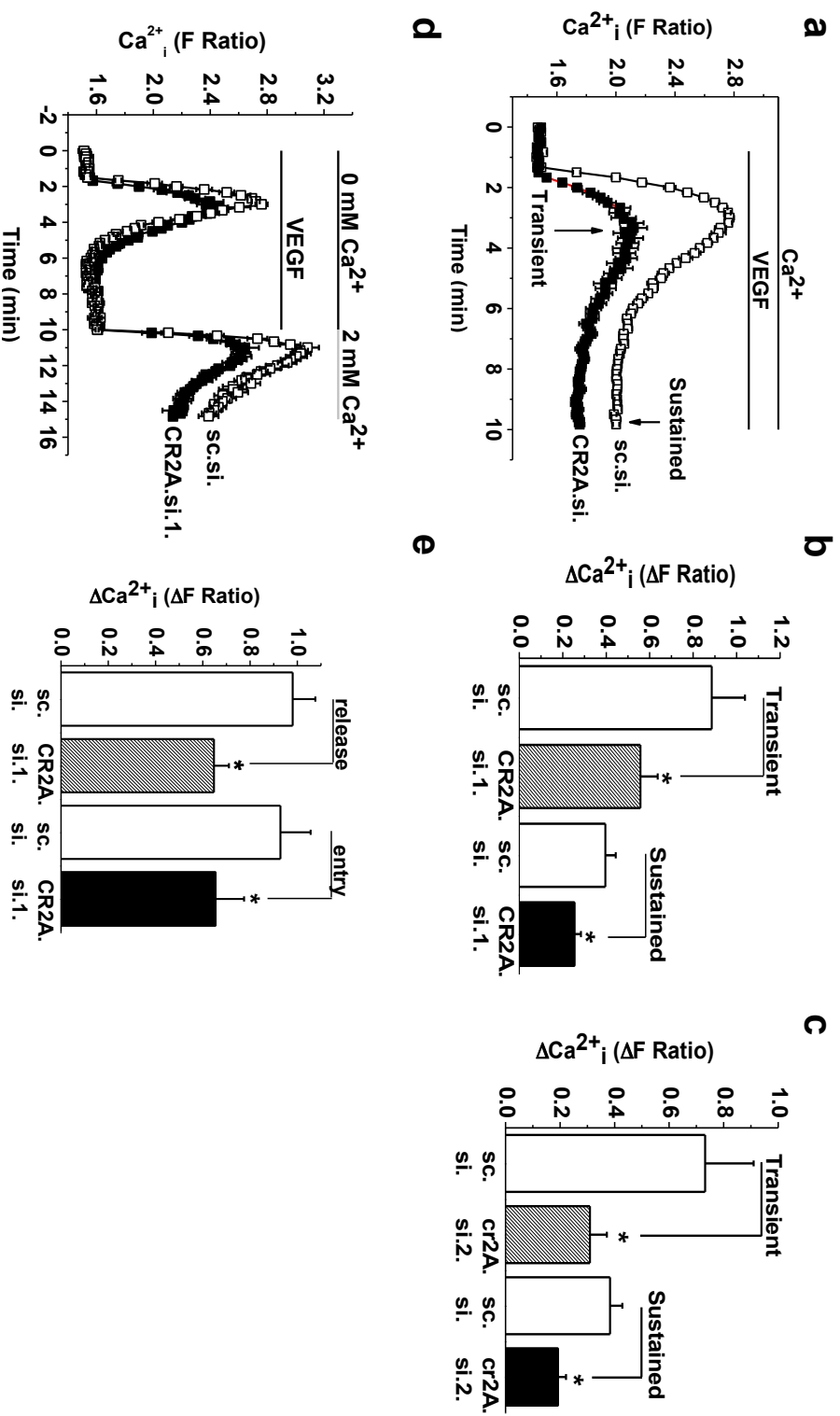
Figure 3-23 siRNA mediated knockdown of EFCAB4B-a inhibits VEGF-induced Ca²⁺ signal.

a. Example trace showing 30 ng/ml VEGF-A$_{165}$-induced Ca²⁺ response in 1.5 mmol/L extracellular Ca²⁺ with CRACR2A (CR2A.si.1) or scrambled (sc.si) siRNA (N=8). **b and c**. Summary data for the experiment of the type illustrated in a. showing measurements for the transient and sustained effects of VEGF-A$_{165}$ with CR2a.si.1 (n/N=5/35; *P<0.05) or CR2a.si.2 (n/N=3/9; *P<0.05) **d**. Example trace showing 30 ng/ml VEGF-A$_{165}$-induced store-depletion in zero mmol/L Ca²⁺ followed by 2 mmol/L Ca²⁺ addback with CRACR2A (CR2A.si.1) or scrambled (sc.si) siRNA (N=3) **e**. Summary data for the experiments of the type illustrated in **d**. showing measurements for the Ca²⁺ release and Ca²⁺ entry effects of VEGF-A$_{165}$ with CRACR2A knockdown with CR2A.si.1 (n/N=5/19; *P<0.05).
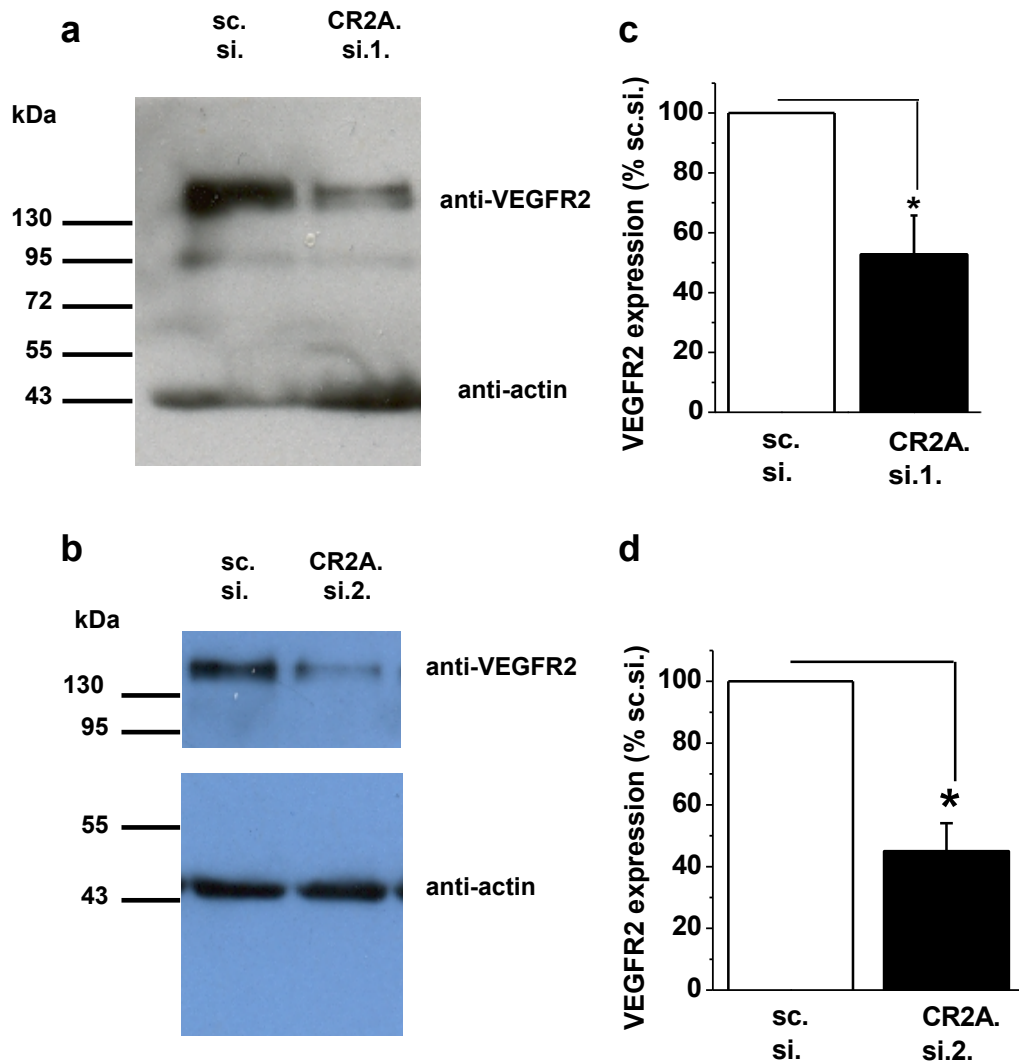
Figure 3-24 EFCAB4B-a enhances VEGFR2 protein expression.

a and b. Example Western blots of HUVEC lysates after transfection with control (sc.ci.) or CRACR2A (CR2A.si.1 **a** or CR2A.si.2 **b**) siRNAs. The blots were probed with an anti-VEGFR2 antibody **c and d**. Quantification of VEGFR2 expression comparing scrambled (sc.si.) and CRACR2A siRNAs (CR2A.si.1 **c**; n=6 or CR2A.si.2 **d**; n=3, both *P<0.05) relative to actin loading controls.

3.10. Knockdown of EFCAB4B-a inhibits histamine-evoked Ca^{2+} entry in HUVECs

The aim of this section was to investigate the role of EFCAB4B-a on histamine-induced Ca^{2+}-responses in endothelial cells. HUVECs were treated with CRACR2A siRNA and 72 hours later, cells were loaded with Fura-2 AM and Ca^{2+} imaging was performed on the FlexStation. The results showed that siRNA mediated knockdown of EFCAB4B-a inhibited histamine-evoked Ca^{2+} entry, with no effect on Ca^{2+} release, compared to scrambled controls (Figure 3-25). The results suggest that EFCAB4B-a does not affect histamine receptor levels, but does affect Ca^{2+} entry through Ca^{2+} permeable ion channels, the identity of which has not been determined in this study.

a

b
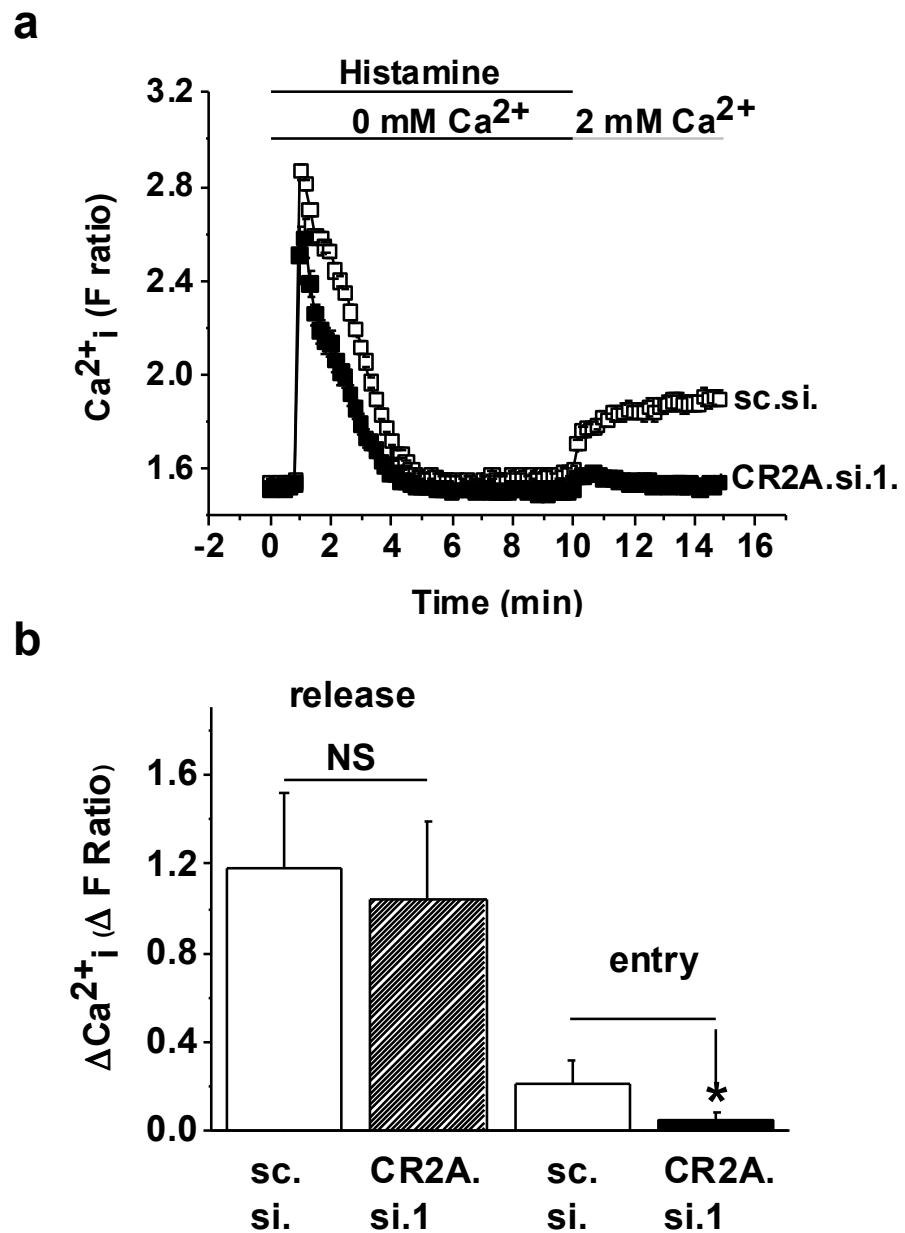
Figure 3-25 EFCAB4B-a knockdown inhibits histamine-evoked Ca^{2+} entry.

a. siRNA transfected HUVECs loaded with Fura-2 AM were treated with histamine (10 µM) in the absence of extracellular Ca^{2+} before Ca^{2+} add-back. Example trace for CRACR2A siRNA 1 (CR2A.si.1; N=11). **b.** Summary data (Mean ± SEM) for the experiments of the type illustrated in a showing measurements for the Ca^{2+} release and Ca^{2+} entry effects with CR2A.si.1 compared to scrambled controls (n/N=3/22; *P<0.05; NS, non-significant).

3.11. Impact of EFCAB4B-a on EC migration and tube formation

To investigate if there were any wider effects of EFCAB4B-a on EC function, the effect of EFCAB4B-a knockdown on EC tube formation and migration *in vitro* was investigated.

An *in vitro* co-culture assay was performed. For this assay HUVECs, which had been pre-treated with scrambled siRNA (sc.si.) or CRACR2A siRNA (CR2A.si.1) were seeded onto a layer of confluent fibroblasts. Over the course of 8 days, the endothelial cells formed tubular-like structures (white arrows, Figure 3-26), which are thought to mimic vessel growth *in vivo*. The tubes were quantified by measuring the mean tube length or area. Typically tubes measured approximately 4 mm/mm^2 in length and 0.11 mm^2/mm^2 in area in control cells. EFCAB4B-a knockdown significantly reduced both tube length and area by 10-12%. The data suggest that EFCAB4B-a positively modulates tube formation, which may be a function of its enhancing effect on VEGFR2.

To examine the effect of EFCAB4B-a on endothelial cell migration alone, HUVECs were transfected with either scrambled or 2 different CRACR2A siRNAs and seeded into 96 well plates. Forty-eight hours post-transfection a wound was made using the 'Wound-maker' (Essen) and migration was imaged using phase-contrast imaging software on the IncuCyte (Essen). Images were taken every 2 hours for 18 hours and the relative wound density was calculated. A small but significant effect was observed for si.2. but no effect was observed with si.1. (Figure 3-27).
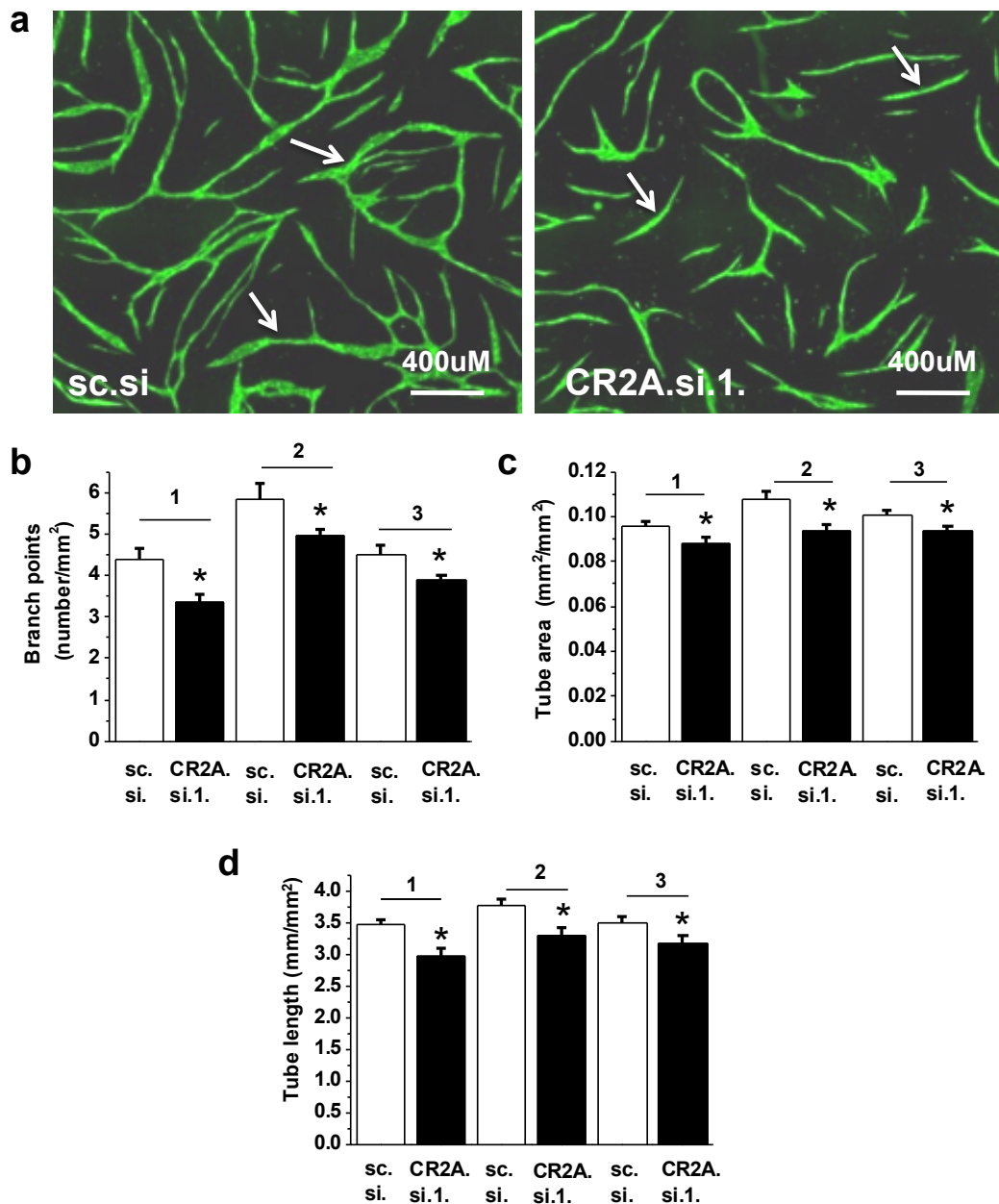
Figure 3-26 EFCAB4B-a enhances tube formation.

a. Representative example images showing HUVEC tube formation with CRACR2A (CR2A.si.1) or scrambled (sc.si.) siRNA. HUVECs are labelled in green by Alexa 488 anti-CD31 antibody. **b−d**. Summary histograms for 3 independent experiments (1-3; n=9 wells for sc.si. and 9 wells for CR2A.si.1. for each experiment) showing the effect of CRACR2A knockdown on mean tube length, branch points and mean tube area. Arrows point to tubes. *$P<0.05$. Data generated by Dr Jing Li.
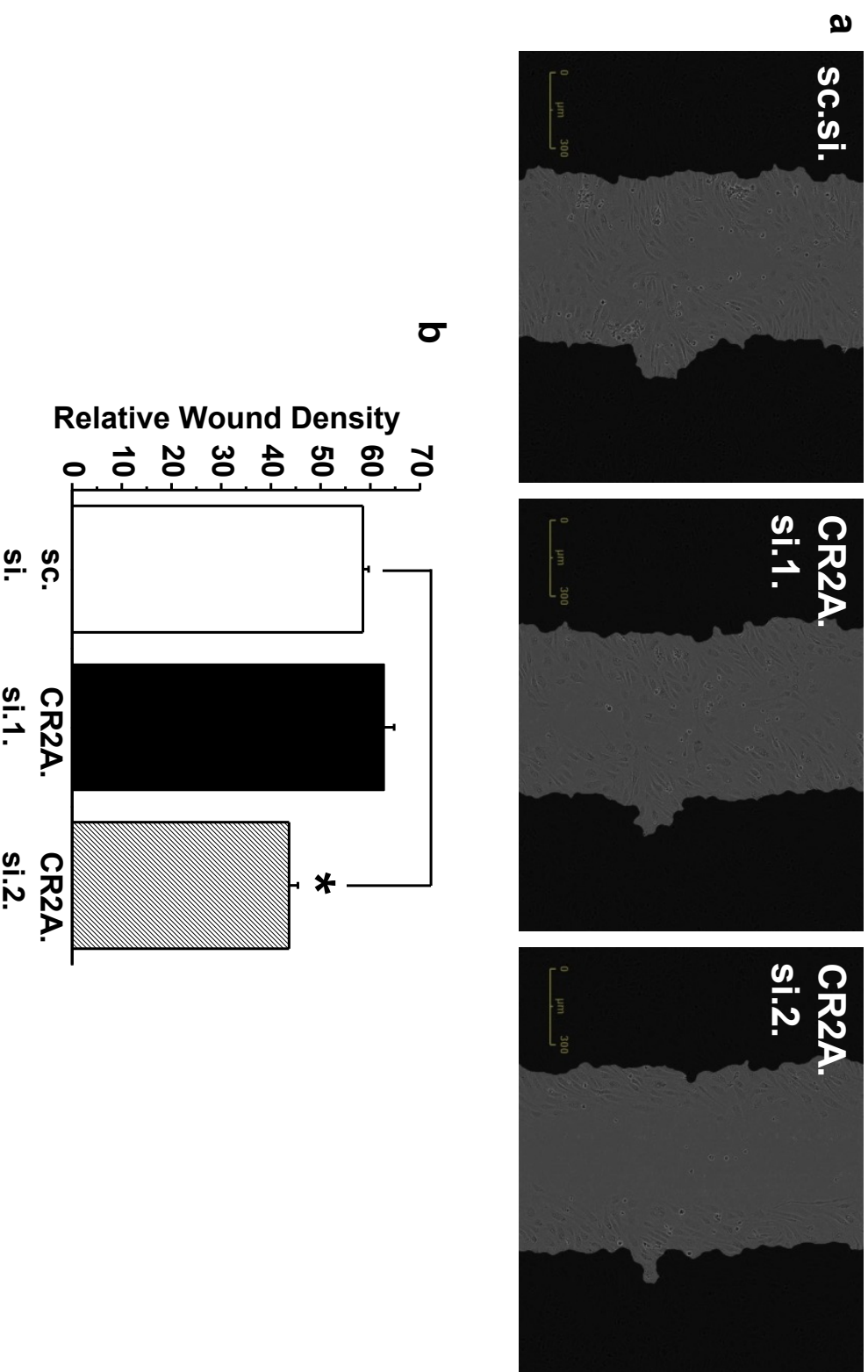
Figure 3-27 EFCAB4B-a may have a modest effect on endothelial cell migration.

HUVECs were transfected with either scrambled (sc.si.) or 2 different CRACR2A siRNAs (CR2A.si.1 and CR2A.si.2.). 48 hours post-transfection cells were seeded into a 96-well ImageLock plate and a wound was made using the WoundMaker (Essen). Migration of cells into the wound was measured every hour for 18 hours. **a.** Representative wound images at the 18 hour time point for sc.si. CR2A.si.1 and CR2A.si.2. **b.** Summary data (mean ± SEM) for the experiments of the type illustrated in a (n/N=3/18; *$P<0.05$). Scale bar 300 μm.

3.12. Discussion and Conclusions

The aim of this study was to investigate the role of CRACR2A as a regulator of SOCE in endothelial cells. In contrast to immune cells, endothelial cells did not express CRACR2A. However, this result led to discovery of a novel splice variant of the CRACR2A gene, EFCAB4B-a, which has distinct function from the previously described CRACR2A. The data from this study provide evidence that EFCAB4B-a is a previously unidentified Rab protein that is expressed on endothelial cell-specific WPBs and negatively influences the abundance of intracellular vWF, without effect on vWF release. Data also showed that EFCAB4B-a could regulate VEGFR2 and its downstream effectors.

3.12.1. CRACR2A gene

This study has revealed for the first time, experimental evidence that a longer splice variant of the CRACR2A gene exists. In fact, according to the Ensembl database, the CRACR2A gene contains a possible seven splice variants (ENSG00000130038). Two of the variants (46 kDa CRACR2A and 83 kDa EFCAB4B-a), which have been described in this thesis, have had their sequences confirmed and exist in the Consensus Coding DNA Sequence (CCDS) database. The CCDS database is one that contains human and mouse protein coding regions that have been consistently annotated and are of high quality (http://www.ncbi.nlm.nih.gov/CCDS/CcdsBrowse.cgi). However, according to Ensembl, another five transcripts may exist, two of which, are predicted to be protein coding. One of these has an incomplete CDS but the other has a predicted length of 462 amino acids and shares the identical N terminal sequence with CRACR2A and EFCAB4B-a, which encodes the Ca^{2+}-binding EF-hands domains. The predicted molecular mass of this variant is 53.8 kDa, which may explain one of the extra bands (approximately 60 kDa) observed on the Western blot with the anti-CRACR2A antibody (Figure 3-3). Since the 46 kDa CRACR2A protein was not detected, subsequent Western blots in this study were cut in half so that one half could be used with the anti-CRACR2A antibody and the other half with the anti-actin antibody as a loading

control. For this reason it could not be determined from these data whether or not the intermediate bands were suppressed by the CRACR2A siRNA. It would be interesting to address this since this protein may be involved in endothelial cell Ca^{2+} signalling. Another point regarding this 53.8 kDa variant is that the region in which its sequence differs from EFCAB4B-a, is where the extra serine was identified in the EFCAB4B-a sequence, suggesting that this may be an important splicing site. Further studies would be needed to determine if this predicted variant is really expressed and what its function is.

Previous data showed that CRACR2A is a binding partner for Orai1 and STIM1 in immune T cells and HEK293 cells (Srikanth et al., 2010) but in this study the 46 kDa CRACR2A protein could not be detected in endothelial cells. This finding raises the possibility that the regulation of CRAC channels differs according to cell type. It also suggests that the CRACR2A gene may be alternatively spliced in different cell types and it would be an interesting to determine how this occurs and whether the expression of the different variants can be controlled and switched on/off.

3.12.2. EFCAB4B-a runs with a greater mass than predicted

In this study, the protein band ascribed to EFCAB4B-a appeared larger than the predicted size of 83 kDa. Rab45, which has the same molecular mass also appeared larger than expected (Oshita et al., 2013a). This could be explained by the acidic nature of these proteins (EFCAB4B-a pI = 5.15; Rab45 pI = 4.83), since it has previously been demonstrated that acidic proteins can negatively affect SDS binding, resulting in a slower migration and an apparent greater mass (Armstrong and Roman, 1993). In this study, the data showed that the band could be significantly reduced following knockdown by two different siRNAs, generating confidence that it really was EFCAB4B-a.

3.12.3. EFCAB4B-a is a novel putative Rab protein

Sequence analysis showed that EFCAB4B-a differed from CRACR2A at its C-terminus where it contained a Rab domain. Several lines of evidence from this study suggest that EFCAB4B-a is a previously undiscovered Rab protein; firstly, Rab proteins contain conserved motifs and the EFCAB4B-a sequence contains all of these conserved Rab motifs including the GTP-binding motifs and the double cysteine (prenylation) motif at its C terminus, a region important in membrane targeting (Colicelli, 2004, Horgan and McCaffrey, 2011). Secondly, GTP binding is important for the localisation and function of Rab proteins and in this study, imaging data showed that by making a mutation in a conserved GTP binding motif (N658I) meant EFCAB4B-a no longer localised to WPBs but instead showed a general cytosolic distribution. Thirdly, the prenylation motif at the C terminus of Rab proteins is critical for their association with intracellular membranes and the data showed that tagging GFP to the C terminus of EFCAB4B-a, resulted in a cytosolic distribution with no localisation to WPBs. Should future biochemical experiments (which will be discussed in detail later) on EFCAB4B-a demonstrate that it has GTP-binding ability, then EFCAB4B-a may be renamed as Rab46.

3.12.4. EF-hand Rab proteins

Whilst EFCAB4B-a is larger than most of the 60 human Rab proteins (around 200-300 amino acids), it is a similar size to Rab44 and Rab45, which have predicted masses of 108 and 83 kDa respectively. Structurally, Rab44, Rab45 and EFCAB4B-a are predicted to be similar in that they all contain two EF-hands at their N termini and a Rab domain at their C termini. Currently no studies have investigated Rab44, only four publications exist for Rab45 (Nakamura et al., 2011, Oshita et al., 2013b, Shintani et al., 2007, Maat et al., 2008) and this is the first account of EFCAB4B-a.

3.12.5. EFCAB4B-a localises to WPBs and a peri-nuclear region: is there a connection?

A key finding from this study was the localisation of EFCAB4B-a on WPBs as revealed by the strong co-localisation between EFCAB4B-a and vWF. This colocalisation of EFCAB4B-a and vWF occurred in fewer than 50% of cells, however when it did occur, the mean Rcoloc value of 0.8 suggested the correlation or relationship between the two proteins was strong. Interestingly, phylogenetic analysis groups EFCAB4B-a protein with other Rab proteins that have been associated with WPBs: Rab3a-d and Rab27a (Figure 3-28). Five of these Rabs (Rab3a, 3d, 27a, 27b and 15) have reported roles in vWF secretion (reviewed in (Nightingale and Cutler, 2013), however I did not find a role for EFCAB4B-a in this process. Some caution is needed in interpreting these data however, since vWF is released from cells as long strings that remain cell attached, which means collecting samples of supernatant, may not accurately reflect the amount of vWF that has been released.

EFCAB4B-a is the first large EF-hand-containing Rab protein to be localised to WPBs and the significance of the Ca^{2+} binding domain would be an interesting future investigation.

EFCAB4B-a also colocalised with vWF in the peri-nuclear region. vWF has been observed in a cluster at the peri-nuclear region before (Rondaij et al., 2006, Vinogradova et al., 2000). Two previous publications have shown that when endothelial cells are stimulated with cAMP raising agents, WPBs travel along microtubules from the cell periphery to accumulate in a peri-nuclear cluster. The region where the WPBs were accumulating was identified as the microtubule organising centre (MTOC) (Rondaij et al., 2006). Interestingly, in a preliminary study looking at the localisation of EFCAB4B-a in endothelial cells, just 24 hours post transfection, I noticed that EFCAB4B-a localised to microtubule-like structures (Figure 3-29).

I hypothesise that the peri-nuclear location observed in this study is therefore the MTOC. This hypothesis is supported by staining results from this study that showed that EFCAB4B-a localised very close to the Golgi but was not colocalised with it, a finding that is consistent with reports that the MTOC is often found closely associated with the Golgi (Sutterlin and Colanzi, 2010).

Microtubules are involved in the transport of cargo around the cell – this cargo can travel in either direction along the microtubules, depending on the balance of activity of the motor proteins kinesin (outward, toward the cell periphery) and dynein (retrograde, toward the cell interior; (Bryantseva and Zhapparova, 2012). In the previous study by Rondaij *et al* it was found that the retrograde transport of WPBS towards the MTOC was dependent on the motor protein dynein (Rondaij et al., 2006).

If this peri-nuclear localisation observed in this study is indeed the MTOC, this suggests that overexpression of EFCAB4B-a favours retrograde transport of WBPs along microtubules and this may involve dynein. In support of this hypothesis, the EFCAB4B-a localisation observed at 24h post-transfection closely resembled the staining that has previously been observed with dynein-GFP (Ma and Chisholm, 2002).

In recent years interactions between microtubule motor proteins and Rab GTPases have been identified and these motor proteins are recognised as Rab effector molecules (Horgan and McCaffrey, 2011). For example, Rab6, which is a regulator in the retrograde transfer of endosomes from the Golgi to the endoplasmic reticulum, has been found to interact with dynein in the Golgi (Wanschers et al., 2008). Given further time, it would be interesting to investigate potential functional interactions between EFCAB4B-a and dynein. Figure 3-30 shows a schematic to illustrate the putative role of EFCAB4B-a in the trafficking of WPBs.

As an interesting side note, images in the Human Protein Atlas show that endogenous Rab45 (structurally very similar to EFCAB4B-a) is also localised to microtubules (http://www.proteinatlas.org/ENSG00000165105/subcellular)

whilst overexpression was identified in a peri-nuclear region (Shintani et al., 2007). These data suggest that EFCAB4B-a and Rab45 may have similar functions.

3.12.6. Could a possible interaction of EFCAB4B-a with dynein affect VEGFR2?

Dynein is also important for the transport of transcription factors to the nucleus. In this study, I found that in cells where EFCAB4B-a had been knocked down, VEGFR2 levels were suppressed. If EFCAB4B-a interacts with dynein, and dynein is responsible for the transport of transcription factors necessary for VEGFR2 expression then it is possible that knockdown of EFCAB4B-a would negatively influence the expression of VEGFR2.

3.12.7. Could EFCAB4B-a effects on VEGFR2 be due to regulation of membrane trafficking in the biosynthetic pathway?

In this study, EFCAB4B-a was found localised in a peri-nuclear localisation close to the Golgi. When EFCAB4B-a was knocked down, total VEGFR2 levels were suppressed. A similar observation was reported with one of the t-SNARE (soluble N-ethylmaleimide-sensitive factor attachment protein receptor) proteins, syntaxin-6 (Manickam et al., 2011). SNARE proteins are important for vesicle fusion and syntaxin-6 is localised predominantly in the Golgi and facilitates trans Golgi and post-Golgi vesicle fusion processes. Manickham *et al* (2011) found that in quiescent endothelial cells, around 25% of VEGFR2 is localised to the Golgi and colocalises with the trans-Golgi marker TFN46. They found that when they suppressed syntaxin-6 either by siRNA or by overexpressing the inhibitory cytosolic domain of syntaxin-6, then total cellular VEGFR2 levels were reduced by approximately 75% and VEGF-stimulated endothelial cell proliferation, migration and tube formation were all inhibited. Further to this they found that if they blocked lysosome function but not proteasome function, then this could reverse the inhibitory effect, suggesting that the VEGFR2 is being targeted to lysosome for degradation (Manickam et

al., 2011). It may therefore be possible that EFCAB4B-a is regulating the biosynthetic pathway of VEGFR2 in a similar manner to syntaxin-6 and this could offer another explanation as to why knocking down EFCAB4B-a suppresses total VEGFR2 levels.

3.12.8. Conclusions

This study has identified a novel putative Rab protein, EFCAB4B-a that is a product of the CRACR2A gene, but has distinct function from CRACR2A. EFCAB4B-a colocalised with vWF in endothelial WPBs but also in a peri-nuclear region, hypothesised to be the MTOC. Overexpression of a predicted GTP-deficient mutant showed a general cytosolic localisation suggesting that GTP-binding was important for EFCAB4B-a localisation to WPBs and the MTOC. I speculate that EFCAB4B-a interacts with the minus-end microtubule motor protein, dynein and favours the reverse trafficking of WPBs.

3.12.9. Future studies

Several lines of evidence suggest that EFCAB4B-a is a novel Rab protein, however the defining feature of Rab proteins is their ability to bind and hydrolyse GTP. The GTP binding ability of EFCAB4B-a has so far not been investigated but the fact that mutations in conserved GTP binding motifs changed the localisation of EFCAB4B-a from WPB expressing to cytosolic, suggests that binding GTP is important for the localisation and function of EFCAB4B-a. Future studies would involve generating a purified EFCAB4B-a protein and performing a GTP binding assay, which may be a colorimetric assay or a radioligand binding assay. Should EFCAB4B-a bind and hydrolyse GTP as predicted, it could be renamed as Rab46.

The exchange between GDP and GTP *in vivo* requires other regulatory proteins. Enzymes termed GEFs (guanine nucleotide exchange factors) and

GAPs (GTPase activating proteins) facilitate the inter-conversion by stimulating the release of bound GDP or the hydrolysis of bound GTP respectively (Pfeffer and Aivazian, 2004). Currently it is not known what the GEFs and GAPs are necessary for EFCAB4B-a so screening approaches and pull-down assays would be needed to determine these. It would certainly be interesting to investigate if there is any relationship between EFCAB4B-a and microtubule motor proteins such as dynein.

For Rabs to effectively bind their respective membranes they undergo post-translational modification in the form of prenylation. Prenylation involves the covalent addition of either a farnesyl (15 carbon) or geranylgeranyl (20 carbon) pyrophosphate and is critical for the function of the modified protein in cellular responses (Leung et al., 2006). EFCAB4B-a has the motif XXXCC, which is one of 6 different carboxyl-terminal motifs on human Rab proteins. To determine if prenylation is important for membrane targeting of EFCAB4B-a, cells would be treated with a statin and these cells should show a more diffuse distribution and only localise to the WPBs on washout of the drug.

To date, only 2 other Rab proteins have EF-hands and the role of these remains unknown. It will be interesting to investigate the role of the EF-hand in the function of EFCAB4B-a.
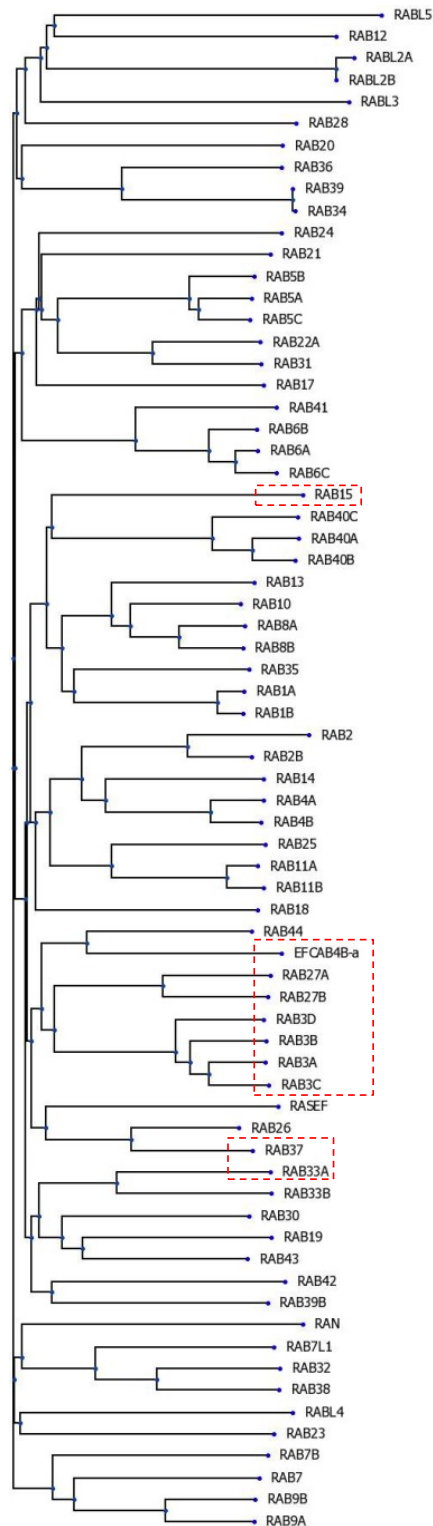
Figure 3-28 Phylogenic tree of Rab family members including the putative Rab family member EFCAB4B-a.

Rab protein sequences were aligned using Clustal Omega online software. The generated Newick tree file was uploaded to Phy.fi (Fredslund, 2006) to generate the phylogenic tree. Rab proteins that have been identified on WPBs are highlighted in the red boxes.
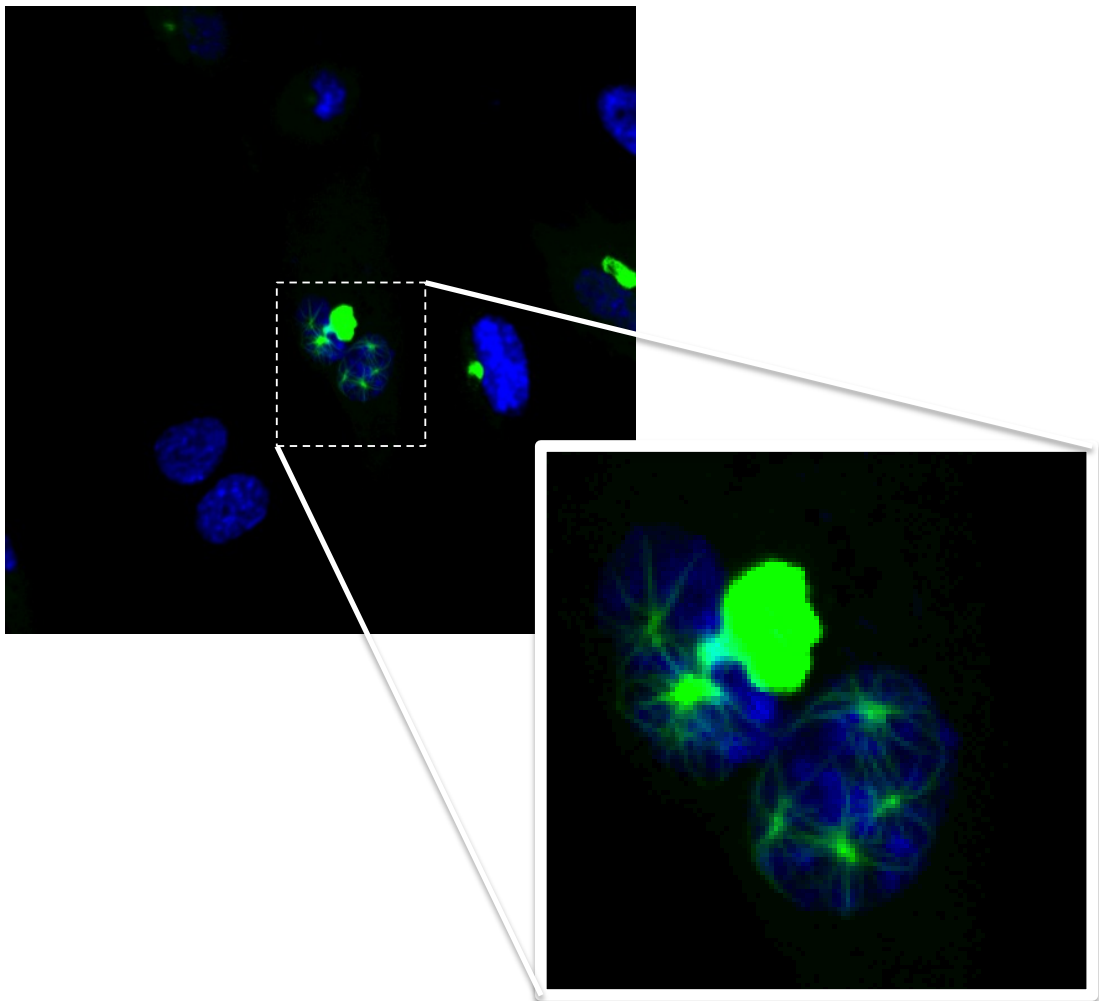
Figure 3-29 Localisation of EFCAB4B-a 24 hours post transfection.

HUVECs were transfected with EFCAB4B-a, fixed and immunostained 24 hours post-transfection with the anti-CRACR2A antibody (green). Nuclei were stained with DAPI (blue).
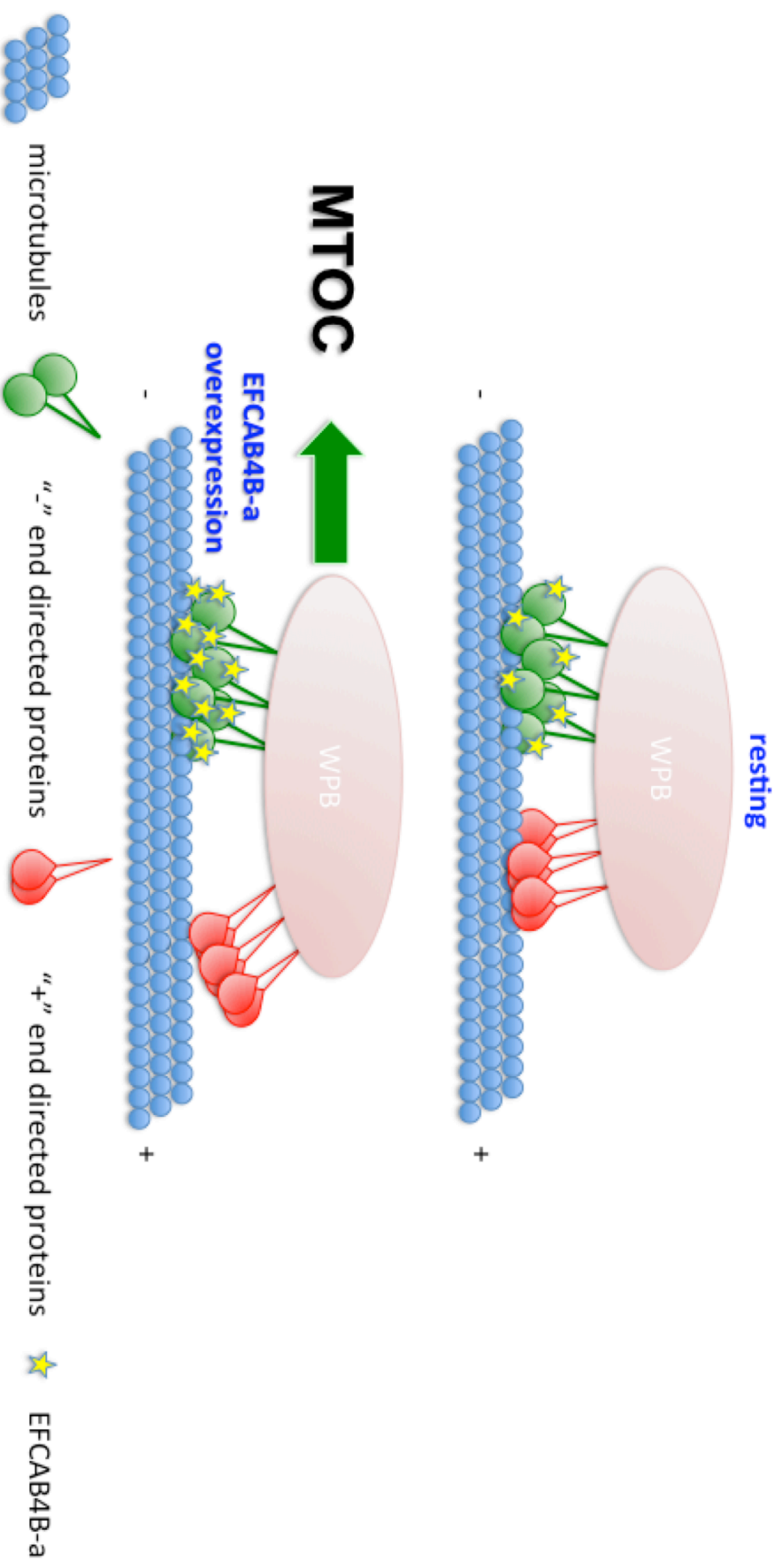
Figure 3-30 A proposed model showing a possible role of EFCAB4B-a in the trafficking of WPBs.

Hypothesis: During normal physiological conditions, EFCAB4B-a interacts with the microtubule minus-end protein dynein. When EFCAB4B-a is overexpressed, there is a stronger interaction with dynein favouring the reverse trafficking and aggregation of WPBs at the MTOC.

CHAPTER 4. GOLLI-MYELIN BASIC PROTEIN IS A POSITIVE REGULATOR OF VEGFR2 EXPRESSION

4.1. Introduction

Myelin basic proteins (MBPs), encoded by the *MBP* gene on chromosome 18, are important structural proteins that make up the myelin sheath surrounding oligodendrocytes and Schwann cells in the central nervous system (CNS). The *MBP* transcription unit however is part of a complex genetic locus that is highly conserved in mouse and human called *Golli*, which stands for *g*ene expressed in the *oli*godendrocyte *li*neage-MBP (Campagnoni et al., 1993, Pribyl et al., 1993). Figure 4-1 shows a diagrammatic representation of the *golli-MBP* gene and the products of its alternative splicing. The *golli-MBP* gene is found upstream of the *MBP* gene and gives rise to at least 2 splice variants. In mouse these splice variants are called *BG21* and *J37* (Campagnoni et al., 1993). Humans have an identical splice variant to mouse *BG21* called *HOG5* or variant 8 and a splice variant which is clearly related to *J37* but contains 2 additional exons and is called *HOG7* or variant 7 (Pribyl et al., 1993). Mouse and human golli-MBP peptides share 79% amino acid similarity (Pribyl et al., 1993). Unlike the classic MBP peptides that are found almost exclusively in the CNS, the golli-MBPs are also expressed in cells and organs of the immune system, including the thymus and spleen, which suggests that golli-MBPs have a different biological role to the classic MBPs (Feng et al., 2000, Pribyl et al., 1993).

4.1.1. Golli-MBP as a negative regulator of SOCE

Whilst the physiological role of golli-MBP is still largely unknown, there is mounting evidence to suggest that golli-MBP regulates intracellular Ca^{2+}. In T lymphocytes, golli-MBP has been identified as a negative regulator of store-operated Ca^{2+} influx (Feng et al., 2004, Feng et al., 2006). A study using golli-deficient mice, showed that ablation of the *golli-MBP* gene in T cells resulted in hyper-proliferation, which could be attributed to an enhanced store-operated

Ca^{2+} entry (SOCE; (Feng et al., 2006). Furthermore, over-expression of *golli-MBP* inhibited SOCE and mutation of the myristolylation site disrupted its ability to associate with the plasma membrane, thereby reversing its inhibitory action on Ca^{2+} influx (Feng et al., 2006). In line with this study, golli-MBP was found associated with the ER Ca^{2+} sensor STIM1 in HeLa cells (Walsh et al., 2010). A bimolecular fluorescence complementation assay using HeLa cells and tagged golli-MBP and STIM1 showed that upon thapsigargin stimulation, golli-MBP and STIM1 came together, but this did not occur in the absence of cell stimulation (Walsh et al., 2010) suggesting that golli-MBP may regulate SOCE. In addition, co-localisation of STIM1 and golli-MBP was observed at the plasma membrane and overexpression of golli-MBP reduced the thapsigargin-induced SOCE, an effect that could be rescued by over-expression of STIM1 (Walsh et al., 2010).

4.1.2. Golli-MBP as a positive regulator of Ca^{2+} entry in oligodendrocytes

Golli-MBP also plays a role in regulating Ca^{2+} influx in oligodendrocyte precursor cells (OPCs) where over-expression resulted in enhanced Ca^{2+} influx with no effect on Ca^{2+} release from intracellular stores (Paez et al., 2007). As observed in studies on T cells, the myristoylation site of golli-MBP was important for its ability to modulate Ca^{2+} homeostasis (Paez et al., 2007). Using golli-overexpressing mice (JOE mice) it was shown that golli-MBP could increase Ca^{2+} entry, both through store-operated Ca^{2+} channels and voltage-operated Ca^{2+} channels (Paez et al., 2009). Another study showed that SOCE was greater in OPCs derived from JOE mice compared to control mice and that this SOCE was dependent on TRPC1, since suppression of TRPC1 using siRNA or a blocking antibody abolished SOCE (Paez et al., 2011).

4.1.3. Aims

SOCE is an important Ca^{2+} entry mechanism for endothelial processes such as migration, proliferation and angiogenesis. STIM1 and Orai1 underlie the main Ca^{2+} entry mechanism in endothelial cells, and Ca^{2+} entry through Orai1 channels is important for endothelial cell migration and angiogenesis (Li et al.,

2011). TRPC1 is also important in angiogenesis (Yu et al., 2010). It is currently unknown if golli-MBPs are expressed and functional in endothelial cells. The aim of this chapter was therefore to investigate golli-MBP in endothelial cells.
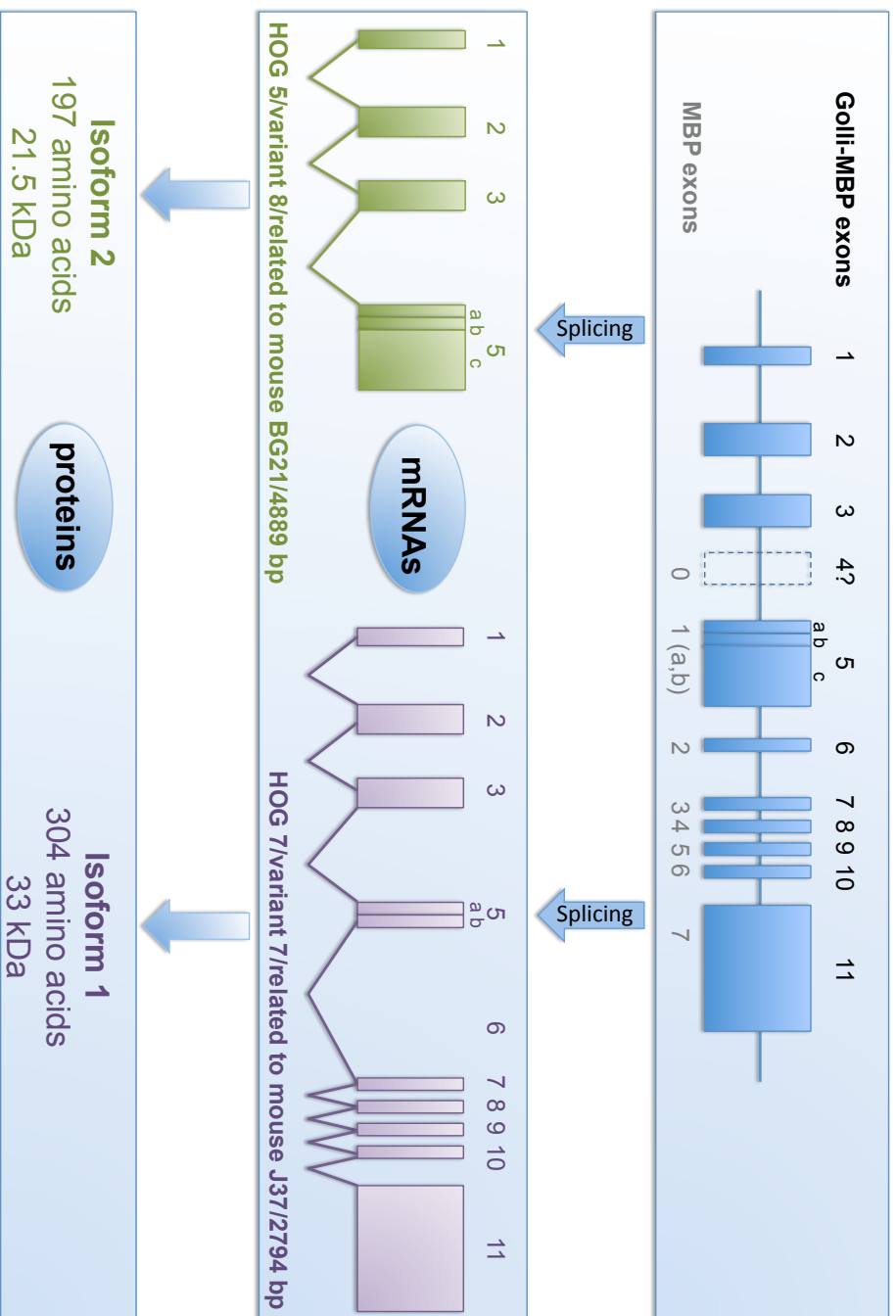
Figure 4-1 Diagram showing the exon structure of the myelin basic protein gene and the golli products generated from this gene.

Adapted from Landry *et al* (1998) (Landry et al., 1998).

4.2. Golli-MBP is expressed in human endothelial cells

Two variants of human golli-MBP, variant 7 and variant 8 have previously been detected in cells and tissues outside of the CNS. To determine if golli-MBP was expressed in endothelial cells, RT-PCR primers were designed in a region that would detect both the long (variant 7) and short (variant 8) transcripts. RT-PCR was performed on cDNA from a range of micro- and macro-vascular endothelial cells and electrophoresis gel images confirm mRNA expression of golli-MBP in all endothelial cells tested (Figure 4-2).

As a first step to determining the functional significance of golli-MBP, the role of golli-MBP in Ca^{2+} influx in response to the major physiological agonist, VEGF-A_{165}, was investigated. HUVECs were transfected with either scrambled or 2 different golli-MBP siRNAs. Knockdown was quantified by RT-PCR and results from 3 independent experiments showed a mean knockdown of golli-MBP at the mRNA level of $75 \pm 2\%$. Cells were loaded with the Ca^{2+} indicator dye Fura-2 AM and Ca^{2+} responses were measured on the FlexStation. In the presence of extracellular Ca^{2+}, VEGF-A_{165} evoked a transient Ca^{2+} elevation followed by a sustained Ca^{2+} response. Both the transient and sustained responses were inhibited in golli-MBP deficient cells compared to controls (Figure 4-3). The next step was therefore to investigate the mechanism underlying this response.

4.3. Golli-MBP is a mild negative regulator of SOCE in HUVECs

Previous studies on immune T cells and HeLa cells showed that golli-MBP had a negative regulatory role on SOCE (Feng et al., 2004, Feng et al., 2006, Walsh et al., 2010) and studies on OPCs showed a positive regulatory role on Ca^{2+} influx (Paez et al., 2011, Paez et al., 2009, Paez et al., 2007). To investigate whether the inhibition of VEGF-A_{165}-induced Ca^{2+} response observed in golli-MBP deficient cells was due to an effect on SOCE, Ca^{2+} imaging experiments were performed as follows. Two different golli-MBP siRNAs and a scrambled control siRNA were individually transfected into HUVECs. Seventy-two hours post-transfection, cells were loaded with the Ca^{2+} indicator dye Fura-2-AM and

SOCE was measured in multi-well intracellular Ca^{2+} ($[Ca^{2+}]_i$) measurement experiments using the FlexStation. To measure SOCE, cells were treated with the SERCA inhibitor TG in the absence of extracellular Ca^{2+} to evoke a release of Ca^{2+} from intracellular stores. Extracellular Ca^{2+} was then added back and the Ca^{2+} entry response measured. The results showed that golli-MBP had no effect on Ca^{2+} release from stores but knockdown of golli-MBP had a small potentiating effect on the Ca^{2+} entry response (Figure 4-4). As a control, STIM1 siRNA-transfected cells showed a significant inhibition of the SOCE response (Figure 4-4).

4.4. Golli-MBP is strong positive regulator of VEGF-A$_{165}$-induced Ca^{2+} responses

Since golli-MBP had only a mild effect on SOCE, another mechanism must exist to explain the large inhibition of the VEGF-A$_{165}$-induced Ca^{2+} response. To investigate the VEGF-A$_{165}$ response in more detail, VEGF-A$_{165}$ was applied in the absence of extracellular Ca^{2+} followed by Ca^{2+} add-back to see individually the effect on Ca^{2+} release and Ca^{2+} entry. In golli-MBP deficient cells, the VEGF-A$_{165}$-induced Ca^{2+} release response was reduced compared to control cells (Figure 4-5). As a control, Ca^{2+} responses in STIM1 deficient cells showed no change in the Ca^{2+} release response compared to scrambled controls (Figure 4-5). On re-addition of extracellular Ca^{2+}, mimicking SOCE, a rise in intracellular Ca^{2+} was observed in control cells but this response was significantly smaller in golli-MBP deficient cells (Figure 4-5). As expected, STIM1 deficient cells showed a significant inhibition of the Ca^{2+} entry response (Figure 4-5c).

To determine whether the knockdown of golli-MBP specifically inhibited VEGF-A$_{165}$-evoked Ca^{2+} release from stores, a second agonist, histamine was used. No significant inhibition of histamine-evoked Ca^{2+} release was observed in golli-MBP deficient cells compared to controls (Figure 4-6) suggesting that golli-MBP preferentially affects VEGF-A$_{165}$-induced Ca^{2+} responses.

4.5. Golli-MBP is a strong positive regulator of VEGFR2 expression

A possible reason why VEGF-A$_{165}$-evoked Ca^{2+} release was reduced in cells deficient in golli-MBP could be that golli-MBP regulates VEGFR2 expression. To test this, Western blotting was performed with an anti-VEGFR2 (anti-KDR) antibody on HUVEC lysates from cells treated with scrambled or golli-MBP siRNAs. Results showed that cells deficient in golli-MBP had significantly reduced expression of VEGFR2 compared to controls (Figure 4-7). Therefore it is suggested that the reason for the inhibition of Ca^{2+} release was lower expression of VEGFR2.
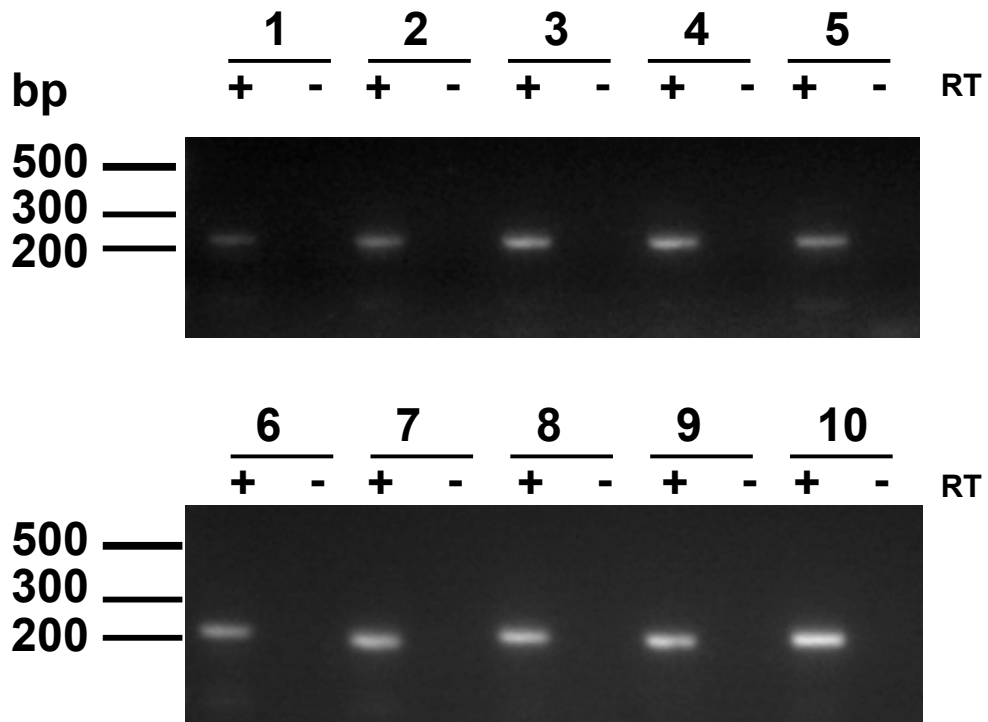
Figure 4-2 Expression of golli-MBP in human endothelial cells.

Gel electrophoresis showing golli-MBP products from RT-PCR analysis of RNA isolated from endothelial cells derived from **1**. HPAEC (pulmonary artery), **2**. HUAEC (umbilical artery), **3**. HDBEC (dermal blood), **4**. HDLEC (dermal lymphatic), **5**. HUVEC (umbilical vein), **6**. HBdMEC (bladder microvascular), **7**. HPMEC (pulmonary microvascular), **8**. HDMEC (dermal microvascular), **9**. HCMEC (cardiac microvascular), **10**. HCoMEC (colonic microvascular). Reactions were performed with (+) or without (-) reverse transcriptase (RT). Expected size of golli-MBP product was 232 bp.
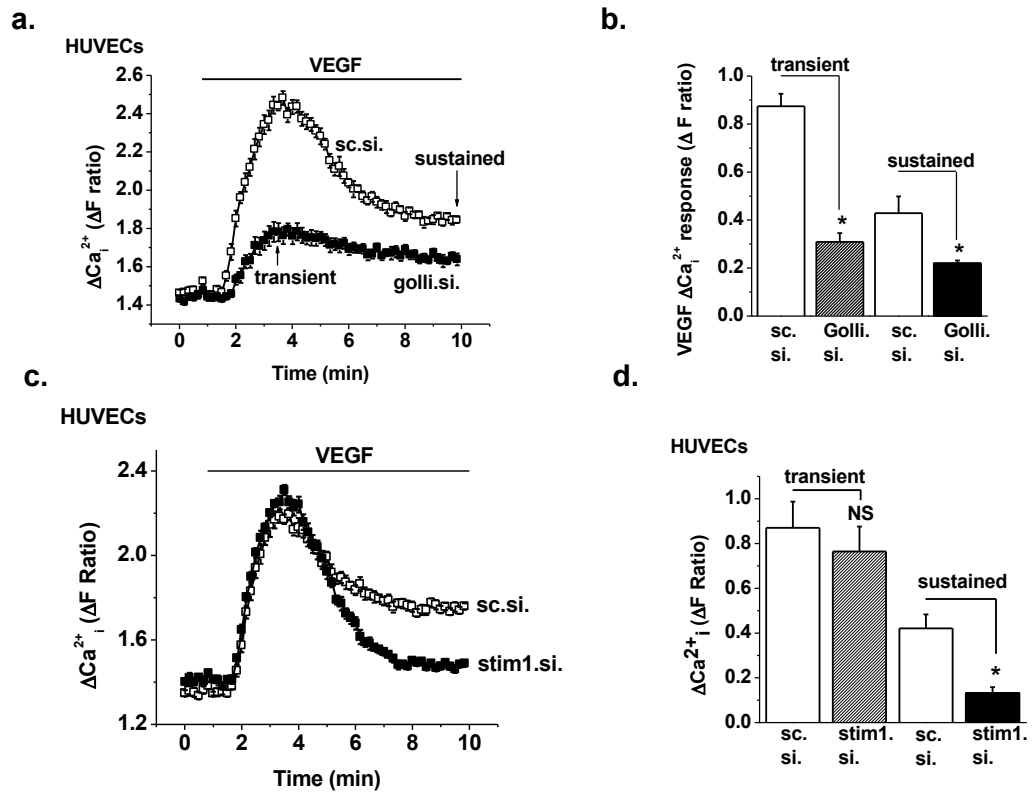
Figure 4-3 Knockdown of golli-MBP inhibits VEGF-A$_{165}$-induced Ca^{2+} response.

a. Example trace showing 30 ng/ml VEGF-A$_{165}$-induced Ca^{2+} response in 1.5 mmol/L extracellular Ca^{2+} with golli siRNA (golli.si.1) or scrambled (sc.si) siRNA (N=7). **b**. Summary data for the experiment of the type illustrated in a. showing measurements for the transient and sustained effects of VEGF-A$_{165}$ with golli.si. (n/N=4/24; *P<0.05) **c**. Example trace showing 30 ng/ml VEGF-A$_{165}$-induced Ca^{2+} response in 1.5 mmol/L extracellular Ca^{2+} with STIM1 siRNA (STIM1.si.) or scrambled (sc.si) siRNA (N=6). **d**. Summary data for the experiment of the type illustrated in c. showing measurements for the transient and sustained effects of VEGF-A$_{165}$ with STIM1.si. (n/N=5/36; *P<0.05; NS, non-significant).
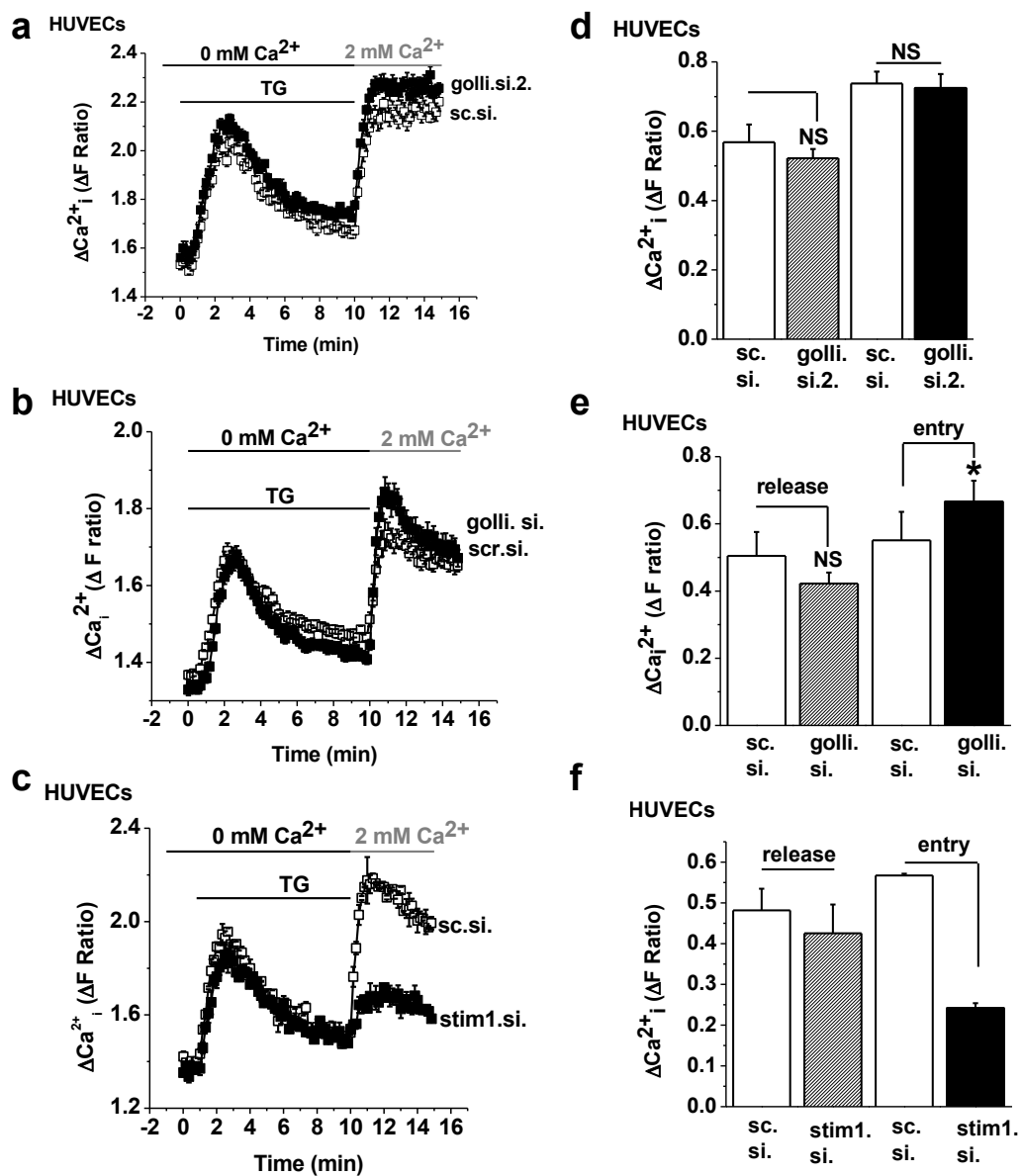
Figure 4-4 Golli-MBP has a small negative effect on SOCE in HUVECs.

a - c. Examples of Ca^{2+} imaging traces showing 1 µmol/L thapsigargin (TG) induced store-depletion in zero mmol/L Ca^{2+} followed by 2 mmol/L Ca^{2+} add-back. Traces show responses in cells treated with scrambled siRNA (sc.si) plus one of the following: golli-MBP siRNA 1 (golli.si.1; a; N=11), golli-MBP siRNA 2 (golli.si.2; b; N=6) or STIM1 siRNA (STIM1.si; c; N=2). (**c**) is repeated from Fig.3.7b. **d – f.** Summary data for the experiments of the type illustrated in a - c. showing measurements for the TG-induced Ca^{2+} release and Ca^{2+} entry effects in cells treated with golli.si.1 (n/N=5/26; d), golli.si.2 (n/N=4/20; e) or STIM1.si. knockdown (n/N=2/8; f) where *P<0.05 and NS, non-significant).
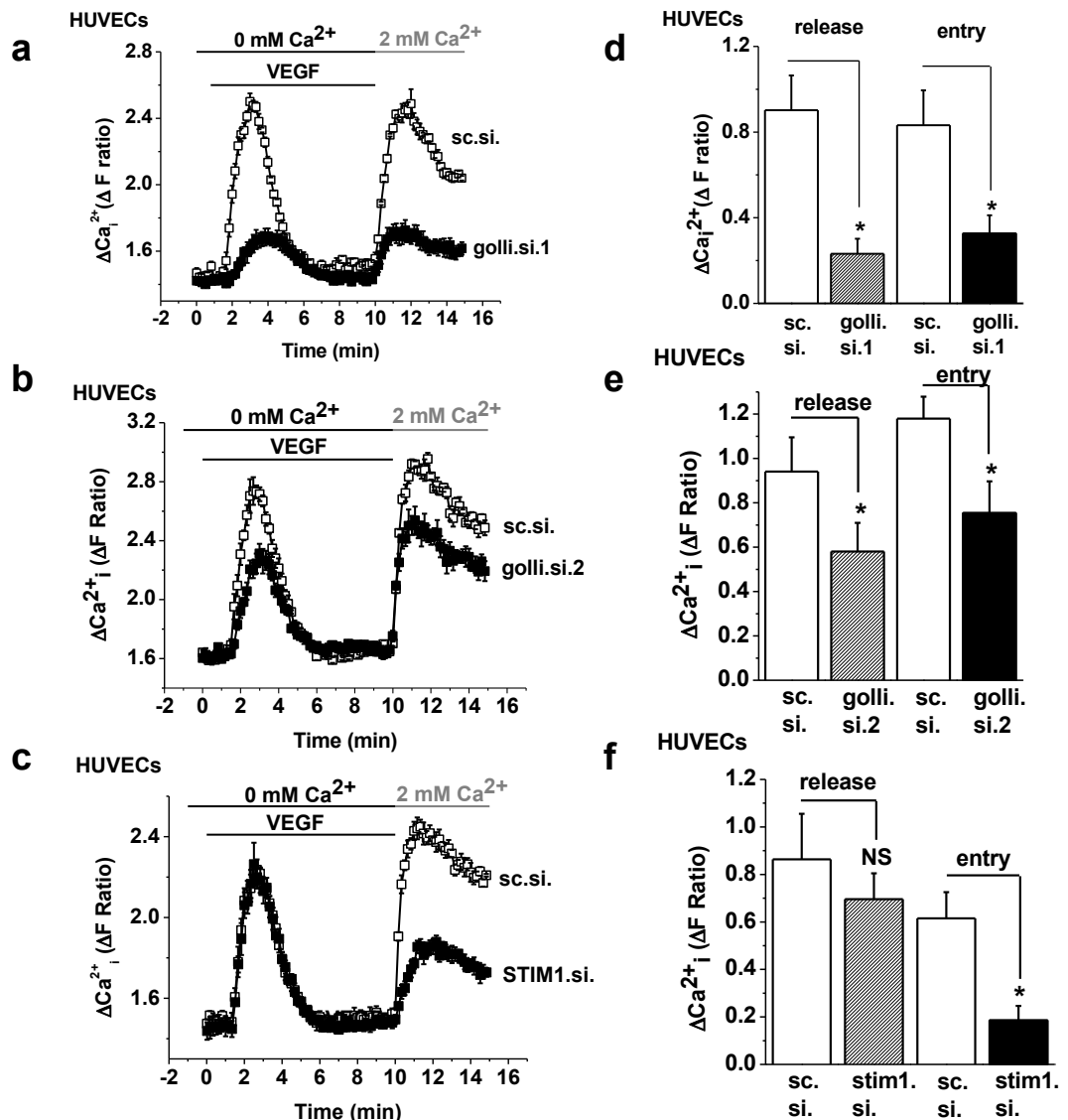
Figure 4-5 Knockdown of golli-MBP inhibits VEGF-A$_{165}$-induced Ca^{2+} response.

a - c. Example traces showing 30 ng/ml VEGF-A$_{165}$-induced store-depletion in zero mmol/L Ca^{2+} followed by 2 mmol/L Ca^{2+} addback. Traces showing cells treated with scrambled siRNA (sc.si) with either golli-MBP siRNA 1 (golli.si.1; a; N=4), golli-MBP siRNA 2 (golli.si.2; b; N=4) or STIM1 siRNA (STIM1.si.;c; N=4). **d − f.** Summary data for the experiments of the type illustrated in a - c. showing measurements for the VEGF-A$_{165}$-evoked Ca^{2+} release and Ca^{2+} entry effects with golli.si.1 (d; n/N = 5/27), golli.si.2 (e; n/N = 3/16) or STIM1.si (f; n/N = 3/11) where *P<0.05 and NS, non-significant.
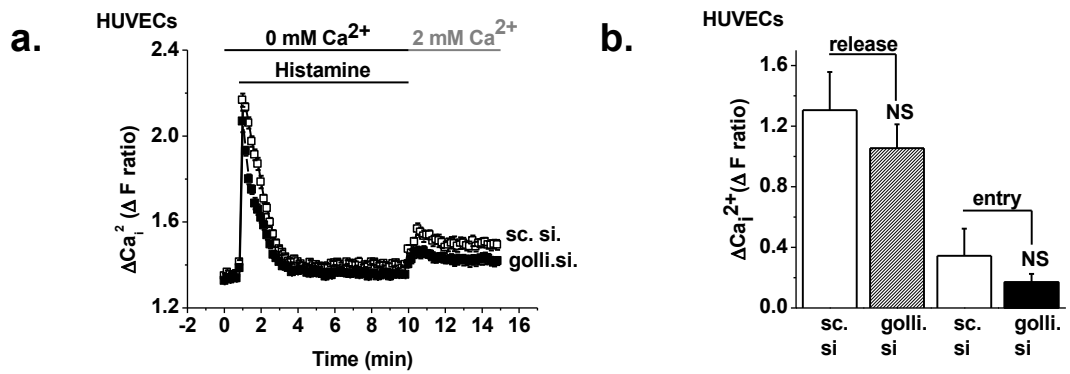
Figure 4-6 Knockdown of golli-MBP has an insignificant effect on histamine-evoked Ca^{2+} response.

a. Example trace showing 10 µM histamine-evoked Ca^{2+} release and Ca^{2+} entry in cells treated with either scrambled siRNA (sc.si) or golli-MBP siRNA (golli.si. N=11) **b.** Summary data for the experiment of the type shown in a showing measurements for the histamine-evoked Ca^{2+} release and Ca^{2+} entry (n/N=3/22; NS, non-significant).
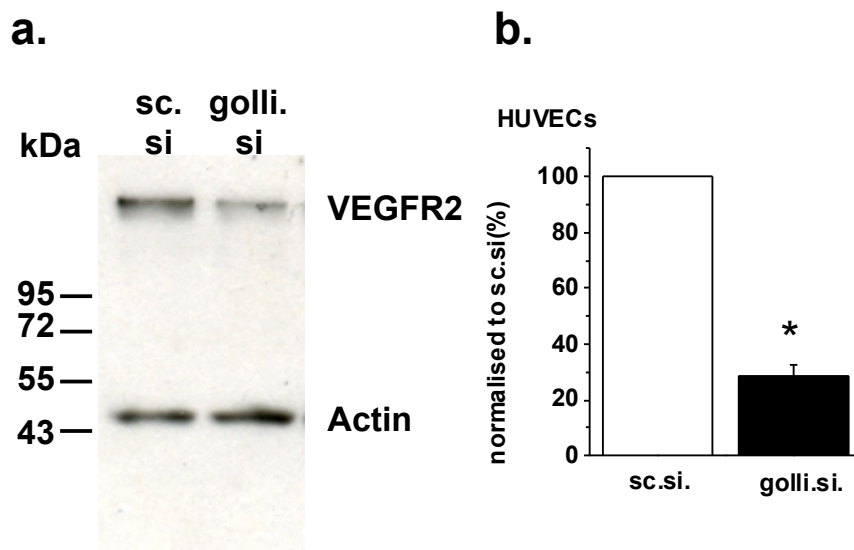
Figure 4-7 Knockdown of golli-MBP reduces VEGFR2 expression.

a. Western blot showing the expression of VEGFR2 in HUVECs treated with scrambled siRNA (sc.si) or golli-MBP siRNA (golli.si). Actin was used as a loading control. **b**. Quantified Western blot data showing VEGFR2/Actin ratio in cells treated with sc.si or golli.si. (n=4; *$P<0.05$).

4.6. Discussion and Conclusions

The main findings from this study are that golli-MBP is expressed in human endothelial cells; that golli-MBP positively regulates VEGFR2 and that golli-MBP has a small negative effect on SOCE.

Golli-MBP was discovered in the early 1990s and one of the main characteristics distinguishing it from the classic MBPs was its expression in a number of different cell types. However, this is the first study to demonstrate expression of golli-MBP in endothelial cells.

There remains an incomplete understanding regarding the functional role of golli-MBPs but a large number of studies point to a role in regulating Ca^{2+} homeostasis. In T cells and HeLa cells it was found that golli-MBP negatively regulated SOCE (Feng et al., 2004, Feng et al., 2006, Walsh et al., 2010). The data presented in this chapter demonstrate a small but significant enhancement of TG-evoked SOCE in HUVECs with one of the golli-MBP siRNAs. The small enhancement compared to that observed in T cells is likely due to methodology, since this study used siRNA to reduce golli-MBP gene expression compared to T cells derived from a golli-knockout mouse. The mechanism by which golli-MBP regulates SOCE is not entirely clear but a recent study showed that golli-MBP can interact with STIM1 complexes at the plasma membrane. The main Ca^{2+} entry pathway in HUVECs is through CRAC channels where STIM1 is the ER Ca^{2+} sensor that triggers activation of Orai1 channels (Li et al., 2011). It is therefore possible that golli-MBP negatively regulates CRAC channels in endothelial cells. Further studies are needed to determine if this is the case. This would not be the first account of a protein regulating CRAC channels as 2 other proteins: the EF-hand proteins CRACR2A and junctate have both been found to regulate CRAC channel activity (Srikanth et al., 2012, Srikanth et al., 2010).

VEGF is a major signalling cytokine in endothelial cells and VEGF-stimulated Ca^{2+} entry occurs through Orai1 ion channels (Li et al., 2011). If golli-MBP was a negative regulator of SOCE in endothelial cells, then an enhancement of VEGF-evoked Ca^{2+} entry might also have occurred. Instead however, knockdown of golli-MBP reduced both the VEGF-induced Ca^{2+} release and subsequent Ca^{2+} entry response. This was in contrast to STIM1 that, as expected, only inhibited the SOCE response. Knockdown of golli-MBP had no effect on histamine-evoked Ca^{2+} release, which suggested that golli-MBP could be involved in the regulation of VEGFR2, the primary receptor for VEGF in endothelial cells. In line with this, the Western blot data showed that the VEGFR2 protein was suppressed in cells that had been treated with golli-MBP siRNA. It remains to be determined whether this suppression occurs at the transcriptional or translational level.

In conclusion, golli-MBP may be an important regulator of endothelial cell Ca^{2+} entry and VEGFR2 expression. Any mechanism that results in reduced VEGFR2 could be relevant for potential new cancer therapies, since this would impair VEGF-driven angiogenesis.

CHAPTER 5. IDENTIFYING NOVEL TRPC6 CHANNEL BLOCKERS

5.1. Introduction

TRPC6 is a 931 amino acid protein that is a member of the TRPC subfamily of TRP ion channels, which comprises TRPC1 – 7. TRPC6 shares around 70-80% sequence homology with TRPC3 and TRPC7 (Trebak et al., 2003). Human and mouse TRPC6 channels share 93% sequence similarity (Hofmann et al., 1999). TRPC6 is widely expressed in the central nervous system and cardiovascular system, and expression has also been detected in the lungs, ovaries and testis (Dietrich and Gudermann, 2007, Garcia and Schilling, 1997, Onohara et al., 2006, Reiser et al., 2005, Riccio et al., 2002, Sours et al., 2006, Zhou et al., 2008).

5.1.1. Structural and biophysical properties of TRPC6

Like other TRPC channels, TRPC6 is predicted to have 6 transmembrane spanning segments with a cation-permeable ion pore located between transmembrane segments 5 and 6 (TM5 and 6) (Dietrich and Gudermann, 2007). TRPC6 has 2 TRP box domains, an ankyrin repeat domain, a coiled-coil domain and a calmodulin and IP_3R binding site (Dietrich and Gudermann, 2007) (Figure 5-1). To form an ion channel, four TRPC6 proteins come together around a central ion channel pore (Beech, 2013). Alternatively, TRPC6 can also form ion channels with TRPC3 and TRPC7 subunits, or indeed other ion channel family subunits, for example Orai1 generating ion channels with distinct biophysical and functional properties (Beech, 2013, Liao et al., 2008, Liao et al., 2007). The native composition of these channels will differ from tissue to tissue and the physiological and pathophysiological relevance of these various compositions remains to be determined (Eder and Groschner, 2008). This chapter will focus on homomeric TRPC6 channels only.

Biophysically TRPC6 currents are both inwardly- and outwardly-rectifying and show a typical S-shaped current-voltage (I-V) relationship with a reversal potential near 0 mV, constituting a non-selective cation channel (Boulay et al., 1997, Hofmann et al., 1999). Human TRPC6 channels have a single channel conductance of around 35 pS as observed in symmetrical 120 mM Cs^+ solutions (Hofmann et al., 1999). TRPC6 channels are permeable to Ca^{2+}, Cs^+, Na^+ and K^+ and show greatest selectivity for Ca^{2+} with a P_{Ca}/P_{Na} in the order of 4-5 (Hofmann et al., 1999).

5.1.2. TRPC6 channel modulation

One of the first observations made following the cloning of TRPC6 in 1997 was that TRPC6 is not activated by store-depletion (Boulay et al., 1997, Hofmann et al., 1999). Electrophysiological studies on both mouse and human TRPC6 showed that currents were not induced with the SERCA inhibitor thapsigargin, the Ca^{2+} ionophore ionomycin, PIP_2 or IP_3 (Boulay et al., 1997, Hofmann et al., 1999). TRPC6 is therefore not considered a store-operated Ca^{2+} channel. Instead, TRPC6 is activated following G-protein coupled receptor stimulation, and a number of receptors have been linked to TRPC6 including muscarinic (Boulay et al., 1997), adrenergic (Inoue et al., 2001) and purinergic receptors (Inoue et al., 2001). Stimulation of tyrosine kinase receptors by growth factors, for example VEGF, has also been shown to activate TRPC6 (Ge et al., 2009, Hamdollah Zadeh et al., 2008). Receptor-activated TRPC6 currents are blocked with the phospholipase C (PLC) inhibitor U73122, but are not blocked with inhibitors of PKC, suggesting that TRPC6 is mainly coupled to PLC activation of diacylglycerol (DAG) and less so to IP_3 or the IP_3Rs (Hofmann et al., 1999, Jung et al., 2002). On this note, TRPC6 can be directly activated by the membrane-permeable analogue of DAG, 1-oleoyl-2-acetyl-sn-glycerol (OAG; (Jung et al., 2002) or by the DAG lipase inhibitor RHC80267 (Inoue et al., 2001). Other lipid activators for TRPC6 include: arachidonic acid and its metabolites 20-HETE and 11,12-EET (Basora et al., 2003, Fleming et al., 2007, Inoue et al., 2009), lysophosphatidylcholine (LPC; (Chaudhuri et al., 2008),

lipopolysaccharide (Tauseef et al., 2012) and c2-ceramide (Samapati et al., 2012). PIP_3 and Ca^{2+}/calmodulin have also been suggested as modulators of TRPC6 channel activity (Kwon et al., 2007). TRPC6 is also modulated by oxidative stress: a study by Graham *et al* (2010) showed that currents through TRPC6 could be augmented by H_2O_2 in a concentration-dependent manner, suggesting that TRPC6 may be more active in an oxidative environment (Graham et al., 2010). Finally, TRPC6 is modulated by intracellular Ca^{2+} concentrations and high concentrations have a negative effect on channel activity, while low concentrations enhance activity (Shi et al., 2004). Figure 5-1 highlights some of the positive and negative modulators of TRPC6.

5.1.3. TRPC6 function in endothelial cells

TRPC6 is important in VEGF-stimulated angiogenesis, as evidenced by two independent studies which overexpressed dominant negative TRPC6 and showed a significant inhibition of VEGF-stimulated tube formation *in vitro* with both micro- and macrovascular endothelial cells (Ge et al., 2009, Hamdollah Zadeh et al., 2008). A recent study has shown that TRPC6 is important for mediating lipopolysaccharide/Toll-like receptor 4–stimulated lung vascular permeability and lung inflammation through NF-κB (Tauseef et al., 2012).

5.1.4. Therapeutic potential

TRPC6 knockout mice are viable, have a broadly normal phenotype, are fertile and produce normal litters (Dietrich et al., 2005), which suggests that the TRPC6 gene is not essential for life. However, overexpression of TRPC6 has been linked to idiopathic pulmonary arterial hypertension, a disease characterised by excessive smooth muscle cell proliferation due to overload of Ca^{2+} (Yu et al., 2004). In addition, a mutation in the TRPC6 gene (P112Q), which results in enhanced Ca^{2+} entry, has been linked to focal segmental glomerulosclerosis (FSG), a disease affecting the kidneys (Winn et al., 2005). The fact that complete loss of TRPC6 is not lethal, but overexpression or mutations are detrimental, suggests that pharmacological manipulation of

TRPC6 may offer a new avenue for therapeutic intervention for the treatment these diseases.

5.1.5. Pharmacology

Flufenamate, a known cation channel blocker, has been to shown to activate TRPC6, but has no effect on TRPC3 or TRPC7 (Inoue et al., 2001). The active ingredient of St John's wort, hyperforin also activates TRPC6 (Leuner et al., 2007). Inhibitors of TRPC6 include lanthanum (La^{3+}), gadolinium (Gd^{3+}) and cadmium (Cd^{2+}) ions, which have IC_{50}s of 4, 1.9 and 253 µM respectively (Inoue et al., 2001). The non-selective cation channel blockers, SKF-96365 and 2-APB, also block TRPC6 channels along with the PLC inhibitor U73122 (Clapham, 2007b, Inoue et al., 2001).

5.1.6. Identifying novel TRPC6 channel blockers

Accumulating evidence including the gene mutation information, *in vitro* and *in vivo* studies suggests that TRPC6 is an important ion channel in vasculature physiology and pathophysiology. However, there remains a lack of selective and potent channel blockers. Identifying novel TRPC6 channel blockers would be beneficial both to fundamental research, to learn and understand more about the functioning of this channel and may also lead to the development of new therapeutics for cardiovascular disease, cancer or other conditions such as FSG. High throughput screening is one approach for the identification of novel channel blockers. Another approach is to mine the literature for molecules, which have shown efficacy *in vivo* or in the clinic but where the mechanism of action or target of the drug remains unknown. One advantage of the latter approach is that the compound will have already passed safety screens. A compound of this type is carboxyamidotriazole. A third approach is to investigate the mechanism of action of herbal or dietary substances that have beneficial effects on health, for example flavonoids found in fruits, vegetables and wine, which are associated with a decreased risk for the development of

cardiovascular disease (Hertog et al., 1993, Knekt et al., 1996, Rimm et al., 1996, Yochum et al., 1999).
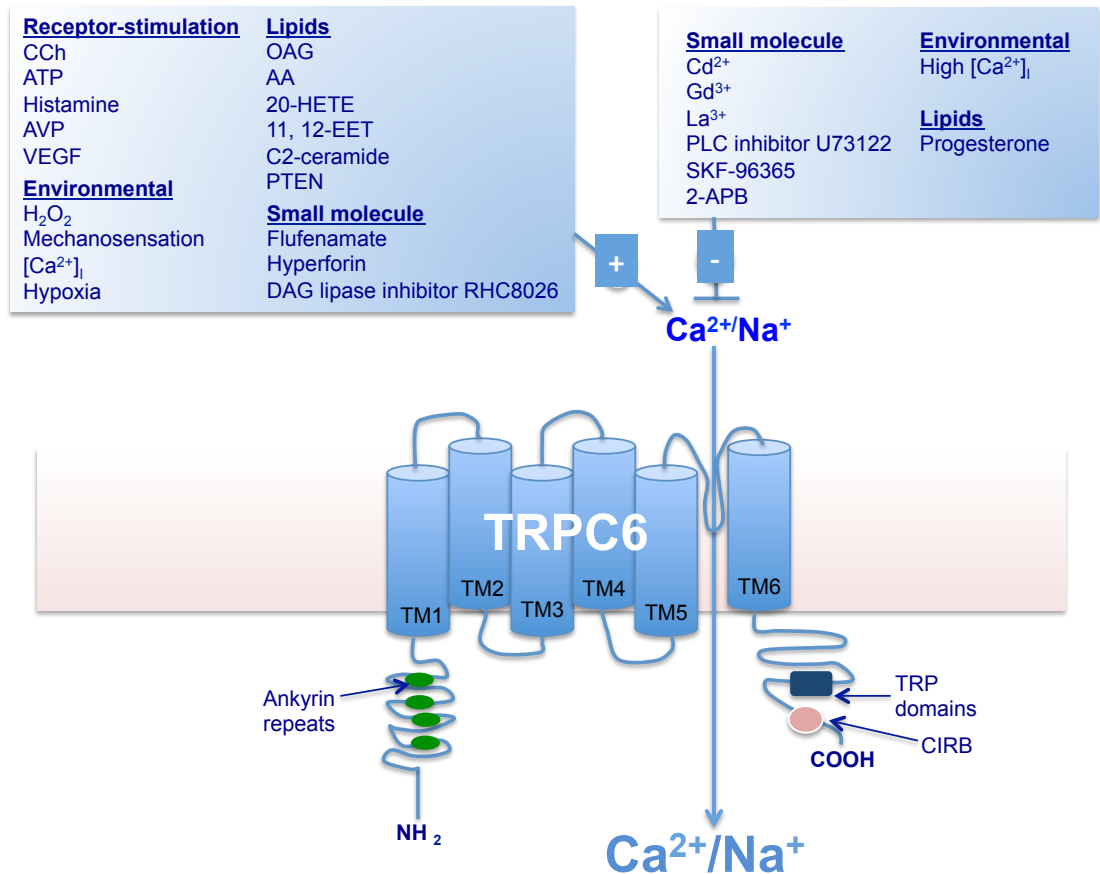
Figure 5-1 TRPC6 channel structure showing positive and negative modulators.

TRPC6 contains 6 transmembrane domains (TM1-TM6) with the channel pore between TM5 and 6. The amino terminal of TRPC6 is cytosolic and contains 4 ankyrin repeat domains and a coiled-coil region. The carboxy terminus is also cytosolic and contains 2 TRP boxes and a calmodulin and IP_3 receptor binding domain (CIRB). Shown in the top left is a list of positive TRPC6 modulators and in the top right, a list of negative TRPC6 modulators.

5.1.7. Carboxyamidotriazole

Carboxyamidotriazole (CAI; Figure 5-4a), also known as L-651,582, was identified in a large pharmaceutical screen that was set up to find novel anti-cancer drugs (Kohn and Liotta, 1990). Initial studies showed that CAI could prolong the life of mice bearing ovarian cancer by 220% compared to untreated mice (Kohn and Liotta, 1990). A large number of studies followed which showed that CAI was effective at inhibiting the development, growth and spread of cancer *in vivo* (Kohn et al., 1995, Kohn and Liotta, 1990, Kohn et al., 1992, Luzzi et al., 1998, Perabo et al., 2005, Qin et al., 1999). Because of the good safety profile and low toxicity effects observed with CAI, this compound was investigated in clinical trials. A large number of trials have taken place, looking at the effects of CAI alone or in combination with other anti-cancer therapies, and the overall results so far have shown some disease stabilisation in various cancers including pancreaticobiliary carcinomas, renal cell carcinoma, melanoma, ovarian cancer and non-small cell lung cancer (Hussain et al., 2003, Kohn et al., 1996).

The mechanism of action for CAI remains incompletely understood but several lines of evidence suggest that CAI affects intracellular Ca^{2+}. Firstly, one of the initial studies on CAI showed that low micromolar concentrations of CAI could block Ca^{2+} entry that is stimulated either by muscarinic receptor agonists or by the Ca^{2+} ionophore A23187 (Felder et al., 1991). Secondly, VEGF-A$_{165}$-induced Ca^{2+} responses in endothelial cells could be blocked by pre-treatment with CAI (Faehling et al., 2002). Thirdly, CAI blocked fMet-Leu-Phe-stimulated Ca^{2+} entry into leukocytes (Hupe et al., 1991). Fourth, CAI was able to block L-type Ca^{2+} channels in guinea-pig atrial cells (Hupe et al., 1991). In addition, Wu *et al* (1997) showed that CAI caused a generalised inhibition of receptor-mediated Ca^{2+} elevation to epidermal growth factor and bradykinin (Wu et al., 1997). Finally, CAI has been shown to inhibit Ca^{2+} entry and mitochondrial Ca^{2+} uptake (Mignen et al., 2005).

There is also substantial evidence that CAI, through the inhibition of Ca^{2+} influx, can inhibit endothelial cell proliferation and angiogenesis: several groups have shown that CAI can strongly inhibit VEGF- and fibroblast growth factor (FGF)-induced endothelial cell proliferation and tube formation (Afzal et al., 2010, Bauer et al., 2000, Faehling et al., 2002, Fiorio Pla et al., 2008). In addition, studies by Fiorio-Pla *et al* (2008 and 2010) showed that CAI caused complete inhibition of arachidonic acid induced Ca^{2+} entry in endothelial cells, and that pre-treatment of breast cancer derived endothelial cells (BTECs) with 1 µM CAI completely abolished BTEC motility in a wound healing assay (Fiorio Pla et al., 2010, Fiorio Pla et al., 2008).

Exactly how CAI inhibits Ca^{2+} influx is not clear. One study shows evidence that CAI works by inhibiting IP_3 formation with no effect on PLC activation (Faehling et al., 2002), whilst another suggests that CAI has no effect on IP_3 formation and may therefore act by blocking Ca^{2+} through receptor-operated ion channels (Hupe et al., 1991). In the recent study by Fiorio-Pla *et al* (2010), it was suggested that CAI may exert its inhibitory effects by blocking endothelial Ca^{2+} permeable channels and the authors postulate that the channel could be TRPV1, TRPV4, TRPC3 or TRPC6 (Fiorio Pla et al., 2010). In guinea-pig atrial cells, it has been shown by patch clamp technique that CAI can block L-type Ca^{2+} channels (Hupe et al., 1991). There has been no study to date that has investigated whether CAI directly blocks any of the endothelial cell Ca^{2+} permeable channels. Owing to the evidence that TRPC6 is involved in angiogenesis, the aim of the first part of this chapter was to investigate if CAI inhibits TRPC6 channels. TRPC5 and TRPV4 were also investigated. Ca^{2+} imaging and whole cell patch clamp recordings on HEK cells overexpressing TRPC6 or TRPC5 or CHO cells overexpressing TRPV4 were used to address these aims.

5.1.8. Galangin

Galangin is a flavonoid found in high concentrations in honey (Kim et al., 2006). Several studies have suggested that galangin has several health benefits

including anti-cancer and anti-inflammatory effects and also decreases the risk for developing cardiovascular disease including stroke and hypertension (Hertog et al., 1993, Knekt et al., 1996, Rimm et al., 1996, Yochum et al., 1999). Studies have suggested that galangin works by modulating intracellular Ca^{2+}. In one study looking at contractile responses of pig bladder it was found that galangin inhibited carbachol- and electrical field stimulated contractions in a concentration-dependent manner (Dambros et al., 2005). In this study they observed that galangin could inhibit responses in the absence of extracellular Ca^{2+}, suggesting that galangin may exert its effect via ryanodine receptors (Dambros et al., 2005). In another study it was found that galangin could inhibit voltage-gated $Ca_v1.2$ channels with an IC_{50} of 13.4 µM (Saponara et al., 2011) whereas the structurally related flavonoids kaempferol and myricetin stimulated $Ca_v1.2$ channels with EC_{50}s of 4.4 and 16 µM, respectively, with the differences in responses being attributed to small changes in the chemical structures of these compounds (Saponara et al., 2011). The second part of this chapter investigates whether galangin and structurally related compounds have any effect on TRPC6 channels.

5.2. TRPC6-mediated Ca^{2+} entry in overexpressing HEK cells

HEK cells stably expressing mouse TRPC6 (mTRPC6) were used in Ca^{2+} measurement experiments on the FlexStation. TRPC6 channels were activated with either the membrane-permeable analogue of DAG, OAG or with carbachol, a muscarinic receptor agonist that stimulates TRPC6 indirectly through activation of PLC_β and production of DAG. In Ca^{2+} measurement experiments, OAG evoked a concentration-dependent increase in intracellular Ca^{2+} (Figure 5-2 a,b). A concentration of 100 µM OAG also evoked a Ca^{2+} response in wild-type HEK cells (Figure 5-2 c,d), which suggests that wild-type HEK cells express endogenous TRPC6 or related channels. However, the response in these cells was smaller and lower concentrations had no effect (Figure 5-2 c,d), indicating that the OAG-evoked Ca^{2+} entry in the TRPC6 expressing cells was primarily through TRPC6 channels.

Carbachol also evoked a concentration-dependent rise in intracellular Ca^{2+}. However, unlike OAG, which evoked a gradual Ca^{2+} entry response, the response to carbachol was rapid and transient, followed by a sustained elevation of the intracellular Ca^{2+} concentration (Figure 5-3a). The EC_{50} generated from the maximal carbachol response was 1.2 µM (Figure 5-3b). In the absence of extracellular Ca^{2+}, only the transient response was observed, with no sustained component. This was likely due to carbachol-evoked Ca^{2+} release from stores following activation of PLC_β and increased levels of IP_3. Carbachol also evoked a Ca^{2+} response in wild-type HEK cells, but this response was transient and showed no sustained component (Figure 5-3d), indicating that the sustained increase in Ca^{2+} concentration in Figure 5-3a was due to carbachol-induced activation of TRPC6 channels.
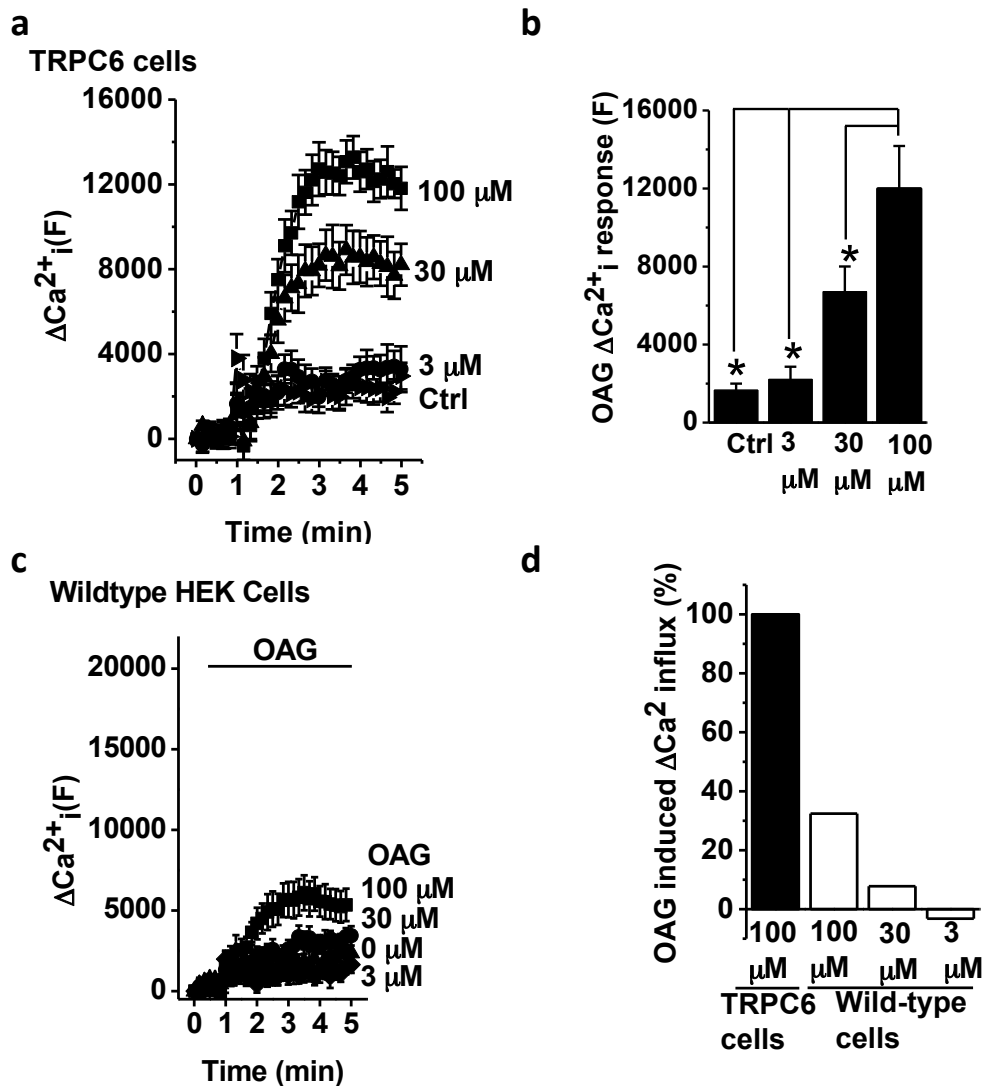
Figure 5-2 OAG induces Ca^{2+} entry through TRPC6 channels.

a. Example time-series graph showing the effect of OAG (0, 3, 30 and 100 µM) in HEK293 cells overexpressing mTRPC6 (N=6). **b.** Summary data for experiments of the type illustrated in a (n/N = 4/23; *$P<0.05$). **c.** Example time-series graph showing the effect of OAG (0, 3, 30 and 100 µM) in wild-type HEK293 cells (N=6). **d.** Summary data for experiments of the type illustrated in c, normalised to the 100 µM OAG response in a (n/N = 2/11).
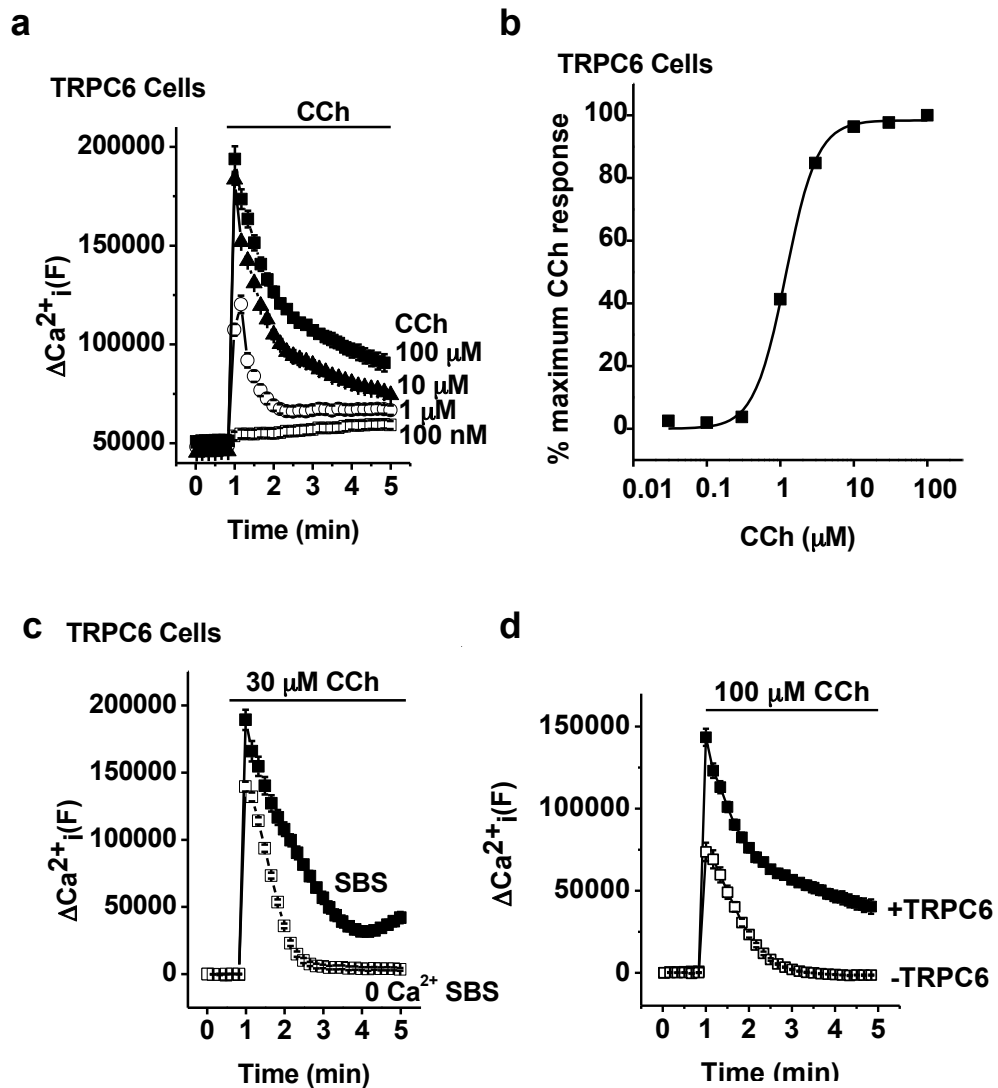
Figure 5-3 Carbachol induces Ca^{2+} entry through TRPC6 channels.

a. Example time-series graph showing the effect of carbachol (0.1, 1, 10 and 100 µM) in HEK293 cells overexpressing mTRPC6 (N=6). **b.** Concentration-response curve showing % maximum carbachol response, EC$_{50}$ = 1.2 µM (N=6). **c**. Example of carbachol-induced Ca^{2+} response in 0 mM extracellular Ca^{2+} **d.** Example of carbachol-induced Ca^{2+} response in wildtype HEK cells compared to 100 µM carbachol response in TRPC6 cells (N=6).

5.3. CAI inhibits TRPC6-mediated Ca^{2+} entry

To determine if CAI (Figure 5-4a) could block TRPC6 channels, cells were pre-treated with CAI or vehicle control for 30 minutes before FlexStation recordings. Pre-treatment of TRPC6 cells with 10 µM CAI significantly inhibited the OAG-induced Ca^{2+} entry compared to DMSO controls (Figure 5-4b,c). CAI also inhibited the carbachol-evoked Ca^{2+} entry in a concentration dependent manner, with an IC$_{50}$ of 1.89 µM for the sustained Ca^{2+} response, compared to vehicle control (Figure 5-5 a-b).

5.4. CAI inhibits TRPC6-mediated ionic currents

To further investigate the blocking effect of CAI on TRPC6-mediated Ca^{2+} responses, electrophysiological studies were performed. TRPC6 channels were activated by 10 µM OAG in a 1.5 mM Ba^{2+} containing extracellular solution in the whole cell patch clamp experiment (Figure 5-6a). Ba^{2+} has a similar permeability to Ca^{2+} through mTRPC6 (Inoue et al., 2001). OAG activated large but transient inward and outward currents (mean current = 1.16 ± 0.21 nA at -80 mV; mean current = 3 ± 0.35 nA at +80 mV; n=11), and the resulting current voltage relationship (I-V) was doubly rectifying, S shaped and reversed close to 0 mV as reported previously (Figure 5-6b) (Hofmann et al., 1999, Boulay, 2002). A high concentration (100 µM) of Gd^{3+} completely inhibited the current. Since OAG-induced currents were of a transient nature, it meant it was not possible to bath-apply CAI to the open channel in the conventional manner. Therefore cells were pre-treated with 10 µM CAI (or vehicle control) for 10 minutes prior to OAG application. Cells that were pre-treated with CAI showed significantly smaller current amplitudes in response to OAG compared to cells pre-treated with DMSO alone (Figure 5-6 c-e).
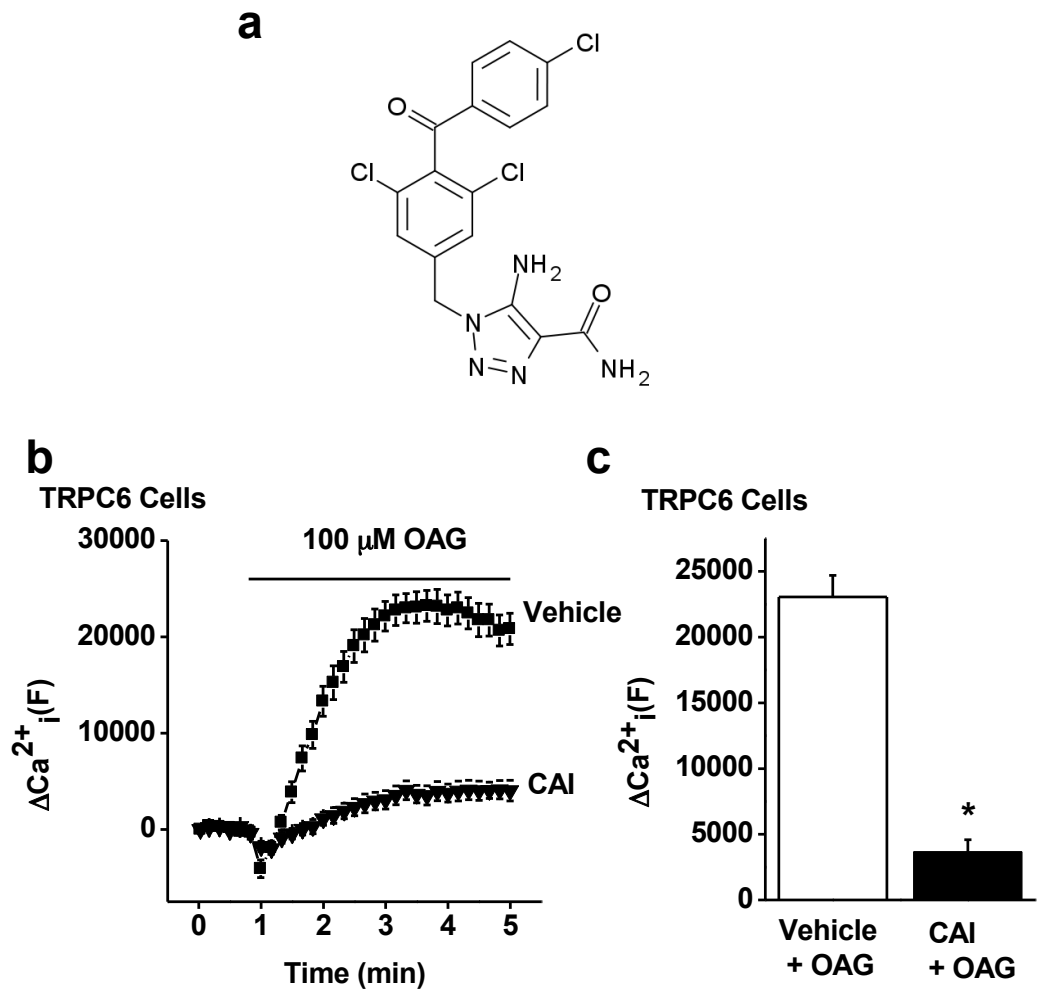
a. chemical structure for CAI. **b**. Example time-series trace showing inhibition of OAG-induced Ca^{2+} entry by 10 μM CAI (n/N=4/10). **c**. Summary data for the experiments of the type illustrated in b (n/N=4/10; *$P<0.05$).

Figure 5-4 CAI inhibits OAG-induced Ca^{2+} entry through TRPC6 channels.

a. chemical structure for CAI. **b**. Example time-series trace showing inhibition of OAG-induced Ca^{2+} entry by 10 μM CAI (n/N=4/10). **c**. Summary data for the experiments of the type illustrated in b (n/N=4/10; *$P<0.05$).
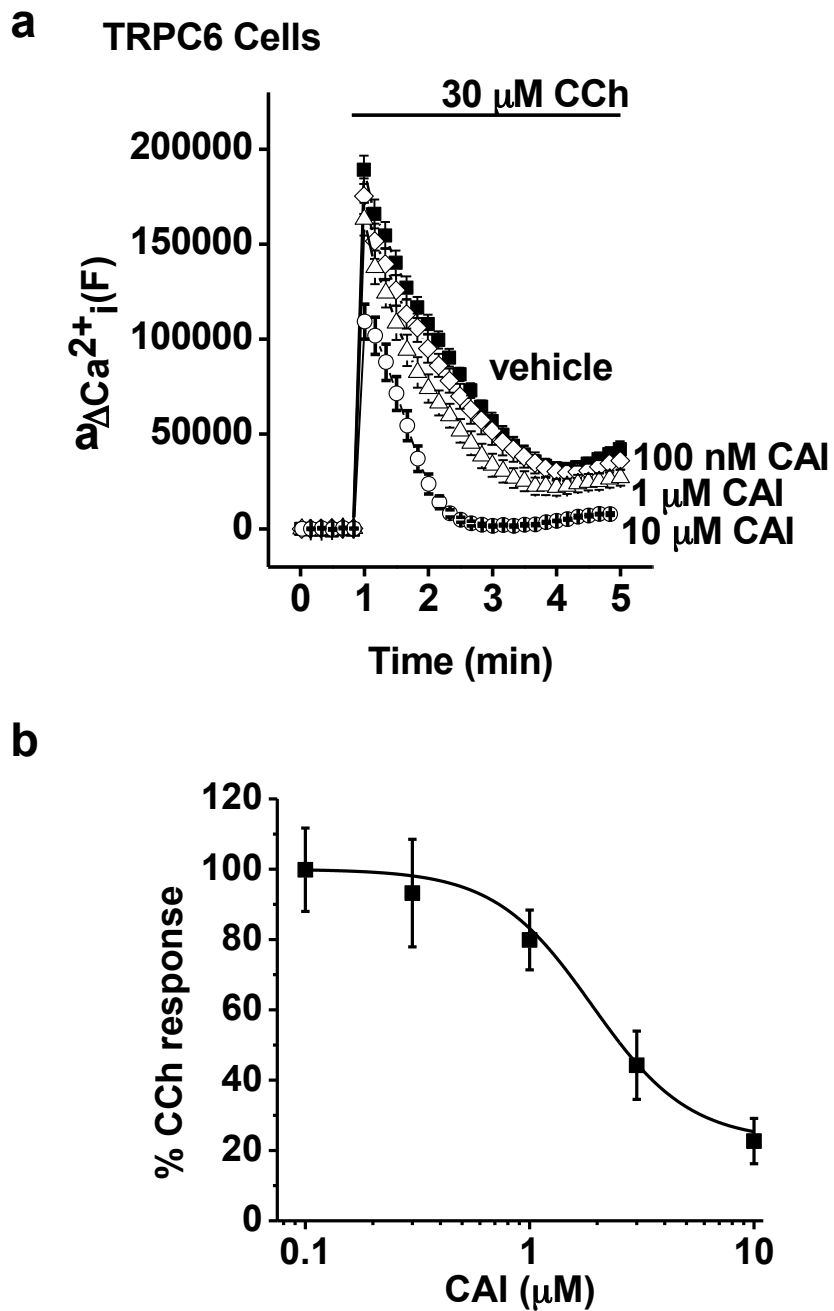
Figure 5-5 CAI inhibits carbachol-stimulated Ca^{2+} responses through TRPC6 channels.

a. Example time-series trace showing concentration-dependent inhibition of CAI on carbachol-induced Ca^{2+} response (N=6). **c**. Concentration-response curve for CAI measuring the sustained Ca^{2+} response (IC_{50} = 1.89 μM; n/N=3/24).
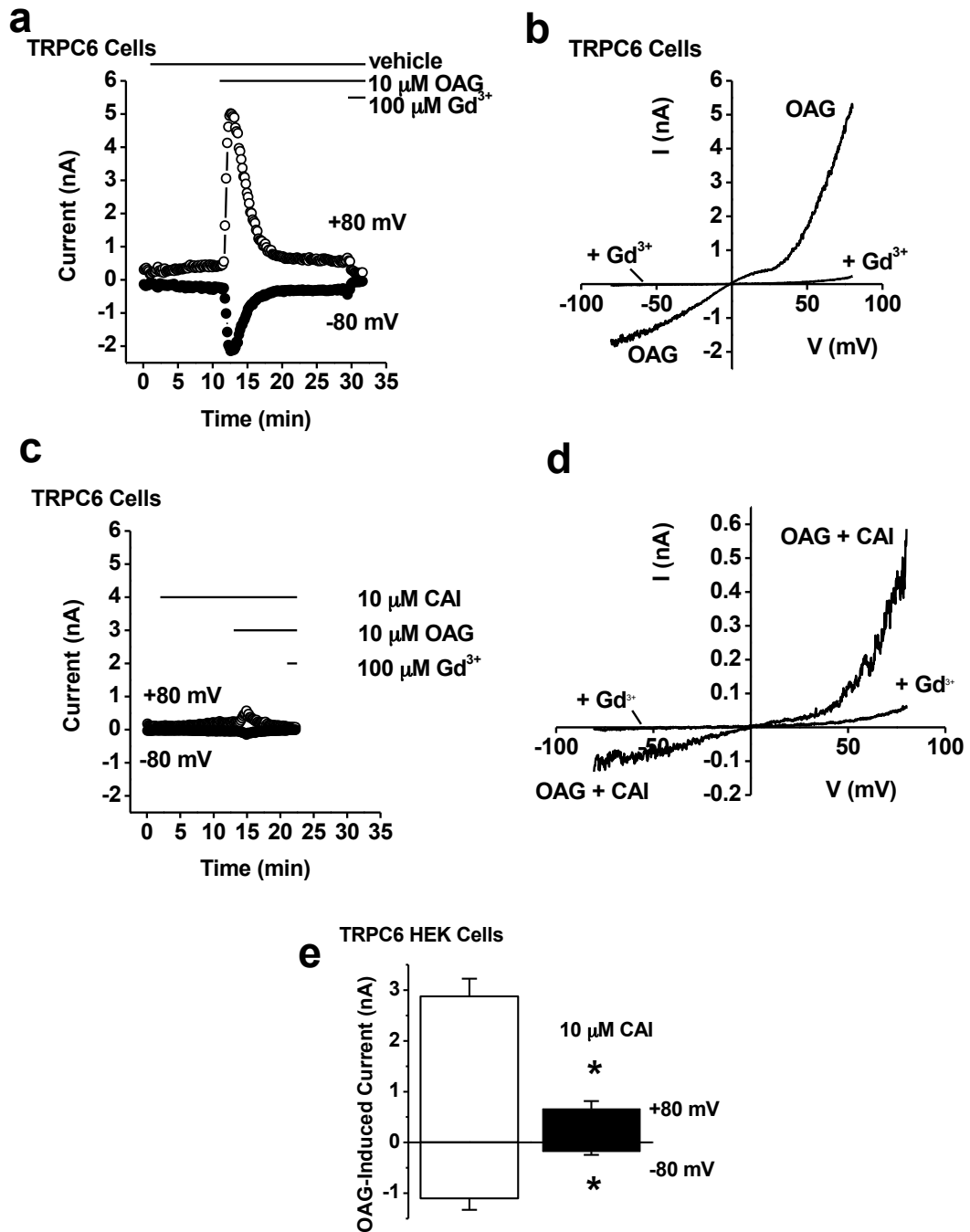
Figure 5-6 CAI inhibits OAG-induced TRPC6 currents.

Recordings were made by whole-cell voltage-clamp from mTRPC6 expressing HEK cells. **a**. Example time course of current sampled at +80 mV and -80 mV during a voltage-ramp protocol, showing bath-application of vehicle control followed by 10 µM OAG and 100 µM Gd^{3+}. **b**. Typical I-V relationship for the experiment shown in a. **c**. Example time course of current sampled at +80 mV and -80 mV during a voltage ramp protocol following, showing bath-application of 10 µM CAI followed by 10 µM OAG and 100 µM Gd^{3+}. **d**. Typical I-V relationship for the experiment shown in c. **e**. Mean data for OAG-induced TRPC6 current following pretreatment with either vehicle (DMSO; n=9) or CAI (n=10; *$P<0.05$).

5.5. CAI does not inhibit TRPC5-mediated ionic currents or TRPV4-mediated Ca^{2+} entry

To investigate if the block observed with CAI was specific for TRPC6, whole cell patch clamp recordings were performed on TRPC5 expressing HEK 293 cells. Ca^{2+} entry through TRPC5 channels was evoked by 30 µM Gd^{3+}. Gd^{3+} evoked large and sustained inward and outward currents and the resulting I-V showed the TRPC5 signature, S shaped, doubly rectifying and crossing at close to 0 mV. In the continued presence of Gd^{3+}, TRPC5 channels remained open, which meant it was possible to bath-apply CAI to determine if it could block the channels. CAI applied to the open channels had no effect on the inward or outward current compared to vehicle controls (Figure 5-7).

TRPV4 is a TRP family member from the vanilloid family and is expressed and functional in endothelial cells (Nilius et al., 2003). In breast cancer derived endothelial cells, arachidonic acid (AA) stimulated Ca^{2+} entry, which was blocked by CAI (Fiorio Pla et al., 2008). TRPV4 is activated by AA, and therefore Fiorio-Pla *et al* (2008) suggested that TRPV4 may be the target for CAI. To determine if this is the case, CHO cells stably expressing TRPV4 were used for Ca^{2+} imaging experiments. 4αPDD (a potent activator of TRPV4) evoked a large and sustained Ca^{2+} response that was absent in wild-type CHO cells. Pre-treatment for 30 minutes with CAI had no significant effect on the 4αPDD-evoked Ca^{2+} entry into TRPV4 cells (Figure 5-7).
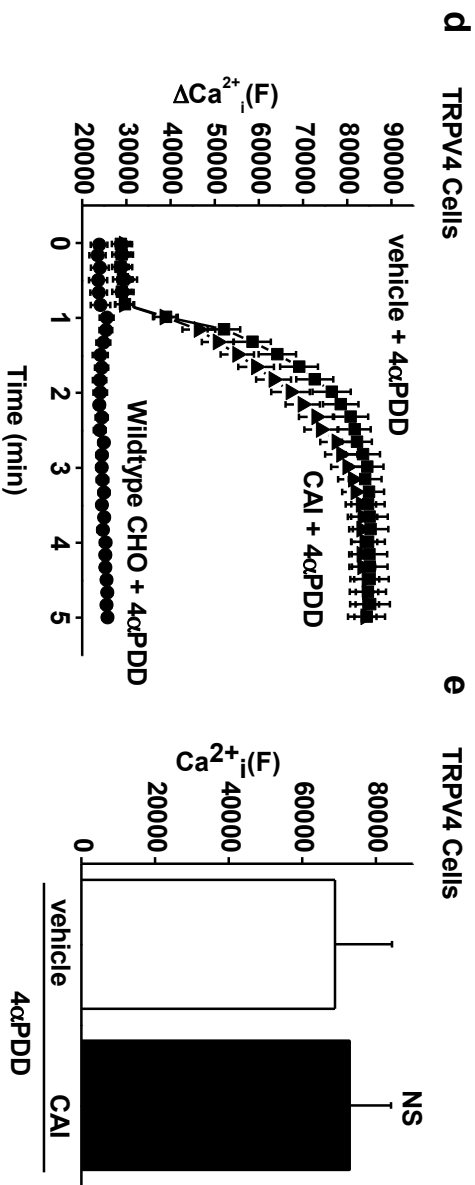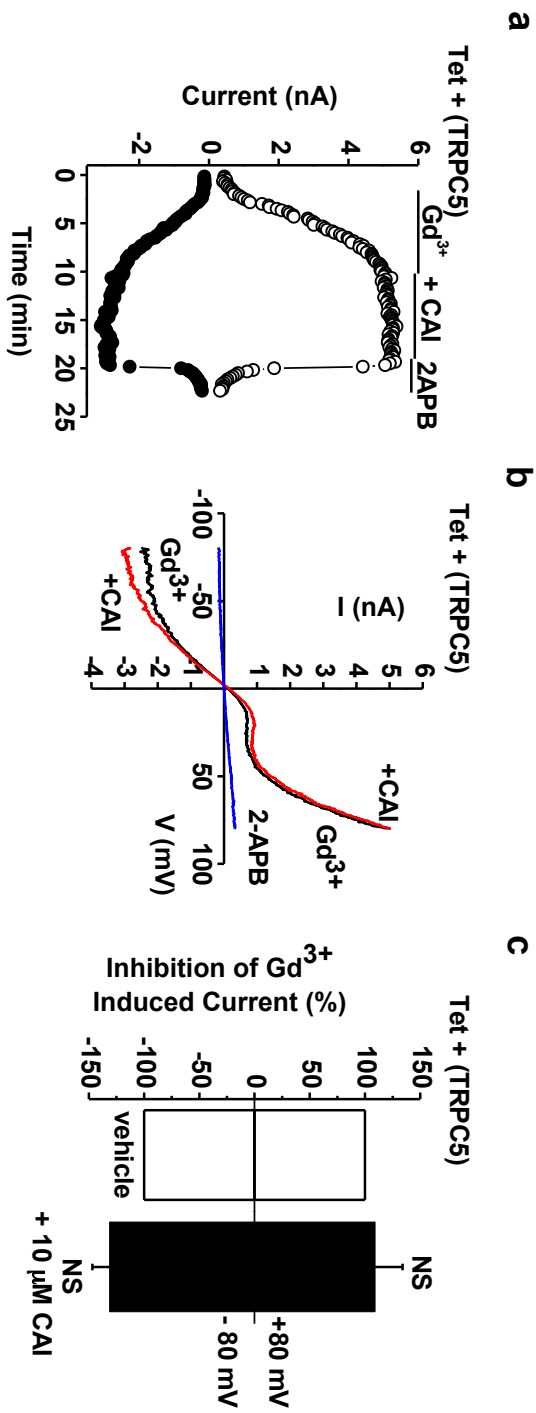
Figure 5-7 CAI does not inhibit Gd³⁺-evoked TRPC5 currents or TRPV4-mediated Ca²⁺ entry.

Recordings were made by whole-cell voltage-clamp from tet + TRPC5 HEK cells (a-c). Ca²⁺ measurements were made on the FlexStation (d-e). **a**. Example time course of current sampled at +80 mV and -80 mV during a voltage-ramp protocol, showing bath-application of 30 μM Gd³⁺, 10 μM CAI and 75 μM 2-APB. **b**. Typical I-V relationship for the experiment shown in a. **c**. Mean normalised data from experiments from the type of experiment shown in a. where NS, non-significant **d**. Example time-series trace showing CAI does not inhibit 4αPDD-induced Ca²⁺ entry into TRPV4 expressing CHO cells. Wildtype CHO cells did not respond to 4αPDD (n=5). **e**. Mean data from experiments of the type illustrated in d (n/N=3/22; NS, non-significant).

5.6. Structure-activity relationship of galangin compounds and TRPC6-mediated Ca^{2+} responses

Previous studies in our lab showed that galangin was an effective blocker of TRPC5 channels, with an IC$_{50}$ of 400 nM generated from Ca^{2+} imaging FlexStation experiments (Ben Green, Yasser Majeed, Jacqueline Naylor, Jing Li, unpublished data). It was found that making substitutions at the R1 position generated compounds that were effective TRPC5 channel blockers though the potency was not as great as that for galangin (Figure 5-8). Conversely, making substitutions at positions R2-R4 generated compounds that were ineffective TRPC5 channel blockers (Figure 5-8). The present study sought to determine the effects of these compounds against TRPC6. TRPC6 cells were seeded into 96 well plates and loaded with the Ca^{2+} indicator dye Fura-2 AM. OAG (100 μM) was used to evoke a Ca^{2+} response through TRPC6 channels. To test the effect of galangin and its derivatives against TRPC6, cells were pre-treated with 10 μM of each compound and OAG was applied in the presence of the compound. The percentage inhibition of the OAG-induced TRPC6 response was measured. Galangin inhibited the OAG-induced response by 65 ± 15.0%. The data for the galangin derivatives with for R1 – R4 substitutions are shown in Tables 5-1 – 5-4 respectively. The data showed that all of the compounds tested had some inhibitory effect on TRPC6 ranging from 21-87% inhibition. However, there was no pattern to suggest any one of the R group substitutions generates better blockers than others. Further experiments would be needed to generate IC$_{50}$ values for these compounds in order to determine how efficacious these compounds really are.
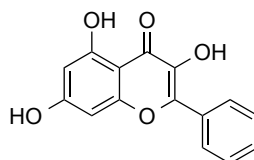
Galangin
(TRPC5 inhibitor)
IC$_{50}$ (FlexStation): 400 nM
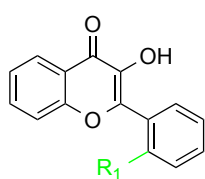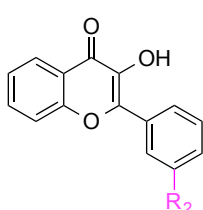
TRPC5 inhibitors   mostly inactive   mostly inactive   mostly inactive
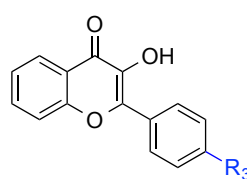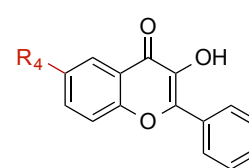
Figure 5-8 Galangin derivatives as TRPC5 inhibitors.

Galangin derivatives with an R1 substitution were effective inhibitors of TRPC5 whereas derivatives with R2, R3 or R4 substitutions were mostly inactive. Unpublished data generated by Ben Green, Yasser Majeed, Jacqueline Naylor, Jing Li. Chemistry by Robin Bon (Leeds University).
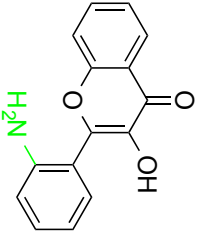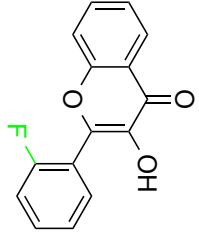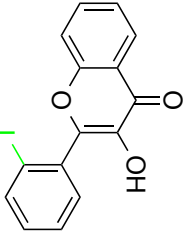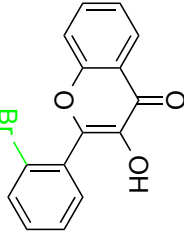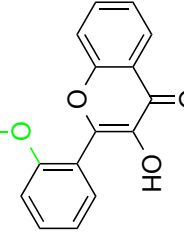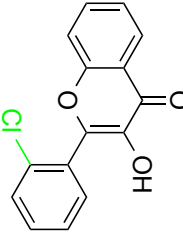
Compound	Structure	% Inhibition	Compound	Structure	% Inhibition
1	H₂N substituted galangin derivative	72.6 ± 1.7	5	F substituted galangin derivative	61.6 ± 7.9
2	I substituted galangin derivative	82.2 ± 6.6	6	HO substituted galangin derivative	41.5 ± 13.1
3	Br substituted galangin derivative	47.5 ± 19.2	7	O-CH₃ substituted galangin derivative	69.5 ± 5.8
4	Cl substituted galangin derivative	62.5 ± 10.3			

Table 5-1 Table showing % inhibition of OAG-induced TRPC6 Ca²⁺ response by galangin-derivatives with substitutions at position R1.
TRPC6 cells were pre-treated with 10 µM compound then stimulated with 100 µM OAG. Table shows the mean % OAG inhibition (n/N=3/6).
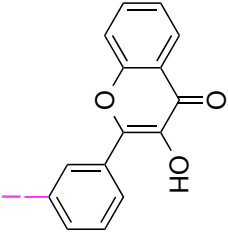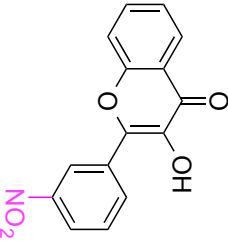
Compound	Structure	% Inhibition	Compound	Structure	% Inhibition
8		61.3 ± 4.1	11		30.0 ± 10.0
9		54.2 ± 8.4	12		47.5 ± 19.2
10		76.5 ± 9.8	13		32.1 ± 18.9

Table 5-2 Table showing % inhibition of OAG-induced TRPC6 Ca^{2+} response by galangin-derivatives with substitutions at position R2.
TRPC6 cells were pre-treated with 10 μM compound then stimulated with 100 μM OAG. Table shows the mean % OAG inhibition (n/N=3/6).
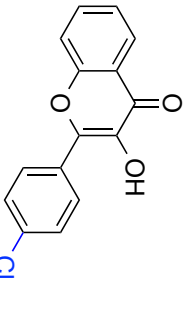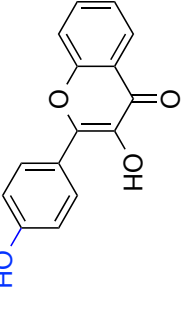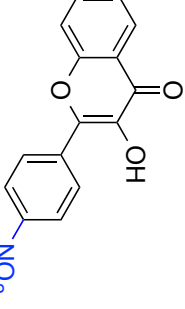
Compound	Structure	% Inhibition	Compound	Structure	% Inhibition
14		21.6 ± 17.9	**17**		59.5 ± 7.3
15		65.7 ± 11.0	**18**		33.3 ± 31.5
16		28.7 ± 6.8	**19**		59.6 ± 8.8

Table 5-3 Table showing % inhibition of OAG-induced TRPC6 Ca^{2+} response by galangin-derivatives with substitutions at position R3. TRPC6 cells were pre-treated with 10 μM compound then stimulated with 100 μM OAG. Table shows the mean % OAG inhibition (n/N=3/6).
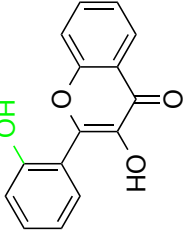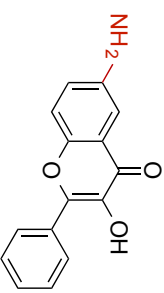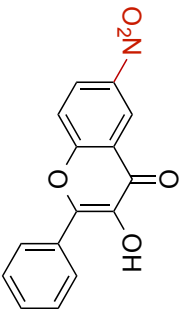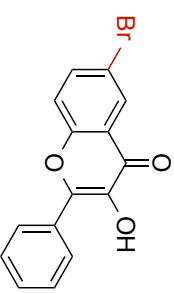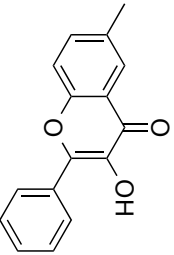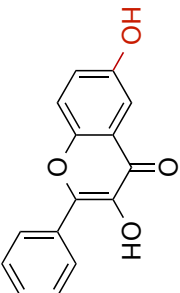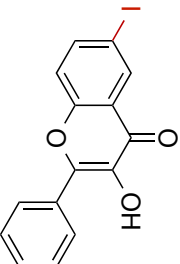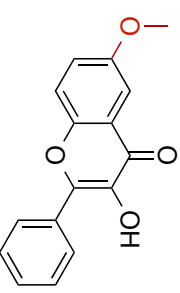
Compound	Structure	% Inhibition	Compound	Structure	% Inhibition
20		63.9 ± 5.1	24		53.8 ± 11.1
21		87.0 ± 12	25		59.1 ± 8.8
22		80.8 ± 14.1	26		59.2 ± 9.6
23		55.7 ± 10.4			

Table 5-4 Table showing % inhibition of OAG-induced TRPC6 Ca^{2+} response by galangin-derivatives with substitutions at position R4.
TRPC6 cells were pre-treated with 10 µM compound then stimulated with 100 µM OAG. Table shows the mean % OAG inhibition (n/N=3/6).
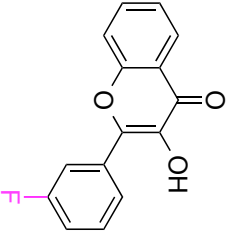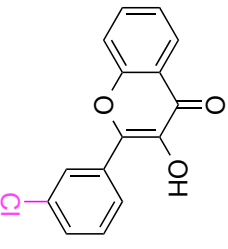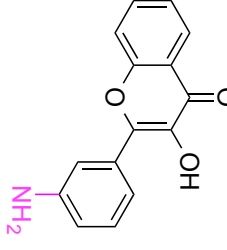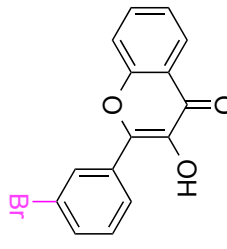
5.7. Discussion and conclusions

The results from this chapter showed that pre-treatment of TRPC6-expressing cells with CAI inhibited Ca^{2+} entry and ionic currents through TRPC6 channels suggesting that CAI is a novel TRPC6 channel blocker. In contrast, CAI had no effect on TRPC5-mediated ionic currents or on TRPV4-mediated Ca^{2+} influx. Galangin, a flavonoid found in honey and derivatives of galangin showed inhibitory effects ranging from 21-87% on TRPC6-mediated Ca^{2+} influx. However, there was no pattern to suggest that certain chemical groups made better or worse blockers which is in contrast to previous data generated in the lab showing structure activity relationships for galangin and its derivatives against TRPC5.

Carbachol, a muscarinic receptor agonist, is widely used to stimulate TRPC6 channels and the resulting Ca^{2+} response is composed of a transient Ca^{2+} response followed by a sustained Ca^{2+} entry response. In the absence of extracellular Ca^{2+} only the transient response remained, which suggested that this was due to Ca^{2+} release from intracellular stores following muscarinic receptor activation followed by PLC activation and IP_3 formation. Importantly, when cells were pretreated with CAI, only the sustained response to carbachol was maximally inhibited, which suggests t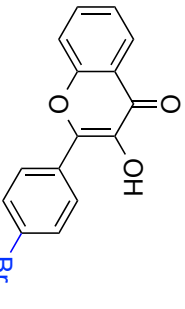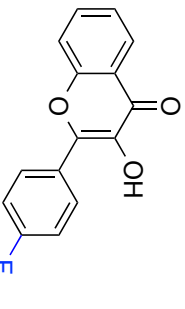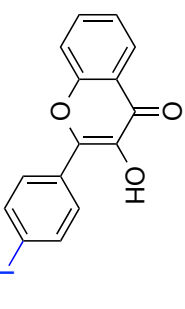hat CAI was blocking Ca^{2+} entry through TRPC6 and having little effect on Ca^{2+} release which would likely be due to IP_3 formation. Faehling *et al* found that CAI inhibited IP_3 formation, but Hupe *et al* found CAI had no effect on IP_3 levels in leukocytes (Faehling et al., 2002, Hupe et al., 1991). The IC_{50} for CAI on carbachol-evoked Ca^{2+} entry was 2.5 μM. This value is comparable to IC_{50}s generated in *in vitro* and *in vivo* angiogenesis studies where CAI was efficacious at concentrations of 1-10 μM (Felder et al., 1991, Kohn and Liotta, 1990, Kohn et al., 1992). In the clinic, cancer patients dosed with CAI maintained steady-state plasma concentrations of approximately 4-10 μM. CAI at these concentrations was well tolerated with adverse events graded 1-2, which included fatigue, depression, nausea, headache and constipation being the common ones (Hussain et al., 2003). Whole cell patch clamp experiments validated the Ca^{2+} imaging experiments

showing that pretreatment of TRPC6 cells with CAI resulted in a significant inhibition of the OAG-evoked ionic currents compared to the vehicle controls, confirming the Ca^{2+} measurement data that CAI inhibits TRPC6 channels at 10 µM, a concentration that is efficacious against cancer and non-toxic.

Under the experimental conditions used in this study, OAG evoked a large and transient current. The conventional method to investigate ion channel blockers is to apply them after channel activation and this is the method that was used to test the effect of CAI on TRPC5 ionic currents. However, the transient nature of the OAG response made this very difficult, therefore cells were pretreated with CAI prior to channel activation and this resulted in a significant inhibition of the OAG response observed in the vehicle control treated cells. The data generated do not entirely support that CAI directly blocks TRPC6 channels and to get this answer, photo-affinity labelling studies could be performed or outside-out patch clamp experiments.

Previous studies in our lab showed that the flavonoid galangin could block TRPC5-mediated Ca^{2+} entry with an IC_{50} of 400 nM. In the present study, galangin had an inhibitory effect on TRPC6 but the block was not as good as for TRPC5, suggesting that galangin has selectivity for TRPC5 over TRPC6. Galangin R1-substituted compounds were also blockers of TRPC5, but the R2-R4 substituted compounds were mostly inactive. For TRPC6 however, there was no pattern to the degree of block measured with the different R group substituted compounds. IC_{50} measurements would be needed to determine the efficacy of these compounds at the TRPC6 channel. The fact that galangin has been found to have health benefits and be anti-cancer suggests that blocking TRPCs may be a good therapeutic strategy for anti-cancer drugs. This fits in with accumulating data showing overexpression of TRPC6 in cancer.

In conclusion, CAI and galangin (and its derivatives) are able to block TRPC6 channels. Whether they directly block the channel remains to be determined but the data so far suggest that TRPC6 may be a good therapeutic target.

CHAPTER 6. FINAL SUMMARY AND CONCLUSIONS

The overall objective of this thesis was to gain further insight into molecular mechanisms and pharmacology of Ca^{2+} entry mechanisms and their downstream signalling in endothelial cells. This was achieved using a range of molecular, biochemical and electrophysiology techniques and cell functional assays.

The first objective was to investigate the putative Ca^{2+} channel regulator proteins, CRACR2A and golli-MBP. Unexpectedly these proteins had functions that were independent of Ca^{2+} channels, this finding lead to alternative hypotheses about their roles in endothelial cells. The second objective was to generate new information about pharmacology targeted to a Ca^{2+} channel subunit, TRPC6, which has been suggested to be important in endothelial cell biology.

In Chapter 3 the putative Ca^{2+} channel regulator protein CRACR2A was investigated. A major finding was that CRACR2A, which had previously been identified as a novel interacting partner for Orai1 and involved in CRAC channel regulation, was not detected in endothelial cells. Instead a longer splice variant arising from the same gene, EFCAB4B isoform *a* (EFCAB4B-a), was detected. CRACR2A and EFCAB4B-a have the same putative Ca^{2+} binding domains at their N termini but EFCAB4B-a, unlike CRACR2A, had no role in the regulation of Ca^{2+} release-activated Ca^{2+} (CRAC) channels. Instead, EFCAB4B-a contained a predicted Rab domain in its C terminus and was therefore a putative monomeric G protein. The results showed that it localised to endothelial cell specific Weibel-Palade bodies (WPBs) where it influenced the abundance of the pro-thrombotic agent von Willebrand factor (vWF). Results also showed that depletion of EFCAB4B-a reduced VEGFR2 protein expression and histamine-stimulated Ca^{2+} entry into endothelial cells. It is therefore possible that EFCAB4B-a is involved in the biosynthetic pathway of VEGFR2 and Ca^{2+} channel subunits, for example TRPC6. This is the first study to show

expression and function of this novel putative Ca^{2+} regulated Rab protein. This discovery is therefore a significant advancement in the field of monomeric G proteins. In addition, this important finding means EFCAB4B-a could be a novel therapeutic target in diseases involving vWF which include von Willebrands disease (VWD), atherosclerosis and cancer.

Chapter 4 investigated golli-MBP and the results unexpectedly showed that golli-MBP had little effect on SOCE in endothelial cells. Instead, the results showed that golli-MBP was a positive regulator of VEGFR2 and suggests that golli-MBP may have a role in the biosynthetic pathway of VEGFR2. Since VEGFR2 is most important for its role in VEGF induced vascular permeability and angiogenesis, golli-MBP may be an important protein in tumour progression by stimulating angiogenesis.

In Chapter 5 the results showed that the small-molecule carboxyamidotriazole (CAI), reported to have anti-cancer activity, was identified as an inhibitor of TRPC6 channels without effect on TRPC5 or TRPV4 channels. Since the first report of CAI as an anti-cancer agent, research has been on-going to try and elucidate the mechanism underlying its effects. The discovery in this study that CAI can inhibit TRPC6 channels at therapeutic concentrations will be of great interest to the field. It also strengthens existing evidence that TRPC6 may be an important ion channel in cancer progression. Not only that, since CAI showed selectivity for TRPC6 over TRPC5 and TRPV4, this finding will also be of interest to the TRP field, where there is a constant interest to find novel TRP channel blockers that can be used as research tools. A range of flavonol compounds was also identified as TRPC6 inhibitors, which will also be of interest to the TRP field in addition to the cardiovascular field where flavonols are continuing to be investigated for their cardiovascular health benefits.

In summary, this research has generated new information and hypotheses about a putative Ca^{2+}-regulated Rab protein of Weibel-Palade bodies, a novel regulator of a key endothelial growth factor receptor, and a molecular target for CAI. It has, therefore, led to understanding of molecular mechanisms and

pharmacology in endothelial cells which may be useful for devising strategies to treat major problems such as cardiovascular disease and cancer.
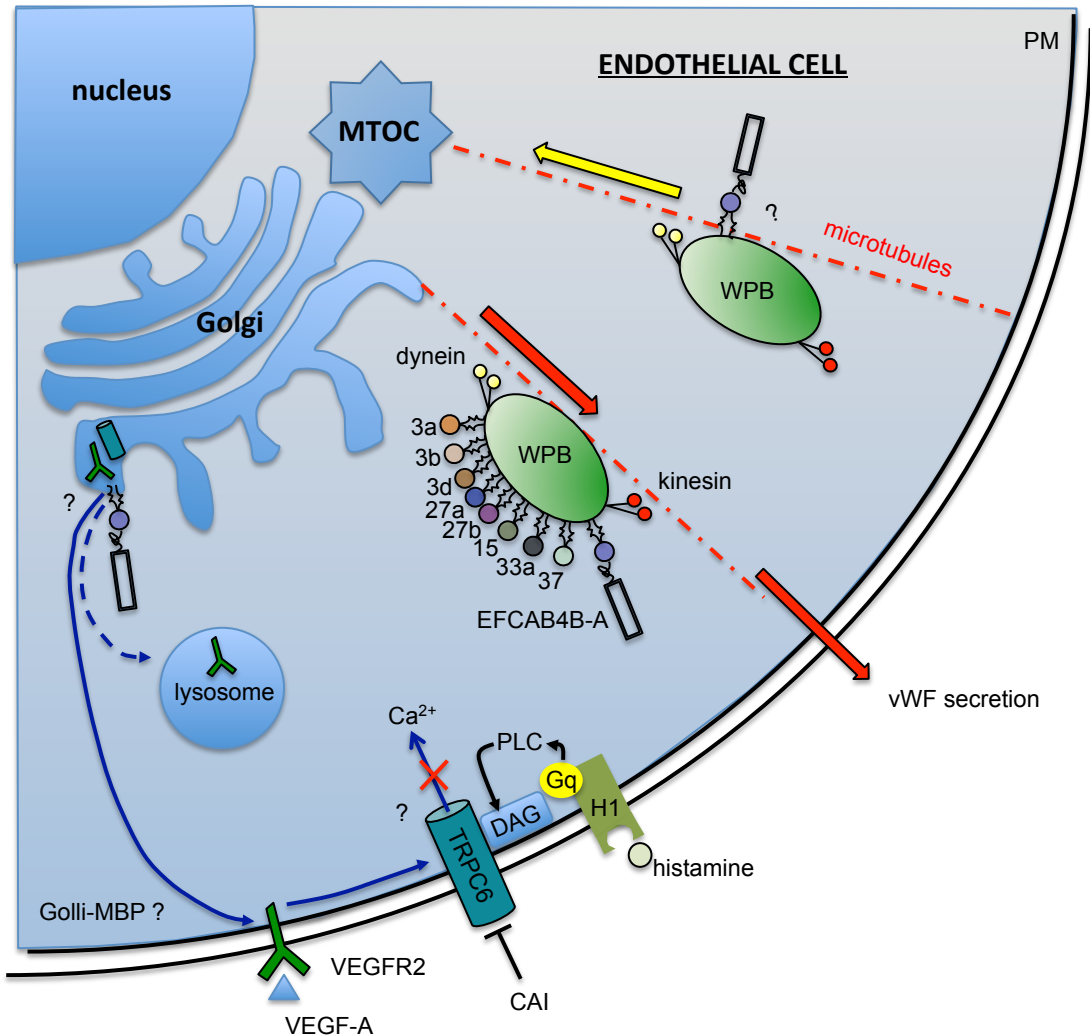
Figure 6-1 Cartoon summarising new hypotheses around EFCAB4B-a, Golli-MBP and the small molecule Ca^{2+} inhibitor, carboxyamidotriazole in endothelial cells, based on the results from this thesis.

A novel Rab protein, EFCAB4B-a has been identified in endothelial cells. EFCAB4B-a localises to Weibel-Palade bodies (WPBs) along with Rabs 3a, 3b, 3d, 27a, 27b, 15, 33a and 37. Rabs 3a, 3d, 15, 27a and 27b have reported roles in vWF secretion (reviewed in (Nightingale and Cutler, 2013). WPBs travel along microtubules using the motor proteins kinesin and dynein, for forward and retrograde traffic respectively. Increases in intracellular Ca^{2+} stimulate the forward trafficking and release of von Willebrand factor (vWF) from the cell, which is particularly important for blood clotting. Increases in intracellular Ca^{2+} or cAMP can result in WPBs travelling in the reverse direction and accumulating at the microtubule organising centre (MTOC). Based on results from this thesis, one hypothesis is that EFCAB4B-a is involved in the retrograde trafficking of WPBs through an interaction with dynein. Since depletion of EFCAB4B-a resulted in a suppression of total VEGFR2 in the cell, another hypothesis may be that EFCAB4B-a is involved in the biosynthetic pathway of VEGFR2, in a similar way to syntaxin-6. The role of the Ca^{2+}-binding EF-hand remains to be determined. Depletion of Golli-MBP had little effect on store-operated Ca^{2+} entry in endothelial cells. Instead depletion of Golli-MBP suppressed total VEGFR2 protein levels, suggesting that Golli-MBP is also involved in the trafficking or biosynthetic pathway of VEGFR2. The role of Ca^{2+} is unknown at present. Finally, the small molecule Cra^{2+} inhibitor,

carboxyamidotriazole (CAI) was found to inhibit TRPC6 channels in HEK293 cells. Expression of TRPC6 has previously been identified on endothelial cells and it has been shown that TRPC6 is involved in VEGF-evoked Ca^{2+} responses that underlie angiogenesis *in vitro*. The hypothesis is therefore that CAI inhibits endothelial TRPC6 channels that are important for VEGF-evoked angiogenesis. Results from this thesis also showed that depletion of EFCAB4B-a using siRNA, resulted in a reduced Ca^{2+} entry following histamine stimulation. It is possible that at least part of this Ca^{2+} entry is through TRPC6 channels. Another hypothesis is therefore that EFCAB4B-a is involved in the biosynthetic pathway of TRPC6 channel subunits. WPB: Weibel-Palade Body; H1: histamine receptor 1; MTOC: microtubule organising centre; CAI: carboxyamidotriazole; vWF: von Willebrand factor; VEGF: vascular endothelial growth factor; VEGFR2: vascular endothelial growth factor receptor 2; DAG: diacylglycerol; PLC: phospholipase C; PM: plasma membrane.

REFERENCES

ABDULLAEV, I. F., BISAILLON, J. M., POTIER, M., GONZALEZ, J. C., MOTIANI, R. K. & TREBAK, M. 2008. Stim1 and Orai1 mediate CRAC currents and store-operated calcium entry important for endothelial cell proliferation. *Circ Res,* 103**,** 1289-99.

AFZAL, A., CABALLERO, S., PALII, S. S., JURCZYK, S., PARDUE, M., GEROSKI, D., EDELHAUSER, H., HOCHHAUS, G., KIM, M., FRANKLIN, A., SHAPIRO, G. & GRANT, M. B. 2010. Targeting retinal and choroid neovascularization using the small molecule inhibitor carboxyamidotriazole. *Brain Res Bull,* 81**,** 320-6.

ALBERTS, B., WILSON, J. & HUNT, T. 2008. *Molecular biology of the cell,* New York, Garland Science.

ANTIGNY, F., KOENIG, S., BERNHEIM, L. & FRIEDEN, M. 2013. During post-natal human myogenesis, normal myotube size requires TRPC1- and TRPC4-mediated Ca2+ entry. *J Cell Sci,* 126**,** 2525-33.

ARMSTRONG, D. J. & ROMAN, A. 1993. The anomalous electrophoretic behavior of the human papillomavirus type 16 E7 protein is due to the high content of acidic amino acid residues. *Biochem Biophys Res Commun,* 192**,** 1380-7.

AYDAR, E., YEO, S., DJAMGOZ, M. & PALMER, C. 2009. Abnormal expression, localization and interaction of canonical transient receptor potential ion channels in human breast cancer cell lines and tissues: a potential target for breast cancer diagnosis and therapy. *Cancer Cell Int,* 9**,** 23.

BASORA, N., BOULAY, G., BILODEAU, L., ROUSSEAU, E. & PAYET, M. D. 2003. 20-hydroxyeicosatetraenoic acid (20-HETE) activates mouse TRPC6 channels expressed in HEK293 cells. *J Biol Chem,* 278**,** 31709-16.

BAUER, K. S., CUDE, K. J., DIXON, S. C., KRUGER, E. A. & FIGG, W. D. 2000. Carboxyamido-triazole inhibits angiogenesis by blocking the calcium-mediated nitric-oxide synthase-vascular endothelial growth factor pathway. *J Pharmacol Exp Ther,* 292**,** 31-7.

BEECH, D. J. 2013. Characteristics of transient receptor potential canonical calcium-permeable channels and their relevance to vascular physiology and disease. *Circ J,* 77**,** 570-9.

BERRIDGE, M. J. 2002. The endoplasmic reticulum: a multifunctional signaling organelle. *Cell Calcium,* 32**,** 235-49.

BERRIDGE, M. J., BOOTMAN, M. D. & RODERICK, H. L. 2003. Calcium signalling: dynamics, homeostasis and remodelling. *Nat Rev Mol Cell Biol,* 4**,** 517-29.

BIERINGS, R., HELLEN, N., KISKIN, N., KNIPE, L., FONSECA, A. V., PATEL, B., MELI, A., ROSE, M., HANNAH, M. J. & CARTER, T. 2012. The interplay between the Rab27A effectors Slp4-a and MyRIP controls hormone-evoked Weibel-Palade body exocytosis. *Blood,* 120**,** 2757-67.

BOLANZ, K. A., HEDIGER, M. A. & LANDOWSKI, C. P. 2008. The role of TRPV6 in breast carcinogenesis. *Mol Cancer Ther,* 7**,** 271-9.

BONETTI, P. O., LERMAN, L. O. & LERMAN, A. 2003. Endothelial dysfunction: a marker of atherosclerotic risk. *Arterioscler Thromb Vasc Biol,* 23**,** 168-75.

BOSSU, J. L., ELHAMDANI, A. & FELTZ, A. 1992a. Voltage-dependent calcium entry in confluent bovine capillary endothelial cells. *FEBS Lett,* 299**,** 239-42.

BOSSU, J. L., ELHAMDANI, A., FELTZ, A., TANZI, F., AUNIS, D. & THIERSE, D. 1992b. Voltage-gated Ca entry in isolated bovine capillary endothelial cells: evidence of a new type of BAY K 8644-sensitive channel. *Pflugers Arch,* 420**,** 200-7.

BOSSU, J. L., FELTZ, A., RODEAU, J. L. & TANZI, F. 1989. Voltage-dependent transient calcium currents in freshly dissociated capillary endothelial cells. *FEBS Lett,* 255**,** 377-80.

BOULAY, G. 2002. Ca(2+)-calmodulin regulates receptor-operated Ca(2+) entry activity of TRPC6 in HEK-293 cells. *Cell Calcium,* 32**,** 201-7.

BOULAY, G., ZHU, X., PEYTON, M., JIANG, M., HURST, R., STEFANI, E. & BIRNBAUMER, L. 1997. Cloning and expression of a novel mammalian homolog of Drosophila transient receptor potential (Trp) involved in calcium entry secondary to activation of receptors coupled by the Gq class of G protein. *J Biol Chem,* 272**,** 29672-80.

BRYANTSEVA, S. A. & ZHAPPAROVA, O. N. 2012. Bidirectional transport of organelles: unity and struggle of opposing motors. *Cell Biol Int,* 36**,** 1-6.

CAHALAN, M. D. 2009. STIMulating store-operated Ca(2+) entry. *Nat Cell Biol,* 11**,** 669-77.

CAMPAGNONI, A. T., PRIBYL, T. M., CAMPAGNONI, C. W., KAMPF, K., AMUR-UMARJEE, S., LANDRY, C. F., HANDLEY, V. W., NEWMAN, S. L., GARBAY, B. & KITAMURA, K. 1993. Structure and developmental regulation of Golli-mbp, a 105-kilobase gene that encompasses the myelin basic protein gene and is expressed in cells in the oligodendrocyte lineage in the brain. *J Biol Chem,* 268**,** 4930-8.

CARMELIET, P., FERREIRA, V., BREIER, G., POLLEFEYT, S., KIECKENS, L., GERTSENSTEIN, M., FAHRIG, M., VANDENHOECK, A., HARPAL, K., EBERHARDT, C., DECLERCQ, C., PAWLING, J., MOONS, L., COLLEN, D., RISAU, W. & NAGY, A. 1996. Abnormal blood vessel development and lethality in embryos lacking a single VEGF allele. *Nature,* 380**,** 435-9.

CASTEELS, R. & DROOGMANS, G. 1981. Exchange characteristics of the noradrenaline-sensitive calcium store in vascular smooth muscle cells or rabbit ear artery. *J Physiol,* 317**,** 263-79.

CHAUDHURI, P., COLLES, S. M., BHAT, M., VAN WAGONER, D. R., BIRNBAUMER, L. & GRAHAM, L. M. 2008. Elucidation of a TRPC6-TRPC5 channel cascade that restricts endothelial cell movement. *Mol Biol Cell,* 19**,** 3203-11.

CHAZIN, W. J. 2011. Relating form and function of EF-hand calcium binding proteins. *Acc Chem Res,* 44**,** 171-9.

CLAPHAM, D. E. 2007a. Calcium signaling. *Cell,* 131**,** 1047-58.

CLAPHAM, D. E. 2007b. SnapShot: mammalian TRP channels. *Cell,* 129**,** 220.

COLICELLI, J. 2004. Human RAS superfamily proteins and related GTPases. *Sci STKE,* 2004**,** RE13.

CZIFRA, G., VARGA, A., NYESTE, K., MARINCSAK, R., TOTH, B. I., KOVACS, I., KOVACS, L. & BIRO, T. 2009. Increased expressions of cannabinoid receptor-1 and transient receptor potential vanilloid-1 in human prostate carcinoma. *J Cancer Res Clin Oncol,* 135**,** 507-14.

DAMBROS, M., VAN DEUTEKOM, M., DE JONGH, R., VAN KOEVERINGE, G. A., DE MEY, J. G. & VAN KERREBROECK, P. 2005. The inhibitory effect of the flavonoid galangin on urinary bladder smooth muscle contractility is mediated in part by modulation of Ca2+ release from intracellular stores. *Planta Med,* 71**,** 962-4.

DEHAVEN, W. I., SMYTH, J. T., BOYLES, R. R. & PUTNEY, J. W., JR. 2007. Calcium inhibition and calcium potentiation of Orai1, Orai2, and Orai3 calcium release-activated calcium channels. *J Biol Chem,* 282**,** 17548-56.

DHARMASHANKAR, K. & WIDLANSKY, M. E. 2010. Vascular endothelial function and hypertension: insights and directions. *Curr Hypertens Rep,* 12**,** 448-55.

DHENNIN-DUTHILLE, I., GAUTIER, M., FAOUZI, M., GUILBERT, A., BREVET, M., VAUDRY, D., AHIDOUCH, A., SEVESTRE, H. & OUADID-AHIDOUCH, H. 2011. High expression of transient receptor potential channels in human breast cancer epithelial cells and tissues: correlation with pathological parameters. *Cell Physiol Biochem,* 28**,** 813-22.

DICKSON, E. J., DUMAN, J. G., MOODY, M. W., CHEN, L. & HILLE, B. 2012. Orai-STIM-mediated Ca2+ release from secretory granules revealed by a targeted Ca2+ and pH probe. *Proc Natl Acad Sci U S A,* 109**,** E3539-48.

DIEKMANN, Y., SEIXAS, E., GOUW, M., TAVARES-CADETE, F., SEABRA, M. C. & PEREIRA-LEAL, J. B. 2011. Thousands of rab GTPases for the cell biologist. *PLoS Comput Biol,* 7**,** e1002217.

DIETRICH, A. & GUDERMANN, T. 2007. Trpc6. *Handb Exp Pharmacol***,** 125-41.

DIETRICH, A., KALWA, H., ROST, B. R. & GUDERMANN, T. 2005. The diacylgylcerol-sensitive TRPC3/6/7 subfamily of cation channels: functional characterization and physiological relevance. *Pflugers Arch,* 451**,** 72-80.

DUDLEY, A. C. 2012. Tumor endothelial cells. *Cold Spring Harb Perspect Med,* 2**,** a006536.

DUNCAN, T. J., AL-ATTAR, A., ROLLAND, P., SCOTT, I. V., DEEN, S., LIU, D. T., SPENDLOVE, I. & DURRANT, L. G. 2008. Vascular endothelial growth factor expression in ovarian cancer: a model for targeted use of novel therapies? *Clin Cancer Res,* 14**,** 3030-5.

DVORAK, H. F. 2002. Vascular permeability factor/vascular endothelial growth factor: a critical cytokine in tumor angiogenesis and a potential target for diagnosis and therapy. *J Clin Oncol,* 20**,** 4368-80.

DVORAK, H. F., NAGY, J. A., FENG, D., BROWN, L. F. & DVORAK, A. M. 1999. Vascular permeability factor/vascular endothelial growth factor and the significance of microvascular hyperpermeability in angiogenesis. *Curr Top Microbiol Immunol,* 237**,** 97-132.

DVORAK, H. F., ORENSTEIN, N. S., CARVALHO, A. C., CHURCHILL, W. H., DVORAK, A. M., GALLI, S. J., FEDER, J., BITZER, A. M., RYPYSC, J. &

GIOVINCO, P. 1979. Induction of a fibrin-gel investment: an early event in line 10 hepatocarcinoma growth mediated by tumor-secreted products. *J Immunol,* 122**,** 166-74.

EDER, P. & GROSCHNER, K. 2008. TRPC3/6/7: Topical aspects of biophysics and pathophysiology. *Channels (Austin),* 2**,** 94-9.

ESPER, R. J., NORDABY, R. A., VILARINO, J. O., PARAGANO, A., CACHARRON, J. L. & MACHADO, R. A. 2006. Endothelial dysfunction: a comprehensive appraisal. *Cardiovasc Diabetol,* 5**,** 4.

ESTACION, M., LI, S., SINKINS, W. G., GOSLING, M., BAHRA, P., POLL, C., WESTWICK, J. & SCHILLING, W. P. 2004. Activation of human TRPC6 channels by receptor stimulation. *J Biol Chem,* 279**,** 22047-56.

ETIENNE-MANNEVILLE, S. & HALL, A. 2002. Rho GTPases in cell biology. *Nature,* 420**,** 629-35.

FAEHLING, M., KROLL, J., FOHR, K. J., FELLBRICH, G., MAYR, U., TRISCHLER, G. & WALTENBERGER, J. 2002. Essential role of calcium in vascular endothelial growth factor A-induced signaling: mechanism of the antiangiogenic effect of carboxyamidotriazole. *FASEB J,* 16**,** 1805-7.

FELDER, C. C., MA, A. L., LIOTTA, L. A. & KOHN, E. C. 1991. The antiproliferative and antimetastatic compound L651582 inhibits muscarinic acetylcholine receptor-stimulated calcium influx and arachidonic acid release. *J Pharmacol Exp Ther,* 257**,** 967-71.

FENG, J. M., FERNANDES, A. O., CAMPAGNONI, C. W., HU, Y. H. & CAMPAGNONI, A. T. 2004. The golli-myelin basic protein negatively regulates signal transduction in T lymphocytes. *J Neuroimmunol,* 152**,** 57-66.

FENG, J. M., GIVOGRI, I. M., BONGARZONE, E. R., CAMPAGNONI, C., JACOBS, E., HANDLEY, V. W., SCHONMANN, V. & CAMPAGNONI, A. T. 2000. Thymocytes express the golli products of the myelin basic protein gene and levels of expression are stage dependent. *J Immunol,* 165**,** 5443-50.

FENG, J. M., HU, Y. K., XIE, L. H., COLWELL, C. S., SHAO, X. M., SUN, X. P., CHEN, B., TANG, H. & CAMPAGNONI, A. T. 2006. Golli protein negatively regulates store depletion-induced calcium influx in T cells. *Immunity,* 24**,** 717-27.

FERRARA, N., CARVER-MOORE, K., CHEN, H., DOWD, M., LU, L., O'SHEA, K. S., POWELL-BRAXTON, L., HILLAN, K. J. & MOORE, M. W. 1996. Heterozygous embryonic lethality induced by targeted inactivation of the VEGF gene. *Nature,* 380**,** 439-42.

FESKE, S. 2010. CRAC channelopathies. *Pflugers Arch,* 460**,** 417-35.

FESKE, S., DRAEGER, R., PETER, H. H. & RAO, A. 2000. Impaired NFAT regulation and its role in a severe combined immunodeficiency. *Immunobiology,* 202**,** 134-50.

FESKE, S., GWACK, Y., PRAKRIYA, M., SRIKANTH, S., PUPPEL, S. H., TANASA, B., HOGAN, P. G., LEWIS, R. S., DALY, M. & RAO, A. 2006. A mutation in Orai1 causes immune deficiency by abrogating CRAC channel function. *Nature,* 441**,** 179-85.

FIORIO PLA, A., GENOVA, T., PUPO, E., TOMATIS, C., GENAZZANI, A., ZANINETTI, R. & MUNARON, L. 2010. Multiple roles of protein kinase a in arachidonic acid-mediated Ca2+ entry and tumor-derived human endothelial cell migration. *Mol Cancer Res,* 8**,** 1466-76.

FIORIO PLA, A., GRANGE, C., ANTONIOTTI, S., TOMATIS, C., MERLINO, A., BUSSOLATI, B. & MUNARON, L. 2008. Arachidonic acid-induced Ca2+ entry is involved in early steps of tumor angiogenesis. *Mol Cancer Res,* 6**,** 535-45.

FIXEMER, T., WISSENBACH, U., FLOCKERZI, V. & BONKHOFF, H. 2003. Expression of the Ca2+-selective cation channel TRPV6 in human prostate cancer: a novel prognostic marker for tumor progression. *Oncogene,* 22**,** 7858-61.

FLEMING, I., RUEBEN, A., POPP, R., FISSLTHALER, B., SCHRODT, S., SANDER, A., HAENDELER, J., FALCK, J. R., MORISSEAU, C., HAMMOCK, B. D. & BUSSE, R. 2007. Epoxyeicosatrienoic acids regulate Trp channel dependent Ca2+ signaling and hyperpolarization in endothelial cells. *Arterioscler Thromb Vasc Biol,* 27**,** 2612-8.

FREDSLUND, J. 2006. PHY.FI: fast and easy online creation and manipulation of phylogeny color figures. *BMC Bioinformatics,* 7**,** 315.

GALLEY, H. F. & WEBSTER, N. R. 2004. Physiology of the endothelium. *Br J Anaesth,* 93**,** 105-13.

GARCIA, R. L. & SCHILLING, W. P. 1997. Differential expression of mammalian TRP homologues across tissues and cell lines. *Biochem Biophys Res Commun,* 239**,** 279-83.

GE, R., TAI, Y., SUN, Y., ZHOU, K., YANG, S., CHENG, T., ZOU, Q., SHEN, F. & WANG, Y. 2009. Critical role of TRPC6 channels in VEGF-mediated angiogenesis. *Cancer Lett,* 283**,** 43-51.

GEE, K. R., BROWN, K. A., CHEN, W. N., BISHOP-STEWART, J., GRAY, D. & JOHNSON, I. 2000. Chemical and physiological characterization of fluo-4 Ca(2+)-indicator dyes. *Cell Calcium,* 27**,** 97-106.

GIROUX, S., TREMBLAY, M., BERNARD, D., CARDIN-GIRARD, J. F., AUBRY, S., LAROUCHE, L., ROUSSEAU, S., HUOT, J., LANDRY, J., JEANNOTTE, L. & CHARRON, J. 1999. Embryonic death of Mek1-deficient mice reveals a role for this kinase in angiogenesis in the labyrinthine region of the placenta. *Curr Biol,* 9**,** 369-72.

GODDARD, L. M. & IRUELA-ARISPE, M. L. 2013. Cellular and molecular regulation of vascular permeability. *Thromb Haemost,* 109**,** 407-15.

GOMES, A. Q., ALI, B. R., RAMALHO, J. S., GODFREY, R. F., BARRAL, D. C., HUME, A. N. & SEABRA, M. C. 2003. Membrane targeting of Rab GTPases is influenced by the prenylation motif. *Mol Biol Cell,* 14**,** 1882-99.

GONZALEZ-COBOS, J. C., ZHANG, X., ZHANG, W., RUHLE, B., MOTIANI, R. K., SCHINDL, R., MUIK, M., SPINELLI, A. M., BISAILLON, J. M., SHINDE, A. V., FAHRNER, M., SINGER, H. A., MATROUGUI, K., BARROSO, M., ROMANIN, C. & TREBAK, M. 2013. Store-independent Orai1/3 channels activated by intracrine leukotriene C4: role in neointimal hyperplasia. *Circ Res,* 112**,** 1013-25.

GRAHAM, S., DING, M., DING, Y., SOURS-BROTHERS, S., LUCHOWSKI, R., GRYCZYNSKI, Z., YORIO, T., MA, H. & MA, R. 2010. Canonical transient receptor potential 6 (TRPC6), a redox-regulated cation channel. *J Biol Chem,* 285**,** 23466-76.

GRAUPERA, M. & POTENTE, M. 2013. Regulation of angiogenesis by PI3K signaling networks. *Exp Cell Res,* 319**,** 1348-55.

GRYNKIEWICZ, G., POENIE, M. & TSIEN, R. Y. 1985. A new generation of Ca2+ indicators with greatly improved fluorescence properties. *J Biol Chem,* 260**,** 3440-50.

GWACK, Y., SRIKANTH, S., OH-HORA, M., HOGAN, P. G., LAMPERTI, E. D., YAMASHITA, M., GELINAS, C., NEEMS, D. S., SASAKI, Y., FESKE, S., PRAKRIYA, M., RAJEWSKY, K. & RAO, A. 2008. Hair loss and defective T- and B-cell function in mice lacking ORAI1. *Mol Cell Biol,* 28**,** 5209-22.

HAMDOLLAH ZADEH, M. A., GLASS, C. A., MAGNUSSEN, A., HANCOX, J. C. & BATES, D. O. 2008. VEGF-mediated elevated intracellular calcium and angiogenesis in human microvascular endothelial cells in vitro are inhibited by dominant negative TRPC6. *Microcirculation,* 15**,** 605-14.

HANAHAN, D. & WEINBERG, R. A. 2000. The hallmarks of cancer. *Cell,* 100**,** 57-70.

HECQUET, C. M., AHMMED, G. U., VOGEL, S. M. & MALIK, A. B. 2008. Role of TRPM2 channel in mediating H2O2-induced Ca2+ entry and endothelial hyperpermeability. *Circ Res,* 102**,** 347-55.

HENDRIX, M. J., SEFTOR, E. A., HESS, A. R. & SEFTOR, R. E. 2003. Vasculogenic mimicry and tumour-cell plasticity: lessons from melanoma. *Nat Rev Cancer,* 3**,** 411-21.

HERNANDEZ, G. L., VOLPERT, O. V., INIGUEZ, M. A., LORENZO, E., MARTINEZ-MARTINEZ, S., GRAU, R., FRESNO, M. & REDONDO, J. M. 2001. Selective inhibition of vascular endothelial growth factor-mediated angiogenesis by cyclosporin A: roles of the nuclear factor of activated T cells and cyclooxygenase 2. *J Exp Med,* 193**,** 607-20.

HERTOG, M. G., FESKENS, E. J., HOLLMAN, P. C., KATAN, M. B. & KROMHOUT, D. 1993. Dietary antioxidant flavonoids and risk of coronary heart disease: the Zutphen Elderly Study. *Lancet,* 342**,** 1007-11.

HOEBEN, A., LANDUYT, B., HIGHLEY, M. S., WILDIERS, H., VAN OOSTEROM, A. T. & DE BRUIJN, E. A. 2004. Vascular endothelial growth factor and angiogenesis. *Pharmacol Rev,* 56**,** 549-80.

HOFMANN, T., OBUKHOV, A. G., SCHAEFER, M., HARTENECK, C., GUDERMANN, T. & SCHULTZ, G. 1999. Direct activation of human TRPC6 and TRPC3 channels by diacylglycerol. *Nature,* 397**,** 259-63.

HOGAN, P. G., CHEN, L., NARDONE, J. & RAO, A. 2003. Transcriptional regulation by calcium, calcineurin, and NFAT. *Genes Dev,* 17**,** 2205-32.

HOGAN, P. G., LEWIS, R. S. & RAO, A. 2010. Molecular basis of calcium signaling in lymphocytes: STIM and ORAI. *Annu Rev Immunol,* 28**,** 491-533.

HOLTON, M. L., WANG, W., EMERSON, M., NEYSES, L. & ARMESILLA, A. L. 2010. Plasma membrane calcium ATPase proteins as novel regulators of signal transduction pathways. *World J Biol Chem,* 1**,** 201-8.

HOOD, J. D. & CHERESH, D. A. 2002. Targeted delivery of mutant Raf kinase to neovessels causes tumor regression. *Cold Spring Harb Symp Quant Biol,* 67**,** 285-91.

HORGAN, C. P. & MCCAFFREY, M. W. 2011. Rab GTPases and microtubule motors. *Biochem Soc Trans,* 39**,** 1202-6.

HOTH, M. & PENNER, R. 1992. Depletion of intracellular calcium stores activates a calcium current in mast cells. *Nature,* 355**,** 353-6.

HOU, X., PEDI, L., DIVER, M. M. & LONG, S. B. 2012. Crystal structure of the calcium release-activated calcium channel Orai. *Science,* 338**,** 1308-13.

HUPE, D. J., BOLTZ, R., COHEN, C. J., FELIX, J., HAM, E., MILLER, D., SODERMAN, D. & VAN SKIVER, D. 1991. The inhibition of receptor-mediated and voltage-dependent calcium entry by the antiproliferative L-651,582. *J Biol Chem,* 266**,** 10136-42.

HUSSAIN, M. M., KOTZ, H., MINASIAN, L., PREMKUMAR, A., SAROSY, G., REED, E., ZHAI, S., STEINBERG, S. M., RAGGIO, M., OLIVER, V. K., FIGG, W. D. & KOHN, E. C. 2003. Phase II trial of carboxyamidotriazole in patients with relapsed epithelial ovarian cancer. *J Clin Oncol,* 21**,** 4356-63.

INOUE, R., JENSEN, L. J., JIAN, Z., SHI, J., HAI, L., LURIE, A. I., HENRIKSEN, F. H., SALOMONSSON, M., MORITA, H., KAWARABAYASHI, Y., MORI, M., MORI, Y. & ITO, Y. 2009. Synergistic activation of vascular TRPC6 channel by receptor and mechanical stimulation via phospholipase C/diacylglycerol and phospholipase A2/omega-hydroxylase/20-HETE pathways. *Circ Res,* 104**,** 1399-409.

INOUE, R., OKADA, T., ONOUE, H., HARA, Y., SHIMIZU, S., NAITOH, S., ITO, Y. & MORI, Y. 2001. The transient receptor potential protein homologue TRP6 is the essential component of vascular alpha(1)-adrenoceptor-activated Ca(2+)-permeable cation channel. *Circ Res,* 88**,** 325-32.

JANSSEN, L. J. & KWAN, C. Y. 2007. ROCs and SOCs: what's in a name? *Cell Calcium,* 41**,** 245-7.

JAULIAC, S., LOPEZ-RODRIGUEZ, C., SHAW, L. M., BROWN, L. F., RAO, A. & TOKER, A. 2002. The role of NFAT transcription factors in integrin-mediated carcinoma invasion. *Nat Cell Biol,* 4**,** 540-4.

JHO, D., MEHTA, D., AHMMED, G., GAO, X. P., TIRUPPATHI, C., BROMAN, M. & MALIK, A. B. 2005. Angiopoietin-1 opposes VEGF-induced increase in endothelial permeability by inhibiting TRPC1-dependent Ca2 influx. *Circ Res,* 96**,** 1282-90.

JI, W., XU, P., LI, Z., LU, J., LIU, L., ZHAN, Y., CHEN, Y., HILLE, B., XU, T. & CHEN, L. 2008. Functional stoichiometry of the unitary calcium-release-activated calcium channel. *Proc Natl Acad Sci U S A,* 105**,** 13668-73.

JUNG, S., STROTMANN, R., SCHULTZ, G. & PLANT, T. D. 2002. TRPC6 is a candidate channel involved in receptor-stimulated cation currents in A7r5 smooth muscle cells. *Am J Physiol Cell Physiol,* 282**,** C347-59.

KALOGRIS, C., CAPRODOSSI, S., AMANTINI, C., LAMBERTUCCI, F., NABISSI, M., MORELLI, M. B., FARFARIELLO, V., FILOSA, A., EMILIOZZI, M. C., MAMMANA, G. & SANTONI, G. 2010. Expression of transient receptor potential vanilloid-1 (TRPV1) in urothelial cancers of human bladder: relation to clinicopathological and molecular parameters. *Histopathology,* 57**,** 744-52.

KAR, P., NELSON, C. & PAREKH, A. B. 2011. Selective activation of the transcription factor NFAT1 by calcium microdomains near Ca2+ release-activated Ca2+ (CRAC) channels. *J Biol Chem,* 286**,** 14795-803.

KAR, P., NELSON, C. & PAREKH, A. B. 2012. CRAC channels drive digital activation and provide analog control and synergy to Ca(2+)-dependent gene regulation. *Curr Biol,* 22**,** 242-7.

KAWASAKI, T., LANGE, I. & FESKE, S. 2009. A minimal regulatory domain in the C terminus of STIM1 binds to and activates ORAI1 CRAC channels. *Biochem Biophys Res Commun,* 385**,** 49-54.

KHAZAEI, M., MOIEN-AFSHARI, F. & LAHER, I. 2008. Vascular endothelial function in health and diseases. *Pathophysiology,* 15**,** 49-67.

KIM, J. D., LIU, L., GUO, W. & MEYDANI, M. 2006. Chemical structure of flavonols in relation to modulation of angiogenesis and immune-endothelial cell adhesion. *J Nutr Biochem,* 17**,** 165-76.

KNEKT, P., JARVINEN, R., REUNANEN, A. & MAATELA, J. 1996. Flavonoid intake and coronary mortality in Finland: a cohort study. *BMJ,* 312**,** 478-81.

KNOP, M., AARESKJOLD, E., BODE, G. & GERKE, V. 2004. Rab3D and annexin A2 play a role in regulated secretion of vWF, but not tPA, from endothelial cells. *EMBO J,* 23**,** 2982-92.

KOHN, E. C., ALESSANDRO, R., SPOONSTER, J., WERSTO, R. P. & LIOTTA, L. A. 1995. Angiogenesis: role of calcium-mediated signal transduction. *Proc Natl Acad Sci U S A,* 92**,** 1307-11.

KOHN, E. C. & LIOTTA, L. A. 1990. L651582: a novel antiproliferative and antimetastasis agent. *J Natl Cancer Inst,* 82**,** 54-60.

KOHN, E. C., REED, E., SAROSY, G., CHRISTIAN, M., LINK, C. J., COLE, K., FIGG, W. D., DAVIS, P. A., JACOB, J., GOLDSPIEL, B. & LIOTTA, L. A. 1996. Clinical investigation of a cytostatic calcium influx inhibitor in patients with refractory cancers. *Cancer Res,* 56**,** 569-73.

KOHN, E. C., SANDEEN, M. A. & LIOTTA, L. A. 1992. In vivo efficacy of a novel inhibitor of selected signal transduction pathways including calcium, arachidonate, and inositol phosphates. *Cancer Res,* 52**,** 3208-12.

KWAN, H. Y., HUANG, Y. & YAO, X. 2007. TRP channels in endothelial function and dysfunction. *Biochim Biophys Acta,* 1772**,** 907-14.

KWON, Y., HOFMANN, T. & MONTELL, C. 2007. Integration of phosphoinositide- and calmodulin-mediated regulation of TRPC6. *Mol Cell,* 25**,** 491-503.

LAMALICE, L., LE BOEUF, F. & HUOT, J. 2007. Endothelial cell migration during angiogenesis. *Circ Res,* 100**,** 782-94.

LANDRY, C. F., PRIBYL, T. M., ELLISON, J. A., GIVOGRI, M. I., KAMPF, K., CAMPAGNONI, C. W. & CAMPAGNONI, A. T. 1998. Embryonic expression of the myelin basic protein gene: identification of a promoter region that targets transgene expression to pioneer neurons. *J Neurosci,* 18**,** 7315-27.

LEE, M. T., MISHRA, A. & LAMBRIGHT, D. G. 2009. Structural mechanisms for regulation of membrane traffic by rab GTPases. *Traffic,* 10**,** 1377-89.

LEUNER, K., KAZANSKI, V., MULLER, M., ESSIN, K., HENKE, B., GOLLASCH, M., HARTENECK, C. & MULLER, W. E. 2007. Hyperforin--a key constituent of St. John's wort specifically activates TRPC6 channels. *FASEB J,* 21**,** 4101-11.

LEUNG, K. F., BARON, R. & SEABRA, M. C. 2006. Thematic review series: lipid posttranslational modifications. geranylgeranylation of Rab GTPases. *J Lipid Res,* 47**,** 467-75.

LEWIS, R. S. 2011. Store-operated calcium channels: new perspectives on mechanism and function. *Cold Spring Harb Perspect Biol,* 3.

LI, J., CUBBON, R. M., WILSON, L. A., AMER, M. S., MCKEOWN, L., HOU, B., MAJEED, Y., TUMOVA, S., SEYMOUR, V. A., TAYLOR, H., STACEY, M., O'REGAN, D., FOSTER, R., PORTER, K. E., KEARNEY, M. T. & BEECH, D. J. 2011. Orai1 and CRAC channel dependence of VEGF-activated Ca2+ entry and endothelial tube formation. *Circ Res,* 108**,** 1190-8.

LIAO, Y., ERXLEBEN, C., ABRAMOWITZ, J., FLOCKERZI, V., ZHU, M. X., ARMSTRONG, D. L. & BIRNBAUMER, L. 2008. Functional interactions among Orai1, TRPCs, and STIM1 suggest a STIM-regulated heteromeric Orai/TRPC model for SOCE/Icrac channels. *Proc Natl Acad Sci U S A,* 105**,** 2895-900.

LIAO, Y., ERXLEBEN, C., YILDIRIM, E., ABRAMOWITZ, J., ARMSTRONG, D. L. & BIRNBAUMER, L. 2007. Orai proteins interact with TRPC channels and confer responsiveness to store depletion. *Proc Natl Acad Sci U S A,* 104**,** 4682-7.

LIOU, J., KIM, M. L., HEO, W. D., JONES, J. T., MYERS, J. W., FERRELL, J. E., JR. & MEYER, T. 2005. STIM is a Ca2+ sensor essential for Ca2+-store-depletion-triggered Ca2+ influx. *Curr Biol,* 15**,** 1235-41.

LIS, A., PEINELT, C., BECK, A., PARVEZ, S., MONTEILH-ZOLLER, M., FLEIG, A. & PENNER, R. 2007. CRACM1, CRACM2, and CRACM3 are store-operated Ca2+ channels with distinct functional properties. *Curr Biol,* 17**,** 794-800.

LOWENSTEIN, C. J., MORRELL, C. N. & YAMAKUCHI, M. 2005. Regulation of Weibel-Palade body exocytosis. *Trends Cardiovasc Med,* 15**,** 302-8.

LUIK, R. M., WU, M. M., BUCHANAN, J. & LEWIS, R. S. 2006. The elementary unit of store-operated Ca2+ entry: local activation of CRAC channels by STIM1 at ER-plasma membrane junctions. *J Cell Biol,* 174**,** 815-25.

LUZZI, K. J., VARGHESE, H. J., MACDONALD, I. C., SCHMIDT, E. E., KOHN, E. C., MORRIS, V. L., MARSHALL, K. E., CHAMBERS, A. F. & GROOM, A. C. 1998. Inhibition of angiogenesis in liver metastases by carboxyamidotriazole (CAI). *Angiogenesis,* 2**,** 373-9.

MA, S. & CHISHOLM, R. L. 2002. Cytoplasmic dynein-associated structures move bidirectionally in vivo. *J Cell Sci,* 115**,** 1453-60.

MAAT, W., BEIBOER, S. H., JAGER, M. J., LUYTEN, G. P., GRUIS, N. A. & VAN DER VELDEN, P. A. 2008. Epigenetic regulation identifies RASEF as a tumor-suppressor gene in uveal melanoma. *Invest Ophthalmol Vis Sci,* 49**,** 1291-8.

MACIAN, F. 2005. NFAT proteins: key regulators of T-cell development and function. *Nat Rev Immunol,* 5**,** 472-84.

MALUMBRES, M. & BARBACID, M. 2003. RAS oncogenes: the first 30 years. *Nat Rev Cancer,* 3**,** 459-65.

MANCINI, M. & TOKER, A. 2009. NFAT proteins: emerging roles in cancer progression. *Nat Rev Cancer,* 9**,** 810-20.

MANICKAM, V., TIWARI, A., JUNG, J. J., BHATTACHARYA, R., GOEL, A., MUKHOPADHYAY, D. & CHOUDHURY, A. 2011. Regulation of vascular endothelial growth factor receptor 2 trafficking and angiogenesis by Golgi localized t-SNARE syntaxin 6. *Blood,* 117**,** 1425-35.

MANJI, S. S., PARKER, N. J., WILLIAMS, R. T., VAN STEKELENBURG, L., PEARSON, R. B., DZIADEK, M. & SMITH, P. J. 2000. STIM1: a novel

phosphoprotein located at the cell surface. *Biochim Biophys Acta,* 1481**,** 147-55.

MATSUSHITA, K., YAMAKUCHI, M., MORRELL, C. N., OZAKI, M., O'ROURKE, B., IRANI, K. & LOWENSTEIN, C. J. 2005. Vascular endothelial growth factor regulation of Weibel-Palade-body exocytosis. *Blood,* 105**,** 207-14.

MAVRIA, G., VERCOULEN, Y., YEO, M., PATERSON, H., KARASARIDES, M., MARAIS, R., BIRD, D. & MARSHALL, C. J. 2006. ERK-MAPK signaling opposes Rho-kinase to promote endothelial cell survival and sprouting during angiogenesis. *Cancer Cell,* 9**,** 33-44.

MCANDREW, D., GRICE, D. M., PETERS, A. A., DAVIS, F. M., STEWART, T., RICE, M., SMART, C. E., BROWN, M. A., KENNY, P. A., ROBERTS-THOMSON, S. J. & MONTEITH, G. R. 2011. ORAI1-mediated calcium influx in lactation and in breast cancer. *Mol Cancer Ther,* 10**,** 448-60.

MCDONAGH, M. S., EDEN, K. B. & PETERSON, K. 2005. *Drug Class Review on Calcium Channel Blockers: Final Report.* Portland (OR).

MEADOWS, K. N., BRYANT, P. & PUMIGLIA, K. 2001. Vascular endothelial growth factor induction of the angiogenic phenotype requires Ras activation. *J Biol Chem,* 276**,** 49289-98.

MEDYOUF, H., ALCALDE, H., BERTHIER, C., GUILLEMIN, M. C., DOS SANTOS, N. R., JANIN, A., DECAUDIN, D., DE THE, H. & GHYSDAEL, J. 2007. Targeting calcineurin activation as a therapeutic strategy for T-cell acute lymphoblastic leukemia. *Nat Med,* 13**,** 736-41.

MIGNEN, O., BRINK, C., ENFISSI, A., NADKARNI, A., SHUTTLEWORTH, T. J., GIOVANNUCCI, D. R. & CAPIOD, T. 2005. Carboxyamidotriazole-induced inhibition of mitochondrial calcium import blocks capacitative calcium entry and cell proliferation in HEK-293 cells. *J Cell Sci,* 118**,** 5615-23.

MIGNEN, O. & SHUTTLEWORTH, T. J. 2000. I(ARC), a novel arachidonate-regulated, noncapacitative Ca(2+) entry channel. *J Biol Chem,* 275**,** 9114-9.

MIGNEN, O., THOMPSON, J. L. & SHUTTLEWORTH, T. J. 2008. Both Orai1 and Orai3 are essential components of the arachidonate-regulated Ca2+-selective (ARC) channels. *J Physiol,* 586**,** 185-95.

MOCCIA, F., BERRA-ROMANI, R. & TANZI, F. 2012. Update on vascular endothelial Ca(2+) signalling: A tale of ion channels, pumps and transporters. *World J Biol Chem,* 3**,** 127-58.

MONTEITH, G. R., DAVIS, F. M. & ROBERTS-THOMSON, S. J. 2012. Calcium channels and pumps in cancer: changes and consequences. *J Biol Chem,* 287**,** 31666-73.

MONTELL, C. & RUBIN, G. M. 1989. Molecular characterization of the Drosophila trp locus: a putative integral membrane protein required for phototransduction. *Neuron,* 2**,** 1313-23.

MOTIANI, R. K., ABDULLAEV, I. F. & TREBAK, M. 2010. A novel native store-operated calcium channel encoded by Orai3: selective requirement of Orai3 versus Orai1 in estrogen receptor-positive versus estrogen receptor-negative breast cancer cells. *J Biol Chem,* 285**,** 19173-83.

MOTIANI, R. K., ZHANG, X., HARMON, K. E., KELLER, R. S., MATROUGUI, K., BENNETT, J. A. & TREBAK, M. 2013. Orai3 is an estrogen receptor

alpha-regulated Ca(2)(+) channel that promotes tumorigenesis. *FASEB J,* 27, 63-75.

MUIK, M., FRISCHAUF, I., DERLER, I., FAHRNER, M., BERGSMANN, J., EDER, P., SCHINDL, R., HESCH, C., POLZINGER, B., FRITSCH, R., KAHR, H., MADL, J., GRUBER, H., GROSCHNER, K. & ROMANIN, C. 2008. Dynamic coupling of the putative coiled-coil domain of ORAI1 with STIM1 mediates ORAI1 channel activation. *J Biol Chem,* 283, 8014-22.

NAKAMURA, S., TAKEMURA, T., TAN, L., NAGATA, Y., YOKOTA, D., HIRANO, I., SHIGENO, K., SHIBATA, K., FUJIE, M., FUJISAWA, S. & OHNISHI, K. 2011. Small GTPase RAB45-mediated p38 activation in apoptosis of chronic myeloid leukemia progenitor cells. *Carcinogenesis,* 32, 1758-72.

NIGHTINGALE, T. & CUTLER, D. 2013. The secretion of von Willebrand factor from endothelial cells; an increasingly complicated story. *J Thromb Haemost,* 11 Suppl 1, 192-201.

NIGHTINGALE, T. D., PATTNI, K., HUME, A. N., SEABRA, M. C. & CUTLER, D. F. 2009. Rab27a and MyRIP regulate the amount and multimeric state of VWF released from endothelial cells. *Blood,* 113, 5010-8.

NILIUS, B., VRIENS, J., PRENEN, J., DROOGMANS, G. & VOETS, T. 2004. TRPV4 calcium entry channel: a paradigm for gating diversity. *Am J Physiol Cell Physiol,* 286, C195-205.

NILIUS, B., WATANABE, H. & VRIENS, J. 2003. The TRPV4 channel: structure-function relationship and promiscuous gating behaviour. *Pflugers Arch,* 446, 298-303.

OH-HORA, M., YAMASHITA, M., HOGAN, P. G., SHARMA, S., LAMPERTI, E., CHUNG, W., PRAKRIYA, M., FESKE, S. & RAO, A. 2008. Dual functions for the endoplasmic reticulum calcium sensors STIM1 and STIM2 in T cell activation and tolerance. *Nat Immunol,* 9, 432-43.

ONOHARA, N., NISHIDA, M., INOUE, R., KOBAYASHI, H., SUMIMOTO, H., SATO, Y., MORI, Y., NAGAO, T. & KUROSE, H. 2006. TRPC3 and TRPC6 are essential for angiotensin II-induced cardiac hypertrophy. *EMBO J,* 25, 5305-16.

OSHITA, H., NISHINO, R., TAKANO, A., FUJITOMO, T., ARAGAKI, M., KATO, T., AKIYAMA, H., TSUCHIYA, E., KOHNO, N., NAKAMURA, Y. & DAIGO, Y. 2013a. RASEF is a novel diagnostic biomarker and a therapeutic target for lung cancer. *Mol Cancer Res*.

OSHITA, H., NISHINO, R., TAKANO, A., FUJITOMO, T., ARAGAKI, M., KATO, T., AKIYAMA, H., TSUCHIYA, E., KOHNO, N., NAKAMURA, Y. & DAIGO, Y. 2013b. RASEF is a Novel Diagnostic Biomarker and a Therapeutic Target for Lung Cancer. *Mol Cancer Res,* 11, 937-51.

PAEZ, P. M., FULTON, D., SPREUER, V., HANDLEY, V. & CAMPAGNONI, A. T. 2011. Modulation of canonical transient receptor potential channel 1 in the proliferation of oligodendrocyte precursor cells by the golli products of the myelin basic protein gene. *J Neurosci,* 31, 3625-37.

PAEZ, P. M., FULTON, D. J., SPREUER, V., HANDLEY, V., CAMPAGNONI, C. W., MACKLIN, W. B., COLWELL, C. & CAMPAGNONI, A. T. 2009. Golli myelin basic proteins regulate oligodendroglial progenitor cell migration through voltage-gated Ca2+ influx. *J Neurosci,* 29, 6663-76.

PAEZ, P. M., SPREUER, V., HANDLEY, V., FENG, J. M., CAMPAGNONI, C. & CAMPAGNONI, A. T. 2007. Increased expression of golli myelin basic

proteins enhances calcium influx into oligodendroglial cells. *J Neurosci,* 27**,** 12690-9.

PANZA, J. A., QUYYUMI, A. A., CALLAHAN, T. S. & EPSTEIN, S. E. 1993. Effect of antihypertensive treatment on endothelium-dependent vascular relaxation in patients with essential hypertension. *J Am Coll Cardiol,* 21**,** 1145-51.

PAREKH, A. B. 2010. Store-operated CRAC channels: function in health and disease. *Nat Rev Drug Discov,* 9**,** 399-410.

PAREKH, A. B. & PUTNEY, J. W., JR. 2005. Store-operated calcium channels. *Physiol Rev,* 85**,** 757-810.

PARK, C. Y., HOOVER, P. J., MULLINS, F. M., BACHHAWAT, P., COVINGTON, E. D., RAUNSER, S., WALZ, T., GARCIA, K. C., DOLMETSCH, R. E. & LEWIS, R. S. 2009. STIM1 clusters and activates CRAC channels via direct binding of a cytosolic domain to Orai1. *Cell,* 136**,** 876-90.

PENNA, A., DEMURO, A., YEROMIN, A. V., ZHANG, S. L., SAFRINA, O., PARKER, I. & CAHALAN, M. D. 2008. The CRAC channel consists of a tetramer formed by Stim-induced dimerization of Orai dimers. *Nature,* 456**,** 116-20.

PERABO, F. G., DEMANT, A. W., WIRGER, A., SCHMIDT, D. H., SITIA, M., WARDELMANN, E., MULLER, S. C. & KOHN, E. C. 2005. Carboxyamido-triazole (CAI) reverses the balance between proliferation and apoptosis in a rat bladder cancer model. *Anticancer Res,* 25**,** 725-9.

PERRAUD, A. L., FLEIG, A., DUNN, C. A., BAGLEY, L. A., LAUNAY, P., SCHMITZ, C., STOKES, A. J., ZHU, Q., BESSMAN, M. J., PENNER, R., KINET, J. P. & SCHARENBERG, A. M. 2001. ADP-ribose gating of the calcium-permeable LTRPC2 channel revealed by Nudix motif homology. *Nature,* 411**,** 595-9.

PERTZ, O. 2010. Spatio-temporal Rho GTPase signaling - where are we now? *J Cell Sci,* 123**,** 1841-50.

PFEFFER, S. & AIVAZIAN, D. 2004. Targeting Rab GTPases to distinct membrane compartments. *Nat Rev Mol Cell Biol,* 5**,** 886-96.

PRAKRIYA, M., FESKE, S., GWACK, Y., SRIKANTH, S., RAO, A. & HOGAN, P. G. 2006. Orai1 is an essential pore subunit of the CRAC channel. *Nature,* 443**,** 230-3.

PRIBYL, T. M., CAMPAGNONI, C. W., KAMPF, K., KASHIMA, T., HANDLEY, V. W., MCMAHON, J. & CAMPAGNONI, A. T. 1993. The human myelin basic protein gene is included within a 179-kilobase transcription unit: expression in the immune and central nervous systems. *Proc Natl Acad Sci U S A,* 90**,** 10695-9.

PUTNEY, J. W., JR. 1986. A model for receptor-regulated calcium entry. *Cell Calcium,* 7**,** 1-12.

QIN, L. X., TANG, Z. Y., LI, X. M., BU, W. & XIA, J. L. 1999. Effect of antiangiogenic agents on experimental animal models of hepatocellular carcinoma. *Ann Acad Med Singapore,* 28**,** 147-51.

REISER, J., POLU, K. R., MOLLER, C. C., KENLAN, P., ALTINTAS, M. M., WEI, C., FAUL, C., HERBERT, S., VILLEGAS, I., AVILA-CASADO, C., MCGEE, M., SUGIMOTO, H., BROWN, D., KALLURI, R., MUNDEL, P., SMITH, P. L., CLAPHAM, D. E. & POLLAK, M. R. 2005. TRPC6 is a

glomerular slit diaphragm-associated channel required for normal renal function. *Nat Genet,* 37**,** 739-44.

RICCIO, A., MEDHURST, A. D., MATTEI, C., KELSELL, R. E., CALVER, A. R., RANDALL, A. D., BENHAM, C. D. & PANGALOS, M. N. 2002. mRNA distribution analysis of human TRPC family in CNS and peripheral tissues. *Brain Res Mol Brain Res,* 109**,** 95-104.

RIMM, E. B., KATAN, M. B., ASCHERIO, A., STAMPFER, M. J. & WILLETT, W. C. 1996. Relation between intake of flavonoids and risk for coronary heart disease in male health professionals. *Ann Intern Med,* 125**,** 384-9.

RINNE, A., BANACH, K. & BLATTER, L. A. 2009. Regulation of nuclear factor of activated T cells (NFAT) in vascular endothelial cells. *J Mol Cell Cardiol,* 47**,** 400-10.

RONDAIJ, M. G., BIERINGS, R., KRAGT, A., GIJZEN, K. A., SELLINK, E., VAN MOURIK, J. A., FERNANDEZ-BORJA, M. & VOORBERG, J. 2006. Dynein-dynactin complex mediates protein kinase A-dependent clustering of Weibel-Palade bodies in endothelial cells. *Arterioscler Thromb Vasc Biol,* 26**,** 49-55.

ROOS, J., DIGREGORIO, P. J., YEROMIN, A. V., OHLSEN, K., LIOUDYNO, M., ZHANG, S., SAFRINA, O., KOZAK, J. A., WAGNER, S. L., CAHALAN, M. D., VELICELEBI, G. & STAUDERMAN, K. A. 2005. STIM1, an essential and conserved component of store-operated Ca2+ channel function. *J Cell Biol,* 169**,** 435-45.

ROTHBERG, B. S., WANG, Y. & GILL, D. L. 2013. Orai Channel Pore Properties and Gating by STIM: Implications from the Orai Crystal Structure. *Sci Signal,* 6**,** pe9.

RYBARCZYK, P., GAUTIER, M., HAGUE, F., DHENNIN-DUTHILLE, I., CHATELAIN, D., KERR-CONTE, J., PATTOU, F., REGIMBEAU, J. M., SEVESTRE, H. & OUADID-AHIDOUCH, H. 2012. Transient receptor potential melastatin-related 7 channel is overexpressed in human pancreatic ductal adenocarcinomas and regulates human pancreatic cancer cell migration. *Int J Cancer,* 131, E851-61.

RYEOM, S., BAEK, K. H., RIOTH, M. J., LYNCH, R. C., ZASLAVSKY, A., BIRSNER, A., YOON, S. S. & MCKEON, F. 2008. Targeted deletion of the calcineurin inhibitor DSCR1 suppresses tumor growth. *Cancer Cell,* 13**,** 420-31.

SABBIONI, S., VERONESE, A., TRUBIA, M., TARAMELLI, R., BARBANTI-BRODANO, G., CROCE, C. M. & NEGRINI, M. 1999. Exon structure and promoter identification of STIM1 (alias GOK), a human gene causing growth arrest of the human tumor cell lines G401 and RD. *Cytogenet Cell Genet,* 86**,** 214-8.

SAMAPATI, R., YANG, Y., YIN, J., STOERGER, C., ARENZ, C., DIETRICH, A., GUDERMANN, T., ADAM, D., WU, S., FREICHEL, M., FLOCKERZI, V., UHLIG, S. & KUEBLER, W. M. 2012. Lung endothelial Ca2+ and permeability response to platelet-activating factor is mediated by acid sphingomyelinase and transient receptor potential classical 6. *Am J Respir Crit Care Med,* 185**,** 160-70.

SAPONARA, S., CAROSATI, E., MUGNAI, P., SGARAGLI, G. & FUSI, F. 2011. The flavonoid scaffold as a template for the design of modulators of the vascular Ca(v) 1.2 channels. *Br J Pharmacol,* 164**,** 1684-97.

SCHMIDT, U., FUESSEL, S., KOCH, R., BARETTON, G. B., LOHSE, A., TOMASETTI, S., UNVERSUCHT, S., FROEHNER, M., WIRTH, M. P. & MEYE, A. 2006. Quantitative multi-gene expression profiling of primary prostate cancer. *Prostate,* 66**,** 1521-34.

SHAPIRO, M. S., GOMEZA, J., HAMILTON, S. E., HILLE, B., LOOSE, M. D., NATHANSON, N. M., ROCHE, J. P. & WESS, J. 2001. Identification of subtypes of muscarinic receptors that regulate Ca2+ and K+ channel activity in sympathetic neurons. *Life Sci,* 68**,** 2481-7.

SHI, J., MORI, E., MORI, Y., MORI, M., LI, J., ITO, Y. & INOUE, R. 2004. Multiple regulation by calcium of murine homologues of transient receptor potential proteins TRPC6 and TRPC7 expressed in HEK293 cells. *J Physiol,* 561**,** 415-32.

SHI, Y., DING, X., HE, Z. H., ZHOU, K. C., WANG, Q. & WANG, Y. Z. 2009. Critical role of TRPC6 channels in G2 phase transition and the development of human oesophageal cancer. *Gut,* 58**,** 1443-50.

SHIBUYA, M. & CLAESSON-WELSH, L. 2006. Signal transduction by VEGF receptors in regulation of angiogenesis and lymphangiogenesis. *Exp Cell Res,* 312**,** 549-60.

SHINTANI, M., TADA, M., KOBAYASHI, T., KAJIHO, H., KONTANI, K. & KATADA, T. 2007. Characterization of Rab45/RASEF containing EF-hand domain and a coiled-coil motif as a self-associating GTPase. *Biochem Biophys Res Commun,* 357**,** 661-7.

SHIOJIMA, I. & WALSH, K. 2002. Role of Akt signaling in vascular homeostasis and angiogenesis. *Circ Res,* 90**,** 1243-50.

SINGH, R. B., MENGI, S. A., XU, Y. J., ARNEJA, A. S. & DHALLA, N. S. 2002. Pathogenesis of atherosclerosis: A multifactorial process. *Exp Clin Cardiol,* 7**,** 40-53.

SOBOLOFF, J., ROTHBERG, B. S., MADESH, M. & GILL, D. L. 2012. STIM proteins: dynamic calcium signal transducers. *Nat Rev Mol Cell Biol,* 13**,** 549-65.

SOURS, S., DU, J., CHU, S., DING, M., ZHOU, X. J. & MA, R. 2006. Expression of canonical transient receptor potential (TRPC) proteins in human glomerular mesangial cells. *Am J Physiol Renal Physiol,* 290**,** F1507-15.

SRIKANTH, S., JEW, M., KIM, K. D., YEE, M. K., ABRAMSON, J. & GWACK, Y. 2012. Junctate is a Ca2+-sensing structural component of Orai1 and stromal interaction molecule 1 (STIM1). *Proc Natl Acad Sci U S A,* 109**,** 8682-7.

SRIKANTH, S., JUNG, H. J., KIM, K. D., SOUDA, P., WHITELEGGE, J. & GWACK, Y. 2010. A novel EF-hand protein, CRACR2A, is a cytosolic Ca2+ sensor that stabilizes CRAC channels in T cells. *Nat Cell Biol,* 12**,** 436-46.

STATHOPULOS, P. B., LI, G. Y., PLEVIN, M. J., AMES, J. B. & IKURA, M. 2006. Stored Ca2+ depletion-induced oligomerization of stromal interaction molecule 1 (STIM1) via the EF-SAM region: An initiation mechanism for capacitive Ca2+ entry. *J Biol Chem,* 281**,** 35855-62.

STATHOPULOS, P. B., ZHENG, L., LI, G. Y., PLEVIN, M. J. & IKURA, M. 2008. Structural and mechanistic insights into STIM1-mediated initiation of store-operated calcium entry. *Cell,* 135**,** 110-22.

SUMPIO, B. E., RILEY, J. T. & DARDIK, A. 2002. Cells in focus: endothelial cell. *Int J Biochem Cell Biol,* 34**,** 1508-12.

SUTTERLIN, C. & COLANZI, A. 2010. The Golgi and the centrosome: building a functional partnership. *J Cell Biol,* 188**,** 621-8.

SZEWCZYK, M. M., DAVIS, K. A., SAMSON, S. E., SIMPSON, F., RANGACHARI, P. K. & GROVER, A. K. 2007. Ca2+-pumps and Na2+-Ca2+-exchangers in coronary artery endothelium versus smooth muscle. *J Cell Mol Med,* 11**,** 129-38.

TAKAHASHI, T. & SHIBUYA, M. 1997. The 230 kDa mature form of KDR/Flk-1 (VEGF receptor-2) activates the PLC-gamma pathway and partially induces mitotic signals in NIH3T3 fibroblasts. *Oncogene,* 14**,** 2079-89.

TAUSEEF, M., KNEZEVIC, N., CHAVA, K. R., SMITH, M., SUKRITI, S., GIANARIS, N., OBUKHOV, A. G., VOGEL, S. M., SCHRAUFNAGEL, D. E., DIETRICH, A., BIRNBAUMER, L., MALIK, A. B. & MEHTA, D. 2012. TLR4 activation of TRPC6-dependent calcium signaling mediates endotoxin-induced lung vascular permeability and inflammation. *J Exp Med,* 209**,** 1953-68.

THASTRUP, O., DAWSON, A. P., SCHARFF, O., FODER, B., CULLEN, P. J., DROBAK, B. K., BJERRUM, P. J., CHRISTENSEN, S. B. & HANLEY, M. R. 1989. Thapsigargin, a novel molecular probe for studying intracellular calcium release and storage. *Agents Actions,* 27**,** 17-23.

THIEL, M., LIS, A. & PENNER, R. 2013. STIM2 drives Ca2+ oscillations through store-operated Ca2+ entry caused by mild store depletion. *J Physiol,* 591**,** 1433-45.

TIAN, D., JACOBO, S. M., BILLING, D., ROZKALNE, A., GAGE, S. D., ANAGNOSTOU, T., PAVENSTADT, H., HSU, H. H., SCHLONDORFF, J., RAMOS, A. & GREKA, A. 2010. Antagonistic regulation of actin dynamics and cell motility by TRPC5 and TRPC6 channels. *Sci Signal,* 3**,** ra77.

TRAN, Q. K., OHASHI, K. & WATANABE, H. 2000. Calcium signalling in endothelial cells. *Cardiovasc Res,* 48**,** 13-22.

TREBAK, M., VAZQUEZ, G., BIRD, G. S. & PUTNEY, J. W., JR. 2003. The TRPC3/6/7 subfamily of cation channels. *Cell Calcium,* 33**,** 451-61.

TSAVALER, L., SHAPERO, M. H., MORKOWSKI, S. & LAUS, R. 2001. Trp-p8, a novel prostate-specific gene, is up-regulated in prostate cancer and other malignancies and shares high homology with transient receptor potential calcium channel proteins. *Cancer Res,* 61**,** 3760-9.

VALENTIJN, K. M., SADLER, J. E., VALENTIJN, J. A., VOORBERG, J. & EIKENBOOM, J. 2011. Functional architecture of Weibel-Palade bodies. *Blood,* 117**,** 5033-43.

VELICEASA, D., IVANOVIC, M., HOEPFNER, F. T., THUMBIKAT, P., VOLPERT, O. V. & SMITH, N. D. 2007. Transient potential receptor channel 4 controls thrombospondin-1 secretion and angiogenesis in renal cell carcinoma. *Febs J,* 274**,** 6365-77.

VIG, M., BECK, A., BILLINGSLEY, J. M., LIS, A., PARVEZ, S., PEINELT, C., KOOMOA, D. L., SOBOLOFF, J., GILL, D. L., FLEIG, A., KINET, J. P. & PENNER, R. 2006a. CRACM1 multimers form the ion-selective pore of the CRAC channel. *Curr Biol,* 16**,** 2073-9.

VIG, M., PEINELT, C., BECK, A., KOOMOA, D. L., RABAH, D., KOBLAN-HUBERSON, M., KRAFT, S., TURNER, H., FLEIG, A., PENNER, R. &

KINET, J. P. 2006b. CRACM1 is a plasma membrane protein essential for store-operated Ca2+ entry. *Science,* 312**,** 1220-3.

VINET, R. & VARGAS, F. F. 1999. L- and T-type voltage-gated Ca2+ currents in adrenal medulla endothelial cells. *Am J Physiol,* 276**,** H1313-22.

VINOGRADOVA, T. M., ROUDNIK, V. E., BYSTREVSKAYA, V. B. & SMIRNOV, V. N. 2000. Centrosome-directed translocation of Weibel-Palade bodies is rapidly induced by thrombin, calyculin A, or cytochalasin B in human aortic endothelial cells. *Cell Motil Cytoskeleton,* 47**,** 141-53.

WALSH, C. M., DOHERTY, M. K., TEPIKIN, A. V. & BURGOYNE, R. D. 2010. Evidence for an interaction between Golli and STIM1 in store-operated calcium entry. *Biochem J,* 430**,** 453-60.

WANSCHERS, B., VAN DE VORSTENBOSCH, R., WIJERS, M., WIERINGA, B., KING, S. M. & FRANSEN, J. 2008. Rab6 family proteins interact with the dynein light chain protein DYNLRB1. *Cell Motil Cytoskeleton,* 65**,** 183-96.

WEBER, C. & NOELS, H. 2011. Atherosclerosis: current pathogenesis and therapeutic options. *Nat Med,* 17**,** 1410-22.

WEI, C., WANG, X., CHEN, M., OUYANG, K., SONG, L. S. & CHENG, H. 2009. Calcium flickers steer cell migration. *Nature,* 457**,** 901-5.

WEIBEL, E. R. & PALADE, G. E. 1964. New Cytoplasmic Components in Arterial Endothelia. *J Cell Biol,* 23**,** 101-12.

WIDLANSKY, M. E., GOKCE, N., KEANEY, J. F., JR. & VITA, J. A. 2003. The clinical implications of endothelial dysfunction. *J Am Coll Cardiol,* 42**,** 1149-60.

WILLIAMS, R. T., MANJI, S. S., PARKER, N. J., HANCOCK, M. S., VAN STEKELENBURG, L., EID, J. P., SENIOR, P. V., KAZENWADEL, J. S., SHANDALA, T., SAINT, R., SMITH, P. J. & DZIADEK, M. A. 2001. Identification and characterization of the STIM (stromal interaction molecule) gene family: coding for a novel class of transmembrane proteins. *Biochem J,* 357**,** 673-85.

WINK, M. 2006. *An Introduction to Molecular Biotechnology: Molecular Fundamentals, Methods and Applications in Modern Biotechnology* Wiley VCH.

WINN, M. P., CONLON, P. J., LYNN, K. L., FARRINGTON, M. K., CREAZZO, T., HAWKINS, A. F., DASKALAKIS, N., KWAN, S. Y., EBERSVILLER, S., BURCHETTE, J. L., PERICAK-VANCE, M. A., HOWELL, D. N., VANCE, J. M. & ROSENBERG, P. B. 2005. A mutation in the TRPC6 cation channel causes familial focal segmental glomerulosclerosis. *Science,* 308**,** 1801-4.

WU, M. M., BUCHANAN, J., LUIK, R. M. & LEWIS, R. S. 2006. Ca2+ store depletion causes STIM1 to accumulate in ER regions closely associated with the plasma membrane. *J Cell Biol,* 174**,** 803-13.

WU, Y., PALAD, A. J., WASILENKO, W. J., BLACKMORE, P. F., PINCUS, W. A., SCHECHTER, G. L., SPOONSTER, J. R., KOHN, E. C. & SOMERS, K. D. 1997. Inhibition of head and neck squamous cell carcinoma growth and invasion by the calcium influx inhibitor carboxyamido-triazole. *Clin Cancer Res,* 3**,** 1915-21.

XU, P., LU, J., LI, Z., YU, X., CHEN, L. & XU, T. 2006. Aggregation of STIM1 underneath the plasma membrane induces clustering of Orai1. *Biochem Biophys Res Commun,* 350**,** 969-76.

YAMASHITA, M., NAVARRO-BORELLY, L., MCNALLY, B. A. & PRAKRIYA, M. 2007. Orai1 mutations alter ion permeation and Ca2+-dependent fast inactivation of CRAC channels: evidence for coupling of permeation and gating. *J Gen Physiol,* 130**,** 525-40.

YANG, S. L., CAO, Q., ZHOU, K. C., FENG, Y. J. & WANG, Y. Z. 2009. Transient receptor potential channel C3 contributes to the progression of human ovarian cancer. *Oncogene,* 28**,** 1320-8.

YEE, N. S., ZHOU, W. & LEE, M. 2010. Transient receptor potential channel TRPM8 is over-expressed and required for cellular proliferation in pancreatic adenocarcinoma. *Cancer Lett,* 297**,** 49-55.

YEROMIN, A. V., ZHANG, S. L., JIANG, W., YU, Y., SAFRINA, O. & CAHALAN, M. D. 2006. Molecular identification of the CRAC channel by altered ion selectivity in a mutant of Orai. *Nature,* 443**,** 226-9.

YOCHUM, L., KUSHI, L. H., MEYER, K. & FOLSOM, A. R. 1999. Dietary flavonoid intake and risk of cardiovascular disease in postmenopausal women. *Am J Epidemiol,* 149**,** 943-9.

YU, P. C., GU, S. Y., BU, J. W. & DU, J. L. 2010. TRPC1 is essential for in vivo angiogenesis in zebrafish. *Circ Res,* 106**,** 1221-32.

YU, Y., FANTOZZI, I., REMILLARD, C. V., LANDSBERG, J. W., KUNICHIKA, N., PLATOSHYN, O., TIGNO, D. D., THISTLETHWAITE, P. A., RUBIN, L. J. & YUAN, J. X. 2004. Enhanced expression of transient receptor potential channels in idiopathic pulmonary arterial hypertension. *Proc Natl Acad Sci U S A,* 101**,** 13861-6.

YUAN, J. P., ZENG, W., DORWART, M. R., CHOI, Y. J., WORLEY, P. F. & MUALLEM, S. 2009. SOAR and the polybasic STIM1 domains gate and regulate Orai channels. *Nat Cell Biol,* 11**,** 337-43.

YUAN, T. L. & CANTLEY, L. C. 2008. PI3K pathway alterations in cancer: variations on a theme. *Oncogene,* 27**,** 5497-510.

ZENG, F., XU, S. Z., JACKSON, P. K., MCHUGH, D., KUMAR, B., FOUNTAIN, S. J. & BEECH, D. J. 2004. Human TRPC5 channel activated by a multiplicity of signals in a single cell. *J Physiol,* 559**,** 739-50.

ZHANG, S. L., YU, Y., ROOS, J., KOZAK, J. A., DEERINCK, T. J., ELLISMAN, M. H., STAUDERMAN, K. A. & CAHALAN, M. D. 2005. STIM1 is a Ca2+ sensor that activates CRAC channels and migrates from the Ca2+ store to the plasma membrane. *Nature,* 437**,** 902-5.

ZHOU, C. & WU, S. 2006. T-type calcium channels in pulmonary vascular endothelium. *Microcirculation,* 13**,** 645-56.

ZHOU, J., DU, W., ZHOU, K., TAI, Y., YAO, H., JIA, Y., DING, Y. & WANG, Y. 2008. Critical role of TRPC6 channels in the formation of excitatory synapses. *Nat Neurosci,* 11**,** 741-3.

ZHOU, Y., RAMACHANDRAN, S., OH-HORA, M., RAO, A. & HOGAN, P. G. 2010. Pore architecture of the ORAI1 store-operated calcium channel. *Proc Natl Acad Sci U S A,* 107**,** 4896-901.

ZOGRAFOU, S., BASAGIANNIS, D., PAPAFOTIKA, A., SHIRAKAWA, R., HORIUCHI, H., AUERBACH, D., FUKUDA, M. & CHRISTOFORIDIS, S. 2012. A complete Rab screening reveals novel insights in Weibel-Palade body exocytosis. *J Cell Sci,* 125**,** 4780-90.